THE DESIGN AND SYNTHESIS OF INHIBITORS OF HIV-1 VIRAL ENTRY AND PHOTOAFFINITY LABELED PROBES FOR STRUCTURAL ELUCIDATION OF THE HIV-1 ENV

Althea Erica Gaffney

A DISSERTATION

in

Chemistry

Presented to the Faculties of the University of Pennsylvania

in

Partial Fulfillment of the Requirements for the

Degree of Doctor of Philosophy

2019

Supervisor of Dissertation

_____

Amos B. Smith, III

Rhodes-Thompson Professor of Chemistry

Graduate Group Chairperson

_____

Prof. David W. Christianson

Roy and Diana Vagelos Professor in Chemistry and Chemical Biology

Dissertation Committee

Marisa C. Kozlowski, Professor of Chemistry

Patrick J. Walsh, Professor of Chemistry

David M. Chenoweth, Associate Professor of Chemistry

ABSTRACT

THE DESIGN AND SYNTHESIS OF INHIBITORS OF HIV-1 VIRAL ENTRY AND PHOTOAFFINITY LABELED PROBES FOR STRUCTURAL ELUCIDATION OF THE HIV-1 ENV

Althea Erica Gaffney

Professor Amos B. Smith, III

An estimated 38 million people globally are currently living with Human Immunodefficiency Virus (HIV-1). While HIV-1 can be effectively treated with antiretroviral therapy (ART), the efficacy of ART is challenged by its cost, required access to regular care, and the onset of viral resistance. Methods to both prevent and cure HIV-1 infection are thus desperately needed. Three such strategies are described herein. Firstly, small molecules which mimic CD4 have been developed which inhibit HIV-1 infection. Notably, these compounds increase the ability of the Env trimer to sample a more open conformation which sensitizes the Env to antibody mediated neutralization and elimination (ADCC). Secondly, HIV-1 infection inhibition and lysis of HIV-1 virions has been accomplished via the design, synthesis and validation of a family of small molecule "Dual-Action Virucidal Entry Inhibitors" (DAVEIs). These compounds, comprised of a small molecule warhead tethered to a segment of the gp41 MPER denoted Trp3, have achieved irreversible lytic inactivation of HIV-1 virions. Finally, small molecules appended with photoactivatable crosslinking moieties were developed which stabilize the Env conformation recognized by most broadly neutralizing antibodies. Importantly, no structure of this Env conformation is reported in the literature. This work is expected to enable both structural elucidation of this critical Env conformation and aid the development of an HIV-1 vaccine.

TABLE OF CONTENTS

LIST OF TABLES

LIST OF FIGURES

Chapter One

Chapter Two

LIST OF SCHEMES

Chapter One

Chapter Two

Chapter Three

CHAPTER 1: DESIGN, SYNTHESIS, AND BIOLOGICAL EVALUATION OF SMALL MOLECULE CD4 MIMETIC COMPOUNDS AS INHIBITORS OF HIV-1 VIRAL ENTRY

1.1 Introduction

An estimated 38 million people globally are currently living with Human Immunodefficiency Virus (HIV). Each year, approximately 2 million additional people are infected with HIV.[1] The development of antiretroviral therapies (ARTs) has dramatically increased the life expectancy of patients, and global efforts to curb the HIV epidemic have enabled 24 million people living with HIV access to ART.[1–3] The efficacy of ART is challenged, however, by cost, required access to regular care, and the onset of viral resistance. Methods to cure and prevent HIV infection are thus desperately needed.

The Smith group at the University of Pennsylvania is part of an interdisciplinary collaboration that has probed the fundamental molecular processes of HIV infection and leveraged this into the development of compounds capable of both preventing and curing HIV. Our collaborators have included:

- Virology: Prof. Joseph Sodroski and Dr. Navid Madani (Dana-Farber Cancer Institute)
- Crystallography: Prof. Wayne Hendrickson (Columbia University)
- Equilibrium thermodynamics: Prof. Ernesto Freire and Dr. Arne Schön (Johns Hopkins)
- Trimer dynamics: Prof. Walther Mothes (Yale University)
- Computational Chemistry: Prof. Cameron Abrams (Drexel University, previously Prof. Judith LaLonde, Bryn Mawr College)
- Biochemistry: Prof. Irwin Chaiken (Drexel University)
- Microbiology: Prof. Andres Finzi (University of Montreal)

A primary focus of this collaboration has been investigation of the role of the HIV-1 envelope glycoprotein spike (Env) in HIV-1 infection. The Env mediates viral entry into cells and is the sole HIV-specific protein on the surface of the virus. This makes the Env an appealing target for treatment of HIV.

The Env is initially produced as the monomer gp160, which is post-translationally cleaved into the glycoproteins gp41 and gp120. These subunits ultimately form a non-covalently linked trimer comprised of gp120-gp41 dimers (Figure 1.1).[4,5] The gp41 subunits anchor the Env to the trimer while the outer gp120 subunits make contact with host cells to initiate the infection pathway.

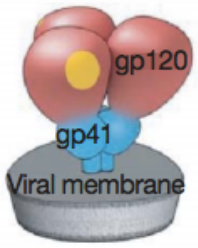

Figure1.1. Cartoon structure of the Env.

1.2 Viral Entry Mechanism

Prior to infection, the unliganded HIV-1 Env trimer adopts a “closed” high energy conformation that will be referred to as State 1 (Figure 1.2).[6] Viral entry begins with binding of gp120 to CD4, a membrane-associated glycoprotein on the surface of helper T cells. This binding event induces conformational changes in the Env that “open” the Env.[7] These conformational changes also form epitopes within gp120 which subsequently bind to chemokine receptors (either CXCR4 or CCR5) on the target cell surface.[8] Chemokine receptor binding causes further conformational changes in gp41. Specifically, the gp41 inserts into the target cell membrane and adopts an extended pre-hairpin intermediate conformation. The “open” pre-hairpin intermediate conformation of the Env is denoted State 3.[9] From the pre-hairpin intermediate State 3, further conformational changes result

in formation a 6-helix bundle within gp41. This 6-helix bundle brings the virus closer to the cell membrane and culminates in gp41-mediated fusion of the cell membrane.[10,11]

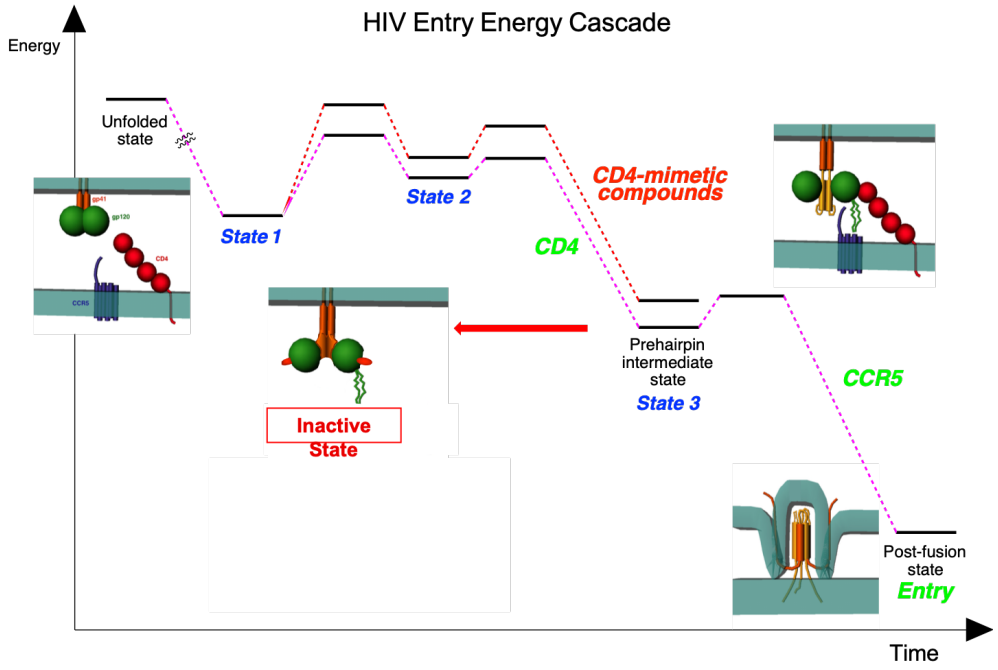

Figure 1.2. HIV-1 Entry Cascade.

The collaborative work described in Chapter One is focused on inhibition of gp120 binding to CD4, the first step of viral infection. This work describes the development of the current family of indane-based CD4 mimetic compounds (CD4mcs) as inhibitors of HIV entry. These compounds operate in three ways:

(i) Direct blockage of the CD4-gp120 interaction,

(ii) Induction of Env conformational changes in the absence of a host cell membrane, resulting in irreversible inactivation of the Env, and

(iii) Exposure of epitopes on the Env which are recognized by antibodies in the host that result in elimination of infected cells in a process denoted antibody-dependent cell-mediated cellular cytotoxicity (ADCC, *vide infra)*.

1.3 Evolution of Small Molecule CD4 Mimics

1.3.1. Initial Discovery of NBD-556 and NBD-557

Two small molecule entry inhibitors which block the CD4-gp120 interaction were identified in 2005 by Debnath and coworkers at the New York Blood Center using high-throughput screening. These compounds, NBD-556 and NBD-557, are shown in Figure 1.3.[12] Mutagenesis studies in combination with co-crystallization studies revealed these compounds bind to gp120 in a hydrophobic pocket referred to as the Phe43 cavity, as this is where the Phe43 residue of CD4 binds to gp120.[12]

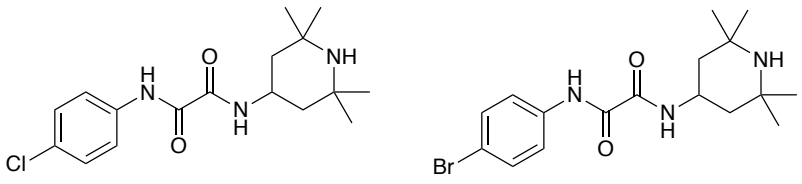

NBD-556
$IC_{50\ YU2} > 100\ \mu m$

NBD-557
$IC_{50\ YU2} > 100\ \mu m$

Figure 1.3. Chemical structures of NBD compounds.

Subsequent work by our collaborators found that these compounds cause conformational structuring of the Env with a thermodynamic signature similar to that of the conformational changes observed on Env-CD4 binding (Figure 1.4).[11] These small molecules, which in many ways act as CD4 surrogates upon their interaction with the Env, are thus termed CD4 mimetic compounds (CD4mcs). [13]

NBD-556 and NBD-557 were also observed to promote infection in cells which lack CD4 (the first required interaction along the viral entry pathway) but possess either a CXCR5 or CCR4 coreceptor (which are required for the second binding event along the entry cascade). Thus, these compounds are agonists of viral infection. That these compounds inhibit infection of cells possessing both CD4 and a coreceptor suggests their binding pushes the Env into a transient

activated state that decomposes in the absence of the co-receptor required to continue the entry cascade.[14] A major effort in the development of CD4mcs was consequently developing compounds that do not function as agonists, but only as inhibitors of viral infection.

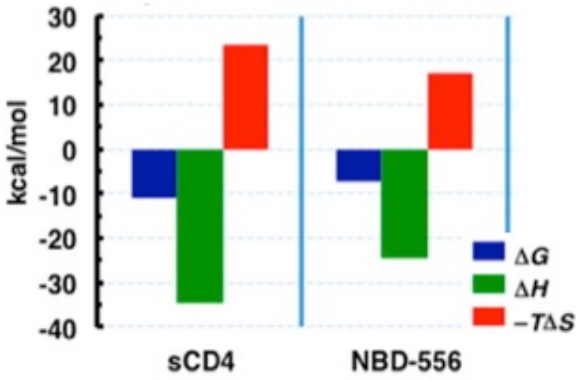

Figure 1.4. Thermodynamic profiles of sCD4 and NBD-556 on binding with gp120.

Further study of the interactions of the Env with both CD4 and the NBD compounds led to the identification of amino acids that have profound impacts on binding.[15,16] The two interactions observed to have the most dramatic impact on Env-CD4 binding were those of (i) ^{CD4}Phe43 with a hydrophobic cavity in gp120, and (ii) an electrostatic interaction between ^{CD4}Arg59-^{gp120}Asp368. Efforts to replicate and improve upon these interactions play a prominent role in the optimization efforts described in this chapter.

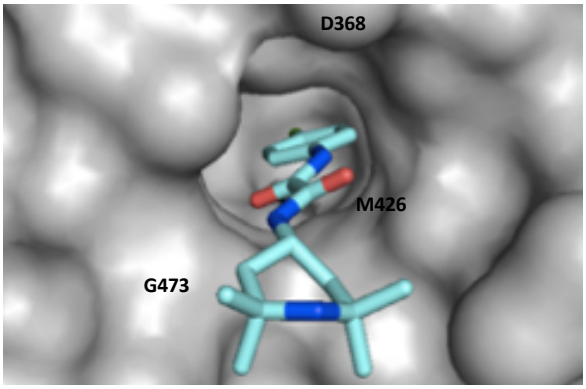

Figure 1.5. Crystal structure of NBD-556 in gp120.

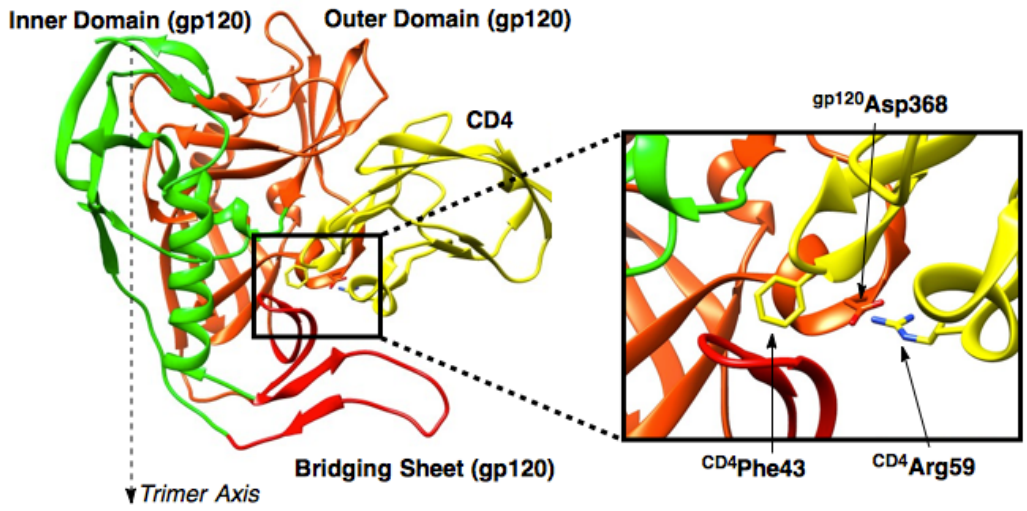

Figure 1.6. Ionic interaction between Arg59 of CD4 and Asp368 of gp120.

1.3.2. Optimization of CD4mcs.

The development of CD4mcs has been divided into three optimization efforts: a halogenated aromatic Region I (green), an oxalamide linker Region II (blue), and Region III (red) (Figure 1.7).

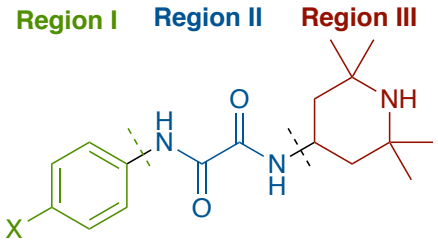

Figure 1.7. Division of CD4mc optimization efforts into three regions.

Optimization of Region I in the Smith Group focused on maximizing the interaction of the moiety within the Phe43 pocket. This effort led to development of JRC-II-191 with addition of a meta-fluorine on the aromatic ring of NBD-556.[17] JRC-II-191, like NBD-556, was observed to both inhibit viral entry into cells equipped with CD4 while enhancing viral entry into cells lacking CD4.

Attempts to modify Region II were not fruitful, and work progressed to optimization of Region III. As Region I effectively mimics ^{CD4}Phe43 by binding in the Phe43 cavity, the ^{CD4}Arg59-^{gp120}Asp368 interaction was targeted next.

Scaffold hopping efforts guided by computational screening ultimately resulted in identification of the current indane-based scaffold. The aminoindane (+)-AWS-I-50 was found to have comparable potency to JRC-II-191, though cytotoxic effects were observed (Figure 1.8).[18] (+)-AWS-I-50 was also observed to enhance infection in cells lacking CD4.[17]

Efforts to position a hydrogen bond donor for interaction with Asp368 led to development of DMJ-I-228 (Figure 1.8). Importantly, DMJ-I-228 was not observed to enhance CD4-independent viral entry.[17] Thus, with the development of DMJ-I-228, CD4mcs had been effectively converted from agonists into antagonists of HIV-1 viral entry.

DMJ-I-228 was observed in co-crystal structures with monomeric gp120 to form a hydrogen bond with Asp368.[17] A methylene linker was added to DMJ-I-228 in an effort to increase potency by improving the interaction with the addition of a guanidinium moiety. Interestingly, this congener, DMJ-II-121, exhibited a 10-fold potency improvement, but co-crystal structures showed interaction with Asp368 was lost in favor of interaction with another hotspot (Met426).[17] Like DMJ-I-228, DMJ-II-121 is also an antagonist of viral entry.

Given the proximity of the guanidinium moiety to Asp368 and the significant role of this amino acid in the CD4-gp120 binding interaction, it was reasoned subtle changes to facilitate interaction with Asp368 may result in a more potent antagonist of viral entry. Computational studies have suggested incorporation of amines at the 5-, 6-, and 7-positions of the indane ring may achieve hydrogen bonding with Asp368. Guided by this work, new compounds with improved potencies were developed, including JP-III-048 and BNM-III-170.[19] The infection inhibition and cytotoxicity profile of BNM-III-170 were the most promising, making it the current lead compound used in studies in animals.[20,21] The evolution of CD4mcs is shown in Figure1.8.

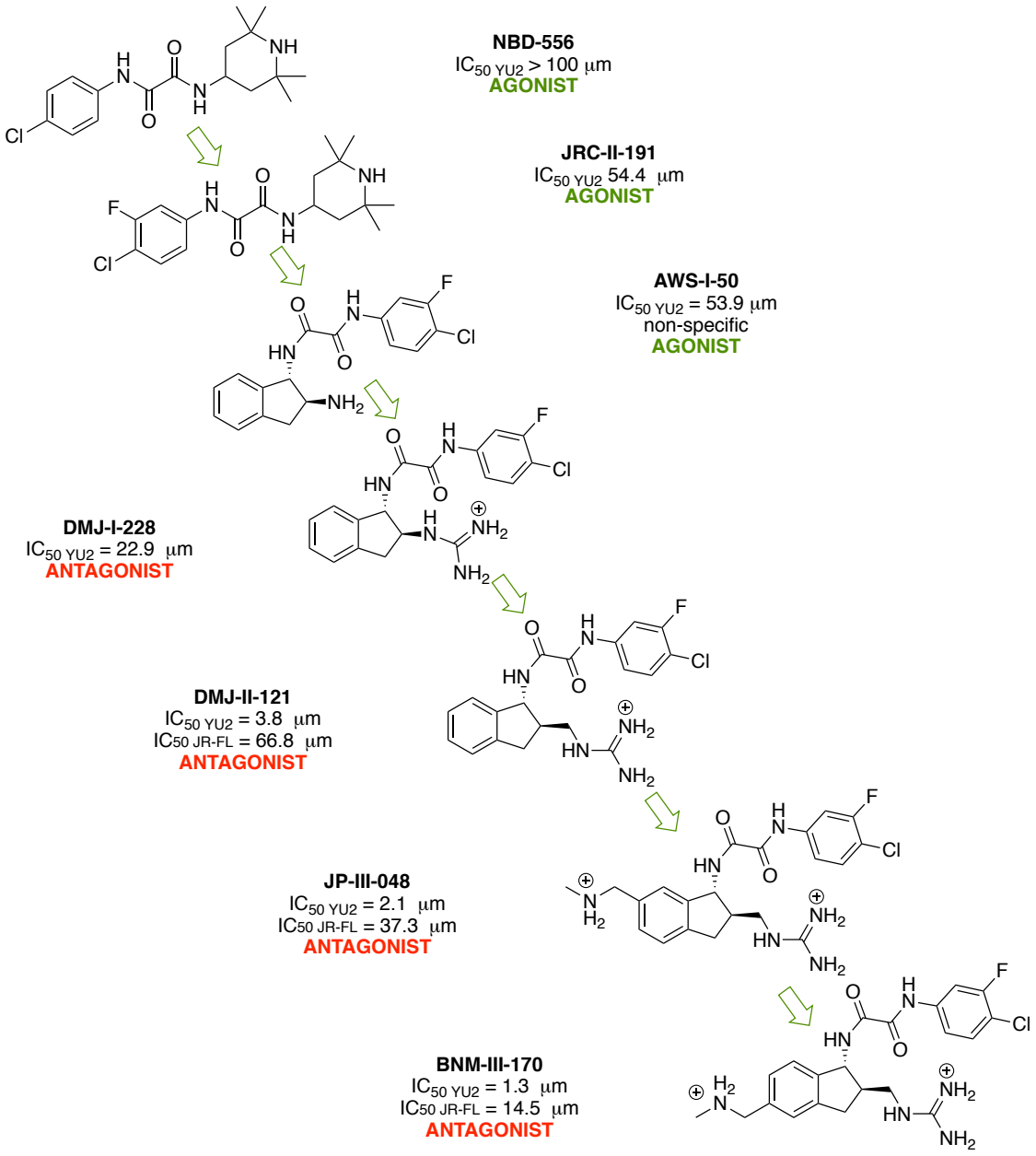

Figure 1.8. Evolution of CD4mcs.

Importantly, in addition to the mechanisms of action described above (i.e., blocking CD4 binding and inactivating the Env through premature activation), BNM-III-170 and other CD4mcs have recently been reported to cause killing of infected cells via antibody-dependent cell-mediated

cellular cytotoxicity (ADCC). CD4mcs have been observed to make infected cells sensitive to neutralization by natural killer immune cells in the body through recognition by antibodies.[22,23] CD4mcs "open" the Env to allow binding of coreceptor binding site antibodies, which subsequently further open the Env to allow recognition of anticluster A antibodies. Natural killer cells in the body recognize anticluster A antibodies and eliminate infected cells (Figure 1.9). [24] This holds promise for eradication of infected cells.[22,23]

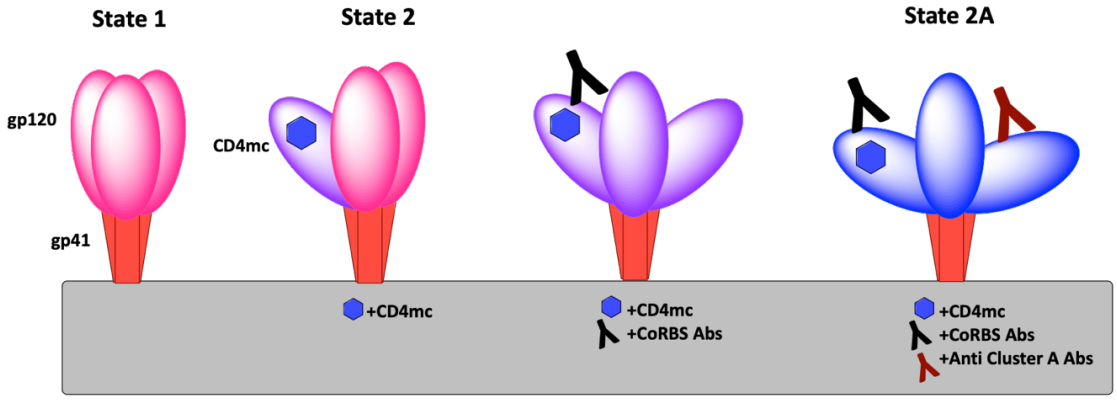

Figure 1.9. Mechanism of ADCC. Binding of a CD4mc to the Env exposes the CoRBS epitope. CoRBS Ab binding exposes anti-cluster A epitopes. Binding of anti-cluster A Abs causes the Env to adopt the conformational state 2A that is recognized for elimination by ADCC.

Furthermore, CD4mcs protect uninfected cells. During the process of infection, gp120 subunits are shed from Env stalks and are able to target other cells. While unable to further spread infection, these shed gp120s bind to CD4 receptors on healthy cells. Unlike infected cells, which are protected by the action of viral Vpu and Nef proteins which downregulate the number of Envs on the surface of virions and infected cells, CD4 present on healthy cells bind shed gp120s. These bystander cells which have bound gp120 are subsequently targeted by natural killer cells, resulting in killing of uninfected cells. CD4mcs bind to and inactivate shed gp120 to protect healthy cells from elimination by the immune system.[25]

Given the promising biological activity of CD4mcs and the improvements in potency made via early efforts at modification of Region III, further optimization was pursued. Docking studies

suggested the positioning of amine-substituted indanes could alter the orientation of Region III outside the pocket. Furthermore, the orientation of the indane is observed in crystal structures to rotate in response to changes in indane substituents (Figure 1.10).

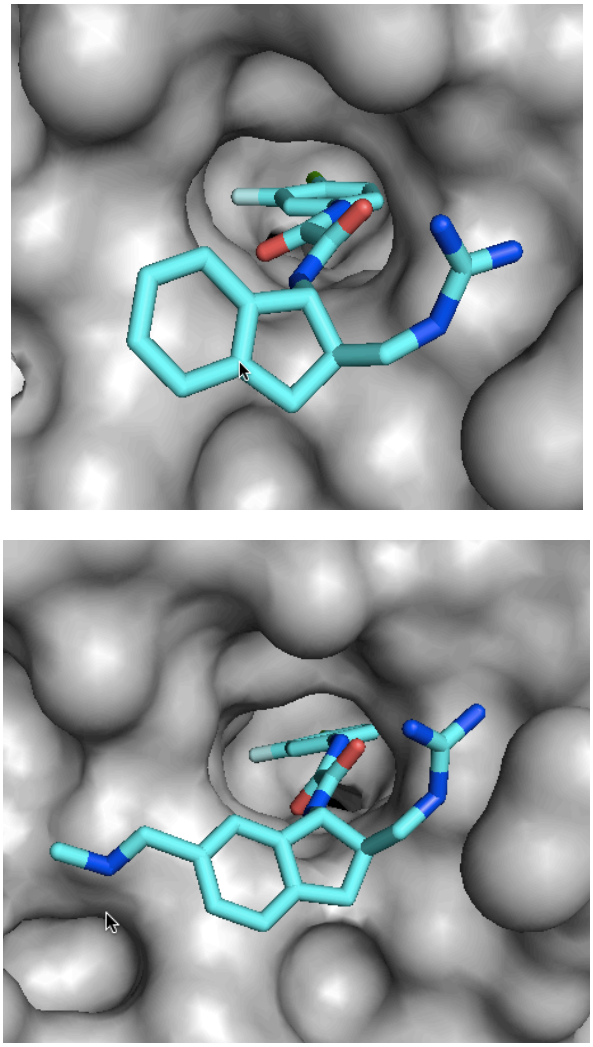

Figure 1.10. Crystal structures of DMJ-II-121 (above) and JP-III-048 (below) in monomeric gp120

In an effort to make contact with Asp368 and to better understand the impact of substitution on the indane region III, a structure-activity relationship (SAR) study of substitution at the 5-, 6-, and 7-positions as well as 5,7-disubstitution was completed (Figure1.11). The synthesis of 6-position congeners as part of this SAR is described below.

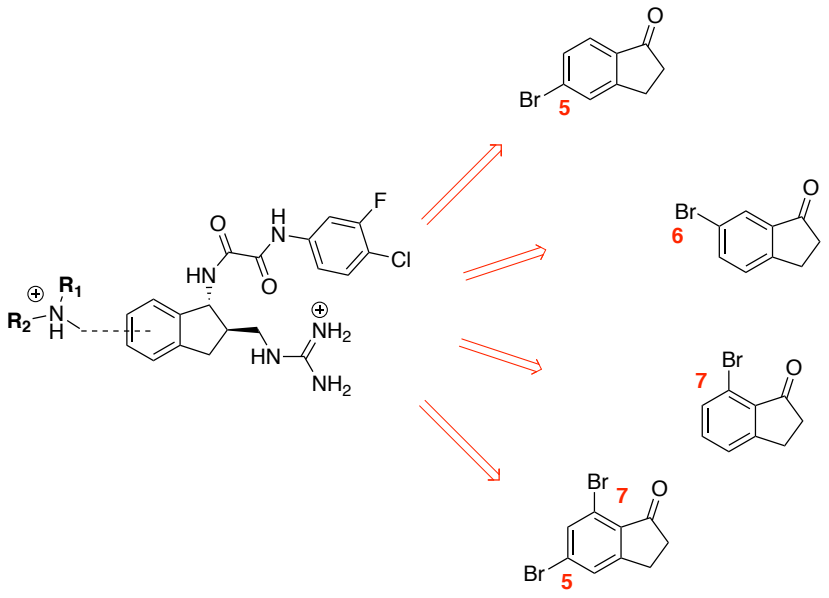

Figure 1.11. Design of SAR study.

1.4 Synthesis of 6-Position Analogs

The synthesis of 6-position CD4mcs following the lead of others in the Smith Group is highlighted (Scheme I). To this end, 6-bromoindanone was carboxylated, subjected to ruthenium-catalyzed transfer hydrogenation in a dynamic kinetic asymetric transformation, reduced to the corresponding diol **1.3**, and selectively protected with TBS at the primary alcohol to afford **1.4**. Reaction with DPPA afforded the corresponding azide **1.5**, which was next subjected to Staudinger reduction. The silyl protecting group was partially cleaved in the acidic reaction mixture. As the isolated aminol **1.6** was observed to selectively perform the desired amide coupling, the Staudinger reduction was modified to include an addition of aqueous HCl to fully remove the silyl ether *in situ* prior to isolation. Guanylation under Mitsunobu conditions produced **1.8**, which then was subjected to Suzuki coupling with vinyltrifluoroborate. Johnson-Lemieux oxidation of the alkene **1.9** afforded the desired aldehyde **1.10**. From this common intermediate, 6-position analogs were synthesized via reductive amination and subsequent deprotection.

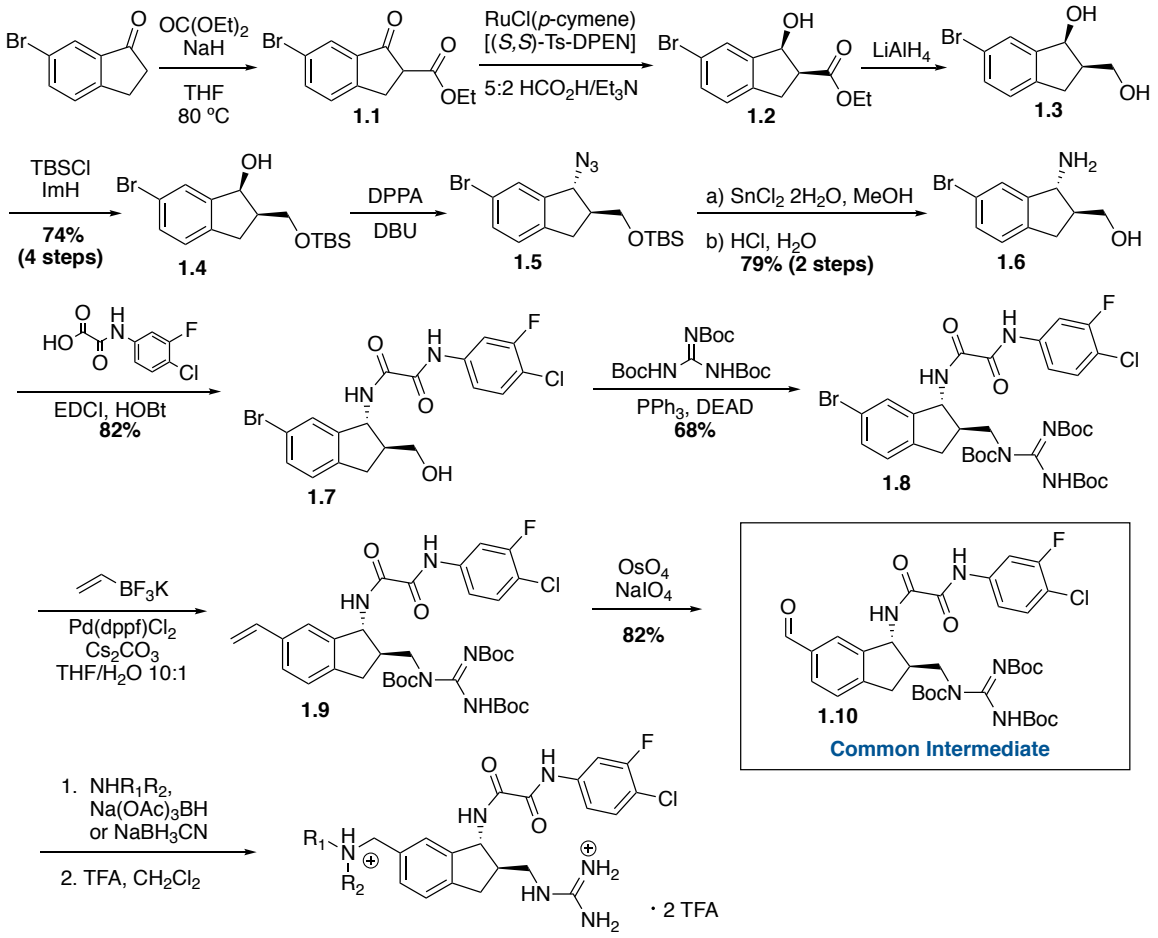

Scheme I. Synthesis of 6-postion analogs of BNM-III-170.

CD4mcs with 5-, 7-, and 5,7- substitution may be synthesized using a similar strategy. Ultimately, a large body of analogs was synthesized with synthetic contributions from Smith group members including Dr. Sharon Kirk (SMK), Dr. Bruno Melillo (BNM), Dr. Melissa Grenier (MCG), and Dr. Jongwoo Park (JP). A summary of this work may be found in Table 1.

Table 1.1. Summary of Structure-Activity-Relationship Study of CD4mcs.

		Compound	Entry Inhibition, IC_{50} (μM)			
			JR-FL	YU-2	AD8	AMLV
	5	SMK-II-222	62.7	28.5	58.5	>100
	6	SMK-II-137	86.8	27	7.1	>100
	7	SMK-II-228	29.6	4.1	7.7	>100
	5,7	MCG-II-032	67.6	15.1	5.4	>100
	5	SMK-I-282	9			16
	6	SMK-II-138	69.9	14.4	4.9	>100
	7	SMK-II-191	49.6	6.3	6.2	>100
	7	SMK-II-236	>100	15.9	37.6	>100
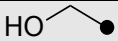	5	SMK-II-012				
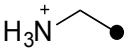	5	SMK-II-117	69.4	17.8	4.9	>100
	6	SMK-II-126	>100	>100	92.7	>100
	7	SMK-II-200	>100	>100	>100	>100
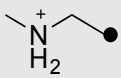	5	BNM-III-170	14.5	1.3	3.1	>100
	6	JP-III-048	37.3	2.1	6.7	>100

	7	SMK-II-169	88.8	83.4	71.6	58.6
	5,7	SMK-III-024	74.6	7.2	10.4	>100
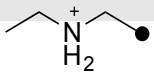	5	SMK-II-195	30.9	2.6	6.6	>100
	6	SMK-II-147	46.3	57.1	18.5	91.5
	7	SMK-II-170	83.3	60.7	55.7	55.9
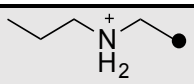	5	SMK-III-016	76.6	>100	57.3	>100
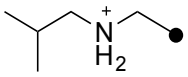	5	SMK-III-017	>100	>100	>100	>100
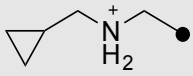	5	SMK-II-048	32.8		6.2	88.1
	6	SMK-II-153	94.8	71.9	46.6	88.7
	7	SMK-II-179	68.7	66.3	59.4	82.3
	5,7	SMK-III-040	17.8	5.1	7.4	>100
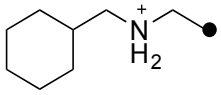	5	SMK-II-194	25.3	24.2	26.8	18.7
	6	SMK-II-159	81.4	62.8	79.6	65.2
	7	SMK-II-239	16.9	16.3	14.6	15.0
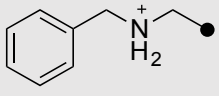	5	SMK-II-124	73.2	25.8	65.2	29.6
	6	SMK-II-125	84.9	70.4	68.5	53.8

	7	SMK-II-178	18.5	23.2	21.0	7.2
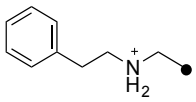	5	SMK-II-026	28			>100
	6	SMK-II-158	23.9	20.7	21.6	23.1
	7	SMK-II-240	16.9	21.3	17.9	18.8
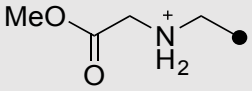	5	SMK-II-058	80			>100
	6	SMK-II-154	>100	89.6	73.1	>100
	7	SMK-II-292	89.7	8.3	6.8	>100
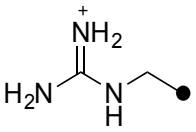	5	SMK-II-019				
	6	SMK-II-112	>100	53.3	22.5	>100
	7	SMK-II-207	90.5	4.6	20.8	>100
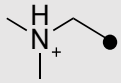	5	SMK-II-233	24.6	1.3	5.4	>100
	6	**AEG-I-189**	51.7	5	4.2	>100
	7	SMK-II-280	18.9	1.2	10.6	>100
	5,7	MCG-III-051	40.1	3.8	12.6	>100
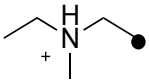	5	BNM-IV-114	11.1	0.9	3.6	17.4
	6	**AEG-I-249**	22.5	1.7	12. 2	>100
	7	SMK-II-281	61.1	10.1	6.3	>100

	5,7	SMK-III-035	20.8	3.6	4.0	>100
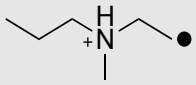	5	BNM-IV-123	24.6	1.4	4.5	>100
	6	**AEG-I-289**	35.5	3.9	11.5	84.0
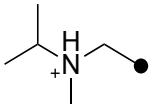	5	BNM-IV-117	20.4	1.6	2.7	>100
	6	**AEG-I-268**	65.8	7.4	14.7	78.9
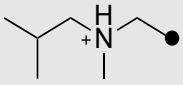	5	BNM-IV-124	24.0	1.5	4.5	>100
	6	**AEG-I-279**	54.3	21.1	25.1	>100
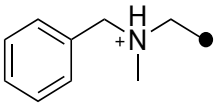	5	BNM-IV-125	18.4	3.1	5.4	61.8
	6	**AEG-I-275**	>100	14.8	65.1	>100
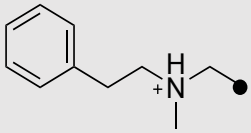	5	BNM-IV-139	17.6	1.4	4.5	>100
	6	**AEG-I-297**	91.8	6.26	14.7	>100
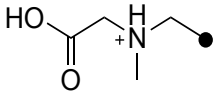	5	BNM-IV-137	23.3	1.3	3.1	>100
	6	**AEG-I-259**	34.3	3.7	25.4	>100
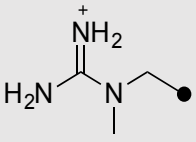	5	BNM-IV-147	6.1	0.8	1.6	>100
	6	BNM-IV-197	19.7	1.6	1.2	83.7
	7	SMK-II-296	62.5	5.9	4.5	>100

1.5 Biological Evaluation

Analysis of the observed antiviral activity indicated that the potency of analogues follows the general trend that tertiary amines are generally more potent as HIV entry inhibitors than secondary amines, which are in turn generally more potent than primary amines. Substitution at the 5-position of the indole leads to the most potent and most specific entry inhibitors of HIV. This may be due to an interaction observed in several crystal structures involving the backbone of the highly conserved Gly^{473} residue.[19] Analogues with amine substituents at the 7-position are typically more potent than 6-position analogues, and both 6- and 7-position analogues are more likely than 5-position analogues to exhibit non-specific cytotoxicity.

While the potencies of some analogs synthesized by AEG as part of this SAR study rival that of BNM-III-170, no substantial potency improvements were observed with the newly synthesized analogs. Furthermore, none of these compounds was observed to make contact with Asp368 in co-crystal structures with gp120.

1.6 Future work

1.6.1. Elongated 5,7-Analogs

Docking studies have suggested that extending the methylene linker to an ethylene may allow the methylamine moiety at the 7-position of 5,7-analogs to reach Asp368. Synthesis of such analogs is underway by Cheyenne Chaplain. The crystal structure of the 5,7-disubstituted compound MCG-III-051 (Figure 1.12, left) suggests the 7-position substituent reaches toward Asp368 but may not have sufficient length to allow interaction. Future synthetic targets (Figure 1.12, right) have an additional methylene in their linkers in an effort to facilitate interaction with Asp368.

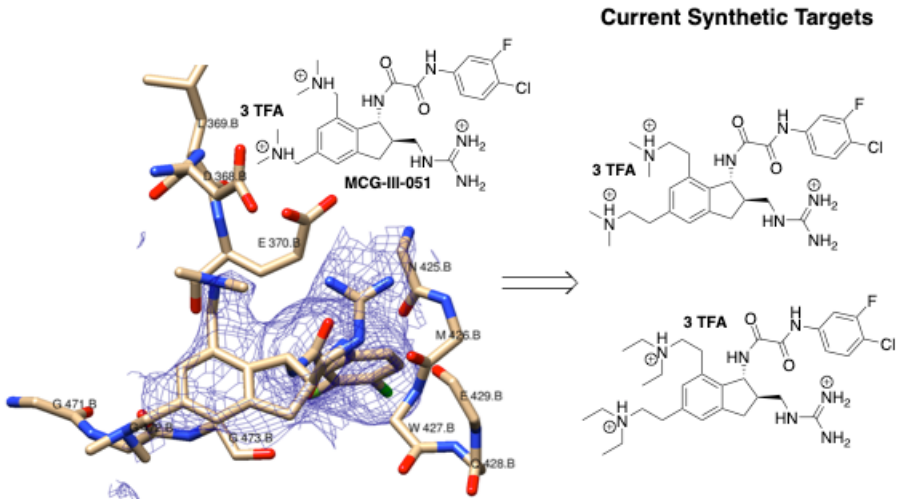

Figure 1.12. The crystal structure of MCG-III-051 (left) and future synthetic targets (right).

1.6.2. Exploration of Guanidinium Bioisosteres

Replacement of the guanidinium moiety of BNM-III-170 with bioisosteres was explored by Cheyenne Chaplain in an effort to make additional contacts along the solvent-exposed surface of the Env. Unfortunately, the synthesized compounds were observed to be non-specific (Fig. 1.13).

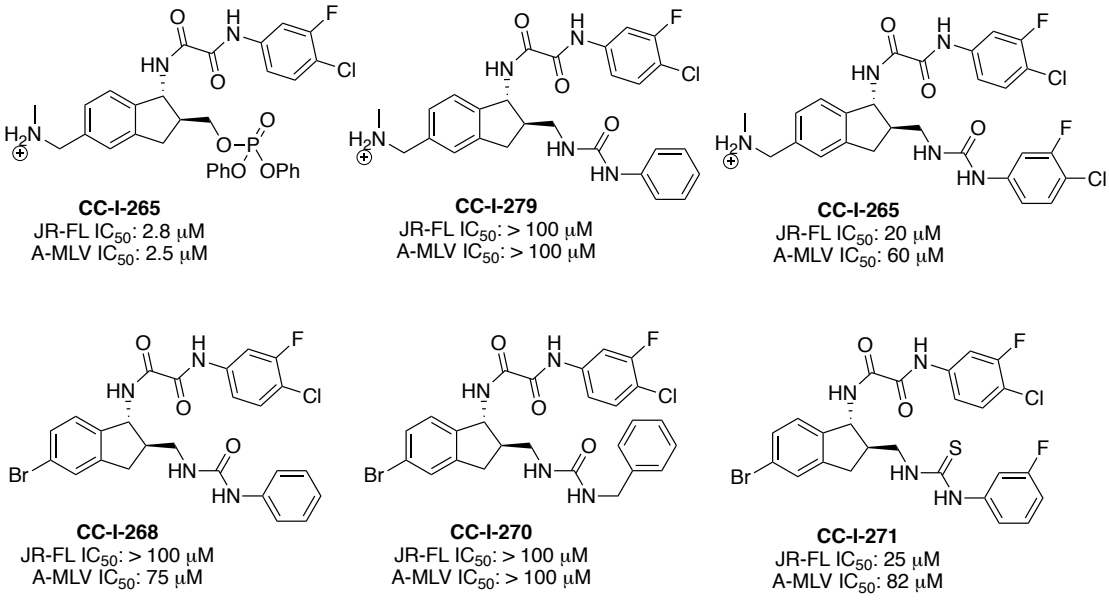

Figure 1.13. Synthesized analogs containing guanidinium bioisosteres and their biological activity.

1.6.3. Exploration of Cyclic Substituents at the Indane 5-Position

Analogs in which aliphatic heterocycles are incorporated at the 5-position have been synthesized by Dr. Jun Park. These compounds have been observed to be slightly more potent than BNM-III-170. Further exploration of these compounds will be done by Christopher Fritschi.

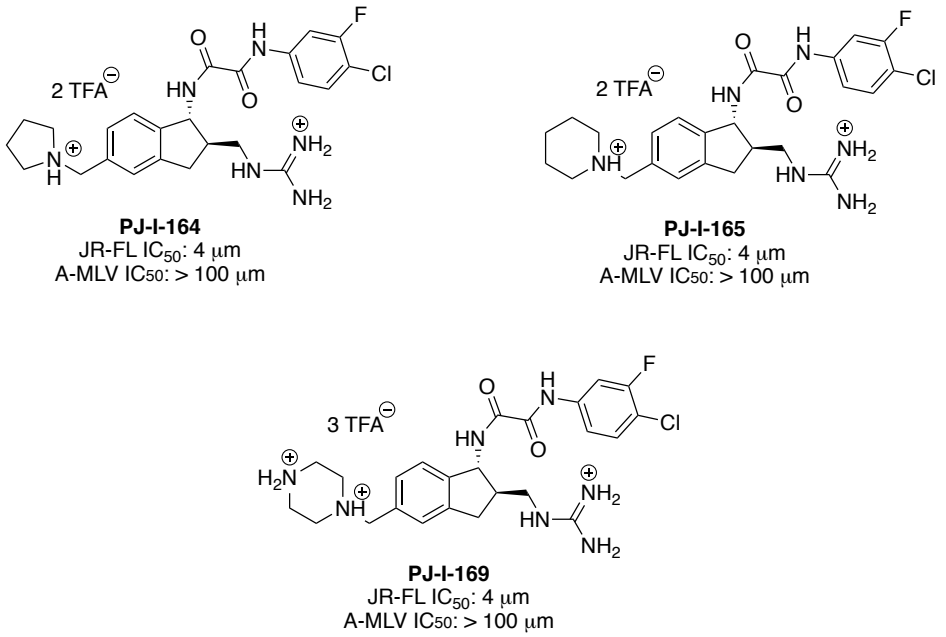

Figure 1.14. Structures and biological data of analogs with aliphatic heterocycles.

1.6.4. Exploration of 3-Position Substitution.

Incorporation of additional substituents at the 3-position has also been explored by Christopher Fritschi and Dr. Junhua Chen. With encouraging biological data from compounds such as CFJ-II-089 and CJF-II-108, this work will be continued by Christopher Fritschi (Figure 1.15).

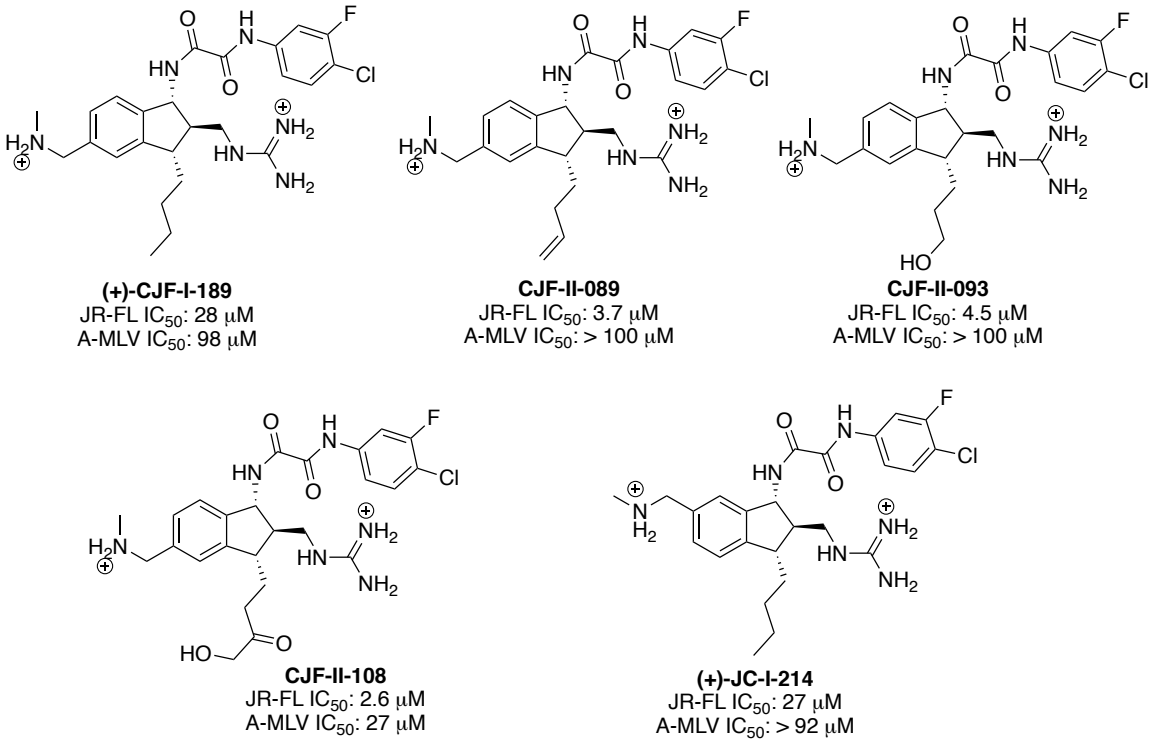

Figure 1.15. Synthesized analogs with 3-position substitution and their biological activity.

1.7 Chapter One References

(1) UNAIDS. UNAIDS Data 2019. Joint United Nationa Programme on HIV/AIDS (UNAIDS) (2019). doi:978-92-9173-945-5

(2) UNAIDS. AIDS by the numbers. AIDS by the Numbers 2015 1–25 (2016). doi:JC2571/1/E

(3) Posse, M.; Meheus, F.; Van Asten, H.; Van Der Ven, A; Baltussen, R. *Trop. Med. Int. Heal*. **2008**, *13*, 904.

(4) Wilen, C. B.; Tilton, J. C.; Doms, R. W. *Cold Spring Harb. Perspect. Med.* **2012,** 2.

(5) Tilton, J. C.; Doms, R. W. *Antiviral Res*. **2010**, *85* (1), 91.

(6) Munro, J. B.; Gorman, J.; Ma, X.; Zhou, Z.; Arthos, J.; Burton, D.R.; Koff, W.C.; Courter, J.R.; Smith, A.B., III; Kwong, P.D.; Blanchard, S.C.; Mothes, W. *Science* **2014**, *346*, 759.

(7) Sattentau, Q. J.; Moore, J. P. *J. Exp. Med.* **1991**.*174* (2) 407-15.

(8) Dragic, T.; Litwin, V.; Allaway, G.; Martin, S.R.; Huang, Y.; Nagashima, K.A.; Cyanan, C.; Maddon, P.J.; Koup, R.A.; Moore, J.P.; Paxton, W.A. *Nature* **1996**, *381*, 667.

(9) Lu, L.; Yu, F.; Cai, L.; Debnath, A. K.; Jiang, S. *Curr. Top. Med. Chem*. **2016**, *16*, 1074.

(10) Langley, D. R.; Kimura, S.R.; Sivaprakasam, P.; Zhou, N; Dicker, I.; McAuliffe, B.; Wang, T.; Kadow, J.F.; Meanwell, N.A.; Krystal, M. *Proteins Struct. Funct. Bioinforma.* **2015**, *83*, 331.

(11) Madani, N.; Schön A.; Princiotto A.M.; Lalonde, J.M.; Courter, J.R.; Soeta, T.; Ng, D.; Wang, L.; Brower, E.T.; Xiang, S.H.; Kwon, Y.D.; Huang, C.C.; Wyatt, R.; Kwong, P.D.; Freire, E.; Smith, A.B., III; Sodroski, J. *Structure* **2008**, *16*, 1689.

(12) Zhao, Q. et al. Identification of N-phenyl-N-(2,2,6,6-tetramethyl-piperidin-4-yl)- oxalamides as a new class of HIV-1 entry inhibitors that prevent gp120 binding to CD4. Virology 339, 213–225 (2005).

(13) LaLonde, J. M.; Le-Khac, M.; Jones, D.M.; Courter, J.R.; Park, J.; Schön, A; Princiotto, A.M.; Wu, X.; Mascola, J.R.; Freire, E.; Sodroski, J.; Madani. N; Hendrickson, W.A. Smith, A.B., III. *ACS Med. Chem. Lett.* **2013**, *4*, 338.

(14) Haim, H.; Si, Z.; Madani, N.; Wang, L.; Courter, J.R.; Princiotto, A.; Kassa, A.; DeGrace, M.; McGee-Estrada, K.; Mefford, M.; Gabuzda, D.; Smith, A.B., III; Sodroski, J. *PLoS Pathog*. **2009**, *5*, e1000360.

(15) Moebius, U.; Clayton, L. K.; Abraham, S.; Harrison, S.C.; Reinherz, E. L. *J. Exp. Med.* **1991**, *176*(2), 507.

(16) Liu, Y.; Schön, A.; Freire, E. *Chem. Biol. Drug Des*. **2013**, *81*, 72.

(17) Courter, J. R.; Madani, N.; Sodroski, J.; Schön, A.; Freire, E.; Kwong, P.D.; Hendrickson, W.A.; Chaiken, I.M.; LaLonde, J.M.; Smith, A.B., III. *Acc. Chem. Res.* **2014**, *47*, 1228.

(18) Lalonde, J. M.; Kwon, Y.D.; Jones, D.M.; Sun, A.W.; Courter, J.R.; Soeta, T.; Kobayashi, T.; Princiotto, A.M.; Wu, X.; Schön, A.; Freire, E.; Kwong, P.D.; Mascola, J.R.; Sodroski, J.; Madani, N. Smith, A.B., III. *J. Med. Chem.* **2012**, *55*, 4382.

(19) Melillo, B.; Liang, S.; Park, J.; Schön. A.; Courter, J.R.; LaLonde, J.M.; Wendler, D.J.; Princiotto, A.M.; Seaman, M.S.; Freire, E.; Sodroski, J.; Madani, N.; Hendrickson, W.A.; Smith, A.B., III *ACS Med. Chem. Lett.* **2016**, *7*, 330.

(20) Madani, N.; Princiotto, A.M.; Easterhoff, D.; Bradley, T.; Luo, K.; Williams, W.B. Liao, H.X.; Moody, M.A.; Phad, G.E.; Vázquez Bernat, N.; Melill,o B.; Santra, S.;, Smith, A.B., III, Karlsson Hedestam, G.B.; Haynes, B.; Sodroski, J. *J. Virol.* **2016**, *90*(10), 5031.

(21) Madani, N.; Princiotto, A.M.; Mach, L.; Ding, S.; Prevost, J.; Richard, J.; Hora, B.; Sutherland, L.; Zhao, C.A.; Conn, B.P.; Bradley, T.; Moody, M.A.; Melillo, B.; Finzi, A,; Haynes, B.F.; Smith, A.B., III; Santra, S.; Sodroski, J. .*Nat. Commun*.**2018**, *9*(1), 2363. .

(22) Madani, N.; Princiotto, A.M.; Schön, A.; LaLonde, J.; Feng, Y.; Freire, E.; Park, J.; Courter, J.R.; Jones, D.M.; Robinson, J.; Liao, H.X.; Moody, M.A.; Permar, S.; Haynes, B.; Smith, A.B., III.; Wyatt, R.; Sodroski, J. *J. Virol*. **2014**, *88*, 617.

(23) Richard, J.; Veillette, M.; Brassard, N.; Iyer, S.S.; Roger, M. Martin, L.; Pazgier, M.; Schön, A.; Freire, E.; Routy, J.P.; Smith, A.B., III; Park, J..; Jones, D.M.; Courter, J.R.; Melillo, B.N.; Kaufmann, D.E.; Hahn, B.H.; Permar, S.R.; Haynes, B.F.; Madani, N.; Sodroski, J.G.; Finzi, A.. *Proc. Natl. Acad. Sci. U. S. A*. **2015**, *112*, E2687.

(24) Richard, J.; Pacheco, B.; Gohain, N.; Veillette, M.; Ding, S.; Alsahafi, N.; Tolbert, W.D.; Prévost, J.; Chapleau, J.P.; Coutu, M.; Jia, M.; Brassard, N.; Park, J.; Courter, J.R.; Melillo, B.; Martin, L.; Tremblay, C.; Hahn, B.H.; Kaufmann, D.E.; Wu, X.; Smith, A.B.,III; Sodroski, J.; Pazgier, M.; Finzi, A.. *EBioMedicine* **2016**,*12*, 208.

(25) Richard, J.; Veillette, M.; Ding, S.; Zoubchenok, D.; Alsahafi, N.; Coutu, M.; Brassard, N.; Park, J.; Courter, J.R.; Melillo, B.; Smith, A.B., III; Shaw, G.M.; Hahn, B.H.;, Sodroski, J.; Kaufmann, D.E.; Finz, A. *EBioMedicine* **2016** , *3*, 122.

CHAPTER 2: DESIGN, SYNTHESIS, AND BIOLOGICAL EVALUATION OF SMALL MOLECULE DUAL-ACTION VIRUCIDAL ENTRY INHIBITORS OF HIV-1 INFECTION

This Chapter describes the development of small molecule Dual-Action Virucidal Entry Inhibitors (DAVEIs), a program in collaboration with the Chaiken and Abrams Laboratories at Drexel University.

2.1 Conceptualization of DAVEIs and Foundational Work

As described in greater detail in Chapter One, the HIV-1 envelope glycoprotein spike (Env) regulates viral entry into host cells. The Env is a metastable trimer of non-covalently linked gp120 and gp41 protein subunits.[1] The unliganded Env trimer exists mainly in a closed conformation (State 1).

The entry mechanism begins *via* binding of gp120 to CD4, a glycoprotein on host T-cells. This binding event triggers major conformational changes within the Env complex, which expose CXCR4 or CCR5 co-receptor binding sites. In turn, the gp41 fusion peptide region inserts into the host cell membrane. Subsequent refolding into a six-helix bundle brings the N and C termini of gp41 together and, in doing so, brings the virion and host cell membranes into sufficient proximity for fusion[2–5] (Figure 2.1).

The virion-cell fusion process requires poration of the viral membrane for transfer of the contents into the host cell. In light of evidence which suggests poration (i.e., lysis) of the virus may occur in the absence of a nearby host cell membrane,[6–8] our collaboration with the Chaiken and Abrams Laboratories at Drexel University set out to investigate whether a compound could be designed to induce sufficient poration of the viral membrane and ultimately to inactivate the virus by draining/lysis of the contents into the extracellular milieu.[6]

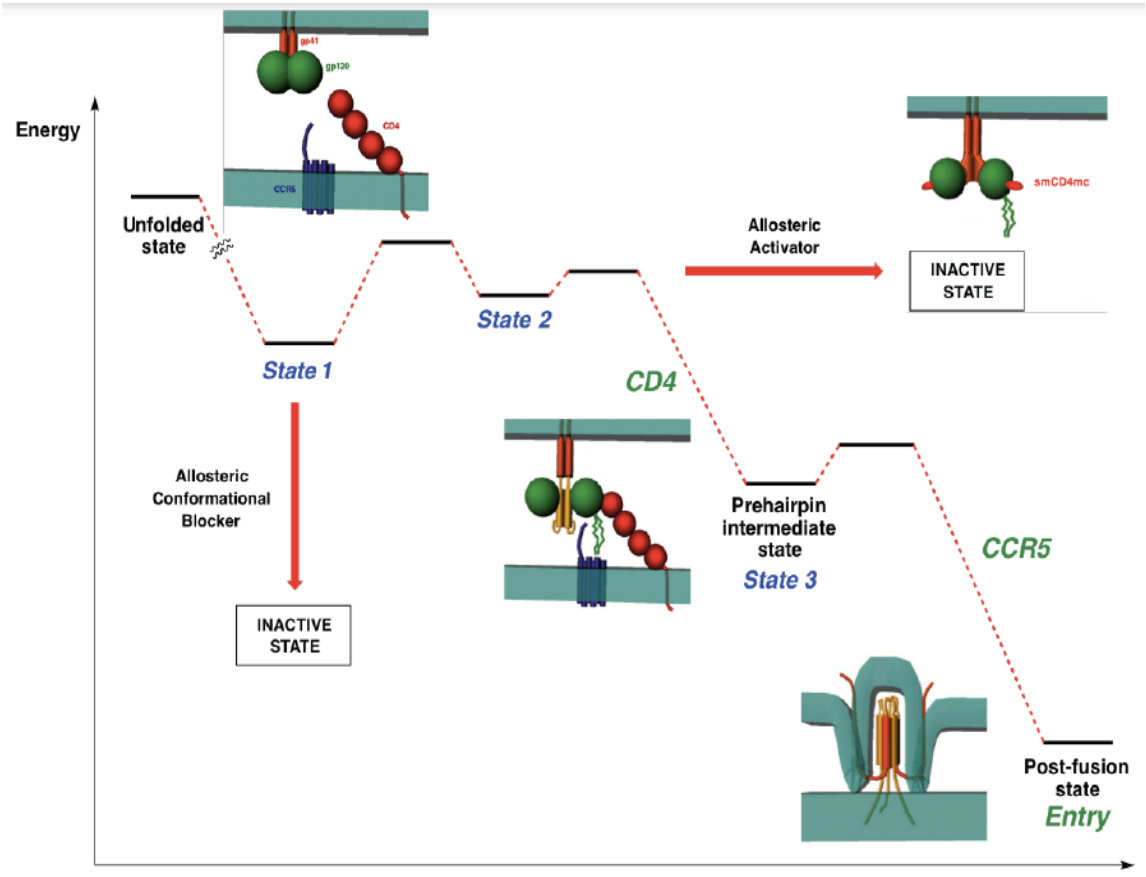

Figure 2.1 Entry cascade initiated by HIV-1 Env interaction with host cell receptors.

This premise inspired earlier work in which our collaborators designed compounds capable of simultaneously binding to the gp120 and gp41 Env components. They hypothesized that binding to both gp120 and to gp41 could impart sufficient stress on the Env spike to trigger viral poration and, consequently, viral inactivation (Figure 2.2).[6] These compounds, which engage both Env subunits, are described as Dual-Action Virucidal Entry Inhibitors (DAVEIs).

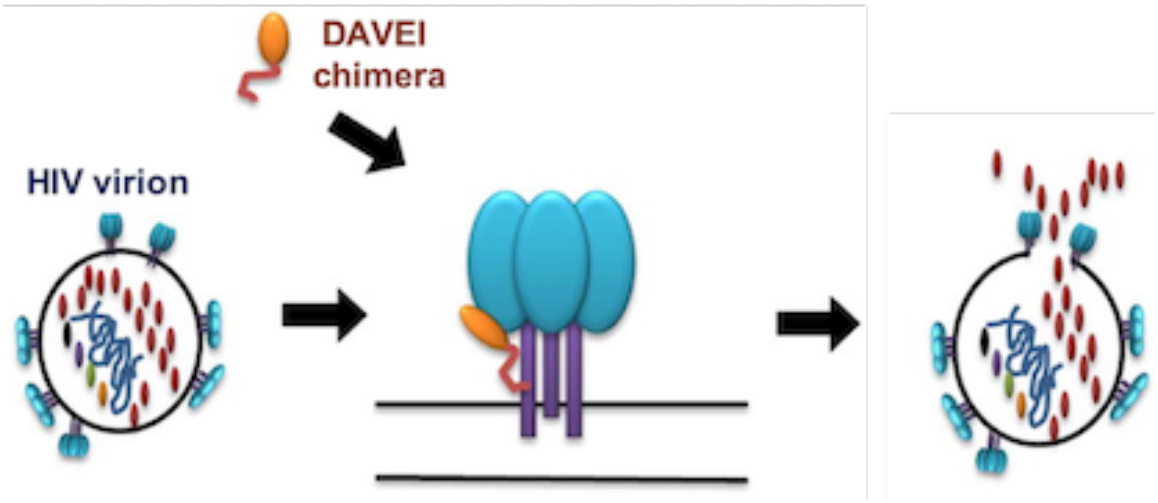

Figure 2.2 Proposed DAVEI mechanism of action. A chimera (orange) comprised of a lectin protein and a segment of the MPER simultaneously engage gp120 (teal) and gp41 (purple) on the surface of a virion, ultimately causing lysis of HIV-1 virions.

The first generation of DAVEIs were recombinant chimeric proteins comprised of the gp120-binding protein cyanovirin tethered to an exogenous segment of the gp41 Membrane Proximal External Region (MPER).[6] Cyanovirin (CVN) is a lectin protein (MW=11.0 kDa)[9] known to inactivate HIV-1,[10] that binds to carbohydrates on the gp120 surface and blocks binding to CD4 on host cells,[11] but does not cause virolysis.[6] The MPER segment is an amphipathic peptide comprised of 20 amino acid residues.[6] For a representative diagram of these lectin DAVEIs refer to Figure 2.3. Pleasingly, our collaborators observed that tethering CVN to the MPER segment produces a recombinant chimeric protein that causes virolysis and inactivation of HIV-1 virions.[6] Importantly, these DAVEIs specifically and irreversibly destroy HIV-1 virions.

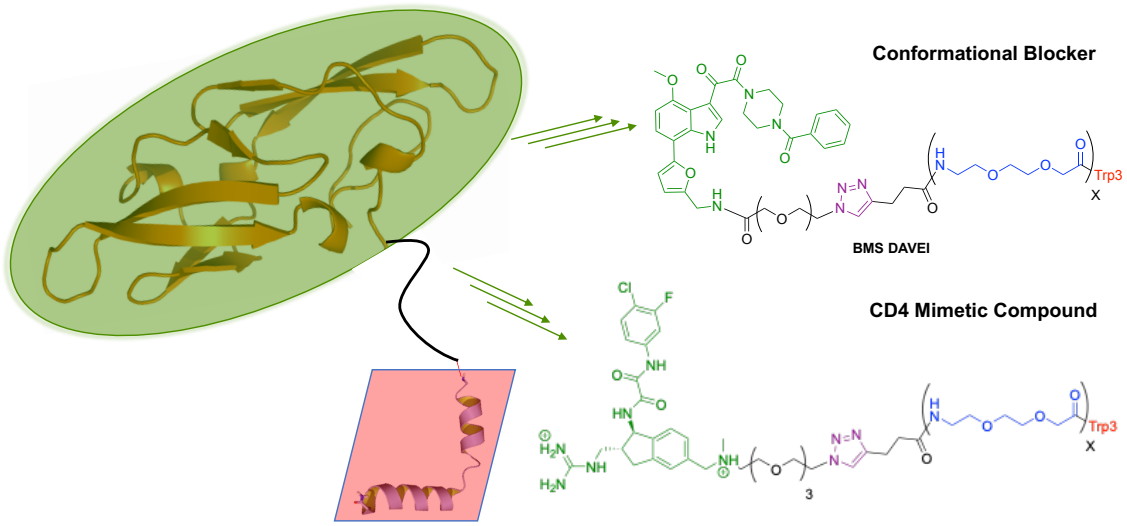

Figure 2.3 Evolution of DAVEIs. The first generation of DAVEIs (left) were comprised of a lectin protein head group (circled in green) tethered to the Trp3 peptide (red). The lectin can be replaced with a small molecule (right), specifically an analog of BMS-529 (top right) or BNM-III-170.

While encouraging as a proof of concept for further development of DAVEIs, study of the CVN DAVEIs was complicated by the fact that CVN is known to bind multiple sites on gp120. This led to development of the second generation of DAVEIs in which cyanovirin is replaced with the lectin microvirin (MW=14.3 kDa)[12], which also inhibits infection of HIV-1 but is only reported to bind at a single site on gp120.[13] Further work identified Trp3, a 9-amino acid segment of the gp41 MPER truncated at the third tryptophan, as a minimized MPER replacement (Figure 2.4).[14] The accumulated findings with cyanovirin-Trp3 and the follow-up with microvirin-conjugated fusion proteins with Trp3 demonstrated[13,14] the overall ability to derive DAVEIs as a new class of irreversible HIV-1 inactivators.

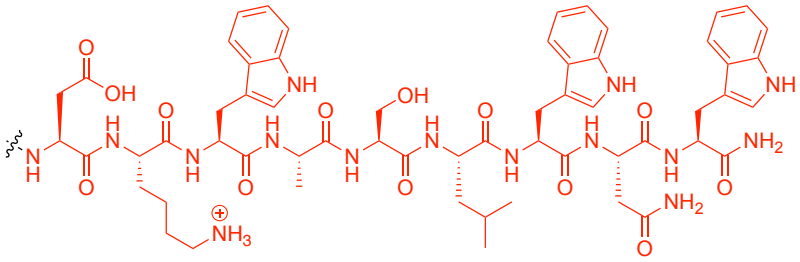

Figure 2.4 Structure of Trp3, a segment of the gp41 MPER.

Nonetheless, the complex binding modes and large size of these proteins impede mechanistic study and reduces the therapeutic potential of such compounds. The work below describes efforts toward a new generation of DAVEI constructs in which small molecules, each with a well-defined mode of Env binding, are used to engage gp120 in lieu of large lectin proteins.

The targeted new classes of small molecule attachments are: (a) conformational blockers inspired by BMS-529 (Fostemsavir, the prodrug of BMS-529 is currently in clinic trials, vide infra), and (b) small-molecule CD4 Mimetic Compounds (CD4mcs) developed in the Smith laboratory (Figure 2.5). Briefly, conformational blockers lock the Env in the “closed” State 1 and prevent adoption of the conformations required for viral entry, whereas small molecule CD4mcs push the Env into more open conformations which ultimately result in activation of the virion (see Figure 2.1).

We expect the results of this work to elucidate the role of the Env conformation elicited by these gp120 ligands in viral inactivation will in turn lead us closer to an understanding of the fundamental mechanism of DAVEI-induced lysis of HIV-1 virions.

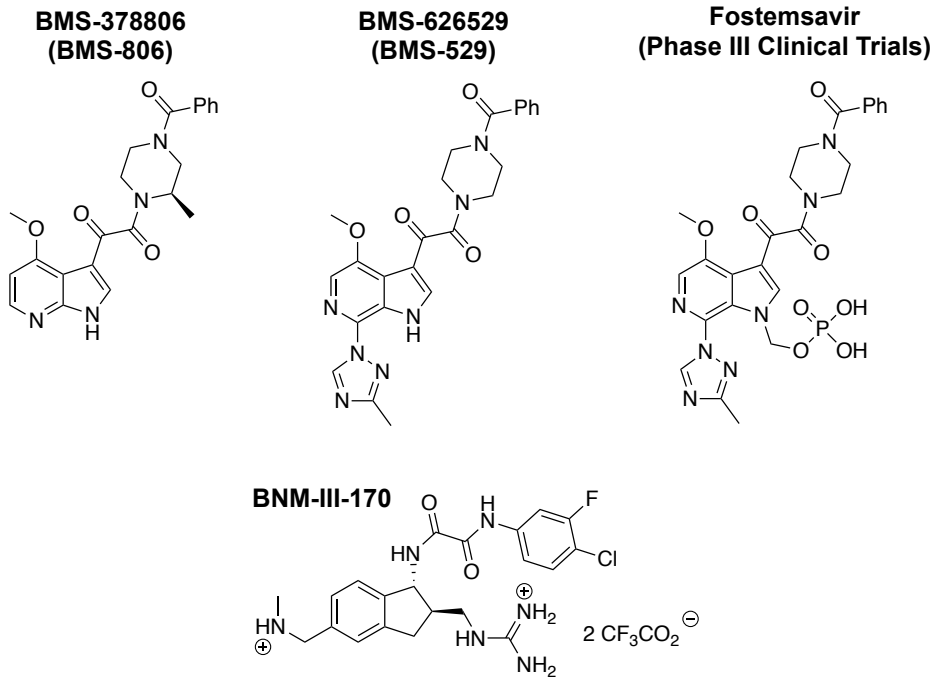

Figure 2.5 Relevant small molecules**.**

2.2 Anatomy of a Small Molecule DAVEI

Small molecule DAVEIs are comprised of a gp120-binding small molecule component (Figure 2.5), which will be referred to here as the "head group," functionalized with a PEG-azido spacer (Figure 2.6). The azide serves as a handle for installation of the alkyne-linker-Trp3 moiety exploiting click chemistry.[15] This alkyne-linker-Trp3 moiety will be referred to as the "tail group" (Figure 2.6).

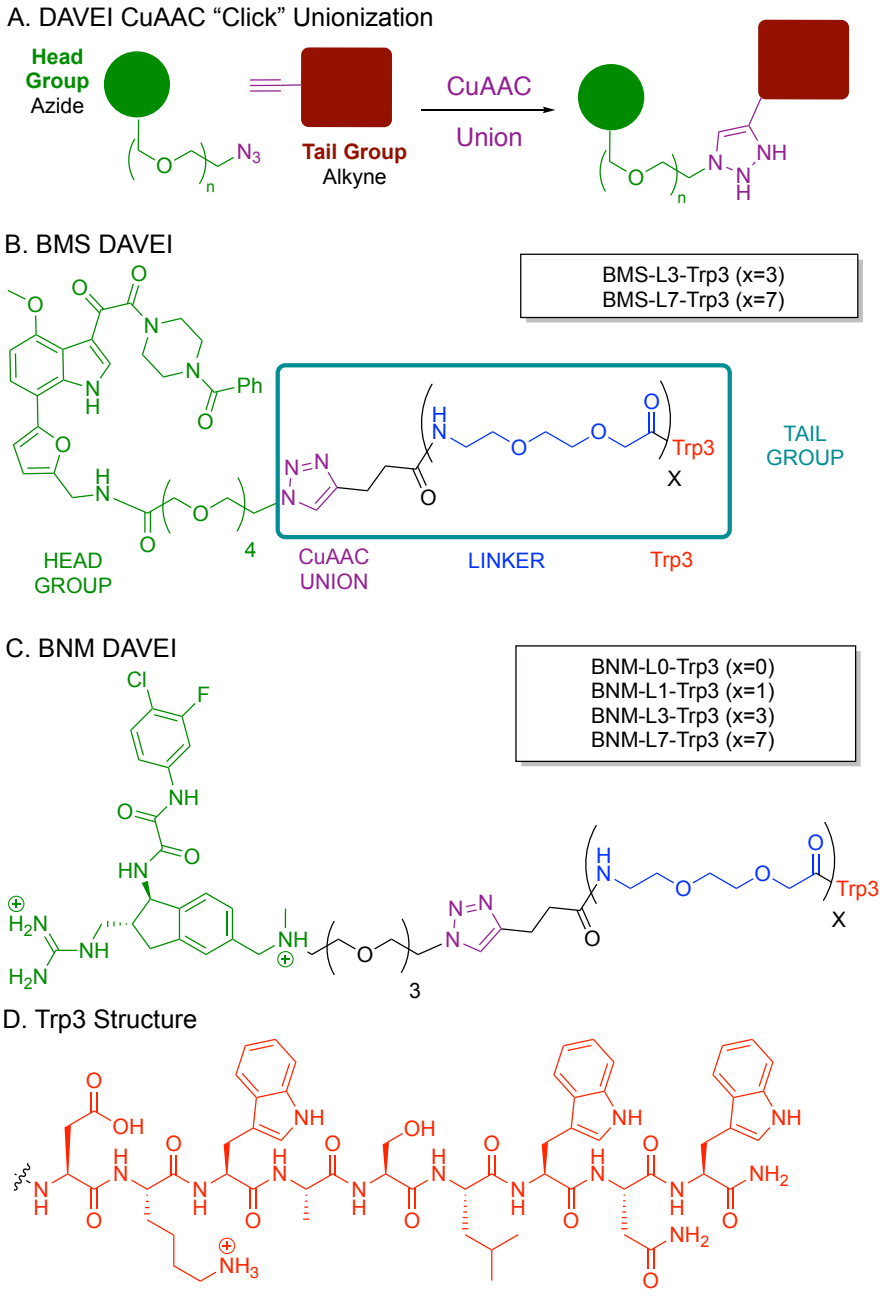

Figure 2.6 Small molecule DAVEI constructs.

2.3 General DAVEI Synthetic Strategy

The small molecule head groups, which will be described in greater detail below, are functionalized with an azide handle to which the peptidic tail group is installed using a copper(I)-catalyzed alkyne-azide cycloaddition (CuAAC) union (i.e., click installation).[15] The tail group is comprised of: (a) the Trp3 optimized MPER segment (sequence DWKASLWNW)[14], (b) an ethoxyamino linker (Lx), and (c) an alkyne. The distance between the small molecule warhead and the Trp3 peptide is varied with incorporation of different numbers of ethoxyamino linkers (Lx) between the alkyne azide acceptor and the Trp3 peptide (Figure 2.6). The alkyne-linker-Trp3 components were synthesized using automated solid phase peptide synthesis. A major advantage to this synthetic strategy is that the solid-phase approach permits rapid, low-cost library construction of tail groups which incorporate various spacer and linker lengths.

2.4 BMS DAVEIs – Incorporation of a Conformational Blocker as a Head Group

The first family of small molecule DAVEIs featured as a head group an analog of BMS-806, an HIV-1 infection inhibitor developed by Bristol Myers Squibb. BMS-806 was an early lead compound which was subsequently optimized to BMS-529 (Figure 2.5). The prodrug of BMS-529, Fostemsavir, is currently in Phase III clinical trials.[16] This family of compounds was selected as the target head group for the first generation of small molecule DAVEI, as both their mechanism of action[17] and the tolerated substitution patterns[16] are well documented.

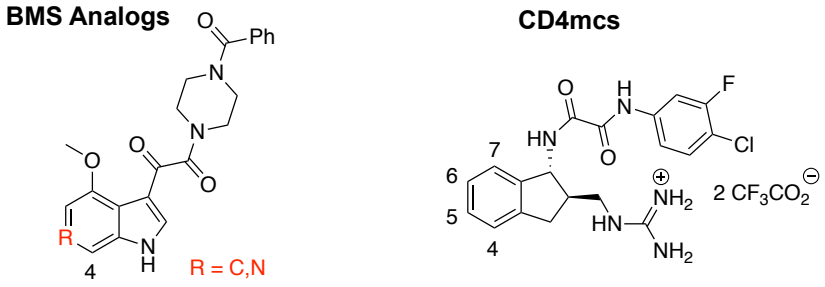

Figure 2.7 Carbon numbering for relevant small molecules.

2.4.1 Binding Site and Mechanism of Action of BMS-529 and Analogs Thereof.

BMS-529 and the analogs thereof inhibit HIV-1 infection by blocking CD4-induced conformational changes[17] required for viral entry. Single-molecule fluorescence resonance energy transfer studies of Env trimers with bound BMS compounds suggest the conformation of BMS-bound Envs and that of the closed unliganded structure (State 1) are nearly identical.[18,19]

The BMS analogs engage the Env in a surface-accessible pocket at the interface between the inner and outer domains of gp120 under the β20–21 loop. For reference, this pocket is on the opposite side of the β20–21 loop relative to the Phe43 cavity where CD4 and CD4mcs bind (see Chapter One).[17,20]

2.4.2 Attachment Strategy

A critical consideration in development of small molecule DAVEIs was incorporation of the sterically large tail group at a position that will not compromise the binding of the small molecule head group. Crystal structures suggested that incorporation of additional bulk at the 4-position of the BMS azaindole core would orient the tail group toward an open, solvent-exposed area on the Env.[17] Substitution at this position is supported by structural studies by BMS[16] (Figure 2.8) and others.[21–23]

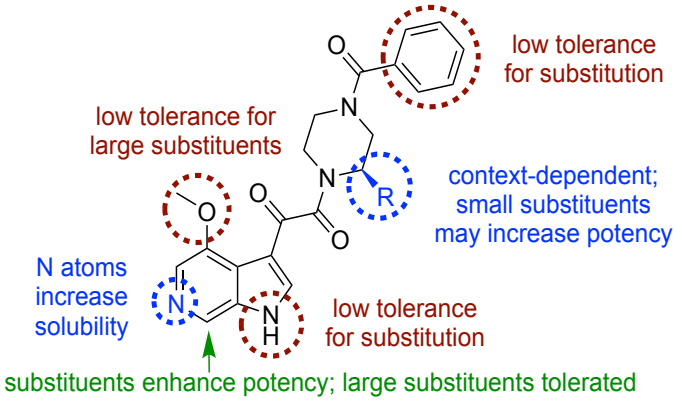

Figure 2.8 Summary of substitution tolerance of BMS analogs.

Incorporation of large substituents on a BMS analog has been explored by the Spiegel group.[21] The Spiegel group designed and synthesized analogs of BMS to which the antibody recruiting agent dinitrophenyl (DNP) was appended. DNP is recognized by anti-DNP antibodies and leads to antibody-mediated immune clearance of Env-expressing cells. The Spiegel group explored at which positions on analogs of BMS-806 a $(PEG)_6$-DNP moiety could be incorporated without drastic reduction in binding of the small molecule.[21] This work found that substitution at the 4-position afforded a compound which successfully bound the Env and had the desired effect – recruiting antibodies for inactivation of the virus (Figure 2.9).

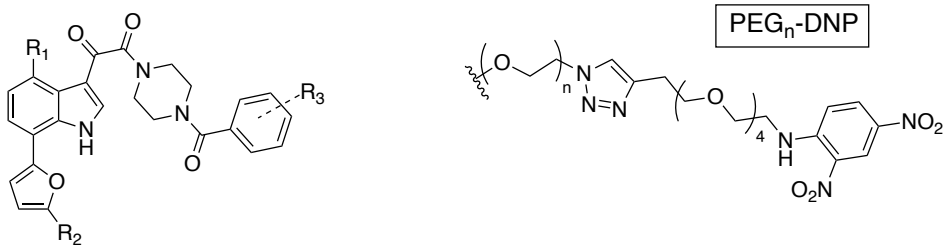

R_1	R_2	R_3	MT-2 IC_{50} (μM)	Ab Recruiting EC_{50} (μM)
PEG_6-DNP	H	H	> 100	> 100
OMe	$(CH_2NHCOCH2_2)$-PEG_5-DNP	H	0.013	1.12
OMe	H	PEG_6-DNP (*ortho*)	7.1	1.21
OMe	H	PEG_6-DNP (*para*)	100	0.90
OMe	H	PEG_6-DNP (*meta*)	0.460	1.15

Figure 2.9 Substitution tolerance of BMS analogs reported by Spiegel et al. with MT-2 HIV.

The Spiegel strategy was selected for proof of concept work on BMS DAVEIs as their synthetic route was developed and simpler than the route required to synthesize the actual BMS compounds. Moreover, the literature suggests BMS analogs have similar modes of action.[16] If these simplified scaffolds were to prove promising, the head group could then be modified to improve DAVEI activity.

2.4.3 Head Group (AEG-I-296) Synthesis

Bartoli indole synthesis of **2.1** afforded **2.2**, which was elaborated to glyoxamide **2.3** as outlined in Scheme 2.10. Deprotection and amide coupling produced **2.4**, which was subjected to Suzuki coupling and deprotected to afford **2.6** (Scheme I).[21]

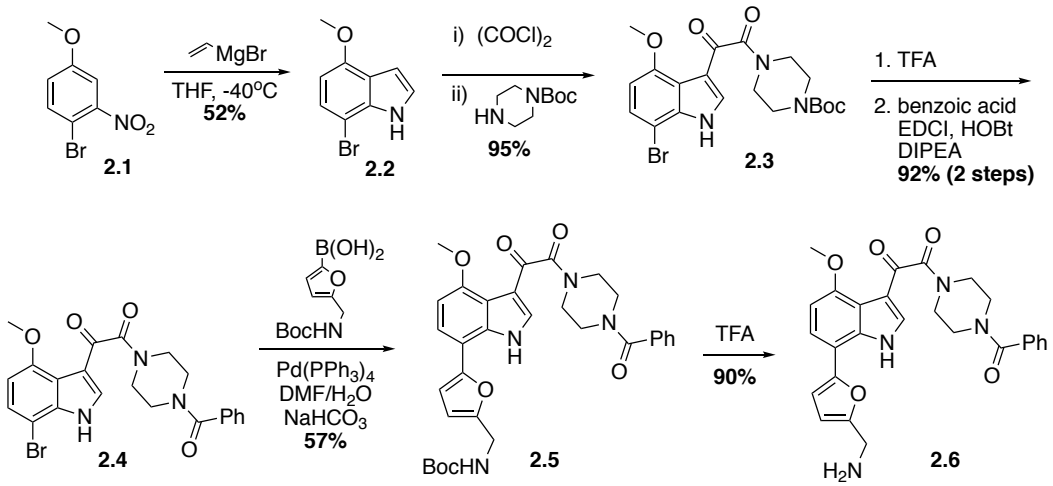

Scheme I. Synthesis of **2.6**.

The PEG-azide handle was next synthesized by tosylation of tetraethylene glycol, followed by azidization and subsequent alkylation of bromoacetic acid to afford azido-carboxylic acid **2.9**.[24] Pleasingly, after union of **2.6** with **2.9**, the BMS-N_3 was found to maintain potent inhibitory activity (IC_{50} = 70 nm in JR-FL), indicating that the functionalization with the PEG spacer had not abrogated the ability of the BMS analog to bind to gp120.

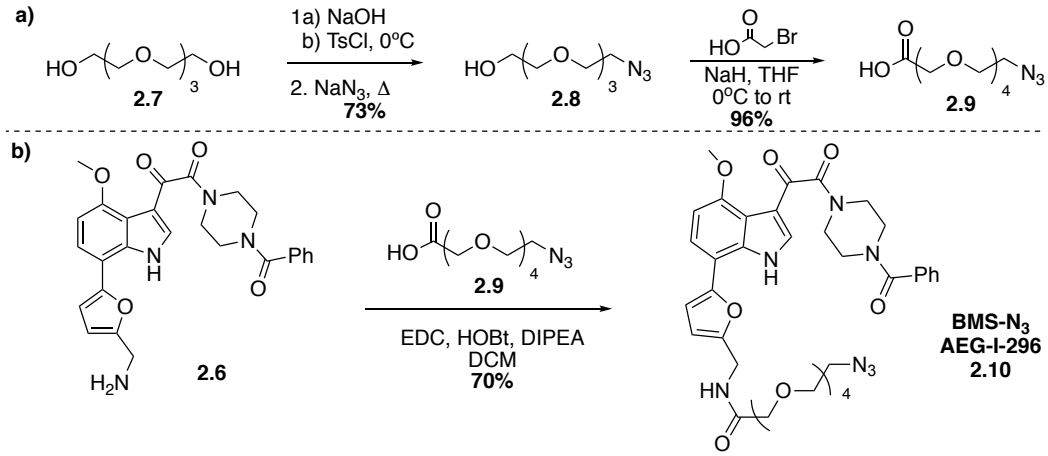

Scheme II. Synthesis of BMS headgroup **AEG-I-296**

2.4.4 Synthesis and Biological Activity of BMS DAVEIs

Two BMS-based DAVEI constructs—BMS-L3-Trp3, and BMS-L7-Trp3— were synthesized employing the click attachment strategy described below (Figure 2.10). Like the parent BMS compounds and the functionalized BMS-N_3, the BMS DAVEI constructs are also inhibitors of HIV-1 infection. However, they were not observed to cause virolysis (Table 2.1).

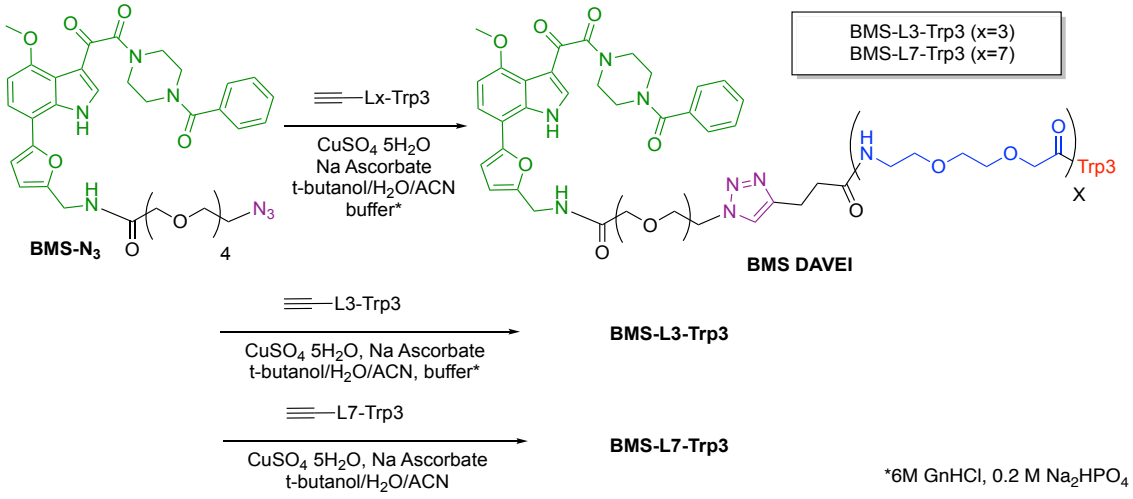

Figure 2.10 CuAAC-mediated synthesis of BMS DAVEIs

Table 2.1 Biological Activity of BMS DAVEIs

	Infection Inhibition IC_{50} (nM)	Virolysis EC_{50}
BMS-N_3 (AEG-I-296)	70 +/- 10	—
BMS-L3-Trp3	14 +/- 3	—
BMS-L7-Trp3	3 +/- 2	—

All-atom in silico models of BMS-DAVEI / Env complexes were generated and analyzed to complement and rationalize the results of the biological observations. Modeling suggests the 7 linking units of BMS-L7-Trp3 are of sufficient length to enable dual engagement with the Env (Figure 2.11). This suggests a factor other than tether length is responsible for the absence of lytic activity in these compounds. Thus, future work with BMS DAVEIs was halted at this time.

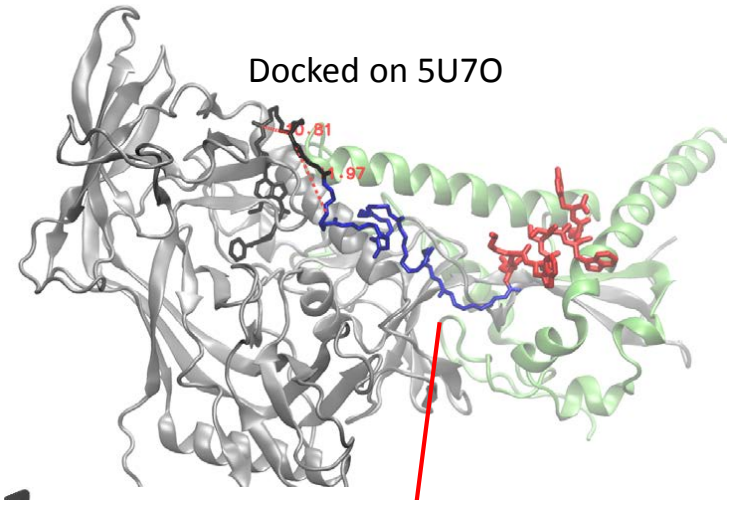

Figure 2.11 BNM-L7-Trp3 docked onto Env crystal structure 5U7O. The small molecule warhead (black) is connected by seven repeating linking units (blue) to Trp3 (red).

2.5 Synthesis of BNM DAVEIs

The BNM family of DAVEIs are derived from analogs of the small-molecule CD4 mimetic compounds (CD4mcs) developed in the Smith Laboratory, exemplified by the indane-oxalamide entry inhibitor, BNM-III-170, demonstrated to prevent vaginal and rectal AIDS infection respectively in mice and primates (i.e., protection), and to sensitize HIV-1 infected cells to ADCC (eradication).[25]

2.5.1 Binding Site and Mechanism of Action

BNM-III-170 and other small molecule CD4mcs bind in the gp120 Phe43 cavity and are reported to push Env into more open conformations vulnerable to antibody attack.[26] While the open conformation induced by CD4 triggers the virus entry cascade into cells, the Env conformational cascade initiated by BNM-III-170 in the absence of CD4 leads ultimately to inactivation of the virion.[26,27] Importantly, the gp120 binding site for BNM-III-170 has been determined at high resolution by X-ray crystallography, making BNM-III-170 ideal as a component for the structurally minimized DAVEI head group constructs.[27] The mechanism of action of this and other CD4mcs is described in greater detail in Chapter One.

2.5.2 Attachment Strategy

BNM-III-170 was chosen as the first small molecule head group because the amine at carbon-5 on the indane was judged an advantageous location for functionalization with an azide spacer to permit construction of DAVEIs. Importantly, crystal structures and docking studies suggest that such substitution at the 5-position would point out towards a solvent-exposed region of the Env thereby tolerating placement of the large tail group.

2.5.3 Head Group Synthesis

BNM-III-170 is available in gram-scale quantities thanks to scale-up efforts in the Smith laboratory completed by Jun Park, Sharon Kirk, Junhua Chen, Xiangqin Li, and Hung-Ching Chen (publication in review). This synthesis is described in the following paragraph.

Carboxylation of commercial 5-bromoindanone affords **2.12**, which is then subjected to a ruthenium-catalyzed dynamic kinetic asymmetric transformation to set the stereochemistry at carbons 1 and 2. Exhaustive reduction with lithium aluminum hydride and selective protection of the primary alcohol then affords **2.14**. Installation of the methylaminomethyl moiety was next achieved by lithium halogen exchange and trapping with dimethylformamide to generate the corresponding aldehyde **2.16**, which was subjected to reductive amination with methylamine. The amine in **2.17** was then protected with Boc-anhydride prior to azidization, and in turn reduced to amine **2.20**. Regions I and II (see Chapter One) were then installed to produce **2.23**. The alcohol was deprotected and mesylated to enable Gabriel synthesis to afford amine **2.25**. The guanidinium moiety was installed to give **2.26**. Finally, TFA-mediated global Boc-deprotection afforded the desired BNM-III-170 (Scheme III).

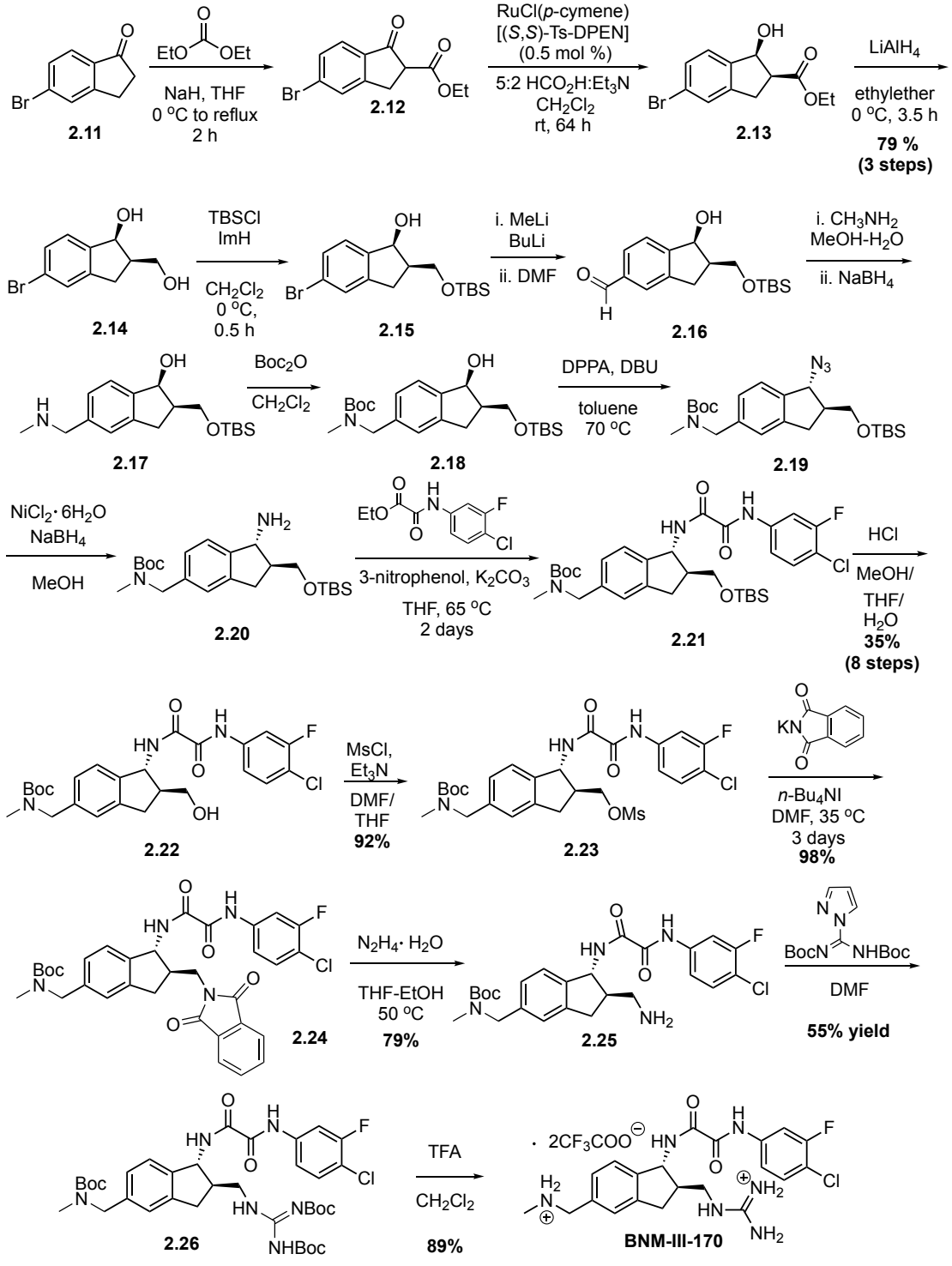

Scheme III. Multi-gram synthesis of BNM-III-170.

The requisite PEG-azide handle was synthesized by tosylation of tetraethylene glycol, followed by azidization and subsequent oxidation to the corresponding aldehyde (Figure 2.12a).[28] Reductive amination with BNM-III-170 afforded the BNM-N_3 (Figure 2.12b).

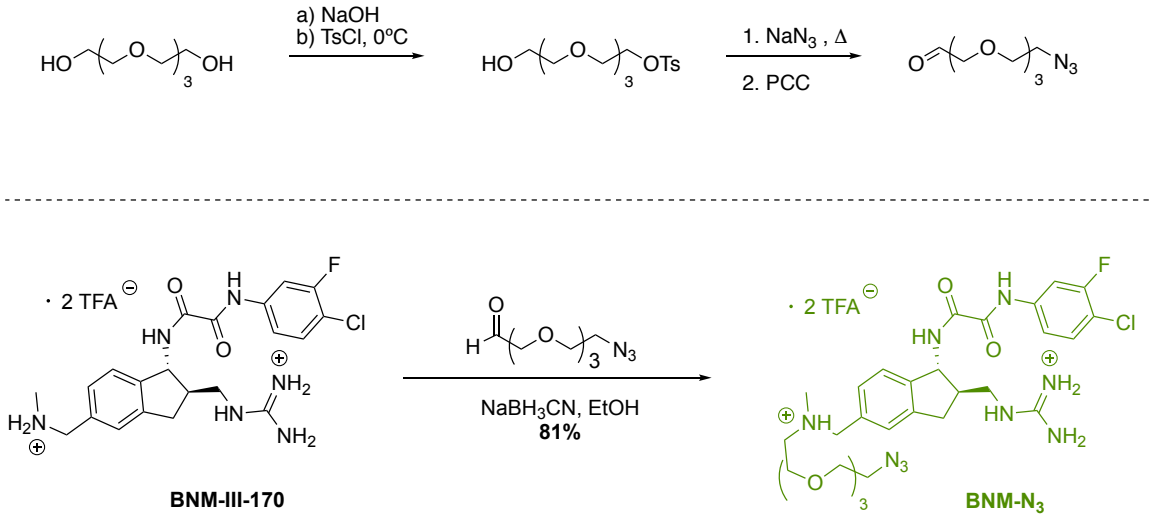

Figure 2.12 a) Synthesis of azide handle for BNM DAVEIs. b) Synthesis of BNM-N_3.

2.5.4 Synthesis of BNM DAVEIs

In turn, CuAAC attachment of the BNM-N_3 with the peptide alkyne-Lx-Trp3 (x = 0, 1, 3, 7) provided BNM-L0-Trp3, BNM-L1-Trp3, BNM-L3-Trp3, and BNM-L7-Trp3, respectively. BNM-N_3 synthesis is depicted in Figure 2.15.

Two routes of conjugate synthesis were employed as illustrated in Figure 2.13. In both, the alkyne-Lx-Trp3 was synthesized using automated solid phase synthesis. These DAVEIs were first generated by performing the CuAAC "click" reaction on the protected, resin-bound peptide, followed by simultaneous deprotection and cleavage from resin (Figure 2.13, left). It was later found that first cleaving peptide, purifying it, and performing the CuAAC click union in solution simplified monitoring of reaction progress (Figure 2.13, right). Purification and structural validations were then carried

out for all intermediates with final products employing reverse phase HPLC and mass spectrometry for structural identification (see Figure 2.14 for a representative case). It should be noted that both routes afford identical structures.

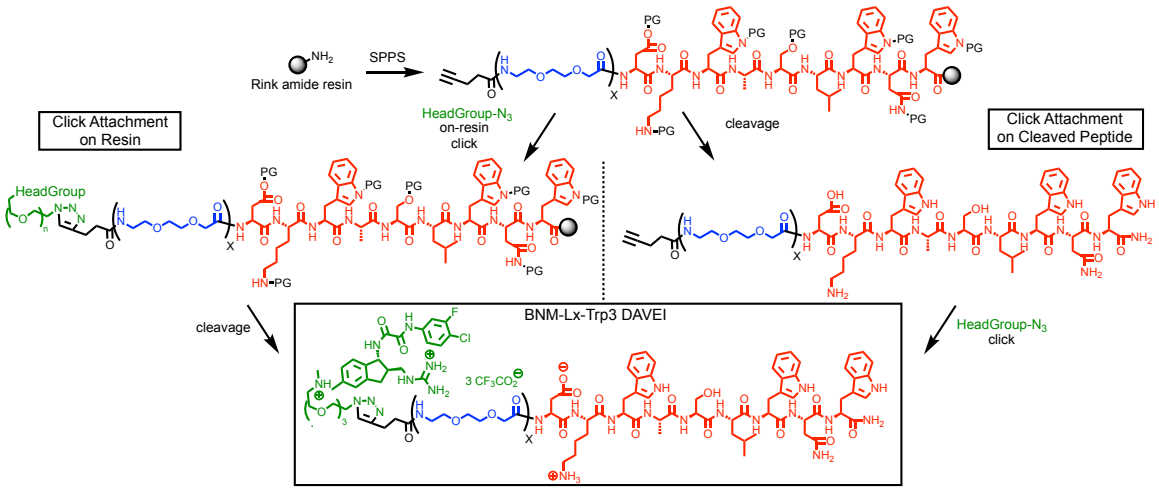

Figure 2.13 DAVEI synthesis strategies. The CuAAC attachment of the headgroup may be performed on the protected, resin-bound peptide (left) or on the cleaved, deprotected and purified peptide (right).

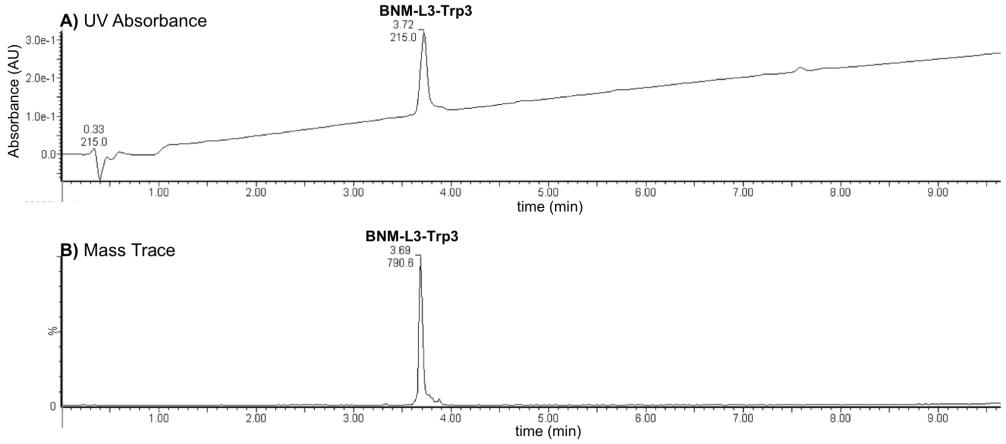

Figure 2.14 Validation of purity of BNM-L3-Trp3 synthesized by solution phase CuAAC protocol using reverse phase LC/MS (10 min, 5-95% acetonitrile/water + 0.1% TFA). A) UV absorbance trace (diode array, 254 nm), B) LC mass trace.

2.5.5 Biological Activity of the BNM-DAVEI Constructs

The BNM-DAVEI constructs were evaluated for their ability to inhibit infection and cause lysis of the HIV-1 virus. The results of these analyses are presented in Table 2.2.

Pleasingly, all four of the covalently-linked BNM-linker-Trp3 constructs synthesized inhibited viral infection. It should be noted that the BNM-L3-Trp3 produced by the full solid phase synthetic protocol (Figure 2.13, left) did not differ functionally from the solution phase synthetic DAVEI constructs (Figure 2.13, right) (IC_{50} = 0.58 ± 0.09 μM, EC50 = 7.2 ± 0.5 μM). These results emphasize the capacity to derive lytic BNM-DAVEIs by multiple synthetic strategies.

Table 2.2 Biological activity of BNM DAVEIs.

	Infection Inhibition IC_{50} (μM)	**Virolysis EC_{50} (μM)**
BNM-N_3	0.73 +/- 0.04	—
BNM-L0-Trp3	0.20 +/- 0.01	1.09 +/- 0.02
BNM-L1-Trp3	0.4 +/- 0.2	1.30 +/- 0.05
BNM-L3-Trp3	0.53 +/- 0.07	3.8 +/- 0.3
BNM-L7-Trp3	0.7 +/- 0.2	4.3 +/- 0.2

Furthermore, all of the tested DAVEI constructs were found to cause virolysis (Table 2.2). Importantly, none of the compounds tested exhibited toxicity against HOS.T4.R5 cells. The BNM-DAVEI constructs with differing linker lengths from L0 to L7 were evaluated. Lytic activity was

significant in all cases, with fractionally greater potency seen with decreasing linker length. The BNM-L0-Trp3 DAVEI was observed to demonstrate the best antiviral and virolytic activity.

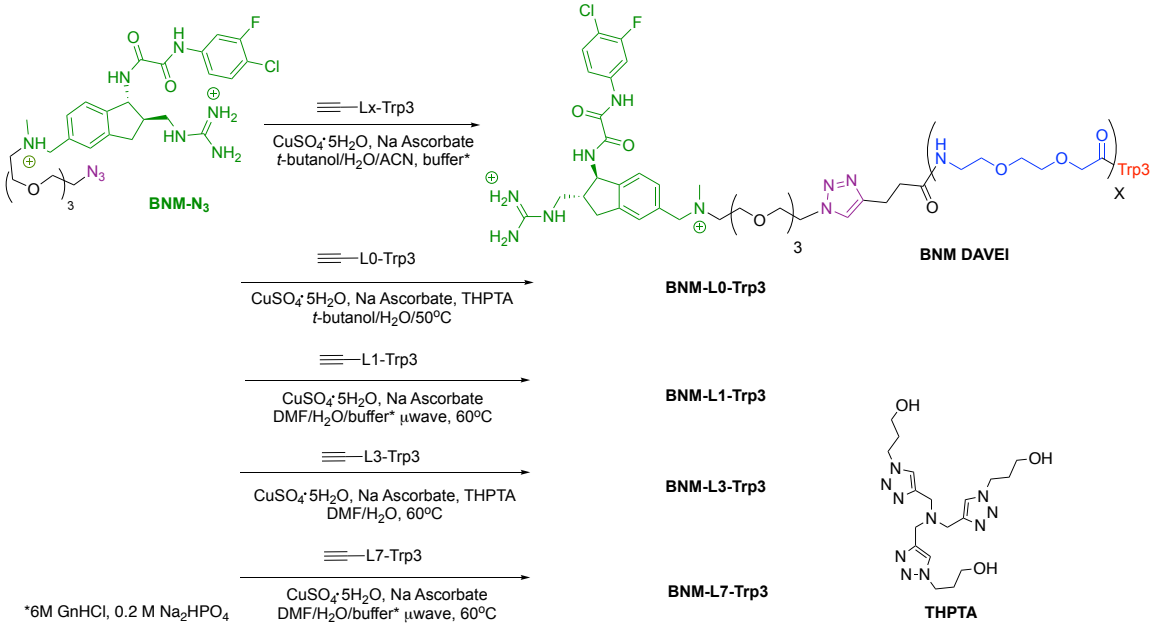

Figure 2.15 BNM DAVEI Synthesis.

To probe further the mechanism of action of these compounds, the role of the covalent linkage of the small molecule CD4 mimic and peptide DAVEI components was evaluated. Importantly, the azide-bearing small molecule head group BNM-N_3 and tail group alkyne- L3-Trp3 (the unclicked linker-peptide moiety) did not cause virolysis when tested alone or as a 1:1 mixture. The simultaneous presence of a gp120-binding compound (i.e., BNM-N_3) and a gp41-binding compound is thus not sufficient to induce virolysis. It should be noted however that BNM-N_3 remains an infection inhibitor with comparable potency to the parent BNM-III-170, and that neither of these compounds induces virolysis. The results are shown in Figure 2.16. These results emphasize the importance of our conjugation strategy, and furthermore suggest the DAVEI constructs engage the Env in a manner fundamentally different from those of the individual components prior to conjugation.

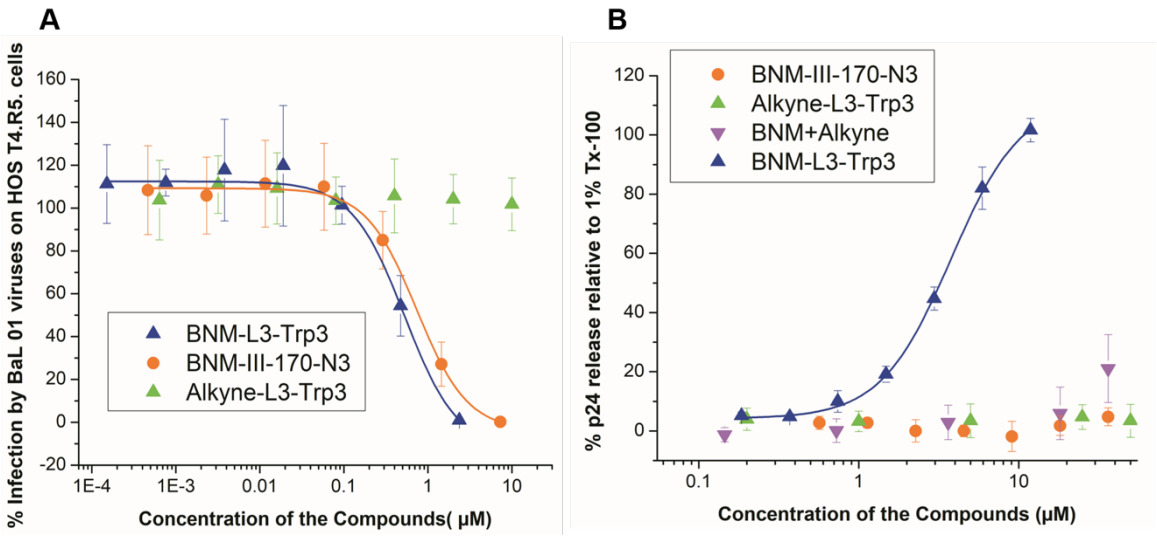

Figure 2.16 Biological Evaluation of BNM DAVEI. Inhibition of infection data (left) and virolysis data (right) are shown above. Neither the head group or tail group alone causes virolysis. Furthermore, the simultaneous presence of both the head group and tail group did not cause virolysis, suggesting covalent linkage is critical to the ability of BNM DAVEIs to cause virolysis.

2.5.6 Computational Study – Molecular Simulation of BNM-DAVEI / Env Complexes

All-atom in silico models of BNM-DAVEI / Env complexes were generated and analyzed by the Abrams laboratory to complement and rationalize the results of the biological observations. Binding models of BNM-Lx-Trp3 (x = 1, 3, 7) were generated using a soluble gp160 SOSIP.664 trimer (PDB ID: 5VN3).[29] 5VN3 was selected because BNM-III-170 is known to bind to gp120 in the CD4-bound conformation.[27] Stable complexes of both BNM-L3-Trp3 and BNM-L7-Trp3 on Env were successfully obtained. However, against a rigid Env structure, it was not possible to form a dually-engaged BNM-L1-Trp3/Env complex. A stable BNM-L1-Trp3 complex was however generated by allowing Env to move during attachment and equilibration, while artificial forces maintained the bound state of both the BNM and the Trp3. Renderings of three representative [BNM-Lx-Trp3]/Env complexes are illustrated in Figure 2.17.

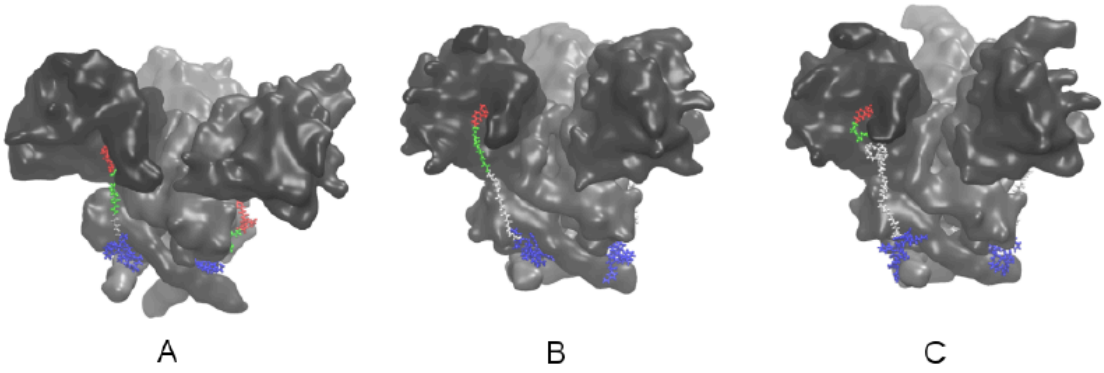

Figure 2.17 Docking of BNM DAVEIs to the Env. (A) BNM-L1-Trp3, (B) BNM-L3-Trp3, (C) BNM-L7-Trp3.

These models suggest that there is sufficient flexibility in the linkers of the L3 and L7 constructs to facilitate simultaneous dual engagement with a gp41 and gp120 subunit on the CD4-activated sgp160 SOSIP.664 Env. This modeling also illustrates that the Env trimer itself possesses sufficient flexibility to allow for the L1 DAVEI to bind stably.

Though instructive, these models are still somewhat speculative because unlike BNM-III-170, there is as yet no precise structural evidence of the Trp3 binding site. Prior work by our collaborators with Trp3 suggests specific binding to Env MPER, yet the lack of structural information on the MPER in the sgp160 SOSIP.664 construct, which does not contain the MPER region of gp41 in its structure, will require modeling of this region of the protein.[6,14]

2.5.7 Further Mechanistic Investigation of Virolysis

To support the proposed mechanism of action, further evaluation of the hypothesis that the small molecule head group of BNM DAVEIs binds in the same place as the parent BNM-III-170 was pursued. Specifically, BNM-L3-Trp3 was tested in a mutant virus in which the Phe43 pocket is not accessible. It has been previously established that mutant Envs in which the Phe43 pocket is partially obscured with mutation of the natural amino acid serine 375 to the significantly larger

tryptophan (S375W) are not susceptible to inhibition of infection by BNM-III-170.[30–32] Thus, it was expected these viral mutants would be resilient to challenge from BNM-based DAVEIs, as the BNM-III-170-based head group was expected to be unable to bind gp120. Indeed, the infectivity of the S375W mutant was not affected by challenge from BNM-L3-Trp3 or the unconjugated BNM-N_3.

Surprisingly, however, the BNM-L3-Trp3 DAVEI did cause virolysis of the S375W mutant! Furthermore, the virolysis data closely resembled that from BaL 01 with an unmodified Env in which the head group can bind (Figure 2.18). As the head group is expected to be unable to bind gp120 in the S375W mutant, this suggests something other than simultaneous dual engagement of gp120 and gp41 causes virolysis. To explore this result further, and to evaluate whether the observed virolytic effect of BNM-DAVEI may extend beyond HIV, BNM-L3-Trp3 was tested in other viruses.

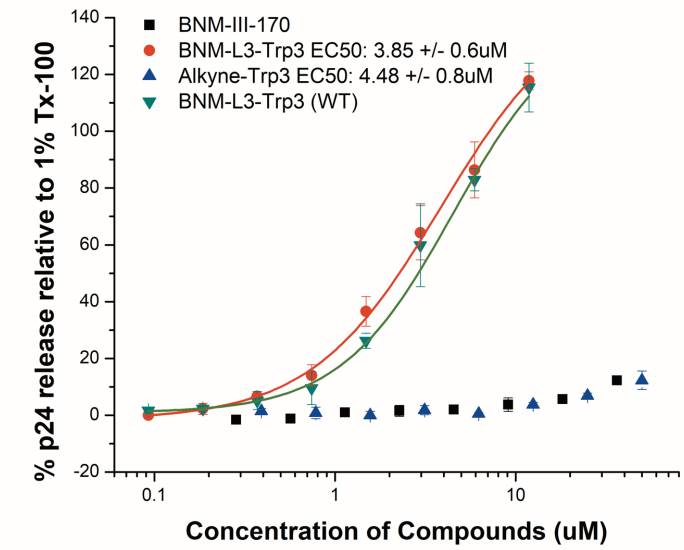

Figure 2.18 Biological data of BNM-L3-Trp3 in the BaL S375W mutant Env. The DAVEI construct BNM-L3-Trp3 causes lysis of virions containing mutant Envs in which the Phe43 pocket is obstructed (red). This activity of BNM-L3-Trp3 is comparable to virolysis observed in the wild type Env (green). The extent of virolysis is evaluated using p24 release from virions upon lysis. An increase in virolysis is suggested by an increase in p24 release.

To explore broader antiviral activity of BNM DAVEI, BNM-L3-Trp3 was tested in vesicular stomatitis virus (VSV), another enveloped virus to which BNM-III-170 does not bind. As expected, BNM-L3-Trp3 did not inhibit VSV infection. However, BNM-L3-Trp3 was again observed to cause virolysis. As with the initial results with BaL 01 virus, both the head group and tail group were required to be covalently bound together for activity – neither the head group azide (BNM-N_3) nor the tail group peptide were able to cause virolysis in VSV. (Figure 2.19)

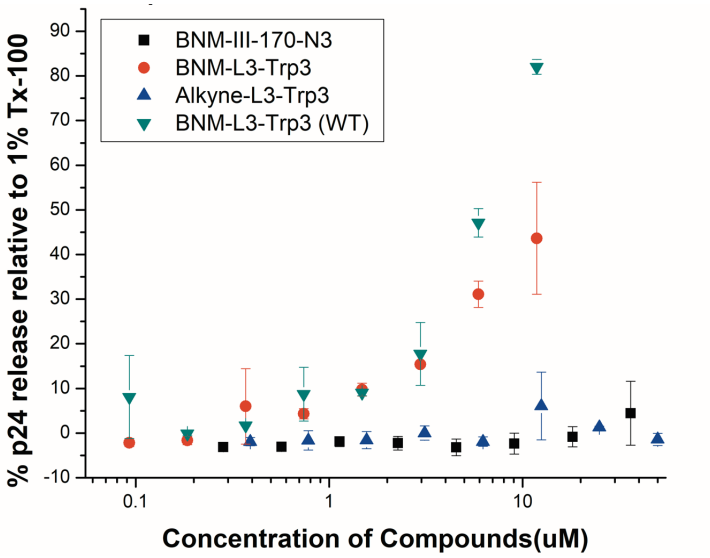

Figure 2.19 Biological activity of BNM-L3-Trp3 in VSV.

To confirm the Env is not required for virolysis, BNM DAVEI activity was evaluated in HIV viruses modified to lack Envs. Again, BNM-L3-Trp3 caused virolysis, confirming the Env is not required for this activity (Figure 1.20).

However, preliminary study of BNM DAVEIs applied to cells (instead of virions as described above) suggests these compounds may have the desired specific killing of HIV-infected cells. In ongoing studies, BNM-L7-Trp3 has been observed to cause cell death in HIV-infected cells. Importantly, cell death was not observed in uninfected cells. This result warrants further study and

may suggest the mechanism by which BNM DAVEIs kill infected cells may differ from the mechanism by which they cause virolysis.

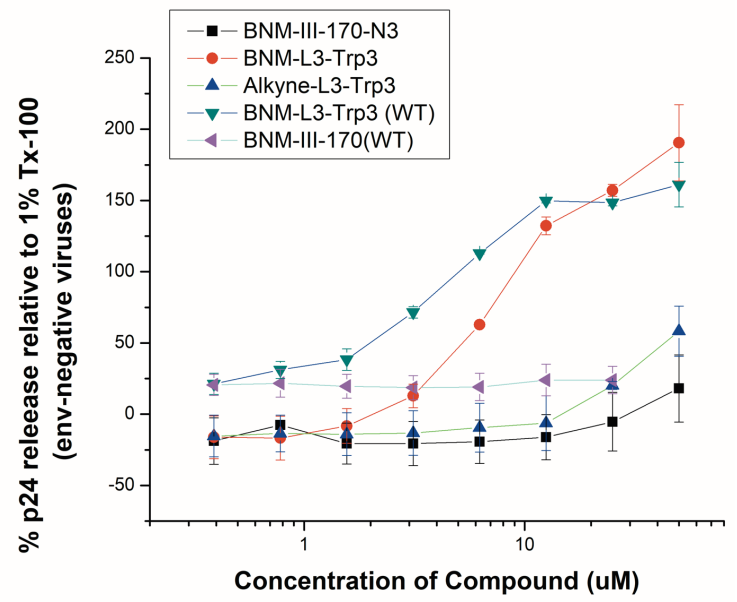

Figure 2.20 Biological activity of BNM-L3-Trp3 in HIV without surface Envs. Activity in wild type virus is shown (teal, purple) for reference.

2.5.8 Conclusion

The family of BNM DAVEIs not only inhibit cell infection but also cause HIV-1 lysis. Importantly, the azide-bearing small molecule warhead BNM-N_3 and the alkyne-L3-Trp3 peptide did not cause significant virolysis when tested independently or when administered together as a mixture of unlinked compounds. This suggests the simultaneous presence of a gp120-binding compound and a gp41-binding compound in the absence of covalent attachment to each other is not sufficient to induce HIV virolysis. It should also be noted that BNM-III-170 and BNM-N_3 retain potent inhibition of viral infection in the presence of the Trp3 peptide.

From the finding that both the small molecule and peptide components must be covalently linked in order for BNM-DAVEIs to cause virolysis, it was initially inferred that simultaneous binding

of gp120 and gp41 likely is required. Computational modeling supported this hypothesis. However, the observed lysis of virions which lack the HIV Env indicate that *this is not the requisite mechanism of action for this observed activity*. While this finding does not completely eliminate the possibility of the originally proposed mechanism of action involving dual engagement, it does necessitate the existence of another mechanism of action that results in virolysis. The extent to which the virolytic properties of DAVEIs extend to other viruses will be explored in future work.

While BNM DAVEI-induced virolysis may apply to a broad spectrum of viruses, BNM DAVEI-mediated killing of cells appears to be limited to HIV-infected cells. This recent area of investigation will also be explored further in future work.

2.6 Comparison of Small Molecule DAVEIs

The disparate results of the BMS and BNM DAVEIs are clearly intriguing and warrant further investigation. BMS-529 and related analogs inhibit infection by locking the Env in a closed state (i.e., State 1), thus preventing it from moving into conformations required for entry into host cells.[17,19] CD4mcs, such as BNM-III-170, however, inactivate the Env by pushing it into more open conformations that ultimately lead to inactivation of the virus. At first it was proposed that a conformation other than the closed Env trimer may be required for virolysis to occur. The observed BNM-L3-Trp3-induced lysis of virions lacking an Env, however, challenges this hypothesis. The specificity of BNM DAVEI-mediated killing of HIV-infected cells, however, is also perplexing. Some future experiments to investigate further these seemingly contradictory observations will be described in the following section.

2.7 Future Directions: Further Biological Evaluation and New Head and Tail Group Evaluation

2.7.1. Biological Evaluation

BNM DAVEIs will be evaluated for potential to cause virolysis in unrelated viruses. BNM DAVEIs will be evaluated collaboratively with the Chaiken group for potential to cause virolysis of enveloped viruses other than HIV-1. The cell work mentioned above is preliminary and requires verification. Additional cell lines should be explored to ensure the observed cytotoxicity is unique to HIV.

2.7.2. Head group exploration

While the preliminary results of the BNM DAVEIs are encouraging, compounds should be designed to both improve their potencies and to better understand the mechanism of DAVEI-induced virolysis.

With the transition from lectins to small molecules as head groups, the molecular weight of small molecule DAVEI constructs are now nearly a tenth of the molecular weight of the original lectin DAVEIs. Further simplification of these head groups is enticing for potential therapeutic compounds. The potency of these compounds should also be improved. Furthermore, it should be noted that the BNM-N_3 and the BMS-N_3 have very different polarities. As alternate head groups are incorporated into DAVEIs, the effects of changes in polarity should be evaluated to determine whether polarity has any effect on observed DAVEI function. Specifically, any potential effects of polarity related to association with the viral membrane should be explored.

2.7.2a The JRC Head Group.

The NBD compounds NBD-556 and NBD-557 were the original hits identified as inhibitors of HIV viral entry.[33] An analog of these, JRC-II-191, was an early improvement en route to BNM-III-

170 antagonism of HIV-1 entry. While substantially less potent than BNM-III-170 as an inhibitor of HIV, JRC-II-191 possesses a significantly lower molecular weight than the later CD4mcs. The difference in polarity may also have interesting results on virolysis.

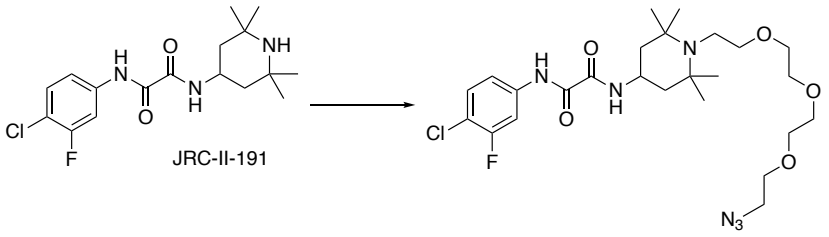

Figure 2.21 Proposed design of a JRC-II-191-based head group.

2.7.2b The Piperidine Head Group.

(S)-MCG-IV-210 is an optimized member of a class of piperidine-based CD4mcs under investigation in our P01 collaboration as inducers of specific antibody-sensitive conformations of native Env, which bind in the Phe43 cavity of gp120. MCG-IV-210 is significantly lighter in molecular weight than BNM-III-170 and presents an amine that is likely to permit facile azide functionalization.

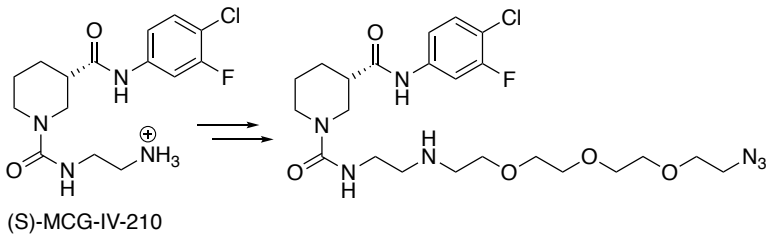

Figure 2.22 Proposed design of an MCG-IV-210-based head group.

2.7.3 Tail Group Exploration

Replacement of the Trp3 peptide component of DAVEI with a small molecule would afford a smaller, more attractive drug candidate. To this end, Andrianov et al.[34] have described compounds

which, based on modeling studies, are proposed to bind the gp41 MPER. This work identified eight lead compounds (Figure 2.23). Three compounds were selected for biological testing based on commercial availability (MMs03555010, MMs01288397) or synthesis (MMs00760407). These compounds have been submitted for biological evaluation. If these compounds are found to bind successfully to gp41, attachment sites may be selected in conjunction with our computational collaborators for incorporation into DAVEIs.

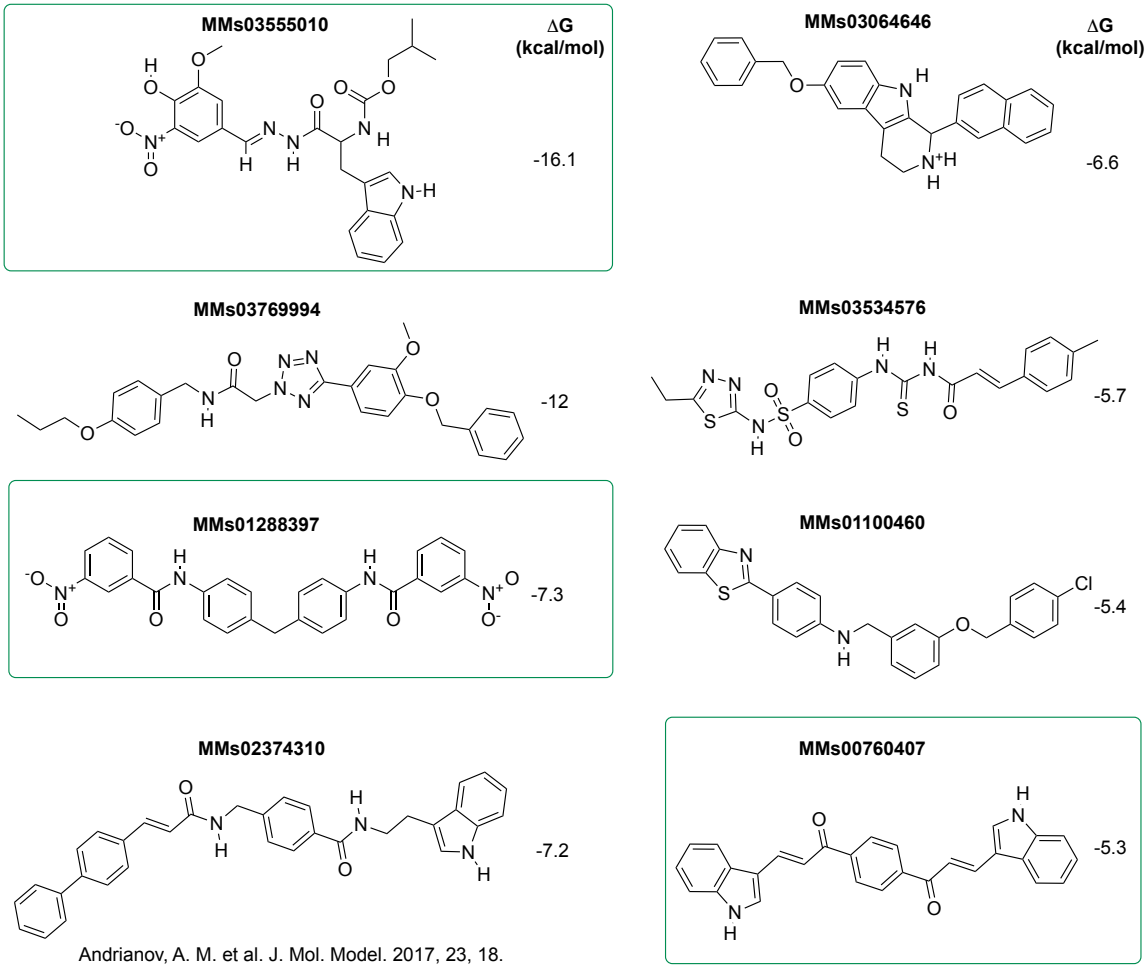

Andrianov, A. M. et al. J. Mol. Model. 2017, 23, 18.

Figure 2.23 Proposed Trp3 surrogates.

2.8 CHAPTER TWO REFERENCES

(1) Herschhorn, A.; Gu, C.; Espy, N.; Richard, J.; Finzi, A.; Sodroski, J. G. *Nat. Chem. Biol.* **2014**, *10* (10), 845.

(2) Chan, D. C.; Kim, P. S. *Cell*. **1998**, 681.

(3) Doms, R. W.; Peiper, S. C. *Virology*. **1997**, 179.

(4) Pierson, T. C.; Doms, R. W. In *Cellular Factors Involved in Early Steps of Retroviral Replication*; **2003**; 1.

(5) Wilen, C. B.; Tilton, J. C.; Doms, R. W. *Cold Spring Harb. Perspect. Med.* **2012**, *2* (8).

(6) Contarino, M.; Bastian, A. R.; Sundaram, R. V. K.; McFadden, K.; Duffy, C.; Gangupomu, V.; Baker, M.; Abrams, C.; Chaiken, I. *Antimicrob. Agents Chemother.* **2013**, *57* (10), 4743.

(7) Bennett, A.; Liu, J.; Van Ryk, D.; Bliss, D.; Arthos, J.; Henderson, R. M.; Subramaniam, S. *J. Biol. Chem.* **2007**, *282* (38), 27754.

(8) Dimitrov, A. S.; Xiao, X.; Dimitrov, D. S.; Blumenthal, R. *J. Biol. Chem.* **2001**, *276* (32), 30335.

(9) Gustafson, K. R.; Sowder, R. C.; Henderson, L. E.; Cardellina, J. H.; Mcmahon, J. B.; Rajamani, U.; Pannell, L. K.; Boyd, M. R. *Biochem. Biophys. Res. Commun.* **1997**, *238*, 223.

(10) Xiong, S.; Fan, J.; Kitazato, K. *Applied Microbiology and Biotechnology*. **2010**.

(11) Esser, M. T.; Lifson, J. D.; Mori, T.; Boyd, M. R.; Mondor, I.; Sattentau, Q. J.; Dey, B.; Berger, E. A. *J. Virol.* **1999**.

(12) Huskens, D.; Férir, G.; Vermeire, K.; Kehr, J. C.; Balzarini, J.; Dittmann, E.; Schols, D. *J. Biol. Chem.* **2010**, *285* (32), 24845.

(13) Parajuli, B.; Acharya, K.; Bach, H. C.; Parajuli, B.; Zhang, S.; Smith, A. B.; Abrams, C. F.; Chaiken, I. **2018**.

(14) Parajuli, B.; Acharya, K.; Yu, R.; Ngo, B.; Rashad, A. A.; Abrams, C. F.; Chaiken, I. M. *Biochemistry* **2016**, *55* (44), 6100.

(15) Rostovtsev, Vsevolod V.; Green, Luke G.; Fokin, Valery V.; Sharpless, K. B. *Angew. Chemie Int. Ed.* **2002**, *41* (14), 2596.

(16) Meanwell, N. A.; Krystal, M. R.; Nowicka-sans, B.; Langley, D. R.; Conlon, D. A.; Eastgate, M. D.; Grasela, D. M.; Timmins, P.; Wang, T.; Kadow, J. F. *J. Med. Chem.* **2018**, *61* (1), 62.

(17) Pancera, M.; Lai, Y.; Bylund, T.; Druz, A.; Narpala, S.; Dell, S. O.; Schön, A.; Bailer, R. T.; Chuang, G.; Geng, H.; Louder, M. K.; Rawi, R.; Soumana, D. I.; Finzi, A.; Herschhorn, A.; Madani, N.; Sodroski, J.; Freire, E.; Langley, D. R.; Mascola, J. R.; Mcdermott, A. B.; Kwong, P. D. *Nat. Publ. Gr.* **2017**, *13* (10), 1115.

(18) Lu, M.; Ma, X.; Castillo-Menendez, L. R.; Gorman, J.; Alsahafi, N.; Ermel, U.; Terry, D. S.; Chambers, M.; Peng, D.; Zhang, B.; Zhou, T.; Reichard, N.; Wang, K.; Grover, J. R.; Carman, B. P.; Gardner, M. R.; Nikić-Spiegel, I.; Sugawara, A.; Arthos, J.; Lemke, E. A.; Smith, A. B.; Farzan, M.; Abrams, C.; Munro, J. B.; McDermott, A. B.; Finzi, A.; Kwong, P. D.; Blanchard, S. C.; Sodroski, J. G.; Mothes, W. *Nature* **2019**, *568* (7752), 415.

(19) Munro, J. B.; Gorman, J.; Ma, X.; Zhou, Z.; Arthos, J.; Burton, D. R.; Koff, W. C.; Courter, J. R.; Smith, A. B.; Kwong, P. D.; Blanchard, S. C.; Mothes, W. *Science* **2014**, *346* (6210), 759.

(20) Herschhorn, A.; Gu, C.; Moraca, F.; Ma, X.; Farrell, M.; Smith, A. B.; Pancera, M.; Kwong, P. D.; Schön, A.; Freire, E.; Abrams, C.; Blanchard, S. C.; Mothes, W.; Sodroski, J. G. *Nat. Commun.* **2017**.

(21) Douglass, E. F.; Shoda, T.; Jawanda, N.; Spasov, K. A.; Lee, S.; Zhou, N.; Domaoal, R. A.; Sutton, R. E.; Anderson, K. S.; Krystal, M.; Jorgensen, L.; Spiegel, D. A. *Chem. Sci.* **2014**, 2311.

(22) Gavrilyuk, J.; Ban, H.; Uehara, H.; Sirk, S. J.; Saye-francisco, K.; Cuevas, A.; Zablowsky, E.; Oza, A.; Seaman, M. S.; Burton, D. R.; Iii, F. B. **2013**, *87* (9), 4985.

(23) Sato, S.; Inokuma, T.; Otsubo, N.; Burton, D. R.; Barbas, C. F. *ACS Med. Chem. Lett.* **2013**, *4* (5), 460.

(24) Sato, R.; Kozuka, J.; Ueda, M.; Mishima, R.; Kumagai, Y.; Yoshimura, A.; Minoshima, M.; Mizukami, S.; Kikuchi, K. *J. Am. Chem. Soc.* **2017**.

(25) Madani, N.; Princiotto, A. M.; Mach, L.; Ding, S.; Prevost, J.; Richard, J.; Hora, B.; Sutherland, L.; Zhao, C. A.; Conn, B. P.; Bradley, T.; Moody, M. A.; Melillo, B.; Finzi, A.; Haynes, B. F.; Smith, A. B.; Santra, S.; Sodroski, J. *Nat. Commun.* **2018**, *9* (1).

(26) Alsahafi, N.; Bakouche, N.; Kazemi, M.; Richard, J.; Ding, S.; Bhattacharyya, S.; Das, D.; Anand, S. P.; Prévost, J.; Tolbert, W. D.; Lu, H.; Medjahed, H.; Gendron-Lepage, G.; Ortega Delgado, G. G.; Kirk, S.; Melillo, B.; Mothes, W.; Sodroski, J.; Smith, A. B.; Kaufmann, D. E.; Wu, X.; Pazgier, M.; Rouiller, I.; Finzi, A.; Munro, J. B. *Cell Host Microbe* **2019**, *25* (4), 578-587.e5.

(27) Melillo, B.; Liang, S.; Park, J.; Schon, A.; Courter, J. R.; Lalonde, J. M.; Wendler, D. J.; Princiotto, A. M.; Seaman, M. S.; Freire, E.; Sodroski, J.; Madani, N.; Hendrickson, W. A.; Smith, A. B. *ACS Med. Chem. Lett.* **2016**, *7* (3), 330.

(28) Park, K. D.; Liu, R.; Kohn, H. *Chem. Biol.* **2009**, *16* (7), 763–772.

(29) Ozorowski, G.; Pallesen, J.; De Val, N.; Lyumkis, D.; Cottrell, C. A.; Torres, J. L.; Copps, J.; Stanfield, R. L.; Cupo, A.; Pugach, P.; Moore, J. P.; Wilson, I. A.; Ward, A. B. *Nature* **2017**, *547* (7663), 360.

(30) Madani, N.; Schon, A.; Princiotto, A. M.; LaLonde, J. M.; Courter, J. R.; Soeta, T.; Ng, D.; Wang, L.; Brower, E. T.; Xiang, S. H.; Do Kwon, Y.; Huang, C. chin; Wyatt, R.; Kwong, P. D.; Freire, E.; Smith, A. B.; Sodroski, J. *Structure* **2008**, *16* (11), 1689.

(31) Xiang, S.-H.; Kwong, P. D.; Gupta, R.; Rizzuto, C. D.; Casper, D. J.; Wyatt, R.; Wang, L.; Hendrickson, W. A.; Doyle, M. L.; Sodroski, J. *J. Virol.* **2002**.

(32) Madani, N.; Princiotto, A. M.; Zhao, C.; Jahanbakhshsefidi, F.; Mertens, M.; Herschhorn, A.; Melillo, B.; Smith, A. B.; Sodroski, J. *J. Virol.* **2017**.

(33) Zhao, Q.; Ma, L.; Jiang, S.; Lu, H.; Liu, S.; He, Y.; Strick, N.; Neamati, N.; Debnath, A. K. *Virology* **2005**, *339* (2), 213.

(34) Andrianov, A. M.; Kashyn, I. A.; Tuzikov, A. V. *J. Mol. Model.* **2017**, *23* (1), 18.

CHAPTER THREE: DESIGN AND SYNTHESIS OF PHOTOAFFINITY-LABELED ANALOGS OF BMS-529

The unliganded Env of the HIV-1 virus is conformationally dynamic. Specifically, the Env spontaneously and reversibly samples conformational states along the HIV-1 entry cascade. The propensity of the Env to sample a given state is dependent on the strain of HIV and can be modified by mutation of key amino acids or exposure to Env ligands.[1] The conformational dynamics of the Env alone and in response to ligands including small molecule inhibitors and antibodies has been the focus of smFRET (single-molecule fluorescence resonance energy transfer)[2] studies by our collaborators in the Laboratories of Professor Walther Mothes at Yale University and Professor Joseph Sodroski at the Dana-Farber Cancer Center. Synthetic efforts in the Smith Laboratory aimed at enabling further study and manipulation of the Env conformational dynamics using photoaffinity labeled compounds will be discussed in this Chapter.

3.1 Background: Study of the Env Conformational Dynamics Using smFRET

Single-molecule fluorescence resonance energy transfer uses the transfer of energy between two fluorophores to calculate the distance between them. When the two fluorophores come within 1-10 nm of each other, the emission energy of the donor fluorophore is transferred to the acceptor fluorophore, causing the acceptor to fluoresce. Intra-fluorophore distance can then be calculated using the ratio of acceptor intensity to total emission intensity.[2] In the context of the work described here, changes in smFRET are used to track the conformational dynamics of the Env in real time.

The conformational dynamics of the HIV-1 Env were investigated using smFRET by the Mothes Laboratory. This ongoing work typically incorporates one donor fluorophore and one acceptor fluorophore into variable loop motifs within the gp120 (Figure 3.1).[1,3]

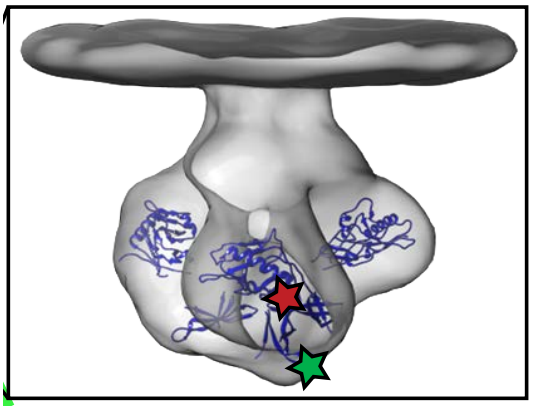

Figure 3.1. A representative example of positioning of fluorophores (stars) on the Env trimer.

FRET labeling was validated in the Env using a variety of incorporation strategies. The first smFRET studies of the Env reported by the Mothes Laboratory were accomplished by incorporating short peptides into the V1 loop and one of the V1, E, or V5 loops.[1] These peptides enabled enzyme-mediated incorporation of fluorophores onto the Env.[4,5] Fluorophores were also installed using an alternative method in which: (i) an unnatural amino acid was mutated into the Env, and (ii) a dye was attached to this residue using click chemistry.[3] Critically, installation of all fluorescence tags was site-specific and did not disrupt Env infectivity or sensitivity to neutralization by trimer-specific antibodies.[1,3,6]

Analysis of the smFRET data demonstrated that the unliganded Env spontaneously fluctuates between at least three conformational states characterized by distinct FRET values. Specifically, states with low (approximately 0.10), intermediate (approximately 0.30) and high (approximately 0.60) values FRET values were identified (Figure 3.2).[1] These values are determined by the ratio of fluorescence resonance energy transfer between the donor and acceptor probes.

As illustrated with NL4-3 and JR-FL viral clades in Figure 3.1, HIV-1 strains have different propensities to sample these conformations. Importantly, the existence of these three states was further validated by repeating FRET analysis with fluorophores incorporated in different positions

within the Env.[3] The smFRET data shown in Figure 3.2 is an aggregate of the behavior N distinct Envs – 173 Envs for NL4-3, and 125 Envs for JR-FL.

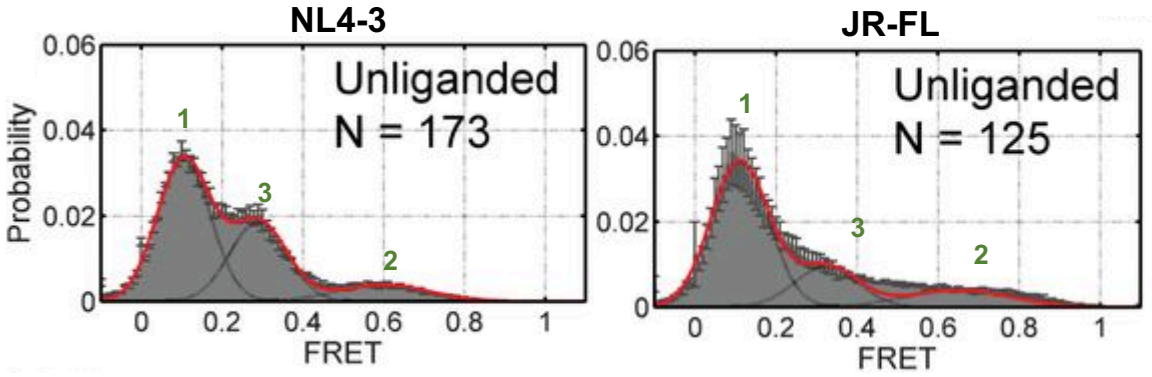

Figure 3.2. Three Env conformational states were observed using smFRET: low-FRET State 1, high-FRET State 2, and intermediate-FRET State 3. Data for strains NL4-3 (left) and JR-FL (right) are shown above.

Evaluation of the transitions between states in each of the observed Envs indicated that the Env transitions from State 1 through State 2 to State 3. State 1 – State 2 and State 2 – State 3 transitions were reversible, though State 2 transitions back to State 1 were observed less frequently. Transitions between State 1 and State 3 were only rarely observed (Figure 3.3).[1]

Assignment of these three states was then accomplished by evaluation of changes in the observed conformational dynamics upon interaction with Env ligands.

The unliganded Env predominantly occupies the low-FRET state. Moreover, mutant Envs with D368R or E370R mutations in the CD4 binding site were also observed to stabilize State 1. These mutations block access to downstream Env conformations by inhibiting formation of the bridging sheet required for CD4 binding.[7-9] Together, this enabled assignment of State 1 as the ground state of the Env. Thus, State 1 is the unliganded Env in a “closed” conformation in which the V1/V2 loop

is orientated toward the Env trimer axis perpendicular to the viral membrane.[1] As the Env "opens," the V1/V2 loops reposition closer to the gp120 outer domain.[10]

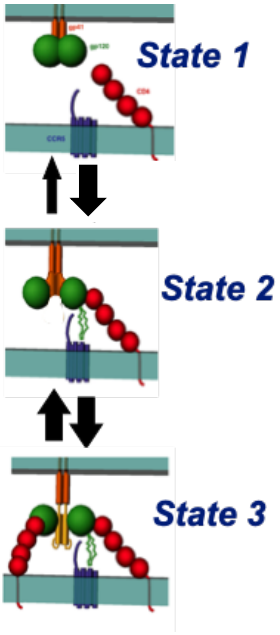

Figure 3.3 Transitions between conformational states of the Env as observed by smFRET.

A large body of experiments in which FRET-labeled Envs were exposed to a variety of ligands including antibodies and soluble CD4 led to identification of States 2 and 3.[3,6] State 2 is an asymmetric intermediate state. State 3 represents the open Env with 3-bound CD4 ligands.[3]

3.2 Changes in Conformational Dynamics on Env Ligand Binding

The closed, unliganded ground state (State 1) of the HIV-1 Env is the conformation recognized by most broadly neutralizing antibodies (bNAbs).[1] While modified trimer structures of the Env have been reported, smFRET studies by our collaborators suggest none of the existing Env crystal structures represents State 1.[18] In addition to advancing the understanding of the scientific community of the mechanism of HIV-1 viral infection, structural elucidation of the ground state (State 1) and an ability to selectively access this conformation could be a major leap in facilitating development of an HIV vaccine.

3.3 Evaluation of the impact of BMS-529 on conformations of the Env using smFRET

BMS-806 and BMS-529 developed by Bristol-Myers Squibb inhibit HIV-1 infection by blocking CD4-induced conformational changes in the Env important for viral entry (Figure 3.4).[11-14] These compounds bind gp120 in a hydrophobic pocket adjacent to the CD4 binding site.[15] For further discussion of this family of inhibitors, please refer to Chapter II.

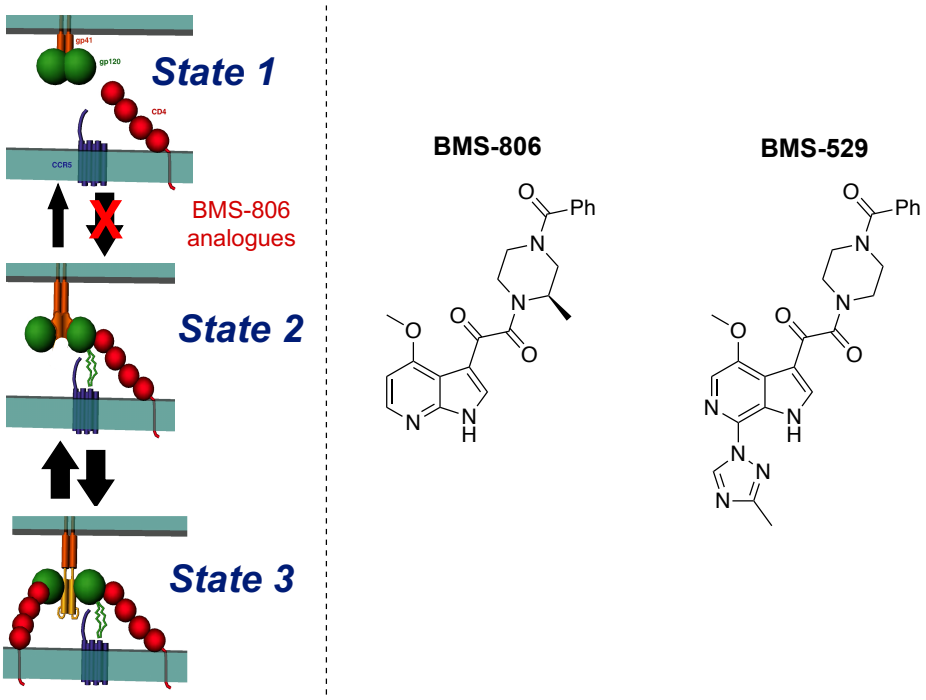

Figure 3.4 (left) Conformational states of the Env. (right) Structures of BMS-806 and BMS-529.

The smFRET studies completed by our collaborators indicated that the BMS family of conformational blockers stabilize State 1 (Figure 3.5).[1]

While these compounds are potent inhibitors of viral infection, BMS-529 and BMS-806 transiently bind the Env. It was hypothesized that appending a photoactive moiety to an analog of BMS-529 would result in covalent attachment, and consequently irreversible binding, upon UV-irradiation. This strategy was expected to covalently lock these analogs in place in the State 1 Env

and enable isolation of the covalently-bound State 1 Env. This, in turn, was expected to permit structural elucidation using cryogenic electron microscopy and mass spectrometry. The Envs covalently bound with a BMS photolabeled analog would also enable development of new antibodies, and possibly vaccines, which recognize State 1.

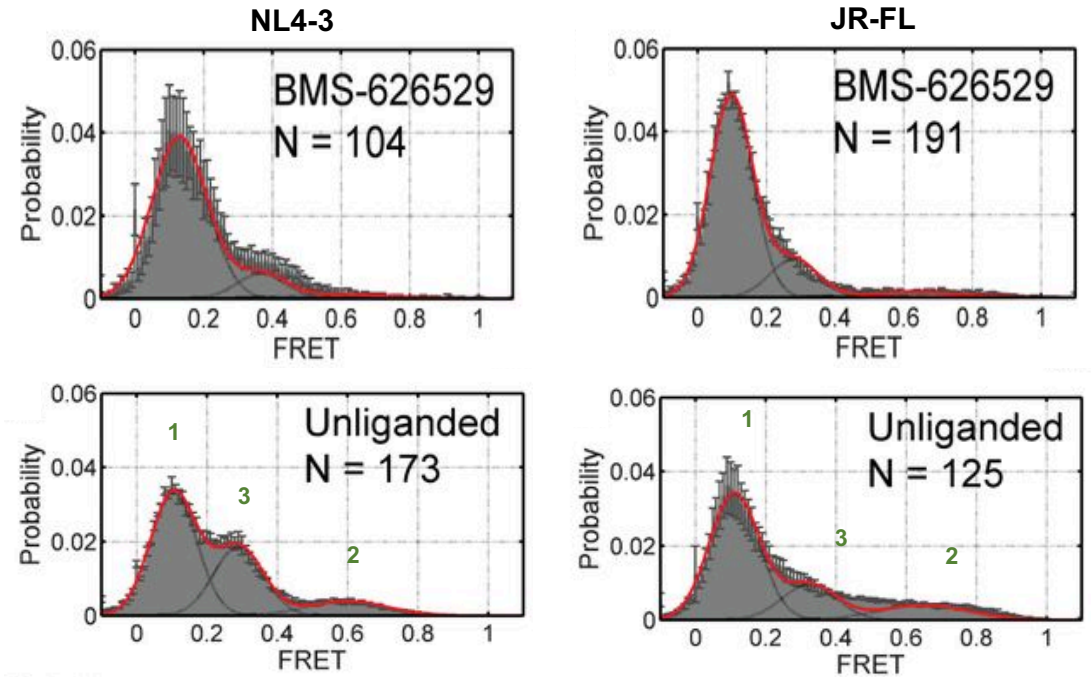

Figure 3.5 The observed FRET data from two HIV-1 strains upon exposure to BMS-806: NL4-3 (left) and JR-FL (right). The unliganded data is shown below for comparison.

3.4 Design and Synthesis of Photoaffinity Labeled BMS Analogs

BMS analogs were therefore designed and synthesized with an appended photoactive moiety. Prior efforts by Mark Farrell, a postdoctoral fellow in the Smith group, toward a photoaffinity-labeled-BMS analog resulted in **MF463** (Figure 3.6), in which a trifluoromethyl diazirine was appended to the phenyl ring of BMS-529. This compound, unfortunately, did not bind the Env.

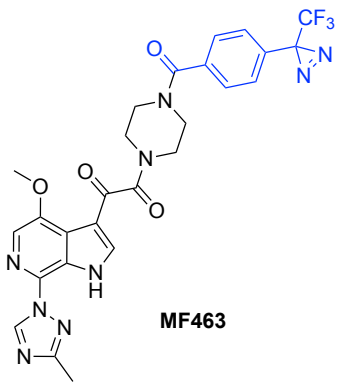

MF463

Figure 3.6. Structure of MF463.

Docking studies of MF463 completed by our computational collaborators in the Abrams Laboratory found no favorable docking conformation, suggesting that the trifluoromethyl diazirine moiety was too large to be accommodated near the Phe43 pocket toward which the aryl ring of BMS-529 projects.[17] This result inspired further docking studies to probe the regions of BMS analogs which may accommodate substitution. A summary of possible tolerated sites for substitution compiled by the Abrams Laboratory is shown in Figure 3.7.

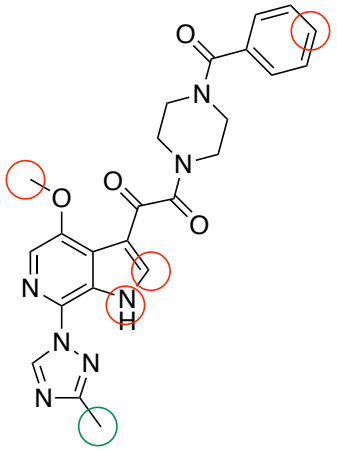

Figure 3.7 Toleration of BMS-529 substitution based on docking studies. Positions circled in green and red are expected to tolerate and not tolerate additional substitution, respectively.

Only the triazole moiety of BMS-529 was observed to tolerate additional substitution in the performed docking studies. This result is consistent with crystal structures of BMS-529 in the BG505 SOSIP trimer which indicates that the triazole moiety projects toward a solvent-exposed surface of the Env (Figure 3.8).[15] It should be noted that the Mothes Laboratory has reported that the BG505 SOSIP trimer Env represents State 2.[3] Pre-binding of the BG505 SOSIP trimer with BMS-529 was not observed to appreciably increase sampling of State 1 as evaluated by antibody binding.[3] Consequently, the binding interactions between BMS-529 and unmodified Envs are likely not represented with complete accuracy in this crystal structure.

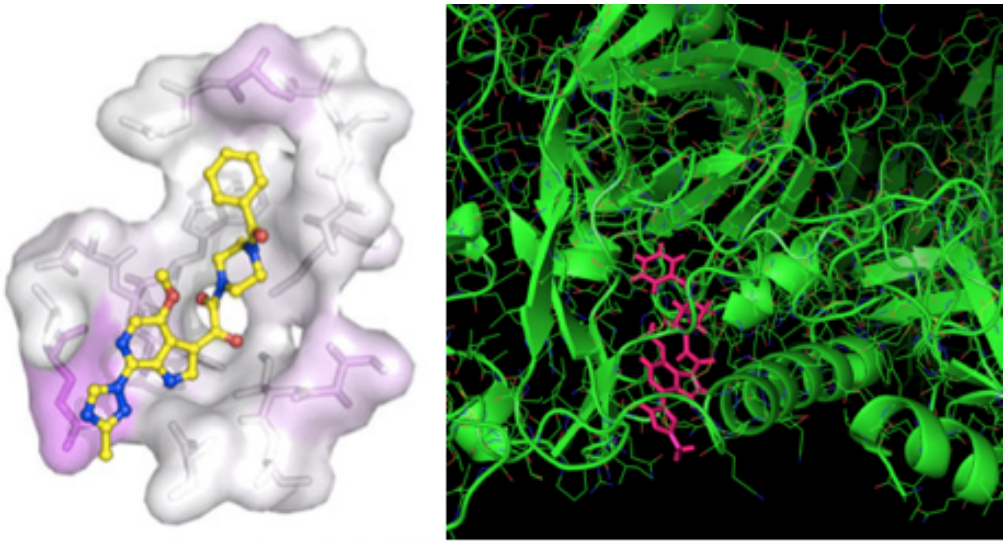

Figure 3.8. X-ray structures of BMS-529 bound to gp120.PDB: 5U7O

Docking studies of designed compound **3.1**, a proposed photoaffinity labeled compound, suggested in this case that the photoactive aryl azide moiety of **3.1** would project into an open area within the Env. In order to form a covalent linkage to the Env, amino acid residues must be present near the photoaffinity label. Encouragingly, the docked structure of **3.1** suggested the presence of many amino acids nearby the photolabile aryl azide for potential formation of a covalent linkage upon photoactivation of the photoaffinity labeled compound (Figure 3.9).

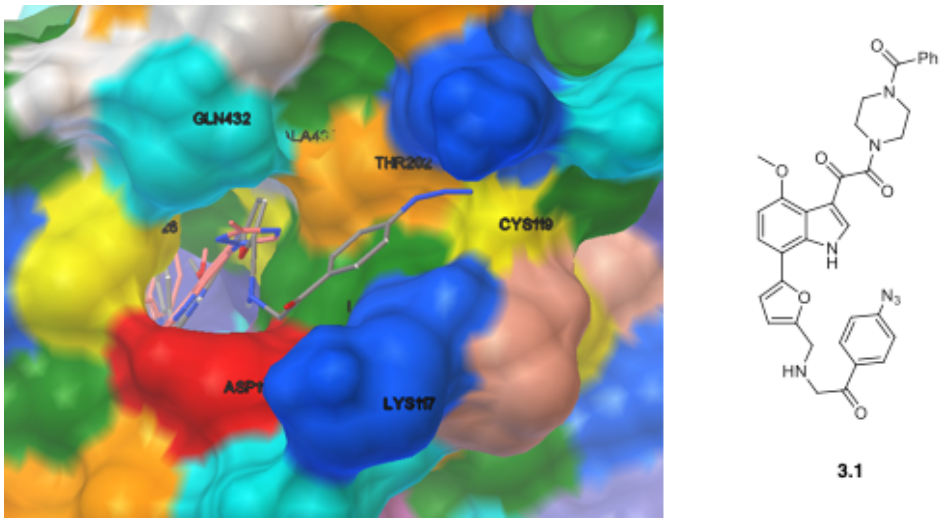

Figure 3.9. (left) Docking of 3.1 in gp120. (right) Structure of 3.1.

Building off the above docking studies, published work by Spiegel,[16] Bristol Myers Squibb,[11] and efforts making BMS-based DAVEIs described in Chapter II, incorporation of a photoaffinity probe projecting from the aza-indole of the BMS-529 or BMS-806 core toward the solvent-exposed region of gp120 was explored. For chemical attachment, the aryl trifluoromethyl diazirine and tetrafluoroaryl azide moieties were selected as photoaffinity labels based on (i) the comparatively low-energy excitation wavelengths required for photoexcitation, and (ii) the commercial availability of these compounds.

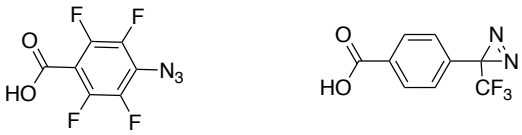

Figure 3.10. Commmercially available photoactivatable moieties. Shown are a tetrafluoroaryl azide (left) and an aryl trifluoromethyl diazirine (right).

Formation of the desired reactive intermediates from a general tetrafluorinated aryl azide and aryl trifluoromethyl diazirine moieties is shown in Figure 3.10.[17] The tetrafluorinatedaryl azides can

release nitrogen gas upon photoexcitation to generate a reactive singlet nitrene. While aryl azides without fluorination are more likely to rearrange into less reactive compounds than remain as the singlet nitrene, the preferred reaction pathway of tetrafluorinatedaryl azides should involve direct insertion of the singlet nitrene.[18] The excitation wavelength of tetrafluoroaryl azides (390 nm) is also reduced compared to other nonfluorinated aryl azides (254 – 400 nm).[18] For example, trifluoromethyl diazirines release nitrogen gas on photoexcitation to ultimately generate a reactive carbene.[19] The trifluoromethyl alpha to the diazirine protects the generated carbene from decomposition into an alkene.

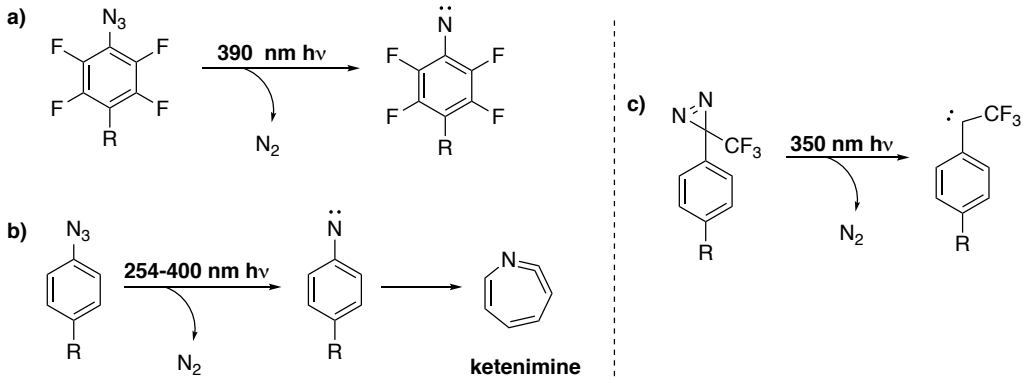

Figure 3.11. Reactive intermediates formed by photoactivation of: (**a)** a tetrafluorinated aryl azide, **(b)** an aryl azide, and **(c)** an aryl trifluoromethyl diazirine.

To incorporate these photoaffinity probes in analogs of BMS-529, BMS-analogs **AEG-II-159** with an appended aryl trifluoromethyl diazirine and **AEG-II-168** bearing a tetrafluoroaryl azide were designed as preliminary targets for photochemical cross-linking studies (Scheme I). Leveraging the common intermediate **3.2** used in the synthesis of BMS-N_3 (Chapter II), photoaffinity-labeled analogs were synthesized pleasingly with only one additional step (Figure 3). It should be noted that only photoactive groups with excitation wavelengths compatible with proteins have been selected. An unlabeled control compound **AEG-III-032** was also synthesized for comparison.

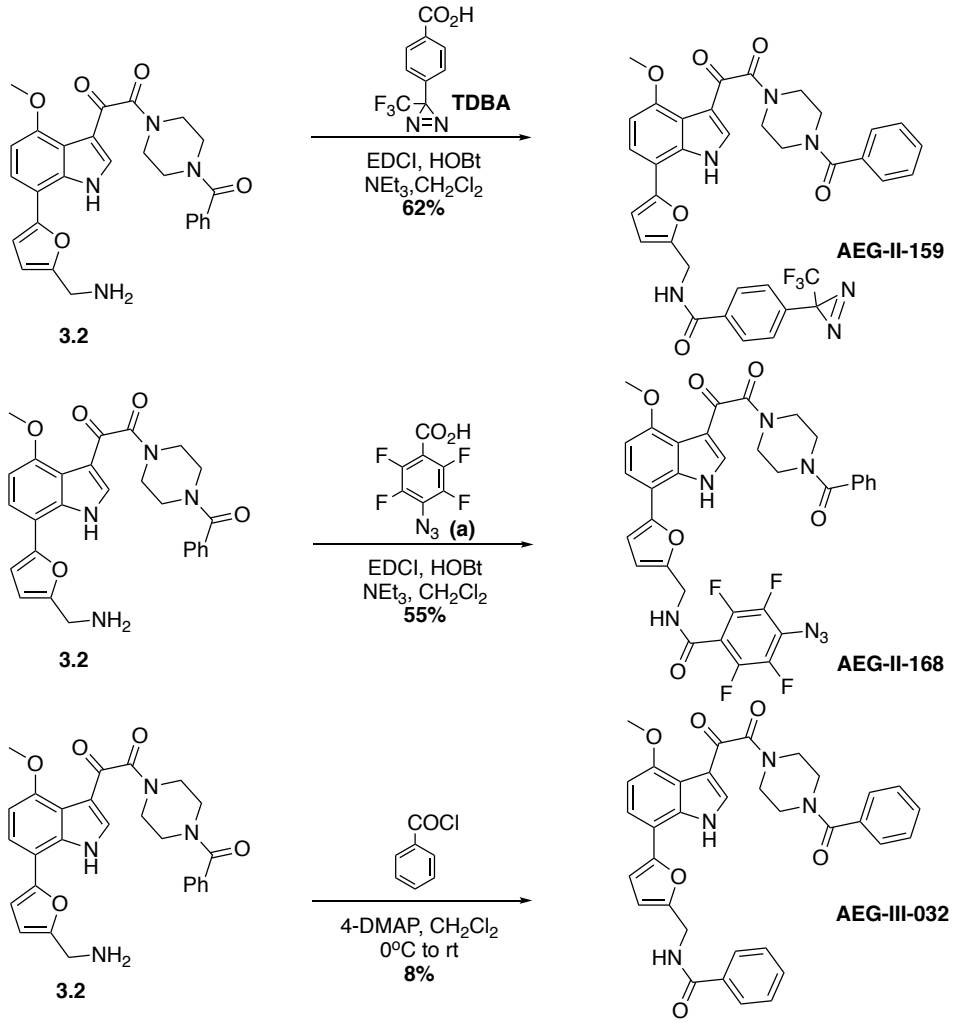

Scheme I. Synthesis and structures of photoaffinity-labeled BMS analogs.

The selected trifluoromethyl diazirine and aryl azide photoaffinity labels are reported to promiscuously form covalent linkages with nearby amino acids.[20] In this respect, the results of photoactivation could potentially be complicated by the greater number of possible interactions enabled by the conformational flexibility of **AEG-II-159** and **AEG-II-168** about the solvent-exposed surface of the Env. In an effort to limit the potential interactions of the photolabeled compound, a second generation of photoaffinity labeled BMS-529 analogs in which the photoactive moiety is

closer to the indole core were also designed and synthesized in an effort to potentially simplify analysis of covalent linkages formed (Scheme II).

As in the previous generation of photoaffinity labeled BMS analogs, compounds bearing the aryl trifluoromethyl diazirine (**AEG-III-087**) and tetrafluoroaryl azide (**AEG-III-095**) were targeted, in addition to a control compound with no photoactive component (**AEG-III-096**). To this end, glyoxamide **3.3** was constructed from 7-nitroindole (Scheme II). Deprotection of **3.3** and coupling with benzoic acid afforded **3.4**. Hydrogenation of **3.4** produced the common intermediate **3.5**. This synthetic strategy was modified from prior work by Brystol-Myers Squibb.[21]

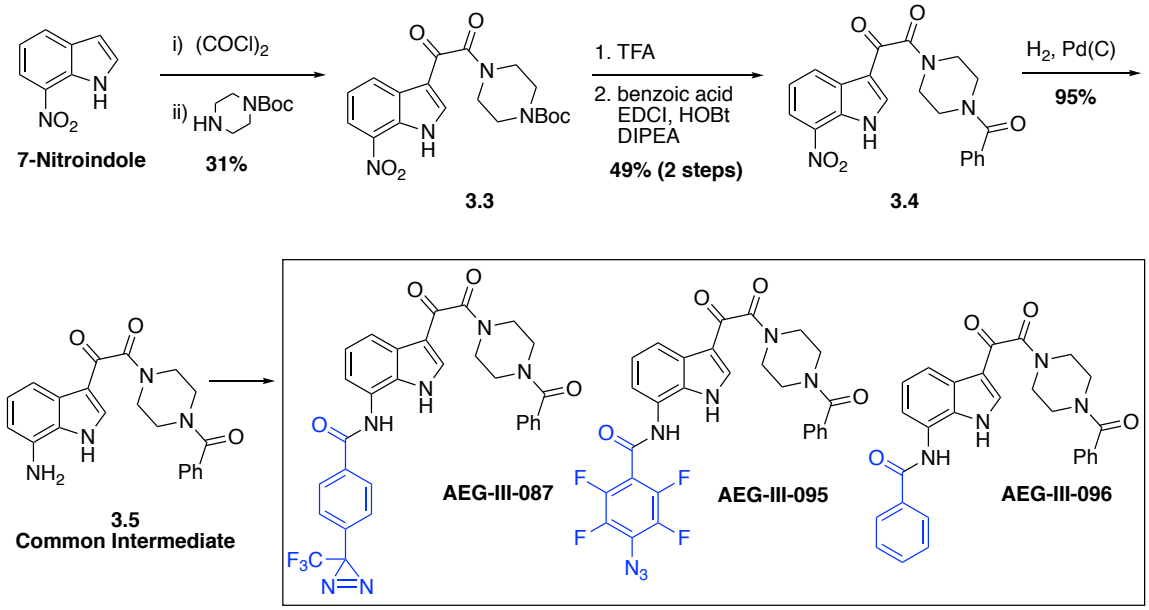

Scheme II. Synthesis and structures of truncated photoaffinity-labeled BMS analogs.

The common intermediate **3.5** was then coupled with photoaffinity labeled moieties or benzoyl chloride (Schemes III). The coupling conditions used to synthesize the first generation of photoaffinity labeled BMS analogs did not translate well for use with the amino-indole **3.5.** These reactions were sluggish and afforded poor yields. Nonetheless significant material was produced

to carry out the binding photolability experiments. If these compounds were to demonstrate promising bioactivity, the coupling conditions would warrant further investigation.

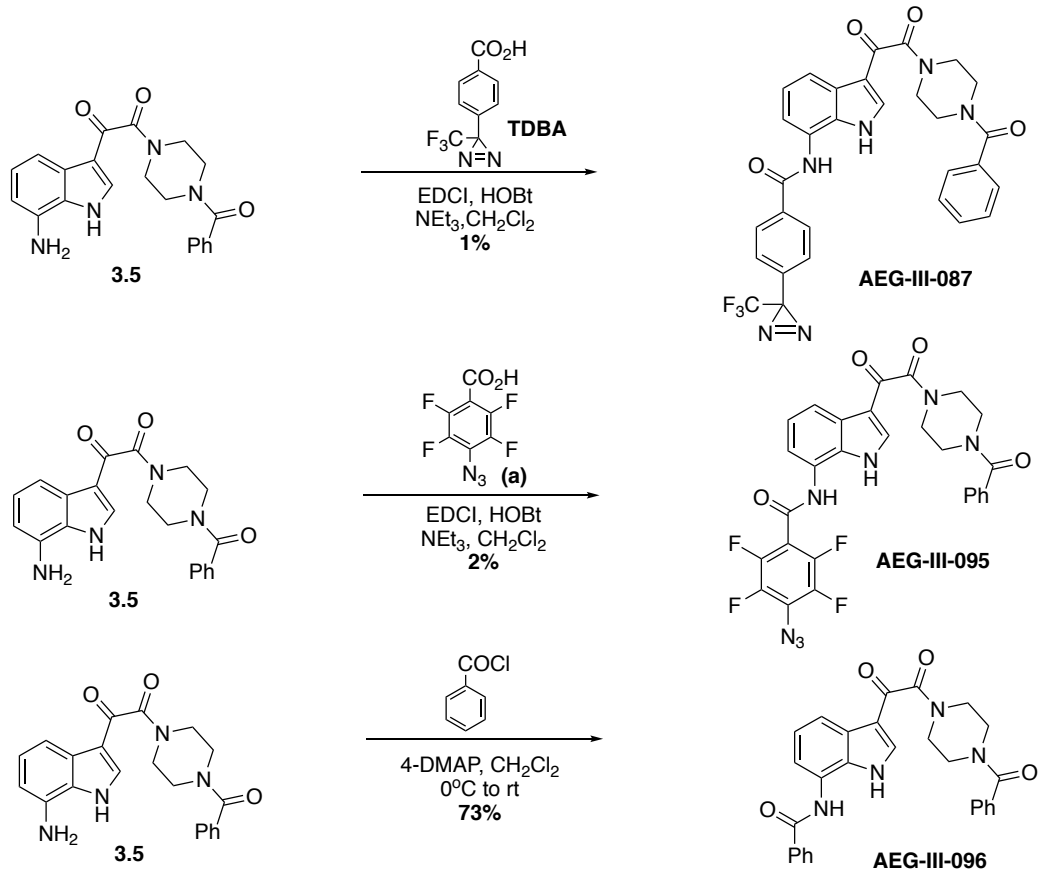

Scheme III. Synthesis of truncated photoaffinity-labled analogs from common intermediate **3.5.**

3.5 Biological Evaluation

Pleasingly, the photolabeled compounds **AEG-II-159**, **AEG-II-168**, **AEG-III-087** and the control compounds **AEG-III-032** and **AEG-III-096** were observed to inhibit HIV-1 infection with low nanomolar to picomolar potencies (Table 1). Particularly significant, **AEG-III-087** was observed to have greater potency as an infection inhibitor than BMS-529 (JR-FL IC50: 0.14 nm), the prodrug of which (Fostemsavir) is currently in Phase III clinical trials!

Table 3.1. IC_{50} (nM) of photoaffinity-labeled BMS analogs.

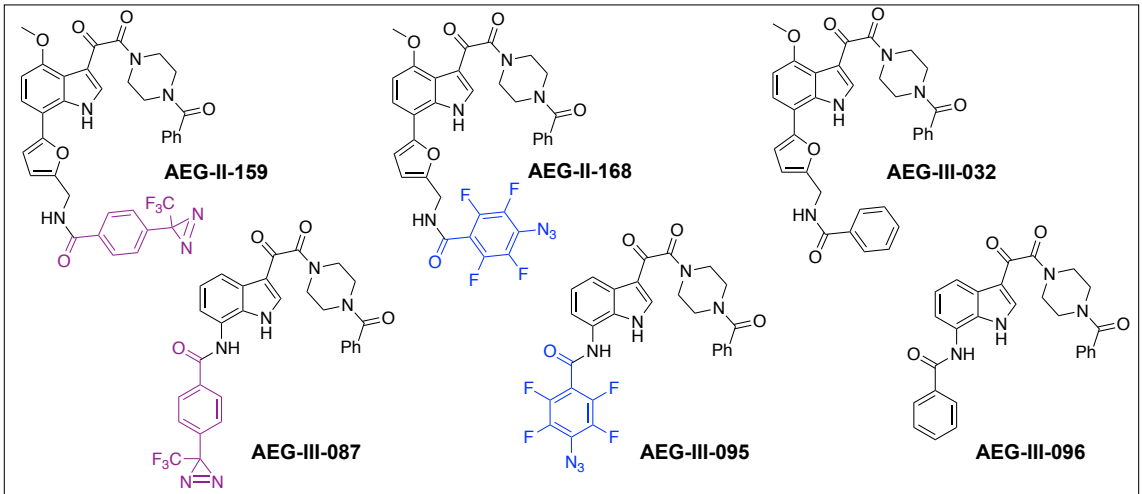

	AEG-II-159	AEG-II-168	AEG-III-032	AEG-III-087	AEG-III-095	AEG-III-096
AD8	0.2+/-0.05	2.8+/-0.1	0.36+/-0.02	0.06+/-0.02	>100	2.4+/-0.1
BG505	0.8+/-0.05	0.22+/-0.08	1.5+/-0.8	1.9+/-0.4	>100	>100
JR-FL	1.6+/-0.1	1.5+/-0.2	0.6+/-0.3	0.1+/-0.01	>100	0.9+/-0.1
JR-FL S375W	>100	>100	>100	>100	>100	>100
AMLV	>100	>100	>100	>100	>100	>100

All of the extended first generation analogs -- **AEG-II-159**, **AEG-II-168**, **AEG-III-032** -- potently inhibited the three tested strains of HIV-1. The truncated second generation trifluoromethyl diazirine **AEG-III-087** also potently inhibited the three strains of HIV. One control compound **AEG-III-096** inhibited the AD8 and JR-FL strains, but was inactive against BG505. The second generation tetrafluoromethyl azide **AEG-III-095** was not observed to have any biological activity as an inhibitor of viral infection.

The JR-FL S375W mutant HIV-1 contains an obscured Phe43 pocket, which interferes with the binding site of BMS-806 and BMS-529. The absence of activity of the photoaffinity labeled compounds in the JR-FL S375W mutant Env supports that these compounds bind in a similar

location to the parent BMS-529 binding site. These compounds also appear to be specific to HIV, as significant inhibition of the unrelated AMLV was not observed.

3.6 smFRET Evaluation of AEG-II-168

The conformational effects of **AEG-II-168** on the Env were studied using smFRET. Like the BMS compounds, **AEG-II-168** was observed to increase the presence of Envs in State 1 compared to the unliganded Env (Figure 3.12).

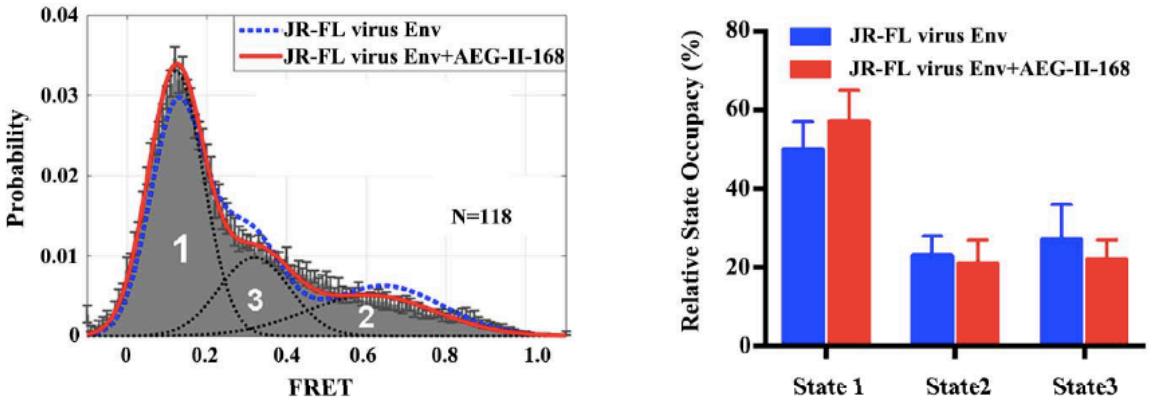

Figure 3.12. (left) FRET traces of labeled HIV-1JR-FL virus Env in the absence (blue) and presence (red) of a saturating concentration (100 μM) of AEG-II-168. (right) Relative state occupancies in the absence (blue) and presence (red) of AEG-II-168 (100 μM).

3.7 Evaluation of the Reversibility of Env Binding with Photoaffinity Labeled BMS Analogs

The conformational effects and reversibility of binding of BMS analogs have been evaluated using recognition of the Env by the 19b antibody, which selectively recognizes State 1. As BMS-806 and BMS-529 stabilize State 1, the binding of these compounds was evaluated by the level of recognition of the Env by the 19b antibody using a Western blot.

Importantly, recognition of the Env by the 19b antibody was observed to diminish in 24 hours with BMS-806, and in 2-4 days with BMS-529. However, and of considerable interest, all of the synthesized analogs were observed to bind with significant reduction in binding reversibility! The

binding effects of the control compounds without photoaffinity labels, as with BMS-806 and BMS-529, only lasted a week or less. Surprisingly, in the absence of UV irradiation, the effects of the photoaffinity labeled compounds were also observed for 3 weeks!

These binding effects lead to considerable perplexity! The binding behavior of these compounds appears to be minimally dependent on exposure to UV light. Interestingly, UV irradiation of Envs incubated with **AEG-II-168** resulted in increased recognition by bNAbs. This effect was not observed, however, with **AEG-III-087** or **AEG-III-095**.

While analysis by mass spectrometry did not identify any specific cross-linking interactions, there is evidence to suggest cross-linking has occurred. BMS-529, BMS-806 and the photoaffinity labeled compounds stabilize the gp120-gp41 dimer and reduce gp120 shedding, which occurs during the infection pathway (see Chapter I). Binding of the photoaffinity labeled compounds increased the amount of gp160 observed. Also observed were new masses which are thought to represent gp120-gp120 linkage and gp120-gp120-gp41 linkage. Structure elucidation by our collaborators is currently underway.

A manuscript describing this work, “Long-Acting BMS378806 Analogues Stabilize the State-1 Conformation of the Human Immunodeficiency Virus (HIV-1) Envelope Glycoproteins” has been submitted to *Nature Communications*.

The encouraging early biological results of the photolabeled BMS analogs clearly warrant further investigation of the reactivity of these BMS analogs in the future.

3.8 References

(1) Munro, J. B.; Gorman, J.; Ma, X.; Zhou, Z.; Arthos, J.; Burton, D.R.; Koff, W.C.; Courter, J.R.; Smith, A.B., III; Kwong, P.D.; Blanchard, S.C.; Mothes, W. *Science* **2014**, *346*, 759.

(2) Roy, R.; Hohng, S.; Ha, T. *Nature Methods*. **2008**, 507.

(3) Lu, M.; Ma, X.; Castillo-Menendez, L. R.; Gorman, J.; Alsahafi, N.; Ermel, U.; Terry, D. S.; Chambers, M.; Peng, D.; Zhang, B.; Zhou, T.; Reichard, N.; Wang, K.; Grover, J. R.; Carman, B. P.; Gardner, M. R.; Nikić-Spiegel, I.; Sugawara, A.; Arthos, J.; Lemke, E. A.; Smith, A. B.; Farzan, M.; Abrams, C.; Munro, J. B.; McDermott, A. B.; Finzi, A.; Kwong, P. D.; Blanchard, S. C.; Sodroski, J. G.; Mothes, W. *Nature* **2019**, *568* (7752), 415–419.

(4) Zhou, Z.; Cironi, P.; Lin, A. J.; Xu, Y.; Hrvatin, S.; Golan, D. E.; Silver, P. A.; Walsh, C. T.; Yin, J. *ACS Chem. Biol.* **2007**.

(5) Lin, C. W.; Ting, A. Y. *J. Am. Chem. Soc.* **2006**, *128*(14), 4542.

(6) Ma, X.; Lu, M.; Gorman, J.; Terry, D. S.; Hong, X.; Zhou, Z.; Zhao, H.; Altman, R. B.; Arthos, J.; Blanchard, S. C.; Kwong, P. D.; Munro, J. B.; Mothes, W. *Elife* **2018**, *7*, 1.

(7) Kwong, P. D.; Wyatt, R.; Robinson, J.; Sweet, R. W.; Sodroski, J.; Hendrickson, W. a. *Nature* **1998**, *393*, 648.

(8) Wu, S. R.; Löving, R.; Lindqvist, B.; Hebert, H.; Koeck, P. J. B.; Sjöberg, M.; Garoff, H. *Proc. Natl. Acad. Sci. U. S. A.* **2010,** *107*(44), 1844.

(9) Olshevsky, U.; Helseth, E.; Furman, C.; Li, J.; Haseltine, W.; Sodroski, J. *J. Virol.* **1990**, *64*(12), 5701.

(10) Henzler-Wildman, K.; Kern, D. *Nature*. **2007**, *450*(7172), 964.

(11) Meanwell, N. A.; Krystal, M. R.; Nowicka-sans, B.; Langley, D. R.; Conlon, D. A.; Eastgate, M. D.; Grasela, D. M.; Timmins, P.; Wang, T.; Kadow, J. F. *J. Med. Chem.* **2018**, *61* (1), 62–80.

(12) Si, Z.; Madani, N.; Cox, J. M.; Chruma, J. J.; Klein, J. C.; Schön, A.; Phan, N.; Wang, L.; Biorn, A. C.; Cocklin, S.; Chaiken, I.; Freire, E.; Smith, A. B.; Sodroski, J. G. *Proc. Natl. Acad. Sci. U. S. A.* **2004**.

(13) Ho, H.-T.; Fan, L.; Nowicka-Sans, B.; McAuliffe, B.; Li, C.-B.; Yamanaka, G.; Zhou, N.; Fang, H.; Dicker, I.; Dalterio, R.; Gong, Y.-F.; Wang, T.; Yin, Z.; Ueda, Y.; Matiskella, J.; Kadow, J.; Clapham, P.; Robinson, J.; Colonno, R.; Lin, P.-F. *J. Virol.* **2006**,*80*(8) 4017.

(14) Herschhorn, A.; Gu, C.; Espy, N.; Richard, J.; Finzi, A.; Sodroski, J. G. *Nat. Chem. Biol.* **2014**, *10* (10), 845.

(15) Pancera, M.; Lai, Y.; Bylund, T.; Druz, A.; Narpala, S.; Dell, S. O.; Schön, A.; Bailer, R. T.; Chuang, G.; Geng, H.; Louder, M. K.; Rawi, R.; Soumana, D. I.; Finzi, A.; Herschhorn, A.; Madani, N.; Sodroski, J.; Freire, E.; Langley, D. R.; Mascola, J. R.; Mcdermott, A. B.; Kwong, P. D. *Nat. Publ. Gr.* **2017**, *13* (10), 1115.

(16) Douglass, E. F.; Shoda, T.; Jawanda, N.; Spasov, K. A.; Lee, S.; Zhou, N.; Domaoal, R. A.; Sutton, R. E.; Anderson, K. S.; Krystal, M.; Jorgensen, L.; Spiegel, D. A. *Chem. Sci.* **2014**, 2311–2317.

(17) Murale, D. P.; Hong, S. C.; Haque, M. M.; Lee, J. S. *Proteome Science*. **2017**, *15*, 14.

(18) Preston, G. W.; Wilson, A. J. *Chem. Soc. Rev.* **2013**, *42*(8), 3289.

(19) Platz, M. S. *Acc. Chem. Res.* **1995**, *28* (12), 487.

(20) Xu, H.; Hett, E. C.; Gopalsamy, A.; Parikh, M. D.; Geoghegan, K. F.; Kyne, R. E.; Menard, C. A.; Narayanan, A.; Robinson, R. P.; Johnson, D. S.; Tones, M. A.; Jones, L. H. *Mol. Biosyst.* **2015**, *11*(10), 2709.

(21) Wang, Tao; Zhang, Zhongxing; Yin, Zhiwei; Kadow, John F.; Meanwell, N. A. Indolyl- and azaindolyloxoacetylpiperazines and related compounds and their preparation and use for the treatment of HIV infection. WO 2012019003, 2012.

CHAPTER FOUR: EXPERIMENTAL PROCUEDURES AND SPECTROSCOPIC DATA

4.1 General Considerations

Microwave heating was conducted with a Biotage Initiator system equipped with an autosampling arm, using 20-mL sealed reaction vials. Reactions were magnetically stirred under a nitrogen atmosphere, unless otherwise noted and reactions were monitored by either thin layer chromatography (TLC) with 0.25 mm E. Merck pre-coated silica gel plates or liquid chromatography mass spectrometry (LCMS). Optical rotations were measured on a JASCO P-2000 polarimeter. Proton (1 H) and carbon (13C) NMR spectra were recorded on a Bruker Avance III 500-MHz spectrometer or on a Bruker DRX500 500-MHz spectrometer. Chemical shifts (δ) are reported in parts per million (ppm) relative to chloroform (δ 7.26) for 1 H NMR, and (δ 77.0) for 13C NMR. Infrared spectra were recorded using a JASCO 480-Plus FT-IR spectrometer, or a Perkin-Elmer Spectrum Two FT-IR spectrometer. Accurate mass measurement data were acquired on Waters Instruments. Waters software calibrates and reports by use of neutral atomic masses. The mass of the electron is not included. Preparative scale HPLC was pre-formed with a Gilson 333/334 preparative pump system equipped with a 5 mL injection loop, Sunfire C18 OBD column (5 µm packing material, 19 x 100 mm column dimensions) equipped with a UV-Vis dual wavelength (210 and 254 nm) detector and 215 liquid handling module. Solvent systems were comprised of H2O containing 0.1% trifluoroacetic acid, and acetonitrile containing 0.1% trifluoroacetic acid. Lyophilization was performed in a Labconco FreeZone 12 Plus lyophilizer (0.035 mbar). Peptides were synthesized on a Liberty Blue microwave peptide synthesizer (CEM Corporation, NC) and purified by HPLC. The purity of new compounds was judged by either NMR or LC/MS. For LCMS, purity of peptides and small molecule-peptide DAVEI constructs were evaluated using a Waters Acquity UPLC, HSS C18 1.8 mm, 5-95% acetonitrile/water + 0.1% TFA gradient over either 2 min or 10 min. UV absorbance traces are at 254 nm.

4.2 Experimental Procedures and Spectroscopic Related to Chapter One

4.2.1 Synthesis of Common Intermediate **10**

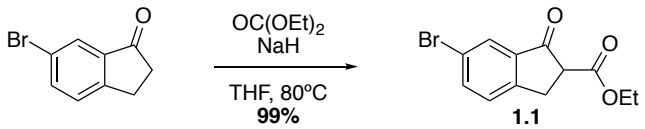

α-ketoester **1.1**. To a mixture of NaH (0.684 g, 17.1 mmol, 2.2 eq., 60% in mineral oil) in diethyl carbonate (5.65 mL, 46.6 mmol, 6 eq.) in a round bottom flask equipped with reflux a condenser under nitrogen gas at room temperature was added a solution of 6-bromoindanone (1.64 g, 7.77 mmol) in THF (13 mL). The reaction mixture was gradually warmed to 80 °C over 45 minutes. After another 2 hours the reaction was quenched with water. The reaction mixture was acidified to pH 2 with 1M aqueous HCl. This mixture was diluted with ethyl acetate and the layers were separated. The aqueous layer was washed with ethyl acetate (2 x 50 mL). The organic layers were combined, dried over sodium sulfate, decanted, and concentrated. Flash column chromatography (SiO_2, 100% hexanes to 25% ethyl acetate/hexanes) afforded a red solid (2.18 g, 99%).

^{1}H NMR (500 MHz, $CDCl_3$) 1:0.5 mixture of tautomers. δ 10.31 (br. s, 0.5 H), 7.89 (s, 1 H), 7.77 (s, 1 H), 7.72 (d, *J* = 8.1 Hz, 1 H), 7.52 (d, *J* = 8.1 Hz, 0.5 H), 7.39 (d, *J* = 8.1 Hz, 1 H), 7.32 (d, *J* = 8.1 Hz, 0.5 H), 4.33 (q, *J* = 7.1 Hz, 1 H), 4.25 (q, *J* = 7.1 Hz, 2 H), 3.74 (dd, *J* = 4.0, 8.2 Hz, 1 H), 3.50 (dd, *J* = 4.0, 17.4 Hz, 2 H), 3.32 (dd, *J* = 8.3, 17.4 Hz, 1 H), 1.38 (t, *J* = 7.1 Hz, 1.5 H), 1.31 (t, *J* = 7.1 Hz, 3 H).

^{13}C NMR (500 MHz, $CDCl_3$): δ 198.2, 168.8, 152.3, 141.8, 139.1, 138.3, 137.2, 132.2, 128.2, 127.6, 126.3, 123.9, 122.1, 120.9, 104.0, 62.1, 60.5, 53.7, 32.5, 30.1, 14.6, 14.3

IR υ_{max} 3379, 2922, 2845, 2300, 1564, 1399, 1108, 803

AMM (ESI) *m/z* 281.9892 [calcd for $C_{12}H_{11}BrO_3$ $(M+H)^+$ 281.98916]

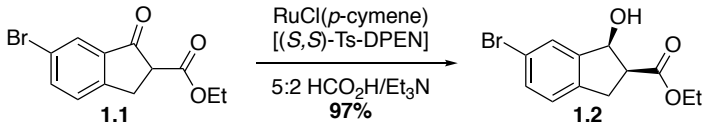

α-hydroxyester **1.1**. To a solution of **1.1** (1.19 g, 4.22 mol) and RuCl(*p*-cymene)[(*S,S*)-Ts-DPEN] (0.0537 g, 0.0843 mmol, 0.02 eq.) in dichloromethane (4.0 mL, 1.0 M) under nitrogen at room temperature was added 5:2 formic acid/triethylamine (1.2 mL). After three days, the reaction mixture was diluted with dichloromethane and water. The layers were separated and the aqueous layer was washed three times with dichloromethane. The organic layers were combined, dried with sodium sulfate, decanted and concentrated. The crude product mixture was purified using flash column chromatography (SiO2, 100% hexanes to 20% ethyl acetate/hexanes) to afford a yellow solid (1.16 g, 97%).

^{1}H NMR (500 MHz, $CDCl_3$) δ 7.55 (s, 1 H), 7.40 (d, *J* = 8.0 Hz, 1 H), 7.13 (d, *J* = 7.7 Hz, 1 H), 5.29 (d, *J* = 5.8 Hz, 1 H), 4.22 (q, *J* = 7.1 Hz, 2 H), 3.35 (m, 2H), 3.04 (dd, *J* = 7.1, 14.9 Hz, 1 H), 1.31 (t, *J* = 7.0 Hz, 3 H).

^{13}C NMR (500 MHz, $CDCl_3$): δ 172.9, 145.1, 140.7, 132.1, 128.3, 126.5, 120.8, 75.6, 61.2, 49.6, 32.7, 14.4.

IR υ_{max} 3409, 2917, 2843, 2362, 2350, 2335, 1365

AMM (ESI) *m/z* 284.0048 [calcd for $C_{12}H_{13}BrO_3$ $(M+H)^+$ 284.00481]

$[\alpha]_D^{23}$ = - 1 ° (*c*, 2.2 CH_2Cl_2)

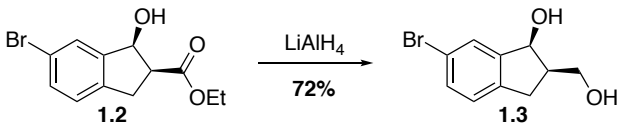

Diol **1.3**. To a solution of **1.3** (0.501 g, 1.76 mmol) in tetrahydrofuran (8.8 mL, 0.2 M) at 0 °C was added lithium aluminum hydride (0.100 g, 2.63 mmol, 1.5 eq.) in 5 equal aliquots in 5 minute intervals. After one hour the reaction was quenched at 0 °C with water, then saturated aqueous sodium potassium tartrate. The biphasic mixture was allowed to stir at room temperature for 30 minutes. The mixture was diluted with ethyl acetate and the layers were separated. The aqueous layer was washed three times with ethyl acetate. The organic layers were combined, dried over sodium sulfate, decanted, and concentrated. Flash column chromatography (SiO_2, 20% ethyl acetate / hexanes to 10% methanol / ethyl acetate) to afford the desired product (0.309 g, 72%).

^{1}H NMR (500 MHz, $CDCl_3$) δ 7.55 (s, 1 H), 7.40 (dd, *J* = 1.9, 8.0 Hz, 1 H), 7.13 (d, *J* = 8.0 Hz, 1 H), 5.31 (d, *J* = 5.9 Hz, 1 H), 3.93 (m, 2 H), 2.88 (m, 2 H), 2.75 (m, 1 H).

^{13}C NMR (500 MHz, $CDCl_3$): δ 146.4, 141.8, 131.9, 128.0, 126.7, 120.5, 77.2, 63.0, 45.4, 32.5

IR υ_{max} 3386, 2910, 2844, 2361, 2340, 1655, 1548

AMM (ESI) *m/z* 241.9640 [calcd for $C_{10}H_{11}BrO_2$ $(M+H)^+$ 241.99424]

$[\alpha]_D^{23}$ = + 41 ° (*c* 0.2, CH_2Cl_2)

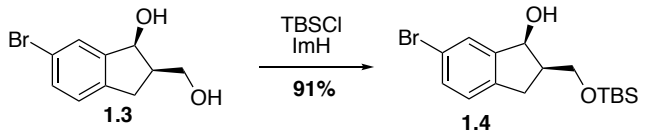

Alcohol **1.4**. To a solution of **1.3** (1.08 g, 4.44 mmol) in dichloromethane (44 mL, 0.1 M) under nitrogen at 0 °C was added imidazole (0.605 g, 8.88 mmol, 1.2 eq.) then TBSCl (0.803 g, 5.33 mmol, 1.2 eq.). After 1.5 hours, the reaction was quenched with water and diluted with dichloromethane. The layers were separated. The aqueous layer was washed three times with dichloromethane. The organic layers were combined, dried over sodium sulfate, decanted, and concentrated. Flash column chromatography (SiO_2, 100% hexanes to 10% ethyl acetate / hexanes) to afford the desired product as an oil (1.45 g, 91%).

^{1}H NMR (500 MHz, $CDCl_3$) δ 7.55 (s, 1 H), 7.35 (d, 1 H, *J* = 8.0 Hz), 7.08 (d, 1 H, *J* = 8.0 Hz), 5.25 (d, 1 H, *J* = 6.5 Hz), 3.96 (dd, 1 H, *J* = 7.0, 10.4 Hz), 3.37 (br s, 1 H), 2.88 (dd, 1 H, *J* = 8.1, 16.0 Hz), 2.77 (dd, 1 H, *J* = 6.1, 16.0 Hz), 2.70 (m, 1 H), 0.87 (s, 9 H), 0.10 (s, 3 H), 0.06 (s, 3 H).

^{13}C NMR (500 MHz, $CDCl_3$): δ 147.2, 141.3, 131.3, 128.1, 126.4, 120.4, 77.1, 63.7, 45.1, 33.0, 29.8, 25.9, 18.2, -5.4, -5.5

IR υ_{max} 3414.35, 2955.38, 2921.63, 2850.27, 2362.37, 2335.37, 1470.46, 1254.47, 1168.65, 1089.58

AMM (ESI) *m/z* 355.0758 obs. $C_{16}H_{23}BrO_2Si$ [356.0807 calcd for $C_{16}H_{25}BrO_2Si$ $(M+H)^+$]

$[\alpha]_D^{23}$ = - 16 ° (*c* 0.07, CH_2Cl_2)

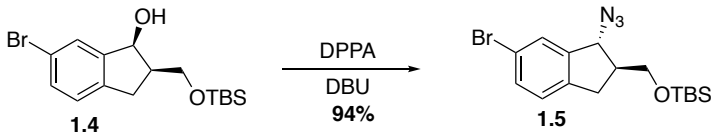

Azide **1.5**. To a solution of **1.5** (4.64 g, 13.0 mmol) in toluene under nitrogen at room temperature was added diphenylphosphoryl azide (5.6 mL, 26.0 mmol, 2 eq.). After ten minutes 1,8-diazabicyclo[5.4.0]undec-7-ene (5.4 mL, 36.4 mmol, 2.8 eq.). The reaction mixture was then warmed to 85 °C and allowed to proceed overnight. The heating bath was removed and the reaction was quenched with water. The crude reaction mixture was diluted with water and ethyl acetate. The layers were separated and the aqueous layer was washed four times with ethyl acetate. The organic layers were combined, dried over sodium sulfate, decanted, and concentrated. Flash column chromatography (SiO_2, 10% to 15 ethyl acetate / hexanes) to afford the desired product as an oil (4.69 g, 94%).

^{1}H NMR (500 MHz, $CDCl_3$) δ 7.51 (s, 1 H) 7.40 (d, 1 H, *J* = 8.1 Hz), 7.11 (d, 1 H, *J* = 8.4 Hz), 4.74 (d, 1 H, *J* = 6.0 Hz), 3.81 (dd, 1 H, *J* = 5.1, 10.3 Hz), 3.67 (dd, 1 H, *J* = 5.9, 10.3 Hz), 2.69 (dd, 1 H, *J* = 7.0, 15.8 Hz), 2.63 (m, 1 H), 0.91 (s, 9 H), 0.09 (overlapping s, 3 H), 0.08 (overlapping s, 3 H).

^{13}C NMR (500 MHz, $CDCl_3$): δ 143.0, 141.4, 131.8, 128.0, 126.7, 120.6, 61.7, 63.38, 49.7, 32.9, 26.0, -5.3

IR υ_{max} 2928, 2857, 2359, 2095, 1472, 1388, 1252, 1113, 984, 837, 777, 668

AMM(ESI)**:** sample did not ionize.

[α]$_D^{23}$ = - 40 ° (*c* 0.22, CH_2Cl_2)

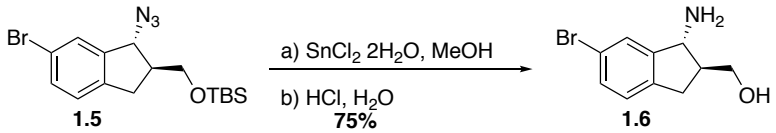

Aminol **1.6**. To a solution of **1.5** (3.32 g, 8.69 mmol) in methanol (29 mL, 0.3 M) under nitrogen at 0 °C was added tin chloride dihydrage (3.92 g, 17.4 mmol, 2 eq.). The reaction was allowed to proceed overnight. To the reaction mixture was then added 1 M aqueous HCl (15 mL). After five hours no starting material was observed. The pH of the reaction mixture was adjusted to 12 with 1 M aqueous NaOH. This solution was diluted with ethyl acetate and brine. The layers were sparated. The aqueous layer was washed three times with ethyl acetate. The organic layers were combined, dried with magnesium sulfate, decanted and concentrated to afford the product (1.59 g, 75%).

^{1}H NMR (500 MHz, DMSO): δ 7.48 (s, 1 H), 7.30 (d, 1 H, *J* = 8.0 Hz), 7.12 (d, 1 H, *J* = 7.9 Hz), 3.93 (d, 1 H, *J* = 8.5 Hz), 3.66 (dd, 1 H, 5.1, 10.6 Hz), 3.58 (dd, 1 H, *J* = 6.2, 10.6 Hz), 2.84 (dd, 1 H, *J* = 8.1, 16.0 Hz), 2.54 (partially obscured dd, 1 H, *J* = 9.5, 16.0 Hz), 2.10 (m, 1 H).

^{13}C NMR (500 MHz, DMSO): δ 151.8, 141.5, 129.9, 127.3, 127.0, 119.7, 62.8, 59.3, 54.0.

IR υ_{max} 3393, 2945, 2843, 2369, 2329, 1659, 1420, 1375, 1247, 1127

AMM(ESI) *m/z* 242.0204 [calcd for $C_{10}H_{12}BrNO$ $(M+H)^+$ 242.0181]

[α]$_D^{23}$ = + 1 ° (*c* 0.18, CH_2Cl_2)

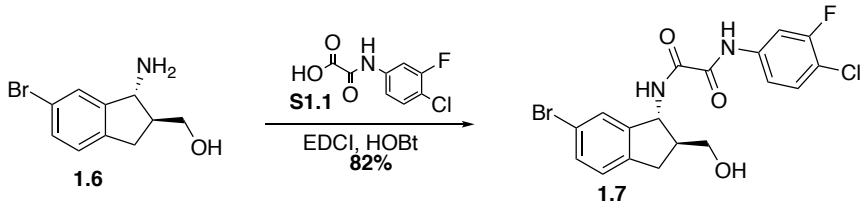

Alcohol **1.7**. To a solution of **1.6** (0.643 g, 2.65 mmol) in **S1.1** (0.693 g, 3.18 mmol, 1.2 eq.) in dimethylformamide (6.6 mL, 0.5 M) at 0 C under nitrogen was added EDCI hydrochloride (0.978 g,

6.36 mmol, 2.4 eq.) and hydroxybenzotriazole hydrate (1.22 g, 6.36 mmol, 2.4 eq.). After five minutes triethylamine was added (1.3 mL, 6.36 mmol, 2.4 eq.) and the reaction was allowed to proceed overnight. The reaction mixture was quenched with saturated aqueous sodium bicarbonate. The reaction mixture was diluted with water and ethyl acetate. The layers were separated and the aqueous layer was washed with ethyl acetate. The aqueous layer was adjusted to pH 9 with 1 M aqueous sodium hydroxide and washed twice with ethyl acetate. The organic layers were combined, dried with magnesium sulfate, and decanted. The organic layer was loaded onto celite and the product was purified with a silica gel plug (50% ethyl acetate / hexanes to 10% methanol / ethyl acetate) to afford the product as a white solid (0.763 g, 65%).

^{1}H NMR (500 MHz, DMSO): δ 11.06 (s, 1 H), 9.42 (d, 1 H, *J* = 8.7 Hz), 7.97 (dd, 1 H, *J* =2.3, 11.8 Hz), 7.75 (app. d, 1 H, *J* = 8.8 Hz), 7.60 (t, 1 H, *J* = 8.7 Hz), 7.39 (app. d, 1 H, *J* = 7.6 Hz), 7.32 (s, 1 H), 7.21 (d, 1 H, *J* = 8.0 Hz), 5.22 (t, 1 H, *J* = 8.4 Hz), 4.75 (t, 1 H, *J* = 5.0 Hz), 3.54 (m, 2 H), 3.00 (m, 1 H), 2.70 (m, 2 H).

^{13}C NMR (500 MHz, DMSO): δ 160.6, 159.5, 157.4 (d, J_{CF} = 244 Hz), 156.4, 146.5, 142.3, 139.0 (d, J_{CF} = 10 Hz), 131.2, 130.9, 127.4, 127.2, 119.7, 118.0 (d, J_{CF} = 3 Hz), 114.9 (d, J_{CF} = 17 Hz), 109.1 (d, J_{CF} = 26 Hz), 62.1, 56.5, 49.1, 33.5.

IR υ_{max} 3372, 3258, 2919, 2367, 1660, 1515, 1060, 956, 674, 441, 426

AMM(ESI) *m/z* 441.0021 [calcd for $C_{18}H_{15}BrClFN_2O_3$ $(M+H)^+$ 441.0017]

[α]$_D^{23}$ = + 16 ° (*c* 0.26, CH_2Cl_2)

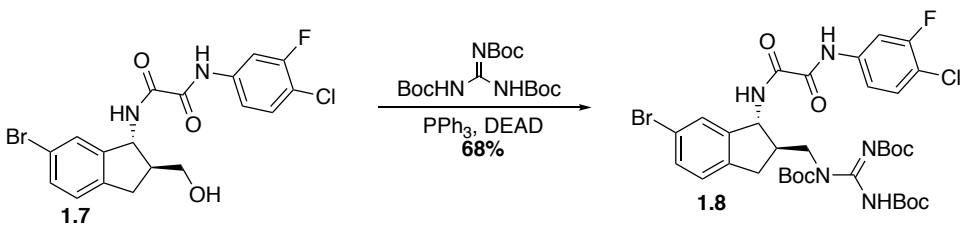

Bromide **1.8**. To a solution of alcohol **1.8** (0.180 g, 0.407 mmol) and triphenylphosphine (0.427 g, 1.63 mmol, 4 eq.) in tetrahydrofuran (15 mL, 0.02 M) under nitrogen at room temperature was added tribocguanidine (0.242 g, 0.403 mmol, 0.99 eq.). To this mixture was slowly added diethyl azodicarboxylate (0.43 mL, 1.63 mmol, 4 eq.) and the reaction was allowed to proceed overnight. The reaction was quenched with aqueous sodium bicarbonate and diluted with ethyl acetate and water. The layers were separated and the aqueous layer was washed three times with ethyl acetate. The organic layers were combined, dried with sodium sulfate, decanted and concentrated. The crude reaction mixture was purified using flash column chromatography (SiO_2, dry loading on celite, 10% ethyl acetate / hexanes) to afford a white solid (0.108 g, 68%)

^{1}H NMR (500 MHz, $CDCl_3$): δ 10.61 (br s, 1 H), 9.38 (s, 1 H), 7.89 (d, 1 H, J = 9.0 Hz), 7.76 (dd, 1 H, J = 2.4, 10.6 Hz), 7.37 (m, 2 H), 7.33 (s, 1 H), 7.27 (m, 1 H), 7.11 (d, 1 H, J = 8.7 Hz), 5.24 (t, 1 H, J = 8.1 Hz), 4.13 (m, 2 H), 3.14 (dd, 1 H, J = 7.9, 15.8 Hz), 2.91 (m, 1 H), 2.74 (dd, 1 H, J = 9.0, 15.8 Hz), 1.51 (m, 27 H).

^{13}C NMR (500 MHz, $CDCl_3$): δ 159.74, 158.2 (d, J_{CF} = 248 Hz), 157.32, 153.39, 153.25, 143.64, 140.81, 136.5 (d, J_{CF} = 9.6 Hz), 131.52, 130.94, 127.20, 126.55, 120.70, 117.2 (d, J_{CF} = 18.1 Hz), 116.04 (d, J_{CF} = 3.5 Hz), 108.59 (d, J_{CF} = 26.1 Hz), 83.79, 58.44, 49.78, 48.12, 34.72, 29.84, 28.38, 28.19, 28.16, 28.13, 28.09, 27.96.

IR υ_{max} 3277, 2972, 2927, 2852, 2360, 1762, 1664, 1610, 1517, 1251, 1148, 664

AMM(ESI) *m/z* 782.1984 [calcd for $C_{34}H_{42}BrClFN_5O_8$ $(M+H)^+$ 782.1968]

[α]$_D^{23}$ = + 15 ° (*c* 0.4, CH_2Cl_2)

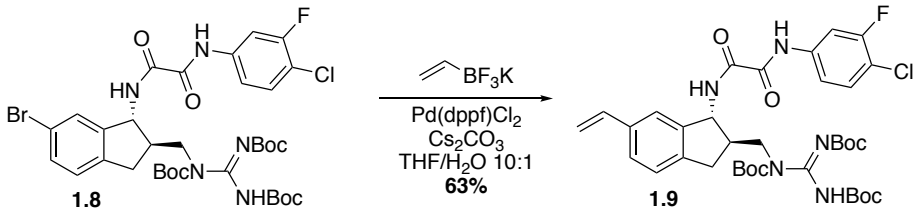

Alkene **1.9**. Bromide **1.8** (0.0987 g, 0.126 mmol), $Pd(dppf)Cl_2$ (0.0082 g, 0.0101 mmol, 0.08 eq.), vinyltrifluoroborate (0.0506 g, 0.378 mmol, 3 eq.) and cesium carbonate (0.164 g, 0.504 mmol, 4 eq.) under nitrogen at room temperature were dissolved in nitrogen-sparged THF/water (32 mL, 10:1, 0.004 M) in a round bottom flask equipped with a reflux condenser. The reaction mixture was heated to reflux overnight. After 21 h, the reaction mixture was cooled to room temperature and diluted with water. The reaction mixture was then filtered through celite with diethyl ether and diluted with water. The layers were separated and the aqueous layer was washed three times with diethyl ether. The organic layers were combined, dried over sodium sulfate, decanted and concentrated. The crude product mixture was purified using flash column chromatography (SiO2, 20% hexanes / ethyl acetate) to afford product as a white solid (0.058 g, 63%).

^{1}H NMR (500 MHz, $CDCl_3$): δ 10.55 (br s, 1 H), 9.38 (s, 1 H), 7.82 (d, 1 H, *J* = 9.1 Hz), 7.76 (dd, 1 H, *J* = 2.5 , 10.6 Hz), 7.38 (t, 1 H, *J* = 8.3 Hz), 7.30 (m, 1 H), 7.25 (m, 1 H), 7.23 (s, 1H), 7.19 (d, 1 H, *J* = 7.8 Hz), 6.67 (dd, 1 H, *J* = 10.9, 17.5 Hz), 5.69 (app. d, 1 H, *J* = 17.6 Hz), 5.25 (t, 1 H, *J* = 8.7 Hz), 5.20 (d, 1 H, *J* = 10.9 Hz), 4.14 (m, 1 H), 3.17 (dd, 1 H, *J* = 7.8, 15.8 Hz), 2.88 (m, 1 H), 2.79 (dd, 1 H, *J* = 8.8, 15.7 Hz), 1.56 - 1.44 (m, 27 H).

^{13}C NMR (500 MHz, $CDCl_3$): δ 159.7, 158.2 (d, J_{CF} = 248 Hz), 157.5, 153.3, 153.2, 141.7 (d, J_{CF} = 8 Hz), 137.0, 136.6, 136.5, 130.9, 126.8, 125.1, 121.5, 117.1 (d, J_{CF} = 18 Hz), 116.0 (d, J_{CF} = 3 Hz), 113.8, 108.4 (d, J_{CF} = 26 Hz), 83.7, 58.5, 50.0, 48.4, 35.0, 28.2, 28.2, 28.1

IR υ_{max} 3277, 2977. 2924, 2857, 2360, 2336, 1757, 1664, 1517, 1366, 1243, 1150 668

AMM(ESI) *m/z* 752.2864 [calcd for $C_{36}H_{45}ClFN_5O_8$ $(M+Na)^+$ 752.2838]

$[\alpha]_D^{23}$ = + 19 ° (*c* 0.5, CH_2Cl_2)

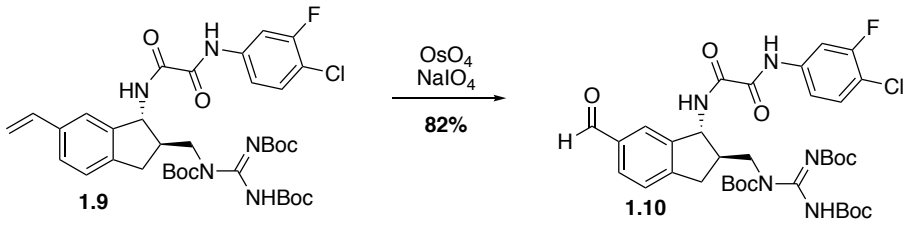

Aldehyde **1.10**. To a solution of aldehyde **1.10** (0.136 g, 0.186 mmol) in THF/water (3:1, 3 mL, 0.05 M) was added osmium tetroxide (2 mol% in water, 0.95 mL, 0.019 mmol, 0.1 eq.) then sodium periodate (0.120 g, 0.559 mmol, 3 eq). After three hours, the reaction was quenched with saturated aqueous sodium thiosulfate and allowed to stir overnight. The reaction mixture was diluted with ethyl acetate and the layers were separated. The aqueous layer was washed three times with ethyl acetate. The organic layers were combined, dried with magnesium sulfate, decanted and concentrated. The crude product mixture was purified using flash column chromatography (SiO_2, 100% hexanes to 30% ethyl acetate / hexanes, ethyl acetate flush) to afford the product as a solid (0.112 g, 82%).

^{1}H NMR (500 MHz, $CDCl_3$): δ 10.59 (br s, 1 H), 9.96 (s, 1 H), 9.31 (s, 1 H), 7.90 (d, 1 H, *J* = 8.7 Hz), 7.79 (d, 1 H, *J* = 7.7 Hz), 7.75 (m, 1 H), 7.72 (s, 1 H), 7.39 (t, 2 H, *J* = 8.3 Hz), 7.24 (d, 1 H, *J* = 8.6 Hz), 5.31 (t, 1 H, *J* = 8.7 Hz), 4.16 (m, 1 H), 3.27 (dd, 1 H, *J* = 7.5, 16.1 Hz), 2.92 (m, 2 H), 1.59 – 1.43 (m, 27 H).

^{13}C NMR (500 MHz, $CDCl_3$): δ 191.7, 159.8, 158.3 (d, J_{CF} = 248 Hz), 157.3, 153.6, 153.2, 149.2, 142.7, 136.4 (d, J_{CF} = 10 Hz), 136.1, 131.0, 130.7, 125.7, 125.1, 117.2 (d, J_{CF} = 18 Hz), 116.0 (d, J_{CF} = 4 Hz), 108.5 (d, J_{CF} = 26 Hz), 83.8, 58.3, 49.8, 48.0, 35.5, 28.2, 28.12, 28.08

IR υ_{max} 3393, 3284, 2979, 2932, 2852,1792, 1725, 1666, 1606, 1517, 1369, 1295, 1248, 1147, 775

AMM(ESI) *m/z* 732.2798 [calcd for $C_{35}H_{43}ClFN_5O_9$ $(M+H)^+$ 732.2812]

[α]$_D^{23}$ = + 31 ° (*c* 2.0, CH_2Cl_2)

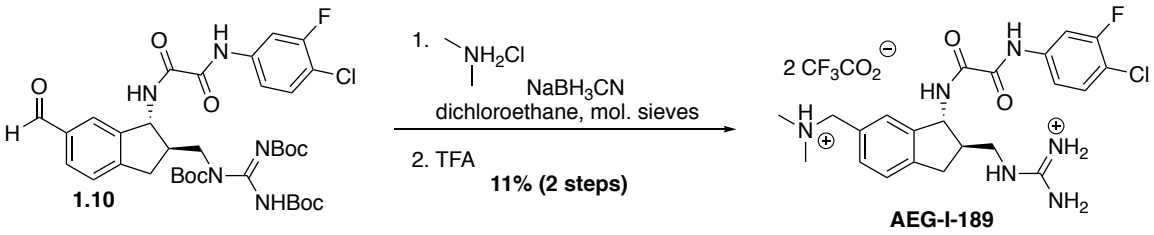

AEG-I-189. To a solution of **1.10** (0.040 g, 0.052 mmol) and dimethylamine-HCl (0.057 g, 0.523 mmol, 10 eq.) in dichloroethane (6.5 mL, 0.008 M) with 3 Å molecular sieves under nitrogen atmosphere at room temperature was added sodium cyanoborohydride (0.016 g, 0.26 mmol, 5 eq.). The reaction was allowed to proceed for 18 h. The reaction was quenched with saturated aqueous sodium bicarbonate. The pH of the reaction solution was adjusted to 12 with 1 M aqueous NaOH, then diluted with water and ethyl acetate. The layers were separated, and the aqueous layer was washed three times with ethyl acetate. The organic layers were combined, dried over sodium sulfate, decanted, and concentrated. Flash column chromatography (SiO_2, 5% MeOH in dichloromethane) afforded a partially purified amine. This amine was dissolved in dichloromethane (5.5 mL, 0.01 M). To this solution was added trifluoroacetic acid (0.12 mL, 1.6 mmol, 30 eq.). After two days the reaction mixture was concentrated, dissolved in 4.0 mL 1:1 acetonitrile/water and purified by reverse phase HPLC (15 mL/min, 10-80% H_2O/ACN + 0.1% TFA, 20 min gradient). The isolated fractions were frozen and concentrated by lyophilization to afford **AEG-I-189** as a white solid (3.9 mg, 11% over two steps).

1H NMR (500 MHz, acetone-d6): δ 8.01 (dd, 1 H, *J* = 2.4, 11.5 Hz), 7.74 (ddd, 1 H, *J* = 1.2, 2.5, 8.8 Hz), 7.51 (m, 3 H), 7.35 (d, 1 H, *J* = 7.7 Hz), 5.35 (d, 1 H, *J* = 8.3 Hz), 4.40 (m, 2 H), 3.63 (m, 2 H), 3.32 (dd, 1 H, *J* = 15.9 Hz), 2.98 (m, 1 H), 2.87 (s, 6 H).

^{13}C NMR (500 MHz, acetone-d6): δ 161.0, 159.2, 159.1, 159.0, 158.6 (d, J_{CF} = 248.8 Hz), 144.5, 143.8, 139.1 (d, J_{CF} = 10.1 Hz), 132.0, 131.6, 130.0, 127.6, 126.3, 117.8 (d, J_{CF} = 3.5 Hz), 116.3 (d, J_{CF} = 18.0 Hz), 109.2 (d, J_{CF} = 26.1 Hz), 61.1, 58.7, 48.0, 44.5, 42.4, 42.2, 35.1.

AMM(ESI) *m/z* 461.1861 [calcd for $C_{22}H_{27}ClFN_6O_2$ $(M+H)^+$ 461.1868]

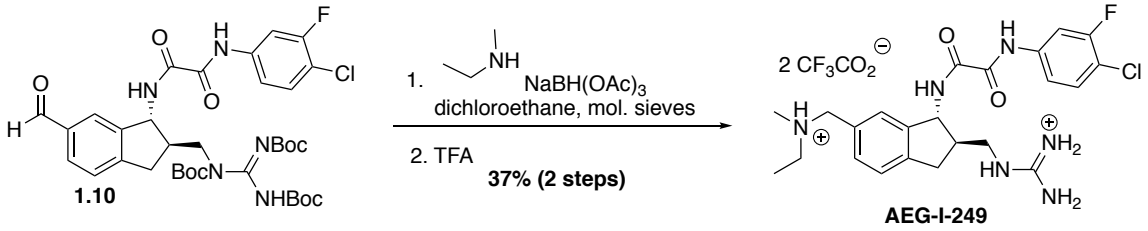

AEG-I-249. To a solution of **1.10** (0.030 g, 0.039 mmol) in dichloroethane (3 mL, 0.02 M) with 3 Å molecular sieves under nitrogen atmosphere at room temperature was added ethylmethylamine (0.08 mL, 0.948 mmol, 20 eq.). After stirring for one hour, sodium triacetoxyborohydride (0.016 g, 0.26 mmol, 5 eq.) was added. After 7 hours, no starting material was observed by TLC or LC/MS. The reaction was quenched with saturated aqueous sodium bicarbonate and diluted with ethyl acetate. The layers were separated, and the aqueous layer was washed three times with ethyl acetate. The organic layers were combined, dried over sodium sulfate, decanted, and concentrated. Flash column chromatography (SiO_2, 0% to 5% MeOH in dichloromethane) afforded a partially purified amine. This amine was dissolved in dichloromethane (3.9 mL, 0.01 M). To this solution was added trifluoroacetic acid (0.12 mL, 1.6 mmol, 40 eq.). After two days complete conversion was observed by LC/MS. The reaction mixture was concentrated, dissolved in 2.3 mL 1:1 acetonitrile/water and purified by reverse phase HPLC (15 mL/min, 15-70% H_2O/ACN + 0.1% TFA, 10 min gradient). The isolated fractions were frozen and concentrated by lyophilization to afford **AEG-I-249** as a white solid (10 mg, 37% over two steps).

^{1}H NMR (500 MHz, acetone-d6): δ 11.79 (s, 1 H), 10.30 (s, 1 H), 8.80 (m, 2 H), 7.99 (ddd, 1 H, *J* = 1.0, 2.4, 11.6 Hz), 7.90 – 7.65 (br s, 2 H), 7.72 (m, 1 H), 7.55 – 7.46 (m, 3 H), 7.33 (d, 1 H, *J* = 7.7 Hz), 5.34 (t, 1 H, *J* = 8.4 Hz), 4.55 – 4.23 (br d, *J* = 80.9 Hz), 3.68 – 3.55 (m, 2 H), 3.41 – 3.24 (br s, 1 H), 3.30 (dd, 1 H, *J* = 8.0, 15.9 Hz) 3.21 – 3.08 (br s, 1 H), 2.96 (m, 1 H), 2.84 (dd, 1 H, *J* = 9.0, 15.9 Hz), 2.78 (s, 3 H), 1.37 (t, 3 H, *J* = 7.2 Hz)

^{13}C NMR (500 MHz, acetone-d6, mixture of rotamers): δ 161.7 (q, J_{CF} = 34.0 Hz, TFA), 161.0609, 160.0 (d, J_{CF} = 249 Hz), 158.6 (d, J_{CF} = 245 Hz), 159.3, 159.2, 159.2, 159.1, 159.1, 144.5, 143.8, 139.2 (d, J_{CF} = 10.1 Hz), 139.1 (d, J_{CF} = 10.0 Hz), 132.0, 131.6, 129.8, 127.7, 126.3, 117.9 (q, J_{CF} = 294 Hz), 117.9 (d, J_{CF} = 3.5 Hz), 117.1 (d, J_{CF} = 3.5 Hz), 116.3 (d, J_{CF} = 18.0 Hz), 109.3 (d, J_{CF} = 26.2 Hz), 109.2 (d, J_{CF} = 26.1 Hz), 59.4, 58.8, 58.7, 51.2, 51.0, 48.0, 48.0, 44.6, 44.5, 38.7, 35.1, 35.1, 9.4.

IR υ_{max} 3355, 2359, 2341, 1682, 1517, 1428, 1203, 1135, 975, 837, 801, 722, 668

AMM(ESI) *m/z* 475.2011 [calcd for $C_{23}H_{29}ClFN_6O_2$ $(M+H)^+$ 475.2025]

[α]$_D^{23}$ = + 9 ° (*c* 0.09, MeOH)

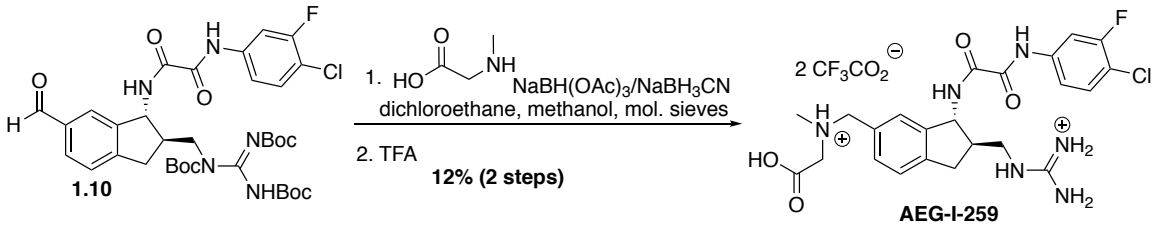

AEG-I-259. To a solution of **1.10** (0.060 g, 0.079 mmol) in dichloroethane (2 mL, 0.04 M) with 3 Å molecular sieves under nitrogen atmosphere at room temperature was added a solution of sarcosine (0.140 g, 1.57 mmol, 20 eq.) in methanol (2 mL). After stirring for 30 minutes, sodium triacetoxyborohydride (0.083 g, 0.39 mmol, 5 eq.) was added. After 24 hours, no conversion was observed by LC/MS. Sodium cyanoborohydride (0.030 g, 0.48 mmol, 6 eq.) was then added. After

two hours, no starting material was observed by TLC or LC/MS. The reaction was quenched with saturated aqueous sodium bicarbonate and diluted with ethyl acetate. The layers were separated, and the aqueous layer was washed three times with ethyl acetate. The organic layers were combined, dried over sodium sulfate, decanted, and concentrated. Flash column chromatography (SiO_2, 0% to 10% MeOH in dichloromethane) afforded a partially purified amine. This amine was dissolved in dichloromethane (5.5 mL, 0.01 M). To this solution was added trifluoroacetic acid (0.16 mL, 2.2 mmol, 40 eq.). After two days complete conversion was observed by LC/MS. The reaction mixture was concentrated, dissolved in 2.3 mL 1:1 acetonitrile/water and purified by reverse phase HPLC (15 mL/min, 5-80% H_2O/ACN + 0.1% TFA, 20 min gradient). The isolated fractions were frozen and concentrated by lyophilization to afford **AEG-I-259** as a white solid (6.8 mg, 12% over two steps).

^{1}H NMR (500 MHz, acetone-d6): δ 11.10 (s, 1 H), 9.47 (d, 1 H, *J* = 9.1 Hz), 7.98 (dd, 1 H, *J* = 2.4, 11.8 Hz), 7.83 (m, 1 H), 7.77 (dd, 1 H, *J* = 2.3, 8.9 Hz), 7.60 (t, 1 H, *J* = 8.7 Hz), 7.31 (s, 1 H), 7.25 (s, 1 H), 5.20 (t, 1 H, *J* = 8.8 Hz), 4.09 (s, 2 H), 3.66 (s, 2 H), 3.39 (m, 1 H), 3.12 (dd, 1 H, *J* = 8.0, 15.8 Hz), 2.83 (m, 1 H), 2.68 (dd, 1 H, *J* = 9.3, 15.7 Hz), 2.58 (s, 3 H).

^{13}C NMR (500 MHz, acetone-d6): 168.5, 159.9, 158.8, 156.8 (q, J_{CF} = 34.0 Hz, TFA), 157.1, 156.8 (d, J_{CF} = 244 Hz),143.0, 142.9, 142.1,138.3 (d, J_{CF} = 10.0 Hz),130.7, 130.2, 125.6, 124.9, 117.3 (d, J_{CF} = 10.0 Hz), 117.2 (q, J_{CF} = 299.7 Hz, TFA), 114.4 (d, J_{CF} = 18.0 Hz), 108.5 (d, J_{CF} = 25.8 Hz), 59.1, 56.9, 55.2, 45.6, 42.9, 40.5, 33.7.

IR υ_{max} 3398, 2917, 2849 2359, 2342, 1683, 1672, 1645, 1635, 1626, 1203, 1138

AMM(ESI) *m/z* 505.1772 [calcd for $C_{23}H_{27}ClFN_6O_2$ $(M+H)^+$ 505.1766]

[α]$_D^{23}$ = + 9 ° (*c* 0.2, MeOH)

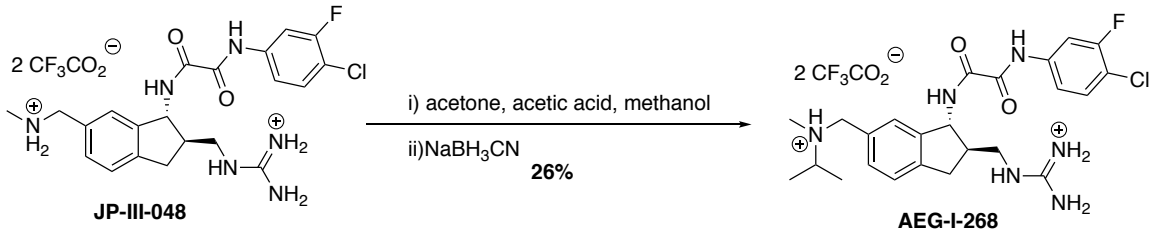

AEG-I-268. To a solution of **JP-III-048** (0.018 g, 0.026 mmol) in methanol (1.1 mL, 0.02 M) under nitrogen atmosphere at room temperature was added a 0.165 M solution of acetone in methanol (0.024 mL, 0.039 mmol, 1.5 eq.) followed by a 0.26 M solution of acetic acid in methanol (0.12 mL, 0.031 mmol, 1.2 eq.). To the reaction solution were added 3 Å molecular sieves then sodium cyanoborohydride (0.012 g, 0.31 mmol, 1.2 eq.). Additional acetone was added as a solution in methanol every 24 hours until minimal starting material was observed by LC/MS. After 4 days, the reaction mixture was filtered through sand and concentrated. The crude reaction mixture was dissolved in 0.7 mL acetonitrile and 1.5 mL water and purified by reverse phase HPLC (15 mL/min, 15-60% H_2O/ACN + 0.1% TFA, 10 min gradient). The isolated fractions were frozen and concentrated by lyophilization to afford **AEG-I-259** as a white solid (4.8 mg, 26%).

^{1}H NMR (500 MHz, acetone-d6): δ 11.25 (s, 1 H), 10.32 (s, 1 H), 8.82 (d, 1 H, *J* = 9.0 Hz), 8.74 (m, 1 H), 7.99 (dd, 1 H, *J* = 2.4, 11.6 Hz), 7.90 – 7.60 (br s, 3 H), 7.72 (m, 1 H), 7.50 (m, 1 H), 7.30 (d, 1 H, *J* = 7.7 Hz), 5.33 (t, 1 H, *J* = 7.7 Hz), 4.38 (m, 2 H), 3.29 (dd, 1 H, *J* = 8.0, 16.0 Hz), 2.94 (m, 1 H), 2.84 (dd, 1 H, *J* = 8.9, 16.0 Hz), 2.71 (s, 3 H), 1.41 (d, 1 H, *J* = 6.5Hz).

^{13}C NMR (500 MHz, acetone-d6): 161.6 (q, J_{CF} = 34.4 Hz, TFA), 161.1, 158.6 (d, J_{CF} = 245 Hz), 159.3, 159.3, 159.2, 144.4, 143.8, 138.3 (d, J_{CF} = 10.2 Hz), 131.9, 131.6, 130.1, 127.5, 126.3, 117.9 (d, J_{CF} = 3.6 Hz, TFA), 116.3 (d, J_{CF} = 34.0 Hz, TFA), 109.3 (d, J_{CF} = 26.0 Hz), 58.8, 57.0, 48.0, 44.6, 35.1, 34.7, 17.6, 15.5, 15.4.

IR υ_{max} 3370, 2360, 2341, 1673, 1517,1427, 1202, 1136, 837, 801, 745, 722, 669

AMM(ESI) *m/z* 489.2188 [calcd for $C_{24}H_{32}ClFN_6O_2$ $(M+H)^+$ 489.2181]

[α]$_D^{23}$ = + 15 ° (*c* 0.2, MeOH)

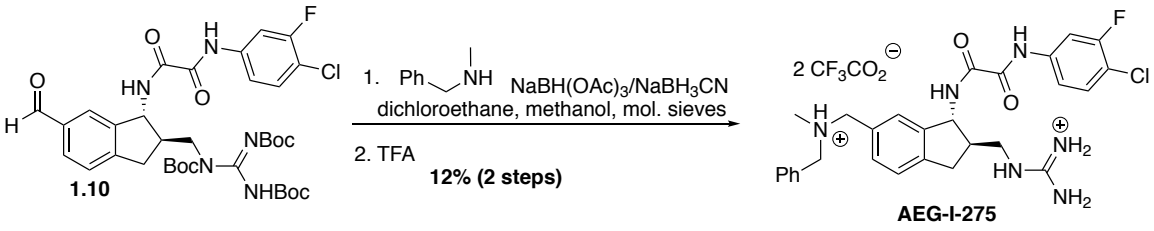

AEG-I-275. To a solution of **1.10** (0.035 g, 0.045 mmol) in dichloroethane (2 mL, 0.04 M) with 3 Å molecular sieves under nitrogen atmosphere at room temperature was added a 0.67 M solution of the amine in methanol (1.35 mL, 0.903 mmol, 20 eq.). After stirring for two hours, sodium triacetoxyborohydride (0.083 g, 0.39 mmol, 5 eq.) was added. After 24 hours, modest conversion was observed by LC/MS. Additional sodium triacetoxyborohydride was added, and again after an additional 48 hours. After an additional 24 hours, incomplete conversion was observed by LC/MS. Sodium cyanoborohydride (0.006 g, 0.090 mmol, 2 eq.) was then added. After 2.5 hours, the reaction was complete by TLC. The reaction was then quenched with saturated aqueous sodium bicarbonate and diluted with ethyl acetate. The layers were separated, and the aqueous layer was washed three times with ethyl acetate. The organic layers were combined, dried over sodium sulfate, decanted, and concentrated. Flash column chromatography (SiO_2, 0% to 10% MeOH in dichloromethane) afforded a partially purified amine. This amine was resubjected to flash column chromatography (SiO_2, 0% to 5% MeOH in dichloromethane). The purified amine was dissolved in dichloromethane (4.3 mL, 0.01 M). To this solution was added trifluoroacetic acid (0.13 mL, 1.7 mmol, 40 eq.). After three days complete conversion was observed by LC/MS. The reaction mixture was concentrated, dissolved in 1 mL acetonitrile and 1.5 mL water and purified by reverse phase HPLC (15 mL/min, 20-70% H_2O/ACN + 0.1% TFA, 10 min gradient). The isolated fractions were frozen and concentrated by lyophilization to afford **AEG-I-275** as a white solid (21.4 mg, 63% over two steps).

^{1}H NMR (500 MHz, acetone-d6): 12.10 (br s, 1 H), 10.30 (s, 1 H), 8.81 (d, 1 H, *J* = 8.9 Hz), 8.73 (m, 1 H), 7.99 (dd, 1 H, *J* = 2.5, 11.6 Hz), 7.71 (m, 4 H), 7.58 (m, 2 H), 7.51 (m, 2 H), 7.47 (s, 1 H), 7.43 (m, 3 H), 7.33 (d, 1 H, *J* = 7.7 Hz), 5.33 (t, 1 H, *J* = 8.6 Hz), 3.61 (m, 2 H), 3.30 (dd, 1 H, *J* = 7.9, 16.0 Hz), 2.94 (m, 1 H), 2.84 (dd, 1 H, *J* = 9.1, 15.9), 2.69 (s, 3 H).

^{13}C NMR (500 MHz, acetone-d6): 161.6 (q, J_{CF} = 34.4 Hz, TFA), 161.08, 158.6 161.6 (d, J_{CF} = 248 Hz), 159.26, 159.20, 159.14, 144.47, 143.82, 139.1, (d, J_{CF} = 10.0 Hz), 132.21, 132.19, 131.61, 131.07, 130.55, 129.91, 129.66, 127.79, 126.29, 117.9 (d, J_{CF} = 3.6 Hz), 116.3 (d, J_{CF} = 17.9 Hz), 109.3 (d, J_{CF} = 26.2 Hz), 59.79, 58.80, 58.69, 48.05, 44.62, 38.95, 35.10.

IR υ_{max} 3353, 1681, 1516, 1428, 1366, 1202, 1136, 974, 836, 801, 745, 722, 701, 632, 500

AMM(ESI) *m/z* 537.2160 [calcd for $C_{28}H_{32}ClFN_6O_2$ $(M+H)^+$ 537.2181]

$[\alpha]_D^{23}$ = + 4 ° (*c* 1.0, MeOH)

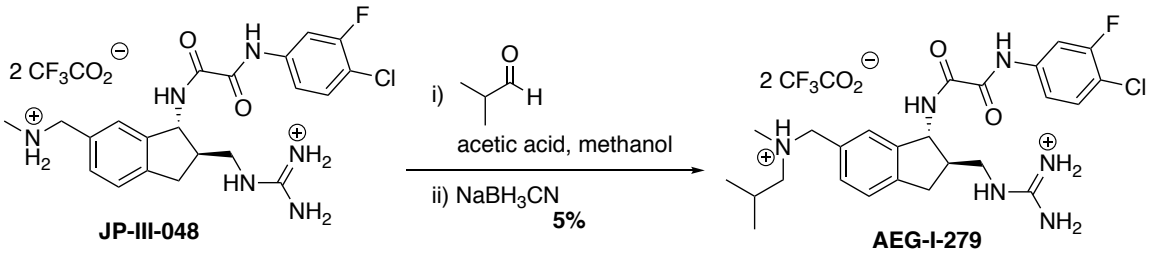

AEG-I-279. To a solution of **JP-III-048** (0.018 g, 0.026 mmol) in methanol (1.1 mL, 0.02 M) under nitrogen atmosphere at room temperature was added a 0.165 M solution of the aldehyde in methanol (0.024 mL, 0.039 mmol, 1.5 eq.) followed by a 0.26 M solution of acetic acid in methanol (0.12 mL, 0.031 mmol, 1.2 eq.). The reaction mixture was allowed to stir for fifteen minutes, then sodium cyanoborohydride (0.012 g, 0.31 mmol, 1.2 eq.) was added and the reaction was allowed

to proceed for 24 hours. The reaction mixture was concentrated, redissolved in 3.2 mL 1:1 acetonitrile/ water and purified by reverse phase HPLC (15 mL/min, 25-65% H_2O/ACN + 0.1% TFA, 15 min gradient). The isolated fractions were frozen and concentrated by lyophilization to afford **AEG-I-279** as a white solid (1 mg, 5%).

^{1}H NMR (500 MHz, acetone-d6): 10.33 (s, 1 H), 8.96 (s, 1 H), 8.82 (d, 1H, *J* = 9.0 Hz), 8.29 - 7.60 (m, 5 H), 7.52 (m, 2 H), 7.48 (s, 1 H), 5.34 (t, 1 H, *J* = 8.5 Hz), 4.38 (s, 2 H), 3.59 (m, 2 H), 3.30 (dd, 1 H, *J* = 8.2, 16.1 Hz), 3.21 (m, 1 H), 2.19 (m, 2 H), 1.94 (m, 2 H), 1.30 (m, 3 H), 0.98 (d, 6 H, *J* = 6.6 Hz).

^{13}C NMR (500 MHz, acetone-d6): 161.6, 161.1, 159.3, 158.6 (d, J_{CF} = 248 Hz), 144.5, 143.8, 139.2 (d, J_{CF} = 10.4 Hz), 132.3, 131.6, 128.0, 126.1, 119.4, 117.9 (d, J_{CF} = 2.8 Hz), 116.2 (d, J_{CF} = 18.2 Hz), 109.3 (d, J_{CF} = 26.1 Hz), 63.1, 60.4, 58.8, 48.0, 46.6, 44.6, 40.5, 35.1, 25.1, 20.8, 8.9.

IR υ_{max} 3357, 2923, 2860, 2834, 2364, 2333, 1677, 1415, 1132, 1025

AMM (ESI) *m/z* 503.2327 [calcd for $C_{25}H_{35}ClFN_6O_2$ $(M+H)^+$ 503.2338]

[α]$_D^{23}$ = - 149 ° (*c* 0.01, MeOH)

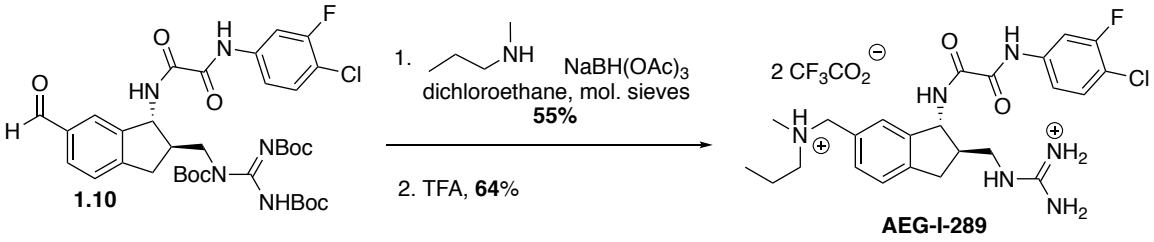

AEG-I-289. To a solution of **1.10** (0.030 g, 0.039 mmol) in dichloroethane (3 mL, 0.02 M) with 3 Å molecular sieves under nitrogen atmosphere at room temperature was added methylpropylamine (0.08 mL, 0.786 mmol, 20 eq.) then sodium triacetoxyborohydride (0.042, 0.20 mmol, 5 eq.) was added. After 24 hours, the reaction was quenched with saturated aqueous sodium bicarbonate and

diluted with ethyl acetate. The layers were separated, and the aqueous layer was washed three times with ethyl acetate. The organic layers were combined, dried over sodium sulfate, decanted, and concentrated. Flash column chromatography (SiO_2, 0% to 10% MeOH in dichloromethane) afforded the amine (17.1 mg, 55%) as a white solid. This amine was dissolved in dichloromethane (0.5 mL, 0.05 M). To this solution was added trifluoroacetic acid (0.07 mL, 0.86 mmol, 40 eq.). After 24 hours complete conversion was observed by LC/MS. The reaction mixture was concentrated, dissolved in 2 mL 1:1 acetonitrile/water and purified by reverse phase HPLC (15 mL/min, 15-70% H_2O/ACN + 0.1% TFA, 15 min gradient). The isolated fractions were frozen and concentrated by lyophilization to afford **AEG-I-289** as a white solid (9.8 mg, 64%).

^{1}H NMR (500 MHz, acetone-d6): 11.82 (s, 1 H), 10.33 (s,1 H), 8.83 (m, 1 H), 8.11 – 7.59 (m, 5 H), 7.50 (m, 5 H), 7.33 (d, 1 H, *J* = 7.7 Hz), 5.34 (t, 1 H, *J* = 8.7 Hz), 4.40 (m, 2 H), 3.61 (m, 2 H), 3.29 (dd, 1 H, *J* = 8.0, 16.0 Hz), 3.10 (d, 2 H, *J* = 70.0 Hz), 2.95 (m, 1 H), 2.85 (m, 1H), 2.79 (m, 3 H), 1.83 (m, 2 H), 0.92 (t, 3 H, *J* = 7.3 Hz).

^{13}C NMR (500 MHz, acetone-d6): 161.9 (q, J_{CF} = 33.8 Hz, TFA), 159.5, 159.2,158.6 (d, J_{CF} = 248 Hz), 144.4, 143.8, 139.2 (d, J_{CF} = 10.0 Hz), 132.1, 131.6, 129.8, 127.7, 126.2, 118.0 (q, J_{CF} = 294 Hz, TFA), 117.9 (d, J_{CF} = 3.6 Hz), 116.3 (d, J_{CF} = 17.8 Hz), 109.3 (d, J_{CF} = 26.1 Hz), 59.7, 58.8, 57.7, 57.4, 48.0, 46.7, 44.6, 39.4, 35.1, 18.1, 11.3, 8.9.

IR υ_{max} 3403, 2931, 2856, 1711, 1678, 1494, 1415, 1364, 1252, 1030, 917, 847

AMM(ESI) *m/z* 489.2188 [calcd for $C_{24}H_{32}ClFN_6O_2$ $(M+H)^+$ 489.2181]

$[\alpha]_D^{23}$ = + 13 ° (*c* 0.1,MeOH)

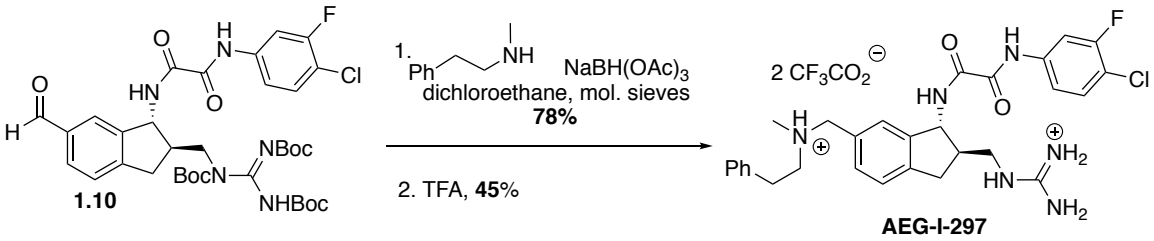

AEG-I-297. To a solution of **1.10** (0.056 g, 0.073 mmol) in dichloroethane (3 mL, 0.02 M) with 3 Å molecular sieves under nitrogen atmosphere at room temperature was added methylphenethylamine (0.10 mL, 0.726 mmol, 10 eq.) then sodium triacetoxyborohydride (0.077, 0.36 mmol, 5 eq.) was added and the reaction was allowed to proceed overnight. The reaction was quenched with saturated aqueous sodium bicarbonate and diluted with ethyl acetate. The layers were separated, and the aqueous layer was washed three times with ethyl acetate. The organic layers were combined, dried over sodium sulfate, decanted, and concentrated. Flash column chromatography (SiO_2, 0% to 10% MeOH in dichloromethane) afforded the amine (48.4 mg, 78%) as a white solid. This amine was dissolved in dichloromethane (1.1 mL, 0.05 M). To this solution was added trifluoroacetic acid (0.17 mL, 2.26 mmol, 40 eq.). After two days complete conversion was observed by LC/MS. The reaction mixture was concentrated, dissolved in 1.5 mL 1:1 acetonitrile/water and purified by reverse phase HPLC (15 mL/min, 25-75% H_2O/ACN + 0.1% TFA, 10 min gradient). The isolated fractions were frozen and concentrated by lyophilization to afford **AEG-I-297** as a white solid (19.8 mg, 45%).

^{1}H NMR (500 MHz, acetone-d6): 7.99 (dd, 1 H, *J* = 2.3, 11.5 Hz), 7.72 (m, 1 H), 7.51 (m, 3 H), 7.36 – 7.20 (m, 6 H), 5.34 (d, 1 H, *J* = 8.3 Hz), 4.50 (d, 2 H), 3.61 (m, 2 H), 3.43 (d, 2 H, *J* = 64.5 Hz), 3.29 (dd, 1 H, *J* = 8.0, 16.0 Hz), 3.20 (s, 2 H), 2.94 (m, 4 H), 2.84 (dd, 1 H, *J* = 9.1, 16.0 Hz). **^{13}C NMR** (500 MHz, acetone-d6): 161.6 (m, TFA), 161.0, 159.1, 158.9, 158.9, 158.6 (d, J_{CF} = 245 Hz), 144.5, 143.9, 139.0 (d, J_{CF} = 9.8 Hz), 137.9, 132.1, 131.6, 129.8, 129.7, 129.6, 127.9, 127.6,

126.3, 121.2, 117.8 (q, J_{CF} = 292 Hz, TFA), 117.8 (d, J_{CF} = 3.6 Hz), 116.3 (d, J_{CF} = 17.8 Hz), 109.2 (d, J_{CF} = 26.3 Hz), 59.86, 58.65, 57.19, 47.90, 44.45, 39.55, 35.05, 30.89.

IR υ_{max} 3281, 2919, 2360, 2340, 1672, 1512, 1428, 1202, 1130

AMM (ESI) *m/z* 551.2339 [calcd for $C_{29}H_{35}ClFN_6O_2$ $(M+H)^+$ 551.2338]

[α]$_D^{23}$ = + 5 ° (*c* 0.5, MeOH)

4.3 Experimental Procedures and Spectroscopic Related to Chapter Two

4.3.1 Synthesis of BMS-DAVEIs

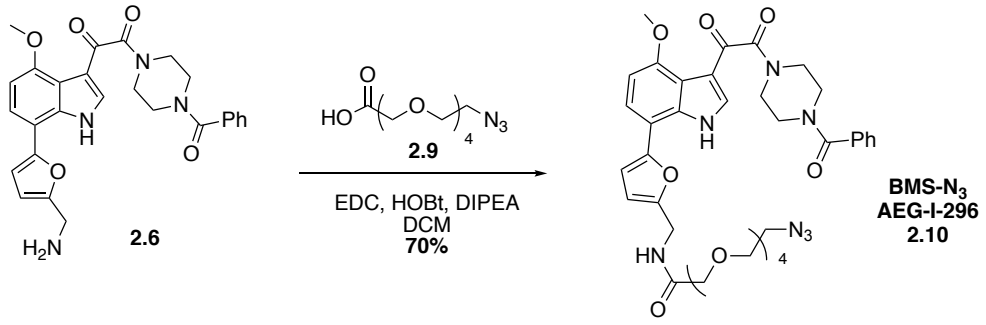

BNM-N3 **AEG-I-296 (2.10)**. To a solution of **2.6** (0.285 g, 0.586m mmol) in dichloromethane (14.6 mL, 0.04 M) under nitrogen gas at room temperature was added diisopropylethyl amine (0.22 mL, 1.17 mmol, 2 eq.), 1-ethyl-3-(3-dimethylaminopropyl)carbodiimide hydrochloride (0.198 g, 1.29 mmol, 2.2 eq.), hydroxybenzotriazole (0.258 g, 1.35 mmol, 2.3 eq.) was added **2..9** as a 0.38 M in dichloromethane (2 mL, 0.762 mmol, 1.3 eq.). After 3.5 h no starting material was observed by TLC. The reaction mixture was diluted with dichloromethane and saturated aqueous sodium bicarbonate. The layers were separated and the aqueous layer was washed once with dichloromethane. The organic layers were combined and washed with ammonium chloride. The aqueous layer was washed with dichloromethane. The organic layers were combined, dried with magnesium sulfate, decanted, and concentrated. The crude material was purified by flash column chromatography (SiO_2, 0 to 5% methanol in dichloromethane) to afford AEG-I-296 (0.306 g, 70%).

^{1}H NMR (500 MHz, $CDCl_3$) δ 11.26 (s, 1H), 8.15 (d, 1 H, *J* = 3.3 Hz), 8.01 (s, 1 H), 7.44 (m, 5 H), 6.72 (d, 1 H, *J* = 8.3 Hz), 6.55 (d, 1 H, *J* = 3.3 Hz), 6.34 (d, 1 H, *J* = 3.3 Hz), 4.54 (d, 1 H, 3.3 Hz), 4.07 (s, 2 H), 3.97 (s, 3 H), 4.00 – 3.39 (m, 22 H), 3.35 (t, 2 H, *J* = 5.0 Hz).

^{13}C NMR (500 MHz, $CDCl_3$): 186.03, 172.17, 171.01, 167.78, 153.90, 152.64, 150.01, 136.15, 135.06, 134.44, 130.34, 128.81, 127.21, 120.40, 115.75, 114.98, 109.65, 109.20, 104.12, 104.06, 100.13, 70.61, 70.52, 70.47, 70.36, 70.08, 70.02, 56.14, 50.74, 36.23.

IR υ_{max} 3296, 2920, 2866, 2359, 2101, 1634, 1512, 1283, 1106

AMM (ESI) *m/z* 746.3156 [calcd for $C_{37}H_{43}N_7O_{10}$ $(M+H)^+$ 746.3150]

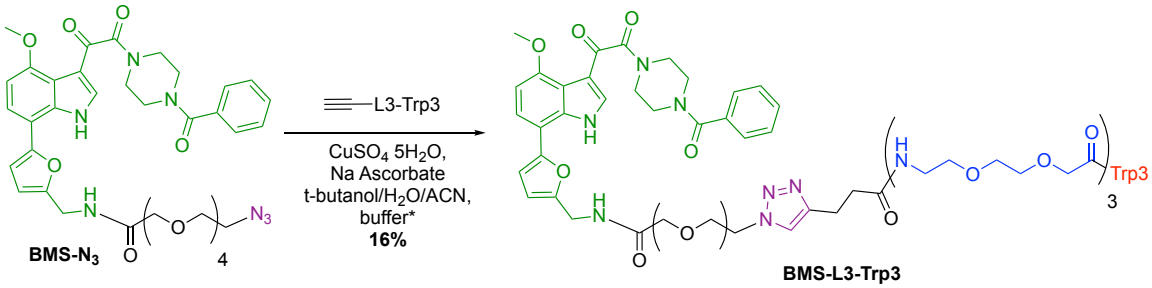

BMS-L3-Trp3. Acetonitrile co-solvent: To **AEG-I-296** (0.006 g, 0.0075, 1.5 eq.) was added a 0.0089 M solution of the alkyne-L3-Trp3 in 1:1 *t*-butanol/water (0.5 mL, 0.005 mmol, 1 eq.), 0.5 mL 6 M guanidinium HCl + 0.2 M sodium hydrogen phosphate aqueous solution, and 0.5 mL acetonitrile. To this solution was added copper sulfate pentahydrate (2.5 mg, 0.010 mmol, 2 eq.) and sodium ascorbate (2 mg, 0.010 mmol, 2 eq.).

Dimethylformamide co-solvent: To **AEG-I-296** (0.006 g, 0.0075, 1.5 eq.) in a separate flask run simultaneously was added a 0.0089 M solution of the alkyne-L3-Trp3 in 1:1 *t*-butanol/water (0.5 mL, 0.005 mmol, 1 eq.), 0.5 mL 6 M guanidinium HCl + 0.2 M disodium phosphate aqueous solution, and 0.5 mL dimethylformamide. To this solution was added copper sulfate pentahydrate (2.5 mg, 0.010 mmol, 2 eq.) and sodium ascorbate (2 mg, 0.010 mmol, 2 eq.).

Monitoring of the reactions overnight indicated the reaction run with acetonitrile had slightly superior conversion to the desired product. The crude reaction mixtures were combined, filtered through cotton, filtered through celite, and concentrated. The crude product was dissolved in 2.5 mL 1:1

acetonitrile/water and purified by reverse phase HPLC (15 mL/min, 25-95% H_2O/ACN + 0.1% TFA, 15 min gradient). The isolated fractions were frozen and concentrated by lyophilization to afford **BMS-L3-Trp3** (4 mg, 16%).

AMM (ESI) *m/z* 1233.0725 [calcd for $C_{37}H_{43}N_7O_{10}$ $(M+2H)^{+2}$/2 1233.0767]

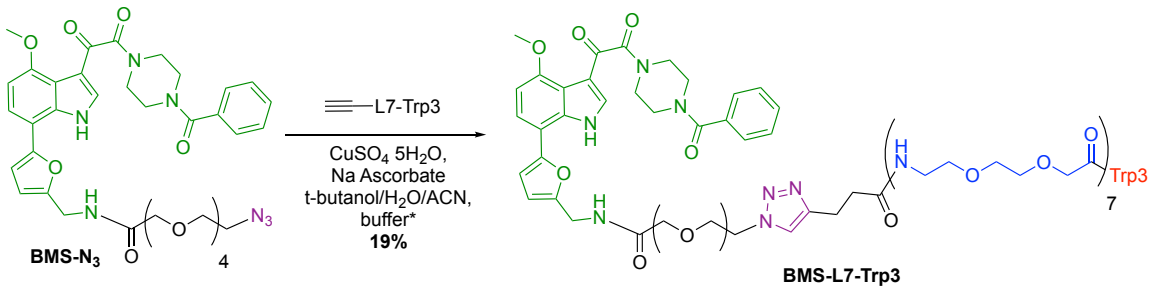

BMS-L7-Trp3. Alkyne-L7-Trp3 (0.013 g, 0.006 mmol, 1 eq.). under nitrogen was dissolved in 0.9 mL 1:1:1 *t*-butanol, water, and buffer (6 M guanidinium HCl + 0.2 M disodium phosphate). To this solution was added BNM-N3 as a 0.02 M solution in acetonitrile (0.007 g, 0.009 mmol, 1.5 eq.), then copper sulfate pentahydrate (0.008 g, 0.03 mmol, 5 eq.) and sodium ascorbate (0.012 g, 0.060 mmol, 10 eq.). After three days, the reaction was concentrated, then diluted with 1:1 acetonitrile/water. The crude product was purified by reverse phase HPLC (15 mL/min, 30-70% H_2O/ACN + 0.1% TFA, 15 min gradient). The isolated fractions were frozen and concentrated by lyophilization to afford **BMS-L3-Trp3** (2 mg, 10%).

AMM (ESI) *m/z* 1015.8165 [calcd for $C_{143}H_{202}N_{29}O_{45}$ $(M+3H)^{+3}$/3 1015.8188]

4.3.2 Synthesis of BNM-DAVEIs

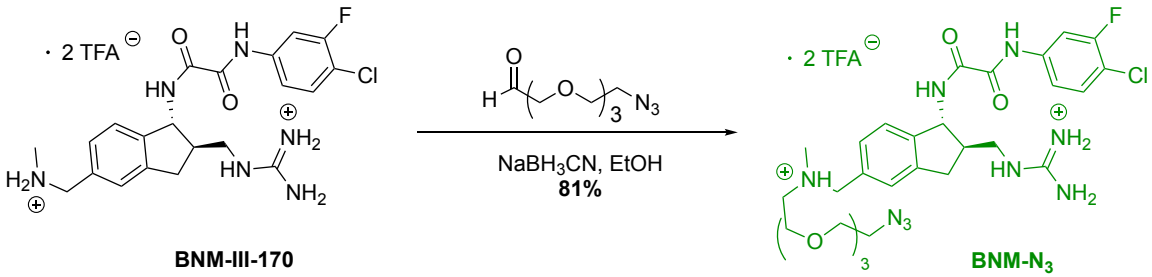

BNM-III-170 **BNM-N_3**

BNM-III-170-N_3. To BNM-III-170 (35 mg, 0.052 mmol) under N2 at room temperature was added the aldehyde21 (17 mg, 0.078 mmol, 1.5 eq) as a 0.1 M solution in 5:3 MeOH/EtOH, followed by $NaBH_3CN$ (0.040 g, 0.062 mmol, 1.2 eq). The reaction mixture was stirred overnight. The crude mixture was concentrated, dissolved in 1.5 mL acetonitrile, 1.5 mL water and 0.2 mL TFA. HPLC purification (15 mL/min, 30-80% acetonitrile/water + 0.1% TFA, 7 min gradient) afforded BNM-N_3 (36 mg, 81% yield).

1 H NMR (500 MHz, acetone-d6) δ 11.74 (bs, 1H), 10.31 (s, 1H), 8.83 (m, 2H), 8.01 (dd, *J* = 2.4, 11.5 Hz, 1H), 7.95-7.60 (bs, 3H), 7.74 (m, 1H), 7.53 (m, 2H), 7.48 (d, *J* = 7.7 Hz, 1H), 7.32 (d, *J* = 7.7 Hz, 1H), 5.33 (t, *J* = 8.7 Hz, 1H), 4.50 (d, *J* = 48.5 Hz, 2H), 3.99 (t, *J* = 4.9 Hz, 2H), 3.74-3.52 (m, 13H), 3.52-3.38 (m, 2H), 3.37 (t, *J* = 4.9 Hz, 2H), 3.31 (dd, *J* = 8.1,16.0 Hz, 1H), 2.99 (dd, *J* = 8.1, 15.7 Hz, 1H), 2.93 (s, 3H), 2.86 (dd, J = 9.0, 16.0 Hz, 1H).

13C NMR (500 MHz, acetone-d6) δ 34.28, 39.93, 43.86, 46.92, 50.57, 54.59, 57.96, 59.86, 64.84, 69.84, 70.20, 70.27, 70.35, 70.38, 108.39, 108.60, 115.45, 115.59, 117.11, 124.55, 127.90,130.03, 130.23, 130.80, 138.19, 138.27, 142.81, 143.91, 156.78, 158.24, 158.41, 158.51, 158.72,159.92, 160.26.

AMM (ESI) *m/z* 648.2819 observed (648.2825 theoretical).

IR νmax: 3357.9, 2918.7, 2874.4, 2359.5, 2340.2, 2104.4, 1675.8, 1513.4, 1428.0,1202.9,1129.6, 668.2, 456.1, 438.7, 421.9, 406.9.

[α]$^{D}_{23}$ = 20 ° (c 0.10, CH3CN).

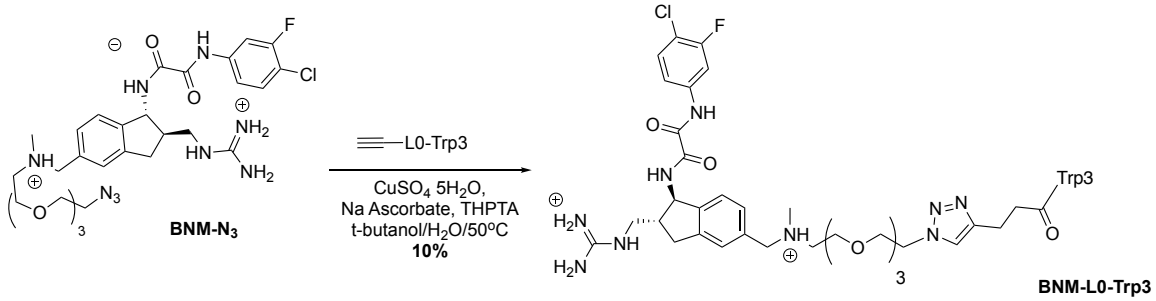

BNM-N$_3$ **BNM-L0-Trp3**

BNM-L0-Trp3. Water and *t*-butanol were sparged with nitrogen for four hours. To BNM-III-170-N_3 under nitrogen in a round bottom flask was added a 9 M solution of alkyne-L0-Trp3 in 1:1 *t*butanol:water (2 mL), then a solution of sodium ascorbate (0.036 g, 0.180 mmol, 10 eq), $CuSO_4$ $5H_2O$ (0.018 g, 0.072 mmol, 4 eq), and THPTA (0.016 g, 0.036 mmol, 2 eq) in 1:1 *t*-butanol:water (1 mL). The reaction mixture was heated to 50 °C overnight. Reaction progress was monitored by LC/MS. The crude reaction mixture was transferred with 1:1 acetonitrile/water, filtered through sand, and concentrated to 3 mL. The crude diluted mixture was purified by reverse phase HPLC (18 mL/min, 25-60% acetonitrile/water, 11 min) to afford 3.93 mg of BNM-L0-Trp3 (10%).

AMM ESI M+2H/2 966.4527 obs. (966.4495 theoretical).

Alkyne-L1-Trp3 [Z-X-D-K-W-A-S-L-W-N-W]. The above peptide (Z = 4-pentynoic acid, X = 8-amino-3,6-dioxaoctanoic acid) was synthesized using a Liberty Blue solid phase peptide synthesizer. The resin-bound peptide was transferred to a synthesis vessel and washed three times with dichloromethane. A pre-mixed solution of TFA (8 mL), TIPS (1 mL), and water (1 mL) was added. The resin-bound peptide was agitated for 90 minutes, drained, and concentrated with a nitrogen stream. The crude peptide was dissolved in acetonitrile/water and purified by HPLC (15 mL/min, 35-65% H_2O/ACN + 0.1% TFA, 13 min gradient).

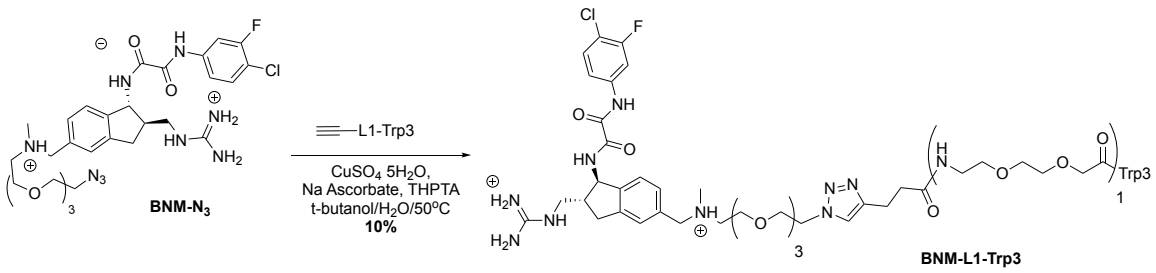

BNM-L1-Trp3. DMF and water were sparged with nitrogen for five hours. A buffer solution (1.45 g guanidine hydrochloride and 0.07 g sodium hydrogen phosphate in 2.5 mL water) was prepared. To the alkyne (0.020 g, 0.010 mmol, 1 eq) in a microwave reactor vessel under nitrogen was added a solution of BNM-III-170-N_3 (0.009 g, 0.010 mmol, 1 eq) in DMF (1 mL) and buffer (1 mL). To this solution were added sodium ascorbate (0.12 g, 0.60 mmol, 60 eq) and $CuSO_4$ $5H_2O$ (0.050 g, 0.20 mmol, 20 eq). The reaction vessel was sealed and subjected to microwave irradiation at 60°C for 13 h. The crude reaction mixture was filtered through sand and diluted with 1:1 acetonitrile/water to 5 mL. The crude diluted mixture was purified by reverse phase HPLC (18 mL/min, 30-60% acetonitrile/water, 9 min) to afford 2.51 mg of BNM-L1-Trp3 (10%).

MALDI-TOF: 2075.214

Alkyne-L3-Trp3 [Z-X-X-X-D-K-W-A-S-L-W-N-W]. The above peptide (Z = 4-pentynoic acid, X = 8-amino-3,6-dioxaoctanoic acid was synthesized using a Liberty Blue solid phase peptide synthesizer. The resin-bound peptide was transferred to a synthesis vessel and washed three times with dichloromethane. A pre-mixed solution of TFA (8 mL), TIPS (1 mL), and water (1 mL) was added. The resin-bound peptide was agitated for 90 minutes, drained, and concentrated with a nitrogen stream. The crude peptide was dissolved in acetonitrile/water and purified by HPLC (15 mL/min, 30-70% H_2O/ACN + 0.1% TFA, 13 min gradient)

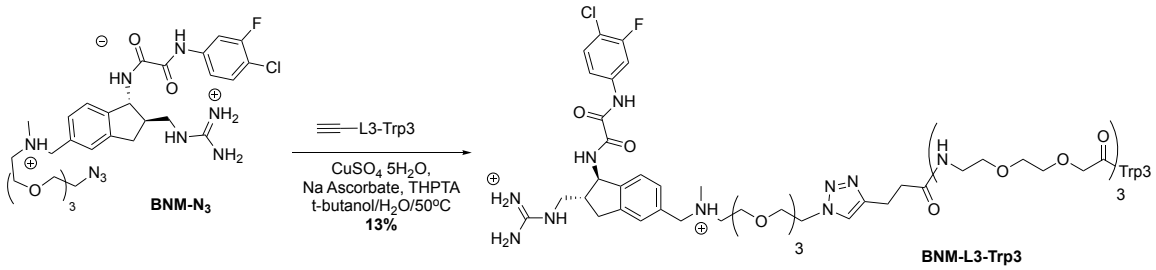

BNM-L3-Trp3. A 1:1 solution of DMF/H2O was sparged with nitrogen for two hours. To alkyne-L3-Trp3 (0.020 g, 0.011 mmol, 1 eq) in a round bottom flask under nitrogen was added 0.1 mL of a 0.1 M solution of BNM-III-170 (0.010 g, 0.011 mmol, 1 eq) in sparged 1:1 DMF/H_2O. To this solution was added a pre-mixed catalyst solution comprised of THPTA (0.019 mg, 0.11 mmol, 10 eq), $CuSO_4$ $5H_2O$ (0.011 g, 0.044 mmol, 4 eq) and sodium ascorbate (0.022 g, 0.044 mmol, 4 eq) in 1 mL 1:1 sparged DMF/H_2O. The crude reaction mixture was transferred with 1:1 water/acetonitrile and filtered through sand. The crude mixture was purified by reverse phase HPLC (15 mL/min, 30-70% H_2O/ACN + 0.1% TFA, 15 min) to afford 4.08 mg of BNM-L3-Trp3 (13%).

AMM (ESI) M+2H/2 1184.0615 obs. (1184.0604 theoretical).

Alkyne-L7-Trp3 [Z-X-X-X-X-X-X-X-D-K-W-A-S-L-W-N-W]. The above peptide (Z = 4-pentynoic acid, X = 8-amino-3,6-dioxaoctanoic acid was was synthesized using a Liberty Blue solid phase peptide synthesizer. The resin-bound peptide was transferred to a synthesis vessel and washed three times with dichloromethane. A pre-mixed solution of TFA (8 mL), TIPS (1 mL), and water (1 mL) was added. The resin-bound peptide was agitated for 90 minutes, drained, and concentrated with a nitrogen stream. The crude peptide was triturated with 3 x Et2O, dissolved in acetonitrile/water and purified by HPLC (15 mL/min, 33-55% H_2O/ACN + 0.1% TFA, 15 min gradient).

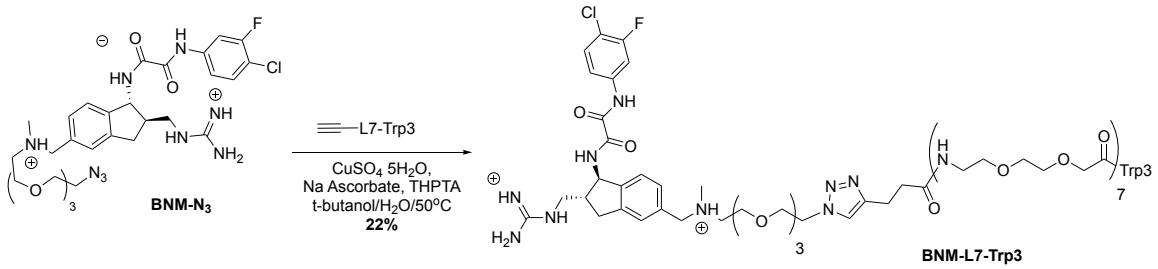

BNM-L7-Trp3. DMF and water were sparged with nitrogen for five hours. A buffer solution (0.58 g guanidine hydrochloride and 0.028 g sodium hydrogen phosphate in 1 mL water) was prepared. To the alkyne (0.027 g, 0.012 mmol, 1 eq) and BNM-III-170-N_3 (0.013 g, 0.015 mmol, 1.3 eq) in a microwave reactor vessel under nitrogen was added buffer solution (2 mL), then sodium ascorbate (0.14 g, 0.70 mmol, 60 eq) and $CuSO_4$ $5H_2O$ (0.058 g, 0.23 mmol, 20 eq). The reaction vessel was sealed and subjected to microwave irradiation at 60oC for 3 h, then stirred at RT for 24 hours. The crude reaction mixture was filtered through sand and diluted with 1:1 acetonitrile/water to 3.5 mL. The crude diluted mixture was purified by reverse phase HPLC (18 mL/min, 30-60% acetonitrile/water, 9 min) to afford 8.52 mg of BNM-L7-Trp3 (22%).

MALDI-TOF: 2946.027

4.4 Experimental Procedures and Spectroscopic Related to Chapter Three

4.4.1 Synthesis of First Generation Photoaffinity Labeled BMS Analogs

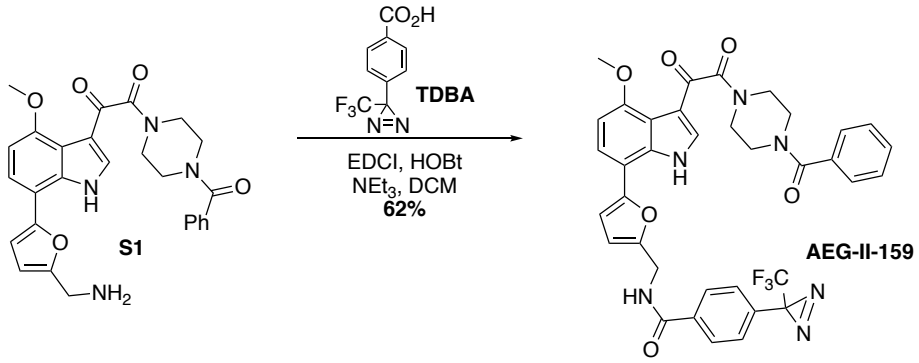

Diazirine **AEG-II-159.** To a solution of **S1** (0.074 g, 0.15 mmol), TDBA (0.052 g, 0.23 mmol, 1.5 eq.), EDCI HCl (0.071 g, 0.46 mmol, 3 eq.), and HOBt H_2O (0.070 g, 0.46 mmol, 3 eq.) in CH_2Cl_2 (6.8 mL) in a round bottom flask shielded from light under N_2 was added NEt_3 (0.11 mL, 0.76 mmol, 5 eq.). After 90 min, no starting material was observed by TLC. The crude reaction mixture was purified by flash column chromatography (SiO_2, 50-100% EtOAc/Hexanes) to afford **AEG-II-159** as a (0.066 g, 62%) yellow solid.

^{1}H NMR (500 MHz, $CDCl_3$) δ 11.26 (s, 1 H), 8.15 (d, 1 H, *J* = 3.3 Hz), 7.82 (app. d, 1 H, *J* = 6.6 Hz), 7.42 (br. s, 5 H), 7.38 (d, 1 H, *J* = 8.3 Hz), 7.20 (d, 2 H, *J* = 8.2 Hz), 7.07 (t, 1 H, *J* = 6.2 Hz), 6.66 (d, 1 H, *J* = 8.3 Hz), 6.52 (d, 1 H, *J* = 3.3 Hz), 6.33 (d, 1 H, *J* =3.3 Hz), 4.66 (d, 2 H, *J* = 6.1 Hz), 3.91 (s, 3 H), 3.97-3.38 (m, 8 H).

^{13}C NMR (500 MHz, $CDCl_3$): 170.9, 167.9, 167.8, 153.8, 152.9, 149.6, 135.7, 135.2, 134.9, 134.4, 133.0, 130.3, 128.8, 127.7, 127.2, 126.8, 120.9, 120.3, 115.6, 115.1, 109.5, 109.4, 103.9, 77.4, 56.1, 37.4, 29.9, 28.6, 28.3.

IR υ_{max} 3849, 3404, 2917, 2849, 2359, 1629, 1577, 1541, 1511, 1467, 1432, 1284, 1155

HRMS (ESI) *m/z* 699.2180 [calcd for $(M+H)^+$ 699.2179]

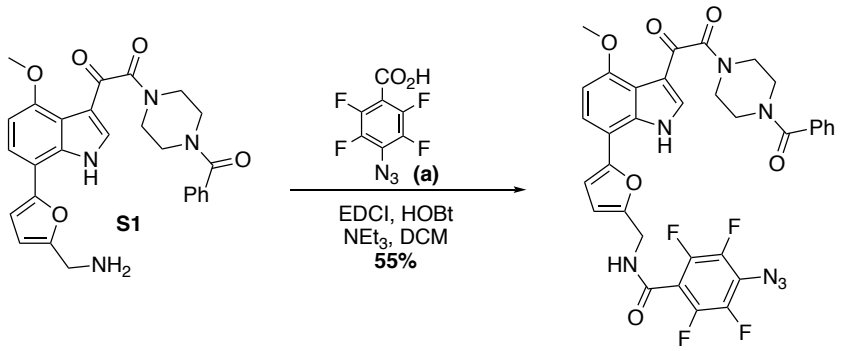

Aryl azide **AEG-II-168**. To a solution of **S1** (0.100 g, 0.206 mmol), **(a)** (0.073 g, 0.31 mmol, 1.5 eq.), EDCI•HCl (0.096 g, 0.62 mmol, 3 eq.), and HOBt•H_2O (0.095 g, 0.62 mmol, 3 eq.) in CH_2Cl_2 (6.8 mL) in a round bottom flask shielded from light under N_2 was added NEt_3 (0.14 mL, 1.03 mmol, 5 eq.). The reaction was allowed to proceed overnight. The crude reaction mixture was concentrated, and purified by flash column chromatography (SiO_2, 60-100% EtOAc/Hexanes) to afford **AEG-II-168** (0.080 g, 55%) as a viscous orange oil.

^{1}H NMR (500 MHz, $CDCl_3$) δ 10.95 (s, 1 H), 8.06 (app. s, 1 H), 7.43 (m, 5 H), 7.20 (m, 1 H), 6.68 (d, 1 H, *J* = 8.3 Hz), 6.56 (d, 1 H, *J* = 3.3 Hz), 6.37 (d, 1 H, *J* = 3.3 Hz), 4.68 (d, 2 H, *J* = 6.1 Hz), 3.90 (s, 3 H), 3.97-3.30 (m, 8 H).

^{13}C NMR (500 MHz, $CDCl_3$): 185.8, 170.8, 167.6, 159.3, 153.7, 152.9, 148.9, 145.3, 139.4, 139.3, 136.1, 134.9, 139.3, 136.1, 134.9, 134.2, 130.2, 128.7, 127.1, 122.3, 120.5, 115.3, 114.8, 110.6, 110.4, 110.3, 109.7, 109.2, 109.1, 108.9, 104.1, 103.9, 55.9, 41.6, 37.3, 29.7

IR υ_{max} 3299, 2918, 2849, 2360, 2341, 2128, 1631, 1545, 1510, 1486, 1429, 1401, 1364, 1271, 1131

HRMS (ESI) *m/z* 704.1859 [calcd for $C_{34}H_{25}F_4N_7O_6$ $(M+H)^+$ 704.1881]

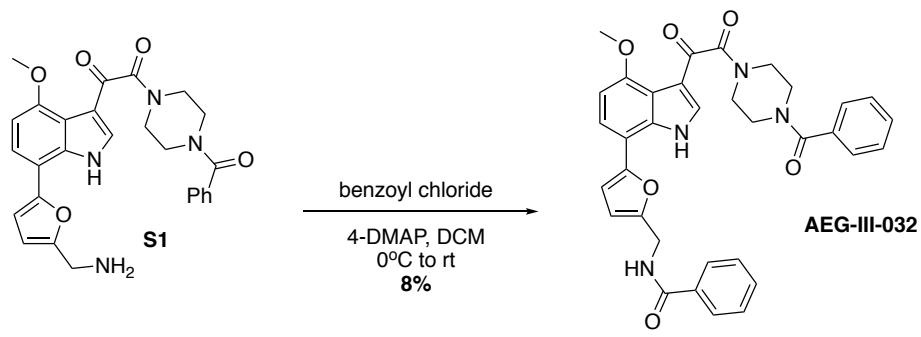

AEG-III-032. To a solution of **S1** (0.039 g, 0.081 mmol) in CH_2Cl_2 (2 mL) under N_2 at 0°C was added 4-DMAP (0.020 g, 0.16 mmol, 2 eq.). After 10 min, benzoyl chloride was added (0.023 g, 0.16 mmol, 2 eq.) and the reaction was allowed to gradually warm to room temperature overnight. The crude reaction mixture was concentrated and subjected to flash column chromatography (SiO_2, 50% EtOAc/Hexanes – 20% MeOH/EtOAc), concentrated, dissolved in 1.5 mL ACN + 0.8 mL water, and further purified by reverse phase HPLC (15 mL/min 45-80% ACN/H_2O + 0.1% TFA, 6 min) to afford **AEG-III-032** (0.004 g, 8%).

^{1}H NMR (500 MHz, $CDCl_3$) δ 11.31 (s, 1 H), 8.21 (s, 1 H), 7.80 (d, 1 H, *J* = 7.3 Hz), 7.52 (t, 1 H, *J* = 7.5 Hz), 7.43 (m, 8 H), 6.99 (t, 1 H, *J* = 6.4 Hz), 6.69 (d, 1 H, *J* = 8.3 Hz), 6.53 (d, 1 H, *J* = 3.3 Hz), 6.34 (d, 1 H, *J* = 3.3 Hz), 4.69 (d, 1 H, *J* = 6.1 Hz), 3.93 (s, 3 H), 3.99-3.39 (m, 8 H)

^{13}C NMR (500 MHz, $CDCl_3$): 171.5, 169.6, 167.9, 158.6, 158.3, 153.9, 152.9, 149.7, 136.1, 134.5, 133.7, 132.4, 130.6, 129.0, 128.9, 127.2, 127.2, 120.4, 116.0, 115.7, 115.0, 113.7, 109.6, 109.4, 104.1, 103.9, 56.1, 37.4

IR υ_{max} 3434, 2360, 2095, 1645, 1517, 1432, 1272, 1206, 1147, 916

HRMS (ESI) *m/z* 591.2265 [calcd for $C_{34}H_{30}N_4O_6$ $(M+H)^+$ 591.2244]

4.3.2 Synthesis of Second Generation Photoaffinity Labeled BMS Analogs

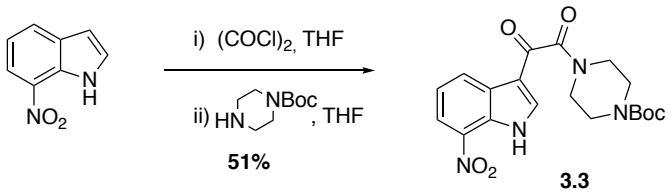

3.3

Piperazine **3.3**. To 7-nitroindole (0.50 g, 3.1 mmol) in THF (8 mL) under N_2 at room temperature was added oxalyl chloride (1.4 mL, 15.4 mmol, 5 eq.). After 23 hours the crude reaction mixture was concentrated and redissolved in THF under N_2. To this solution was added 1-boc-piperazine (0.69 g, 3.7 mmol, 1.2 eq.) then NEt_3 (1.2 mL, 6.16 mmol, 2 eq.). The reaction was allowed to proceed for 24 h. The crude reaction mixture was diluted with CH_2Cl_2 and washed with $NaHCO_3$. The organic layer was dried with $MgSO_4$, decanted, and concentrated. The crude reaction mixture was purified using flash column chromatography (SiO_2, 0-100% EtOAc/Hexanes) to afford **3.3** as a (0.626 g, 51%) yellow solid.

^{1}H NMR (500 MHz, $CDCl_3$) □ 10.56 (s, 1 H), 8.76 (d, 1 H, *J* = 7.9 Hz), 8.28 (d, 1 H, *J* = 8.1 Hz), 8.21 (d, 1 H, *J* = 3.1 Hz), 7.47 (app. t, 1 H, *J* = 8.0 Hz), 3.75 (m, 2 H), 3.58 (m, 2 H), 3.55-3.47 (m, 4 H).

^{13}C NMR (500 MHz, $CDCl_3$): 185.3, 165.3, 154.6, 137.0, 133.6, 130.5, 129.8, 128.8, 123.1, 121.2, 115.7, 80.8, 46.2, 41.8, 28.5

IR □$_{max}$ 3273, 2976, 1699, 1634, 1532, 1485, 1412, 1364, 1332, 1302, 1286, 1249, 1166, 1125, 1063, 1035, 995, 974, 928, 863, 810, 795, 772, 734, 659

HRMS (ESI) *m/z* 425.1255 [calcd for $C_{19}H_{22}N_4O_6$ (M+Na) 425.1437]

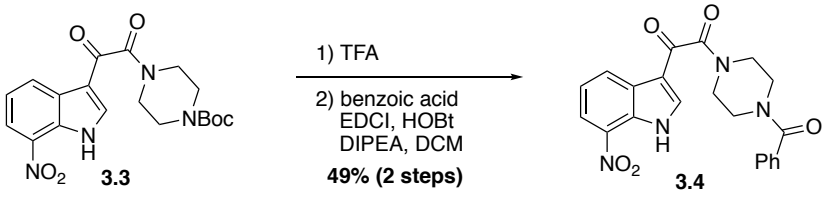

3.3 **3.4**

Amide **3.4**. To a solution of **3.3** (0.386 g, 0.959 mmol) in CH_2Cl_2 (6.5 mL) was added TFA (1.5 mL, 1.5 mL / mmol). After four hours, no starting material was observed by LC/MS. The reaction mixture was concentrated repeatedly with CH_2Cl_2. The crude product was then put under N_2 atmosphere and dissolved in CH_2Cl_2 (10 mL). To this solution was added benzoic acid (0.129 g, 1.05 mmol, 1.1 eq.), EDCI•HCl (0.203 g, 1.05 mmol, 1.1 eq.), and HOBt•H_2O (0.142 g, 1.05 mmol, 1.1 eq). After 25 minutes NEt_3 was added and to the reaction mixture, and the reaction was allowed to proceed overnight. The crude reaction mixture was washed with $NaHCO_3$ then NH_4Cl. The organic layer was dried with $MgSO_4$, decanted, and concentrated. The crude reaction mixture was purified using flash column chromatography (SiO_2, 50% EtOAc/Hexanes – 10% MeOH/EtOAc) to afford **3.4** as a (186 mg, 49%) yellow solid.

^{1}H NMR (500 MHz, $CDCl_3$) δ 10.58 (s, 1 H), 8.74 (s, 1 H), 8.27 (d, 1 H, *J* = 8.1 Hz), 8.23 (d, 1 H, *J* = 2.9 Hz), 7.45 (m, 6 H), 4.08-3.41 (m, 8 H).

^{13}C NMR (500 MHz, $CDCl_3$): 185.0, 170.9, 165.2, 137.2, 135.0, 133.6, 130.4, 129.8, 128.9, 128.8, 127.2, 123.2, 121.3, 115.6, 42.1, 29.9

IR υ_{max} 3449, 2925, 2854, 1741, 1631, 1532, 1438, 1369, 1333, 1251, 1116, 1050, 975, 792, 736, 440, 425, 410

HRMS (ESI) *m/z* 407.1341 [calcd for $C_{21}H_{18}N_4O_5$ (M+H) 407.1355]

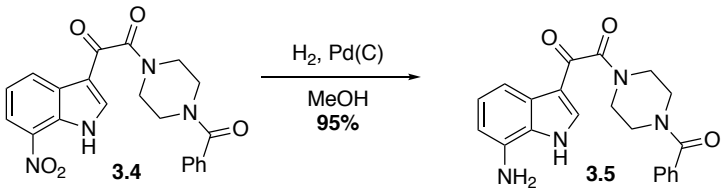

Amine **3.5**. To a solution of **3.4** (0.186 g, 0.458 mmol) in methanol (10 mL) under N_2 was added Pd/C (0.010 g). H_2 gas was then bubbled into the solution and the reaction was allowed to stir overnight. The crude reaction mixture was filtered through sand and concentrated to afford **3.5** (163 mg, 95%) as an olive green solid.

^{1}H NMR (500 MHz, $CDCl_3$) □ 10.89 (s, 1 H), 7.64 (app. s, 1 H), 7.40 (m, 6 H), 7.07 (t, 1 H, *J* = 7.7 Hz), 6.56 (d, 1 H, *J* = 7.6 Hz), 3.49 (s, 2 H), 3.94-3.32 (m, 8 H).

^{13}C NMR (500 MHz, $CDCl_3$): 185.0, 171.0, 167.2, 135.2, 134.8, 132.8, 130.5, 129.8, 128.9, 127.2, 127.0, 126.3, 124.7, 114.6, 112.1, 110.2, 51.0, 46.3, 41.7

IR υ_{max} 3583, 3366, 3237, 2914, 1717, 1621, 1522, 1434, 1251, 1158, 1003, 427

HRMS (ESI) *m/z* 377.1600 [calcd for $C_{21}H_{20}N_4O_3(M+H)^+$ 377.1614]

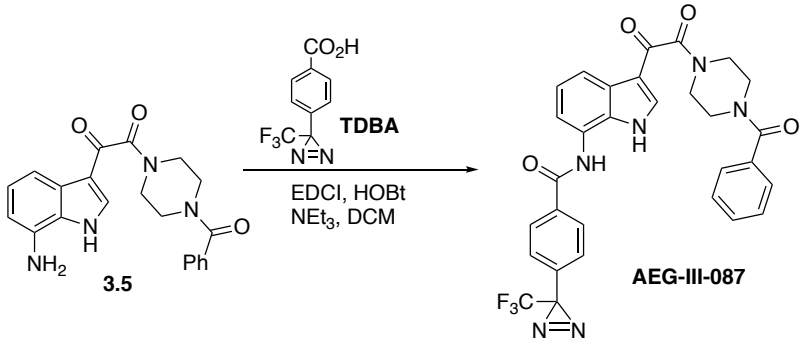

Diazirine **AEG-III-087**. To a solution of **S4** (0.156 g, 0.414 mmol), TDBA (0.143 g, 0.622 mmol, 1.5 eq.), EDCI•HCl (0.119 g, 0.622 mmol, 1.5 eq.), and HOBt•H_2O (0.095 g, 0.622 mmol, 1.5 eq.) in CH_2Cl_2 (18.4 mL) in a round bottom flask shielded from light under N_2 was added NEt_3 (0.11 mL,

0.828 mmol, 2 eq.). After 18 h, the crude reaction material was concentrated, dissolved in 1:1 ACN/H_2O and purified using reverse phase HPLC (15 mL/min 20-95% ACN/H_2O + 0.1% TFA, 15 min) to afford **AEG-III-087** as a green-yellow solid (3.4 mg, 1.4%).

^{1}H NMR (500 MHz, $CDCl_3$) δ 9.10 (s, 1 H), 8.10 (s, 1 H), 8.00(d, 2 H, *J* = 8.1 Hz), 7.64 (s, 1 H), 7.43 (m, 5 H), 7.30 (d, 2 H, *J* = 8.1 Hz), 7.20 (m, 1 H), 7.01 (d, 1 H, *J* = 7.6 Hz), 4.02-3.33 (m, 8 H)

^{13}C NMR (500 MHz, $CDCl_3$): 184.9, 171.3, 166.7, 165.2, 135.6, 134.7, 134.5, 133.5, 130.6, 130.5, 128.9, 128.7, 128.2, 127.7, 127.2, 126.9, 126.5, 123.6, 123.1, 122.9, 120.9, 119.9, 116.8, 114.2, 41.8, 29.9, 28.7, 28.4, 28.0

IR υ_{max} 3281, 2923, 2861, 1784, 1717, 1627, 1429, 1250, 1156, 999, 939, 440, 425, 409

HRMS (ESI) *m/z* 589.1798 [calcd for $C_{30}H_{23}F_3N_6O_4$ $(M+H)^+$ 589.1811]

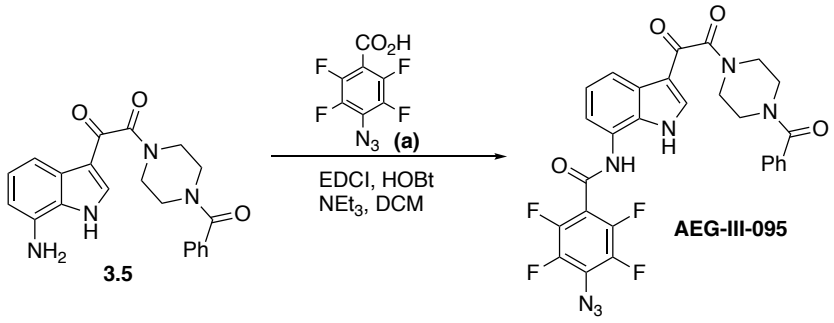

Azide **AEG-III-095**. To a solution of **(a)** (0.024 g, 0.10 mmol, 1.5 eq.) in CH_2Cl_2 (4 mL) in a round bottom flask shielded from light under N_2 at 0°C was added EDCI•HCl (0.016 g, 0.010 mmol, 1.5 eq.), HOBt•H_2O (0.015 g, 0.10 mmol, 1.5 eq.), NEt_3 (0.02 mL, 0.13 mmol, 2 eq.), then **S4** (0.025 g, 0.066 mmol). The reaction mixture was allowed to gradually warm to room temperature overnight. The crude reaction mixture was concentrated, dissolved in 1:1 ACN/H_2O, and purified using reverse phase HPLC (15 mL/min 20-95% ACN/H_2O + 0.1% TFA, 15 min) to afford **AEG-III-095** as a green-yellow solid (0.68 mg, 2%).

^{1}H NMR (500 MHz, $CDCl_3$) δ 10.47 (s, 1 H), 8.80 (s, 1 H), 8.24 (s, 1 H), 7.81 (s, 1 H), 7.45 (m, 5 H), 6.96 (d, 1 H, *J* = 7.6 Hz), 4.03-3.40 (m, 8 H).

^{13}C NMR (500 MHz, $CDCl_3$): 184.7, 171.0, 166.4, 156.3, 135.5, 134.5, 130.4, 128.8, 128.1, 127.8, 127,1, 123.5, 121.8, 120.5, 116.4, 114.3, 29.7

IR υ_{max} 3265, 2359, 2127, 1634, 1486, 1422, 1257, 1157, 999, 912, 731, 668

HRMS (ESI) *m/z* 594.1520 [calcd for $C_{28}H_{19}F_4N_7O_4$ $(M+H)^+$ 594.1513]

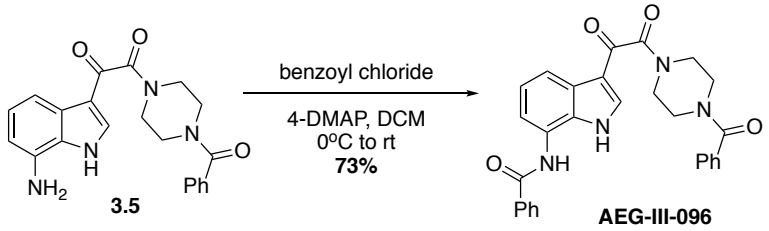

Amide **AEG-III-096**. To a solution of **S4** (0.044 g, 0.12 mmol) in CH_2Cl_2 (2.5 mL) under N_2 at 0°C was added benzoyl chloride (0.049 g, 0.35 mmol, 3 eq.), then 4-DMAP (0.043 g, 0.35 mmol, 3 eq.). The reaction mixture was allowed to gradually warm to room temperature overnight. After 15 h, the crude reaction mixture was purified using flash column chromatography (SiO_2, 0-100% EtOAc/Hex) to afford **AEG-III-096** (0.041 g, 73%) as a white solid.

^{1}H NMR (500 MHz, $CDCl_3$) δ 11.07 (s, 1 H), 8.95 (s, 1 H), 8.10 (s, 1 H), 7.96 (d, 1 H, *J* = 7.6 Hz), 7.70 (s, 1 H), 7.58 (t, 1 H, *J* = 7.5 Hz), 7.40 (m, 5 H), 7.18 (app. s, 1 H), 7.06 (d, 1 H), *J* = 7.51 Hz), 3.93-3.29 (m, 8 H).

^{13}C NMR (500 MHz, $CDCl_3$): 185.1, 170.9, 166.6, 166.4, 135.6, 135.0, 133.8, 132.5, 130.4, 129.0, 128.9, 128.8, 127.7, 127.2, 123.5, 123.4, 119.5, 116.6, 114.4, 29.9

IR υ_{max} 3283, 1629, 1528, 1425, 1251, 1157, 998, 710, 427

HRMS (ESI) *m/z* 481.1876 [calcd for $C_{28}H_{24}N_4O_4$ $(M+H)^+$ 481.1876]

APPENDIX

Spectroscopic Data Relevant to Chapter One

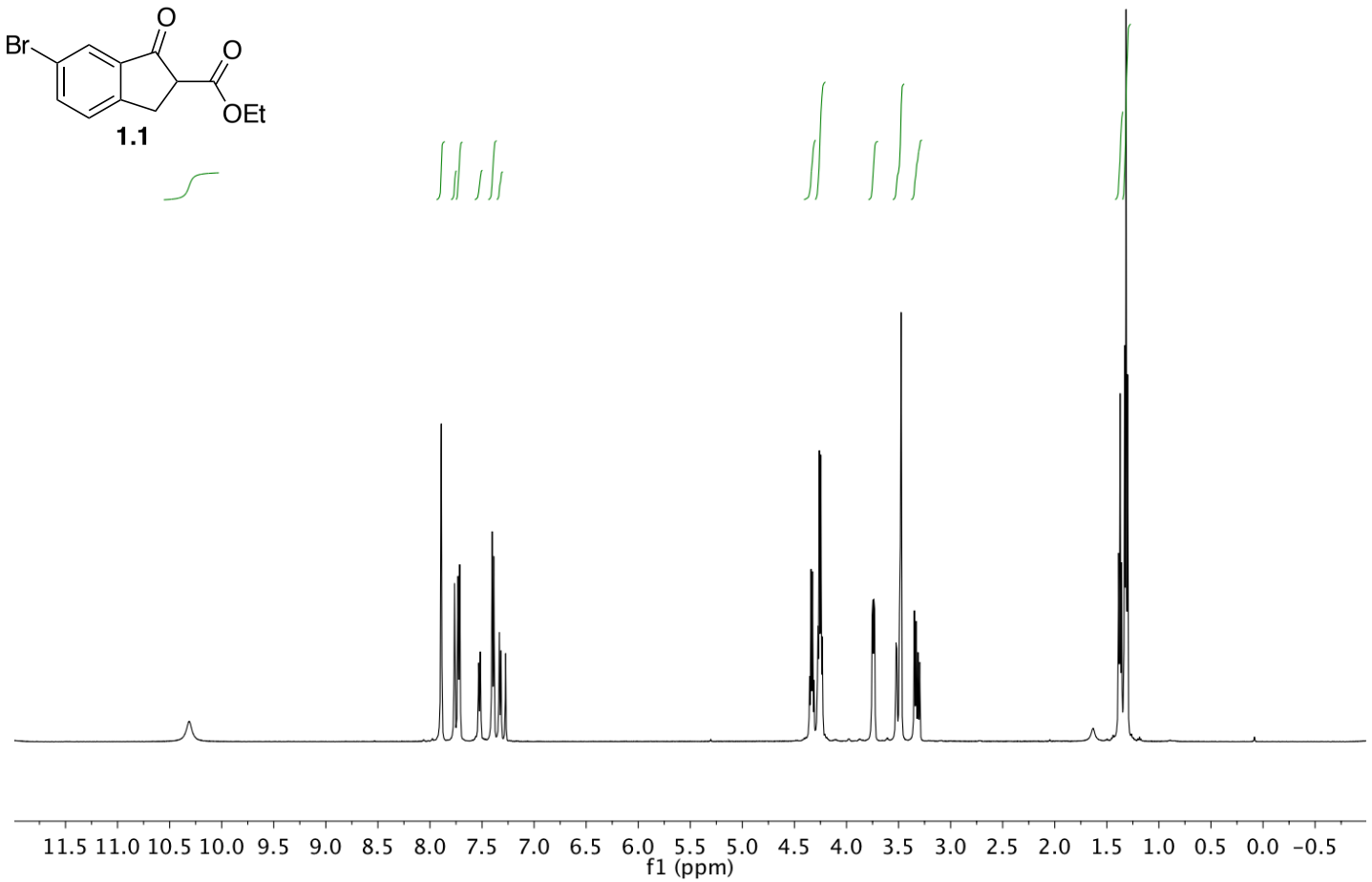

Figure A.1.1.1. The 500 MHz ^{1}H NMR Spectrum of Compound **1.1** in $CDCl_3$.

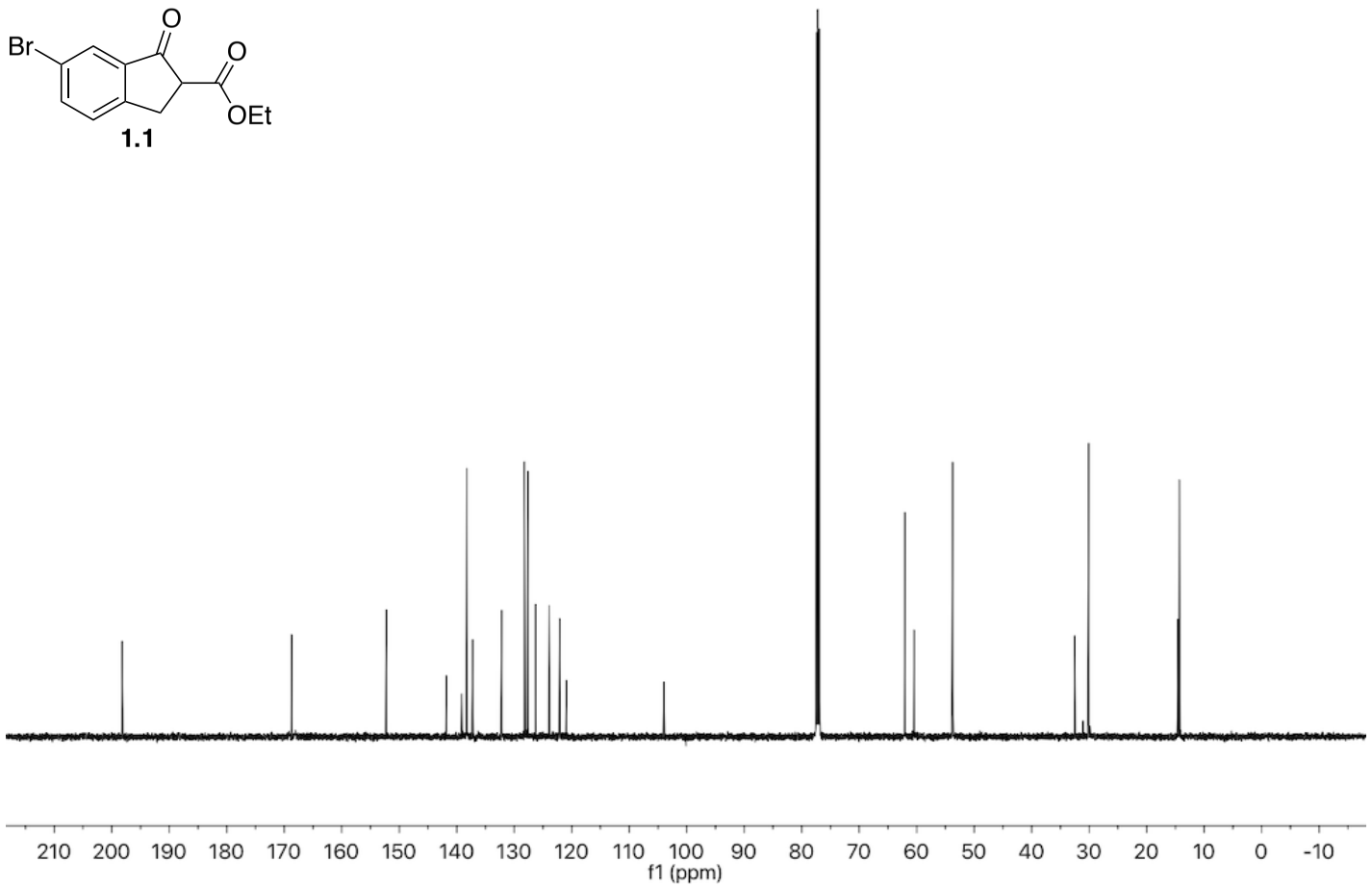

Figure A.1.1.2. The 500 MHz ^{13}C NMR Spectrum of Compound **1.1** in $CDCl_3$.

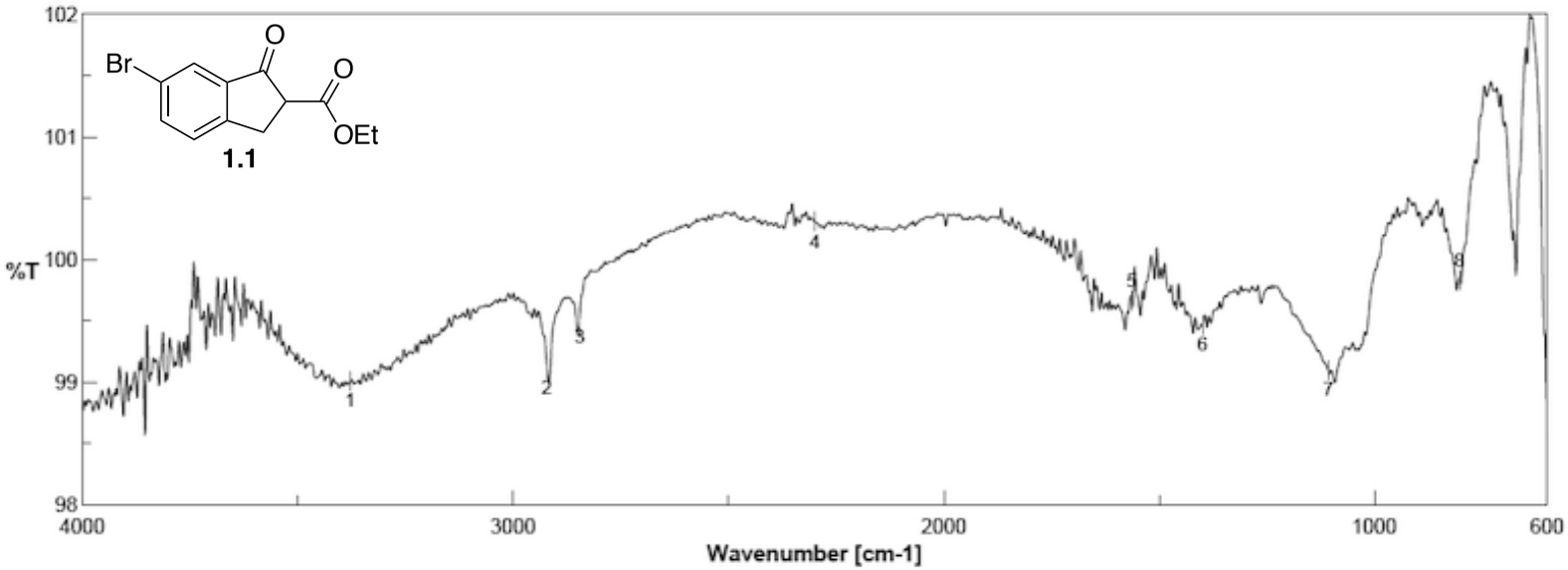

Figure A.1.1.3. The Infrared Spectrum of Compound **1.1**.

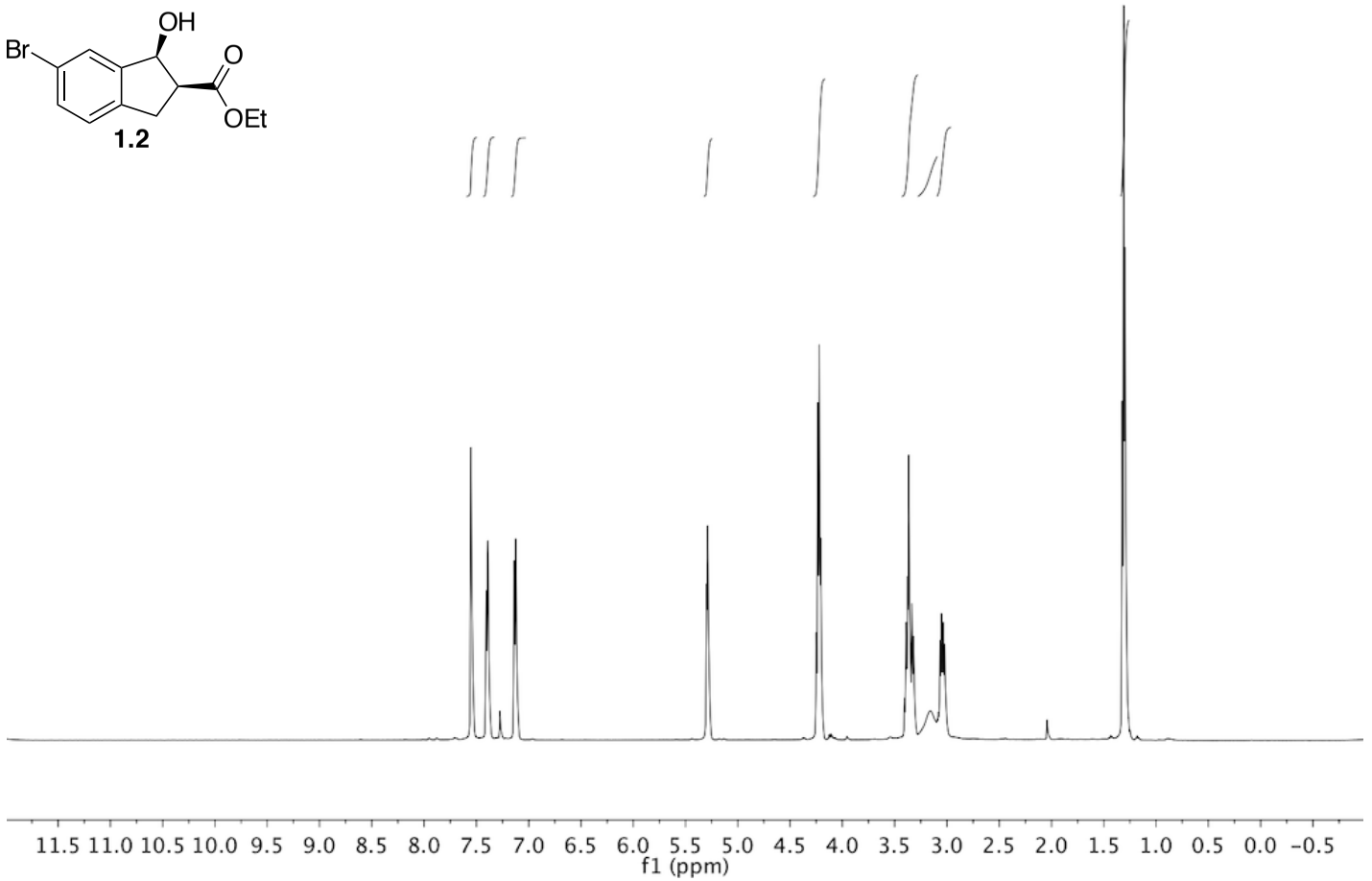

Figure A.1.2.1. The 500 MHz ^{1}H NMR Spectrum of Compound **1.2** in $CDCl_3$.

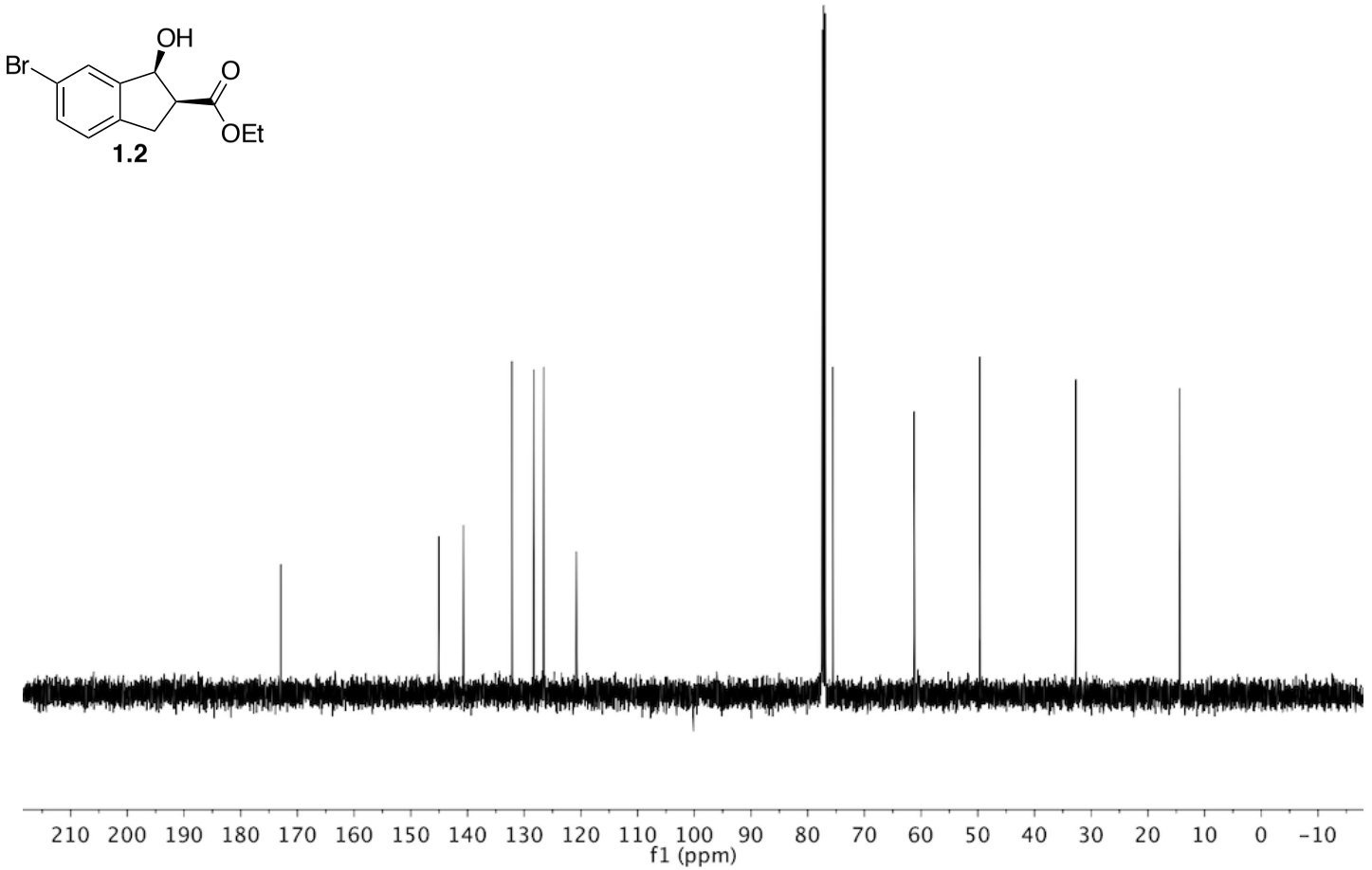

Figure A.1.2.2. The 500 MHz ^{13}C NMR Spectrum of Compound **1.2** in $CDCl_3$.

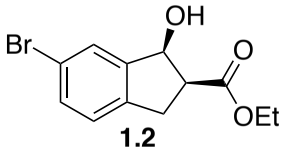

1.2

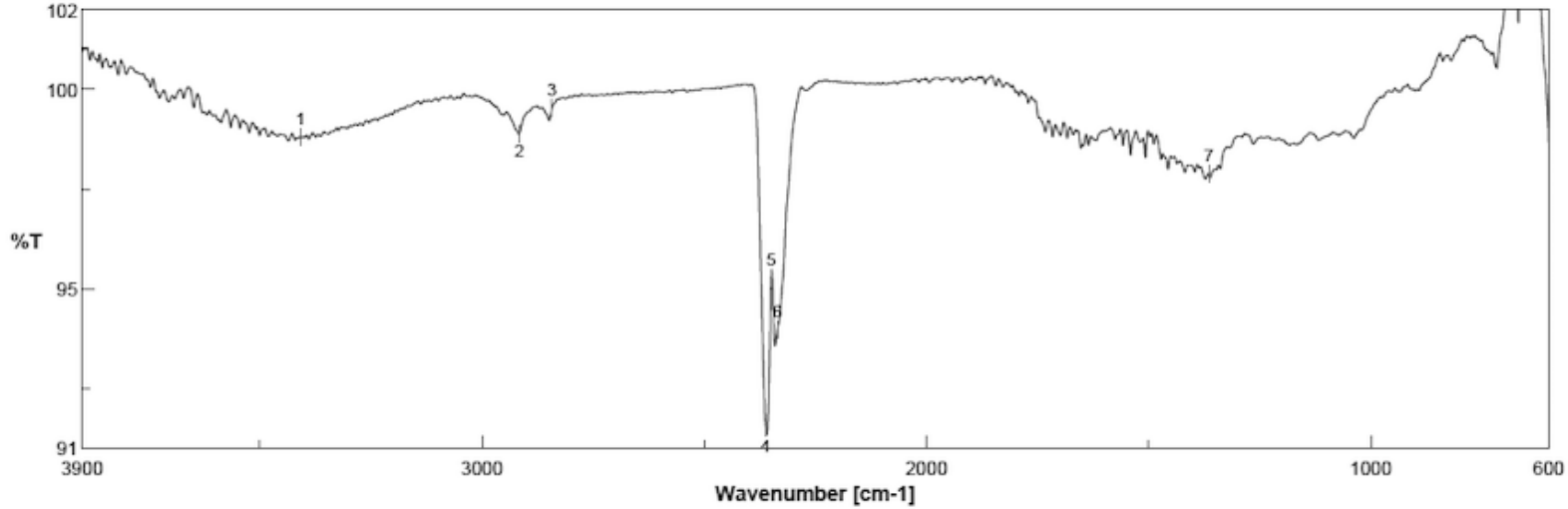

Figure A.1.2.3. The Infrared Spectrum of Compound **1.2**.

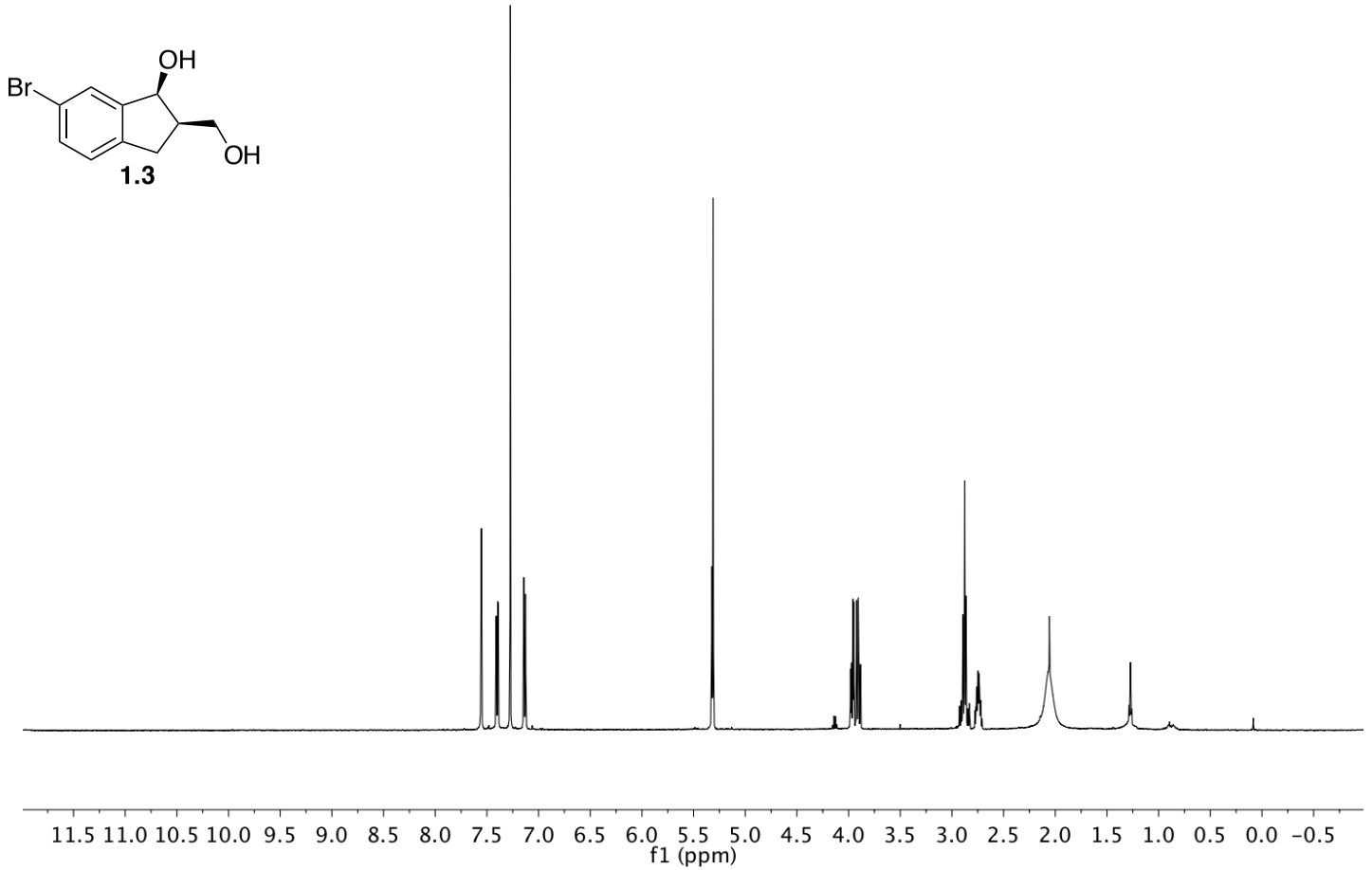

Figure A.1.3.1. The 500 MHz ^{1}H NMR Spectrum of Compound **1.3** in $CDCl_3$.

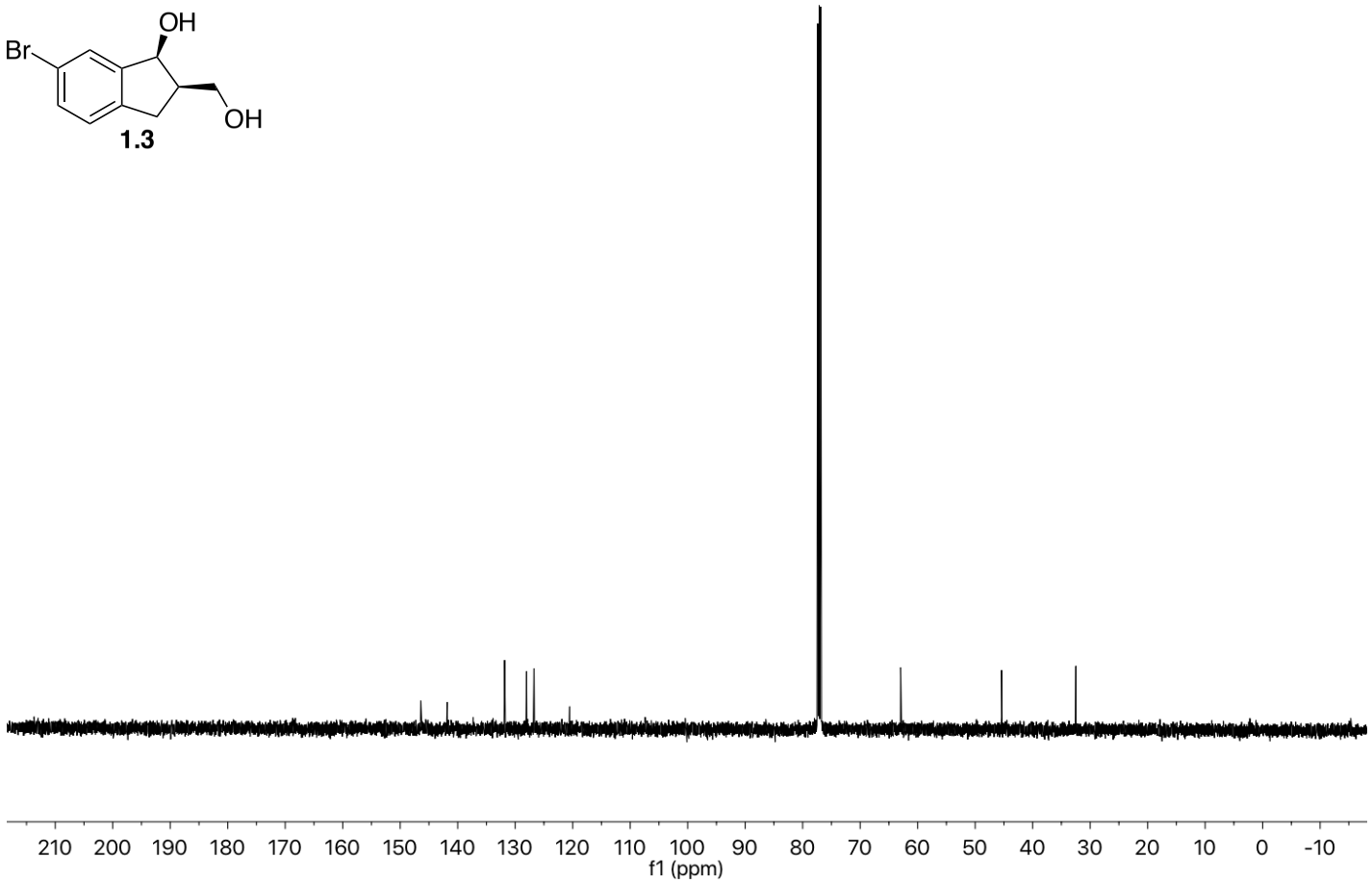

Figure A.1.3.2. The 500 MHz ^{13}C NMR Spectrum of Compound **1.3** in $CDCl_3$.

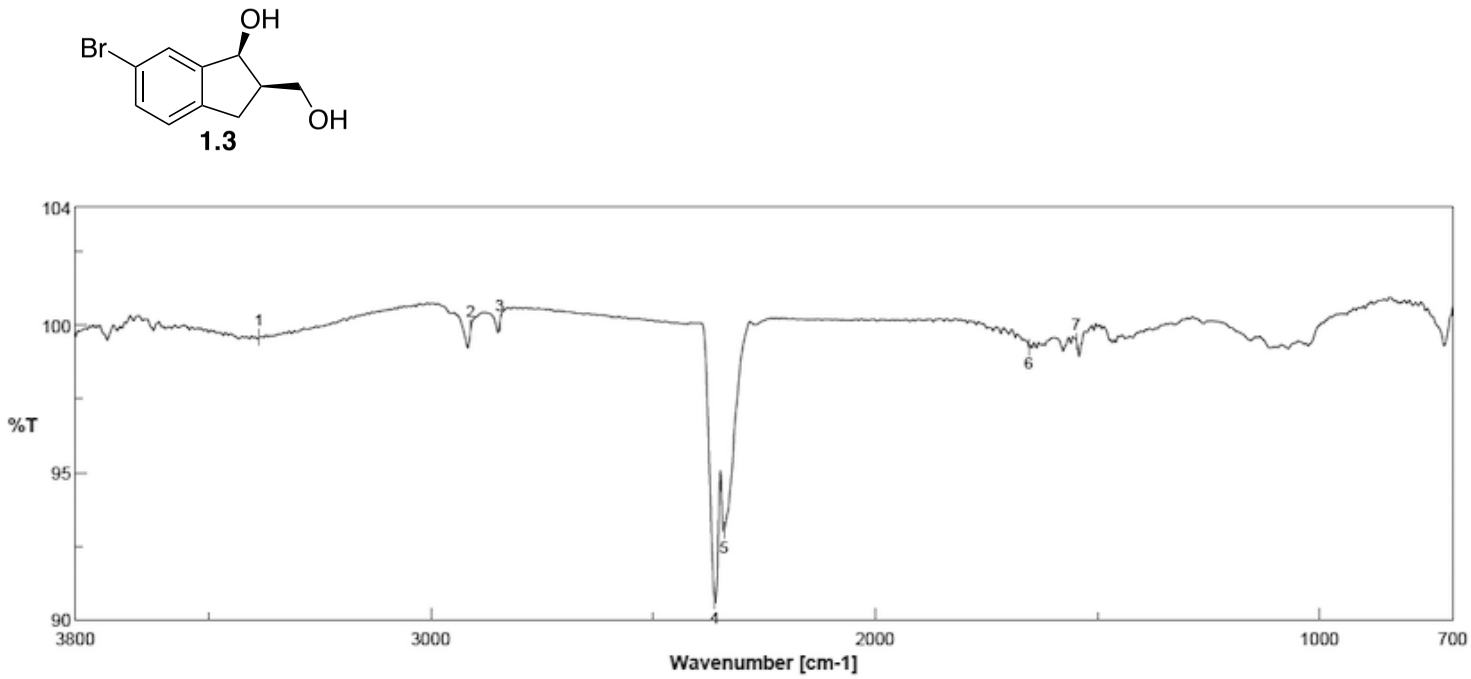

Figure A.1.3.3. The Infrared Spectrum of Compound **1.3**.

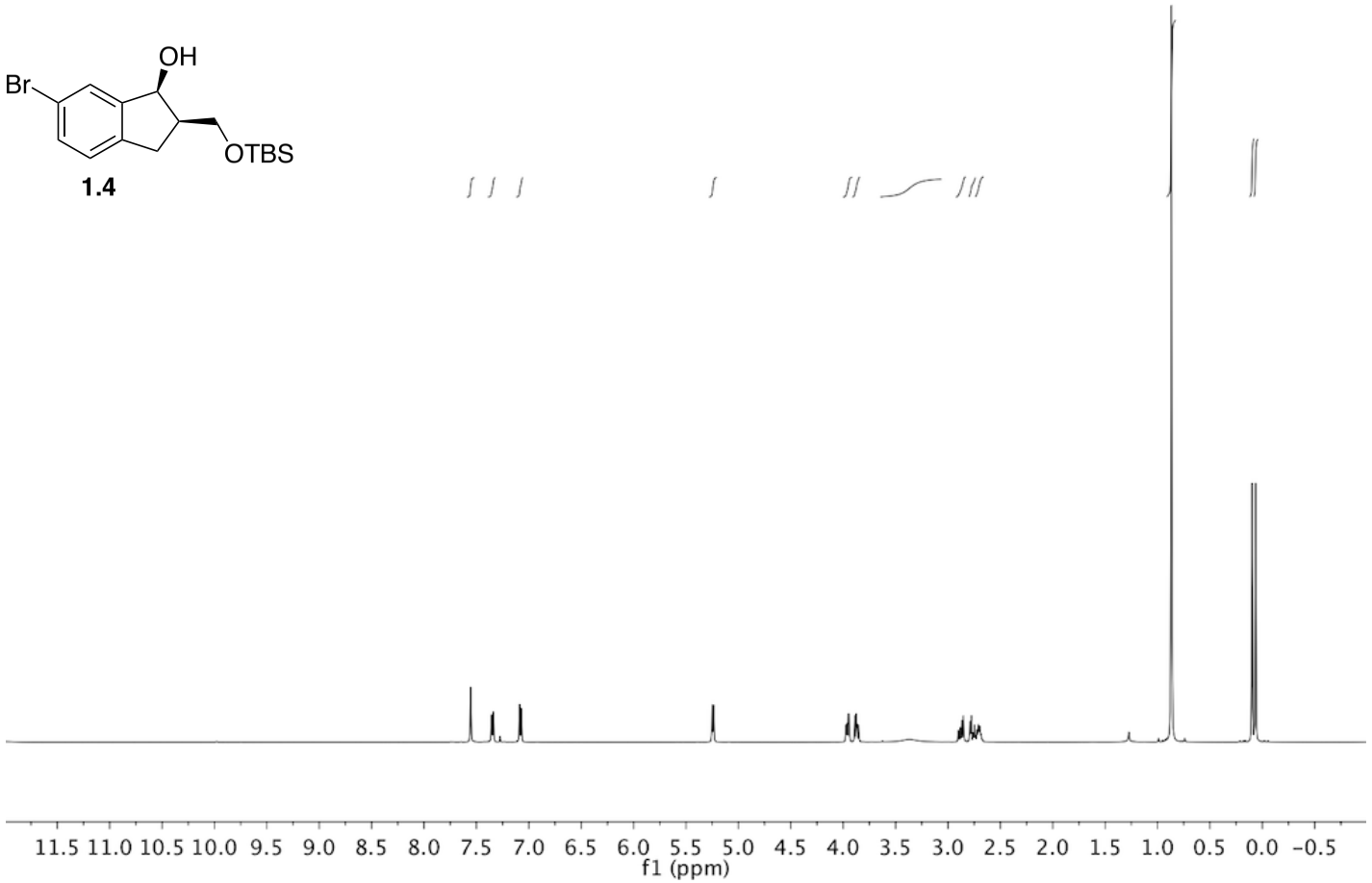

Figure A.1.4.1. The 500 MHz ^{1}H NMR Spectrum of Compound **1.4** in $CDCl_3$.

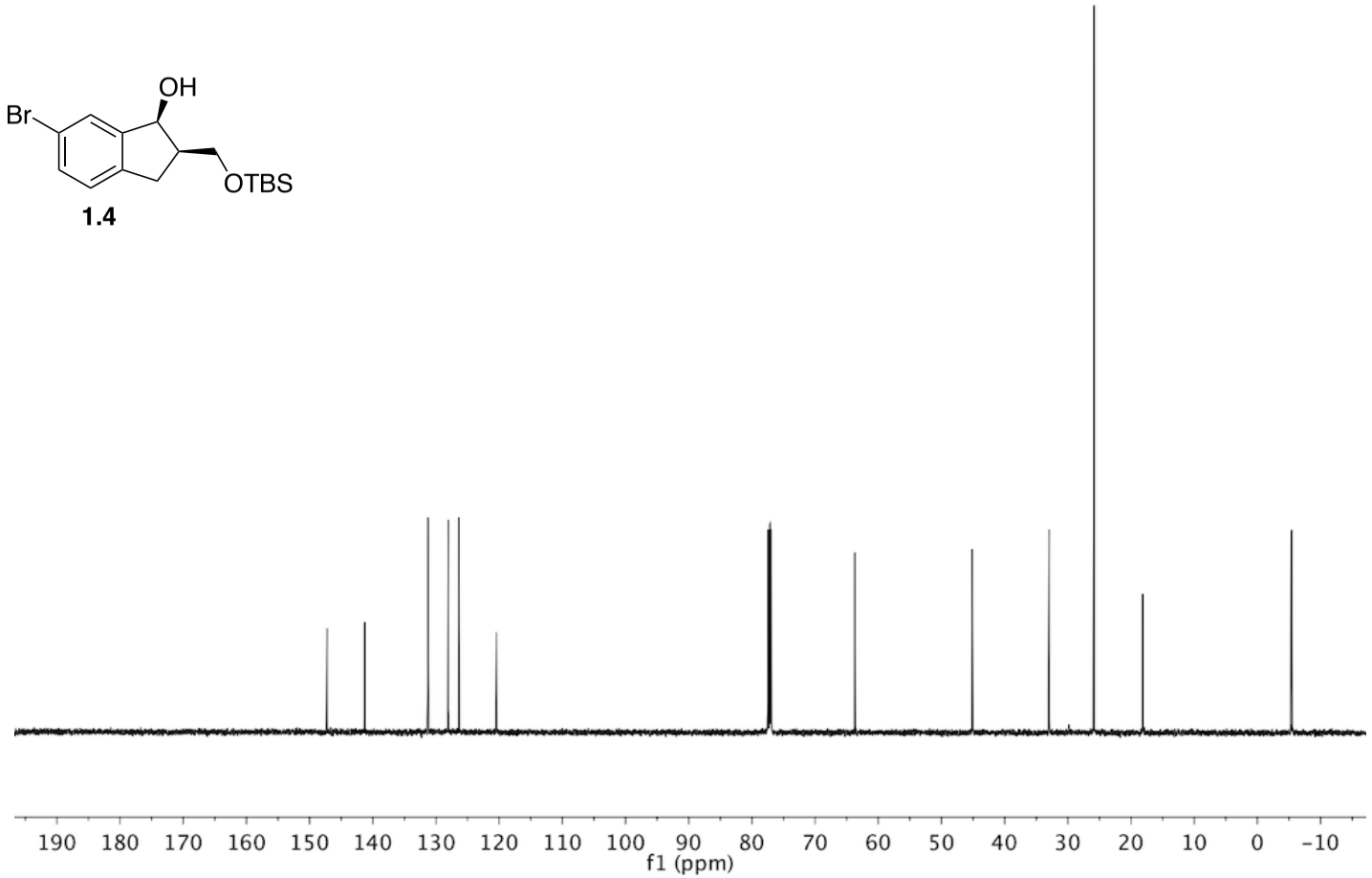

Figure A.1.4.2. The 500 MHz ^{13}C NMR Spectrum of Compound **1.4** in $CDCl_3$.

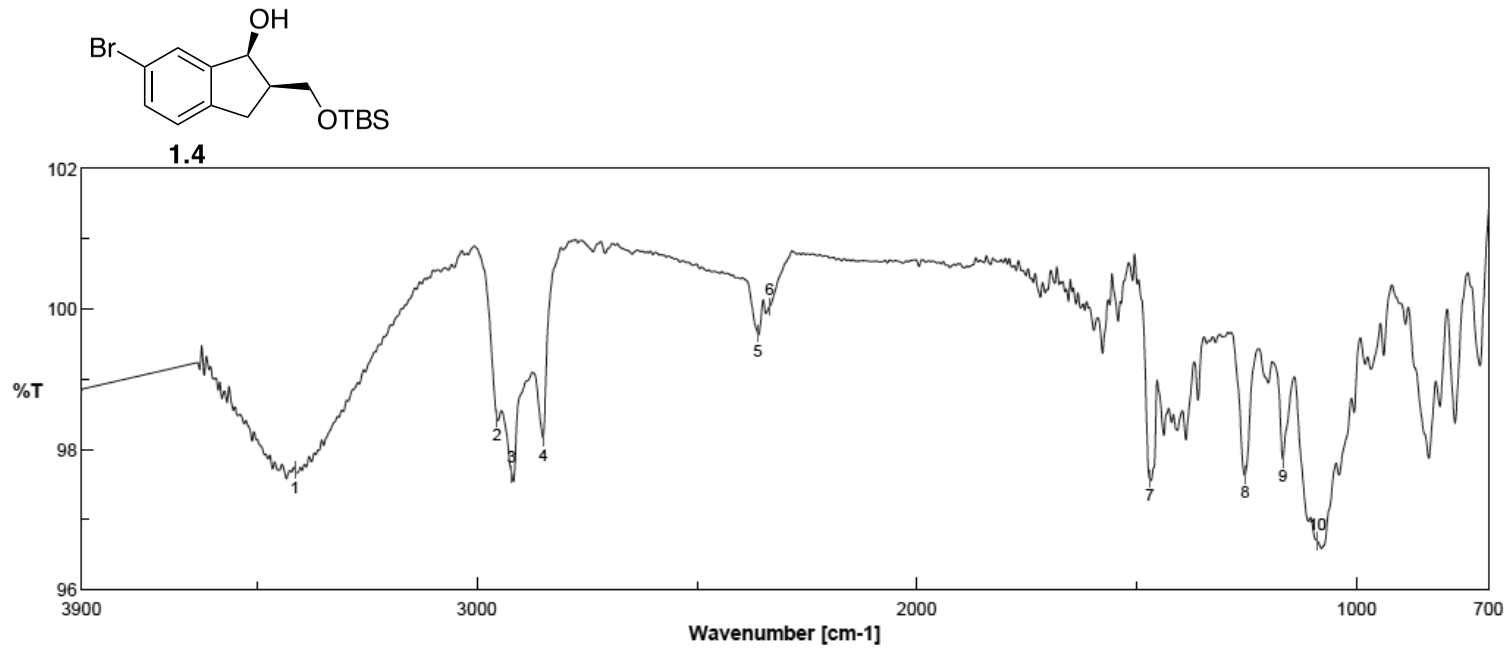

Figure A.1.4.3. The Infrared Spectrum of Compound **1.4**.

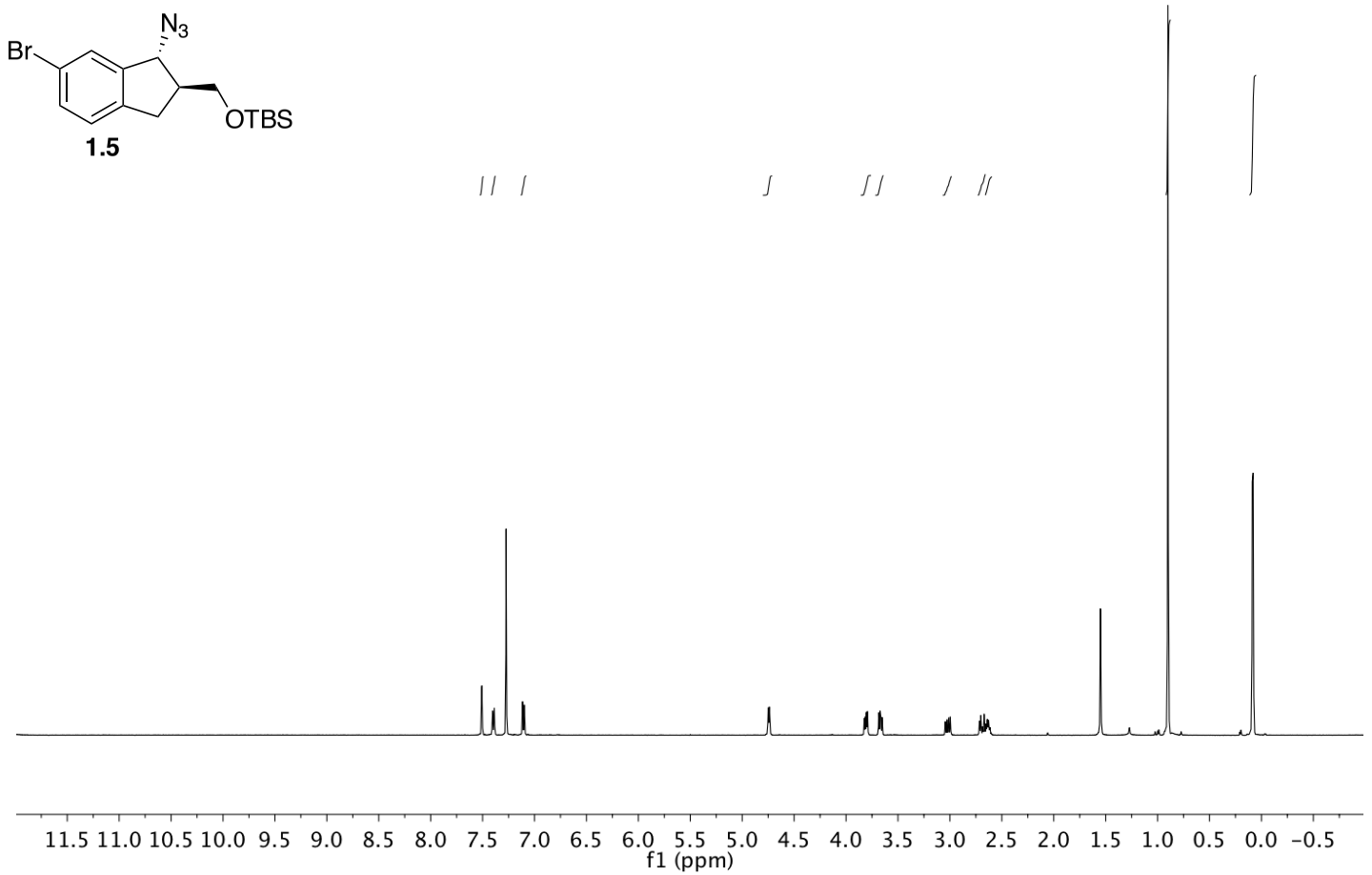

Figure A.1.5.1. The 500 MHz ^{1}H NMR Spectrum of Compound **1.5** in $CDCl_3$.

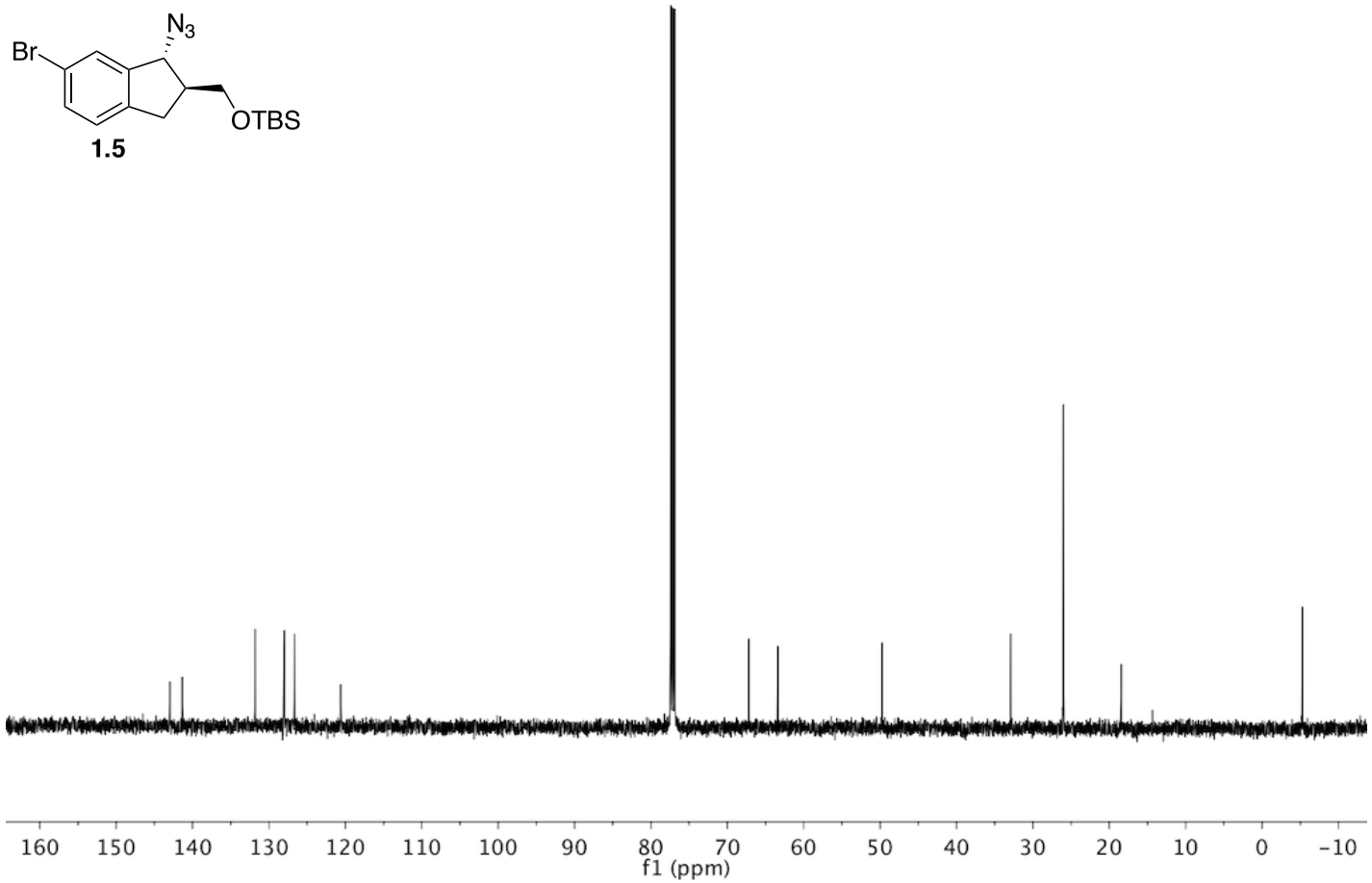

Figure A.1.5.2. The 500 MHz ^{13}C NMR Spectrum of Compound **1.5** in $CDCl_3$.

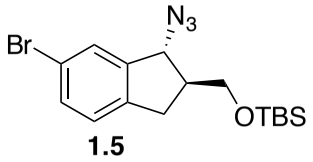

1.5

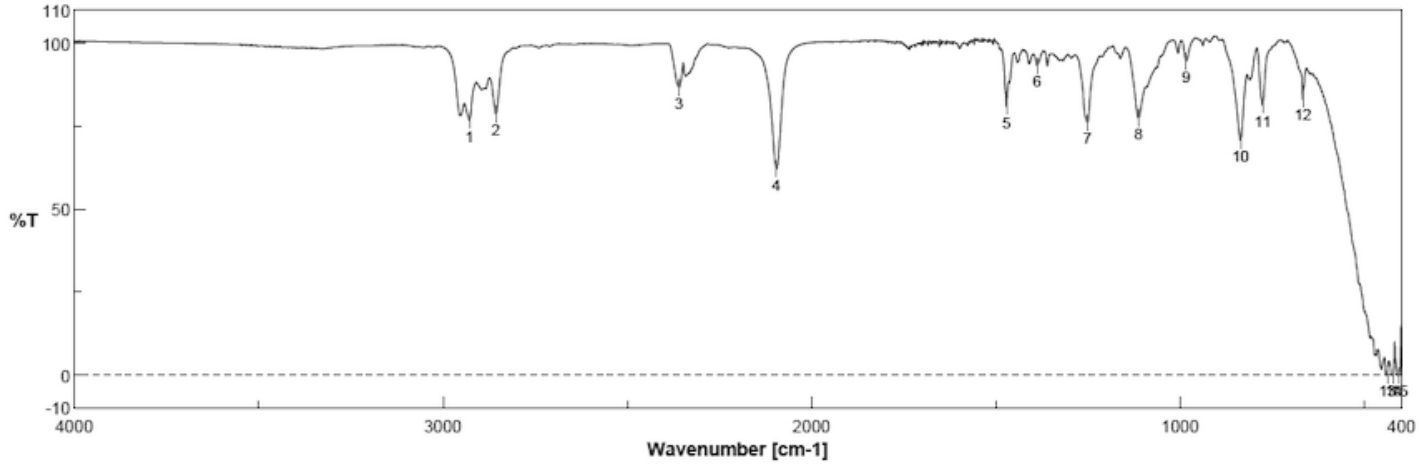

Figure A.1.5.3. The Infrared Spectrum of Compound **1.5**.

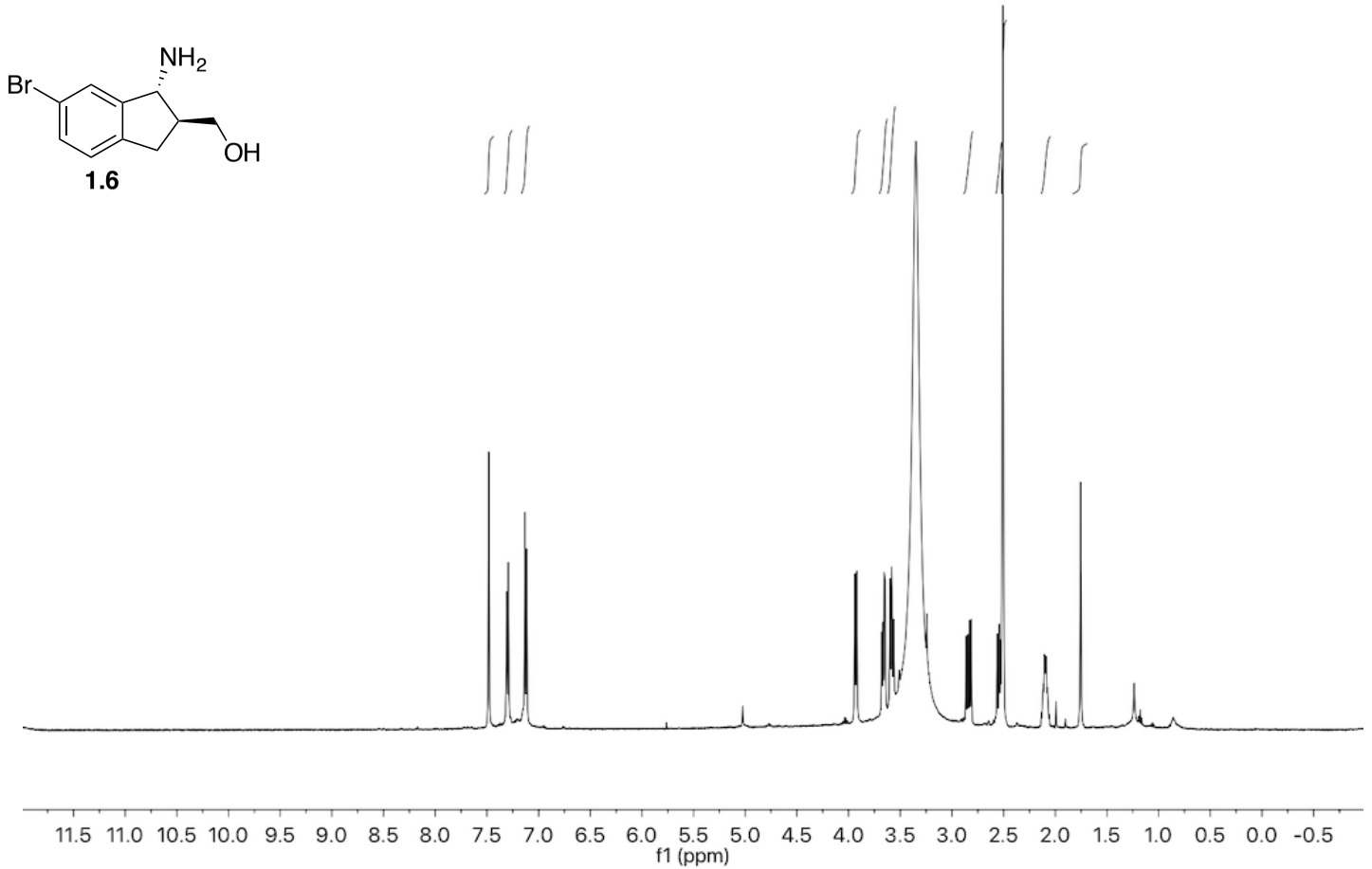

Figure A.1.6.1. The 500 MHz ^{1}H NMR Spectrum of Compound **1.6** in DMSO.

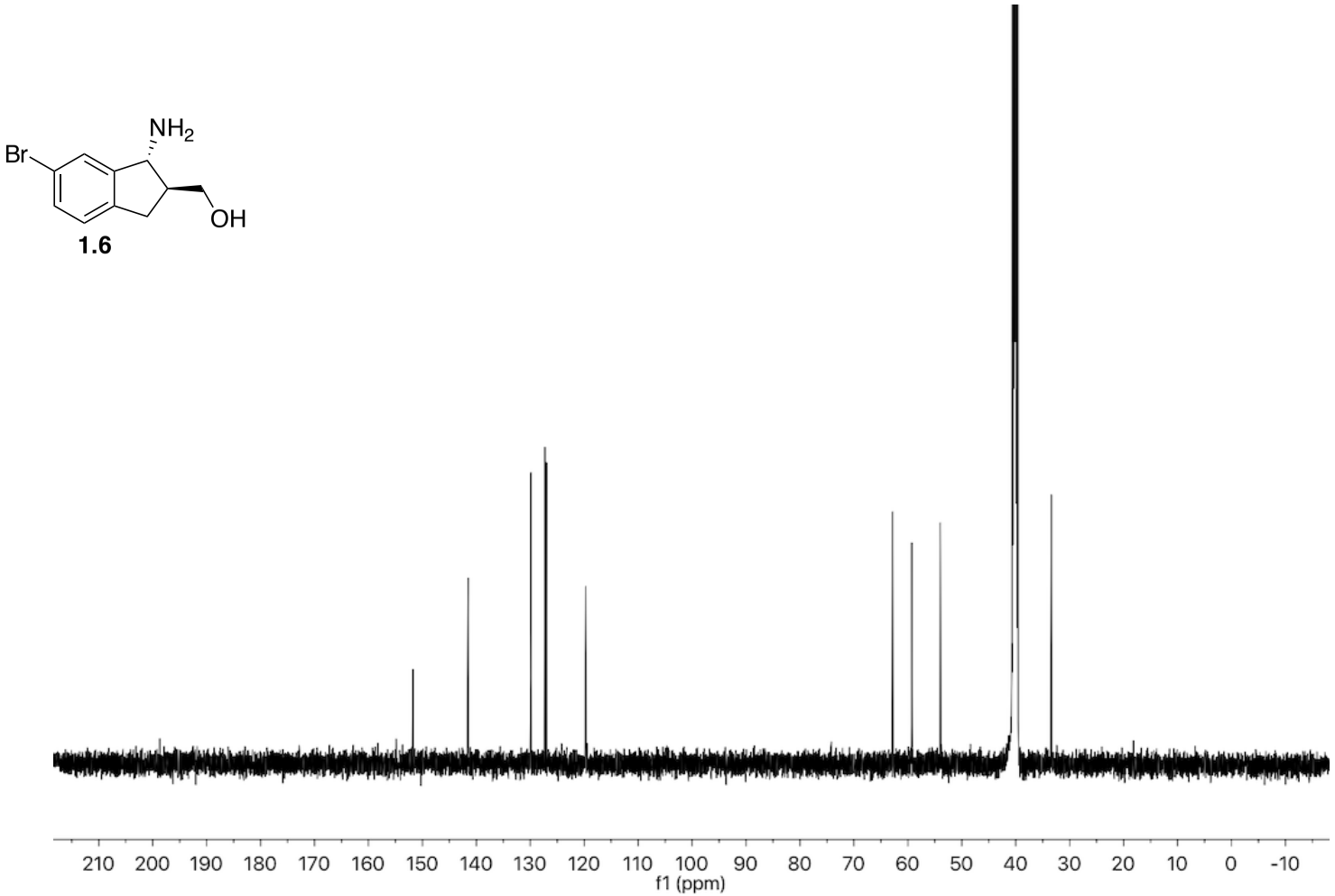

Figure A.1.6.2. The 500 MHz ^{13}C NMR Spectrum of Compound **1.6** in DMSO.

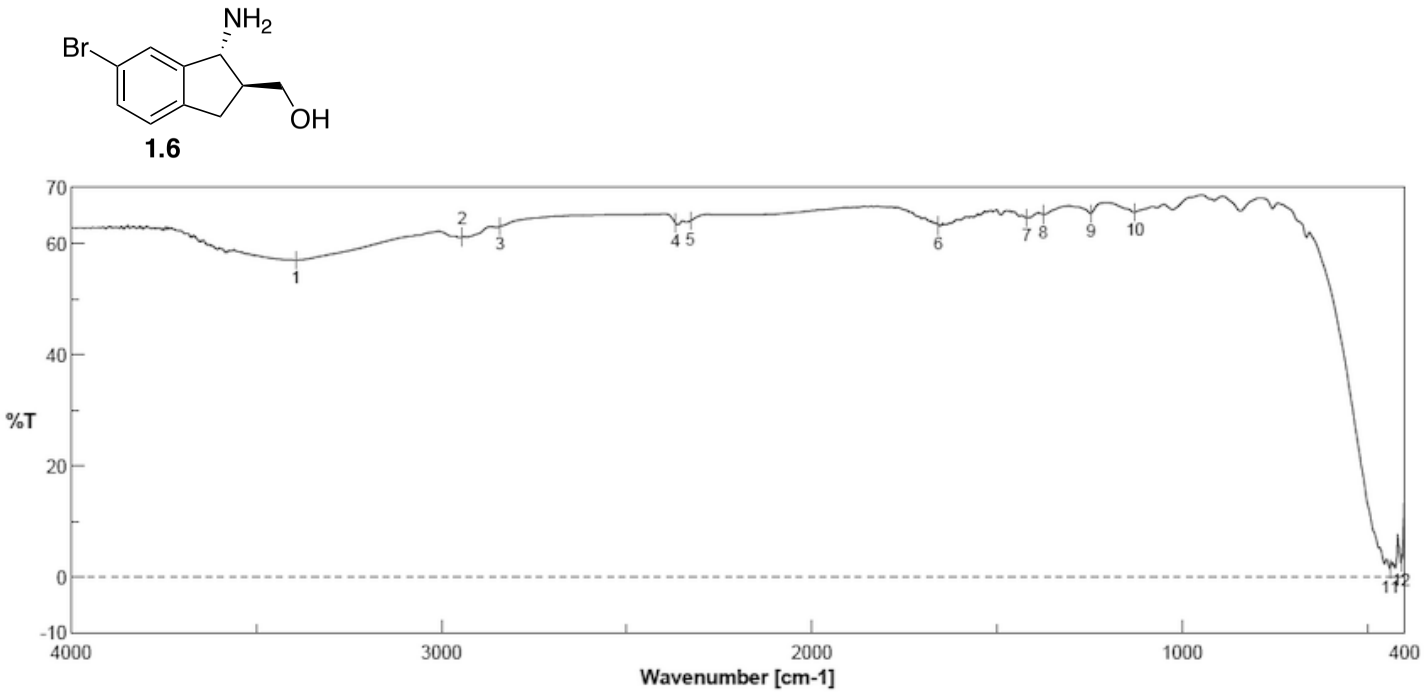

Figure A.1.6.3. The Infrared Spectrum of Compound **1.6**.

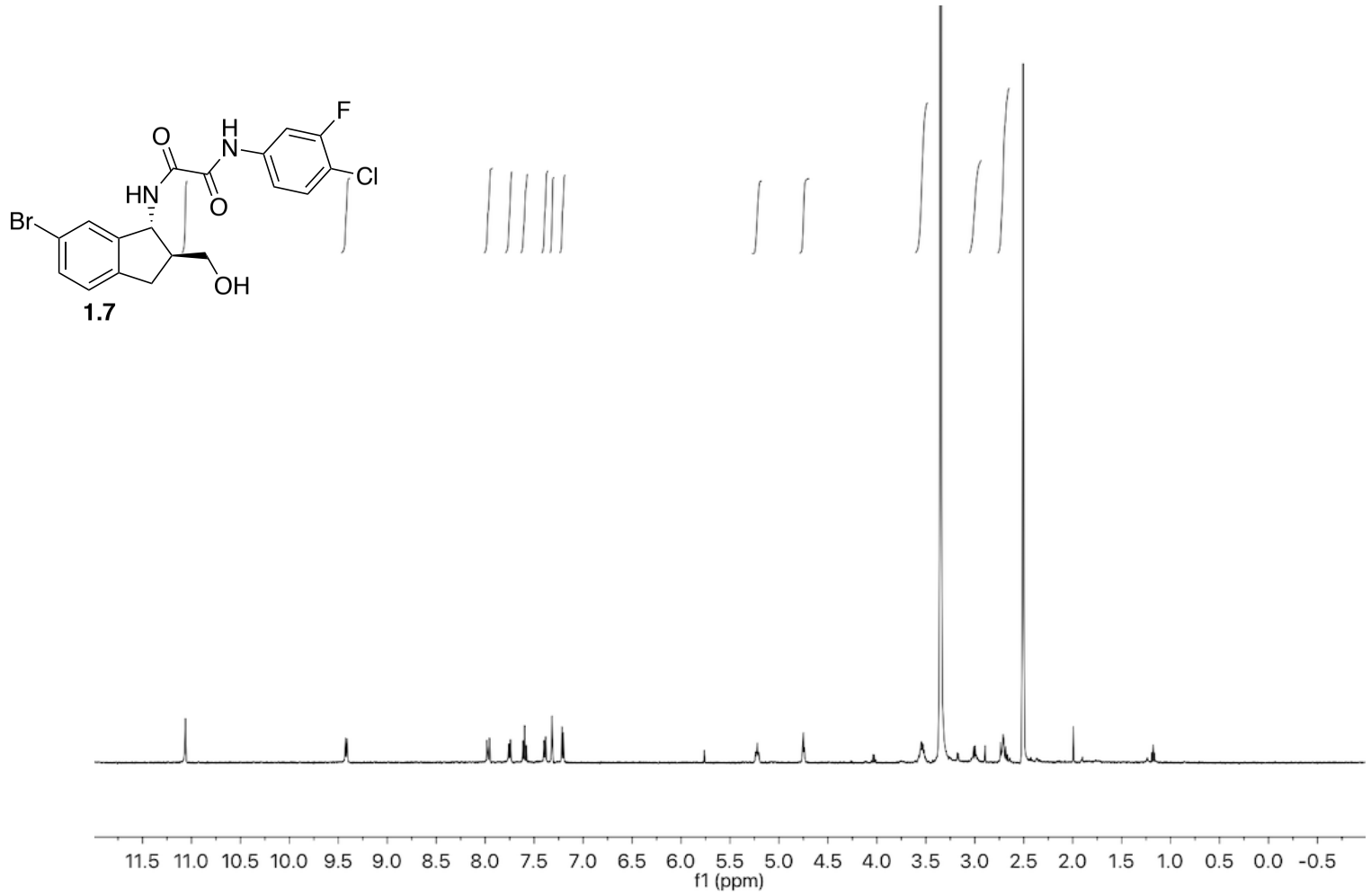

Figure A.1.7.1. The 500 MHz ^{1}H NMR Spectrum of Compound **1.7** in DMSO.

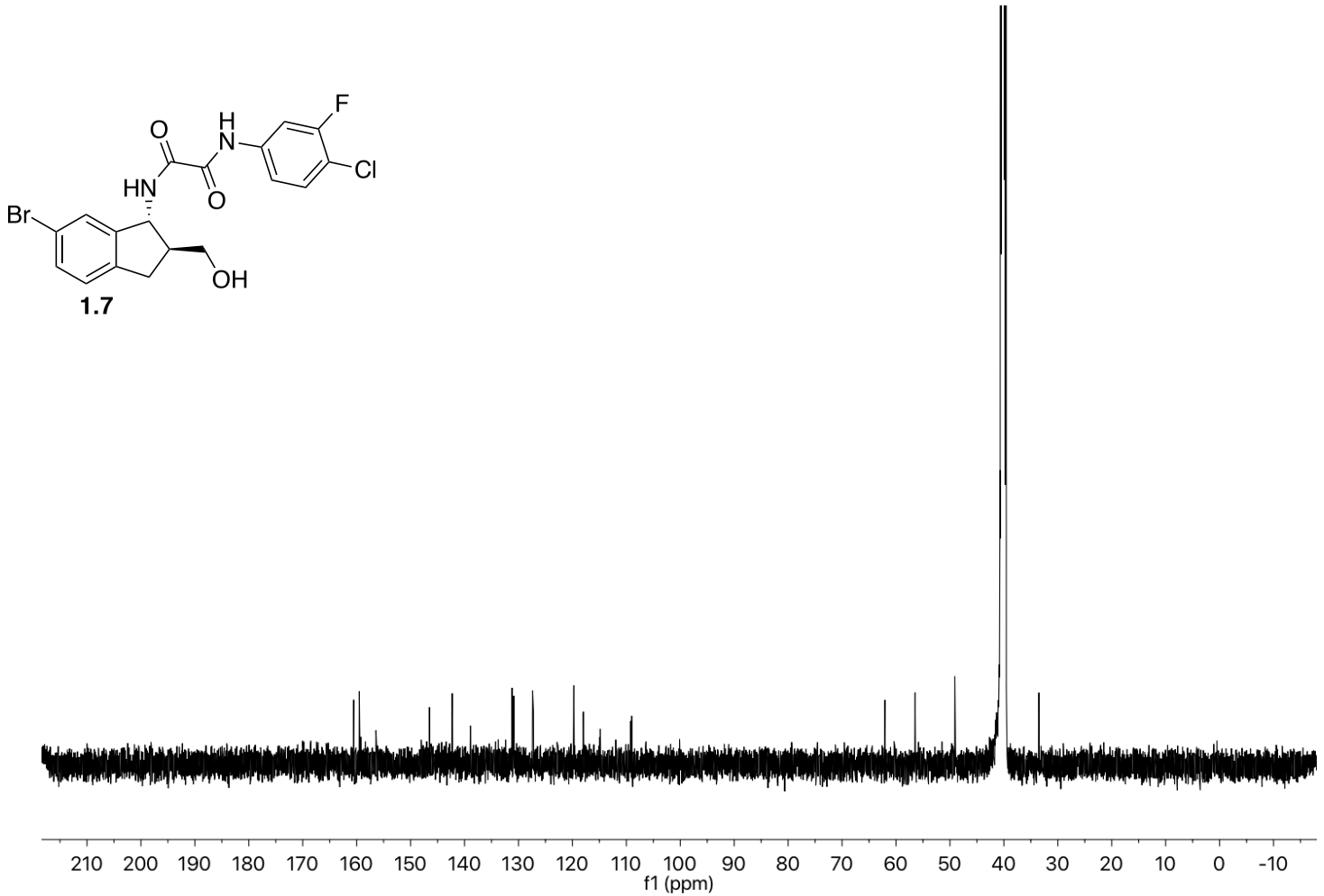

Figure A.1.7.2. The 500 MHz ^{13}C NMR Spectrum of Compound **1.7** in DMSO.

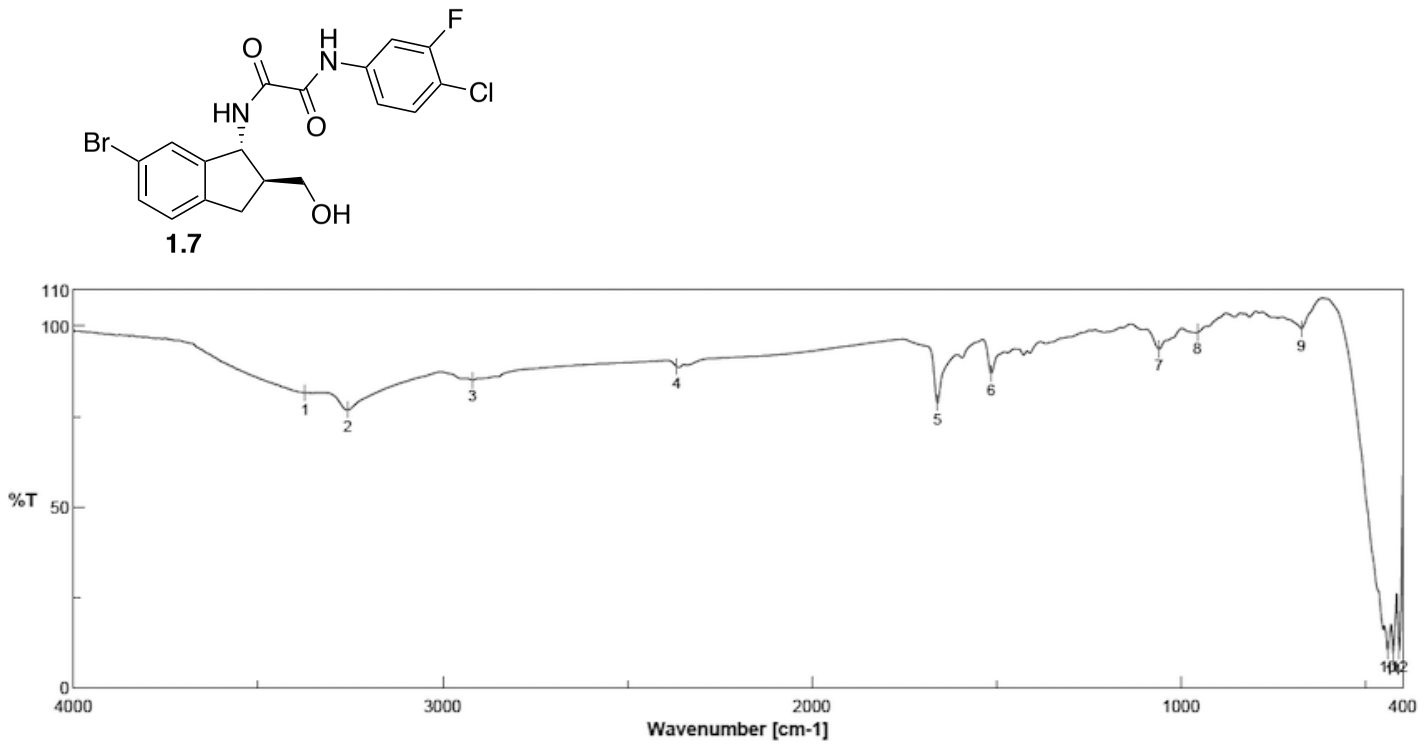

Figure A.1.7.3. The Infrared Spectrum of Compound **1.7**.

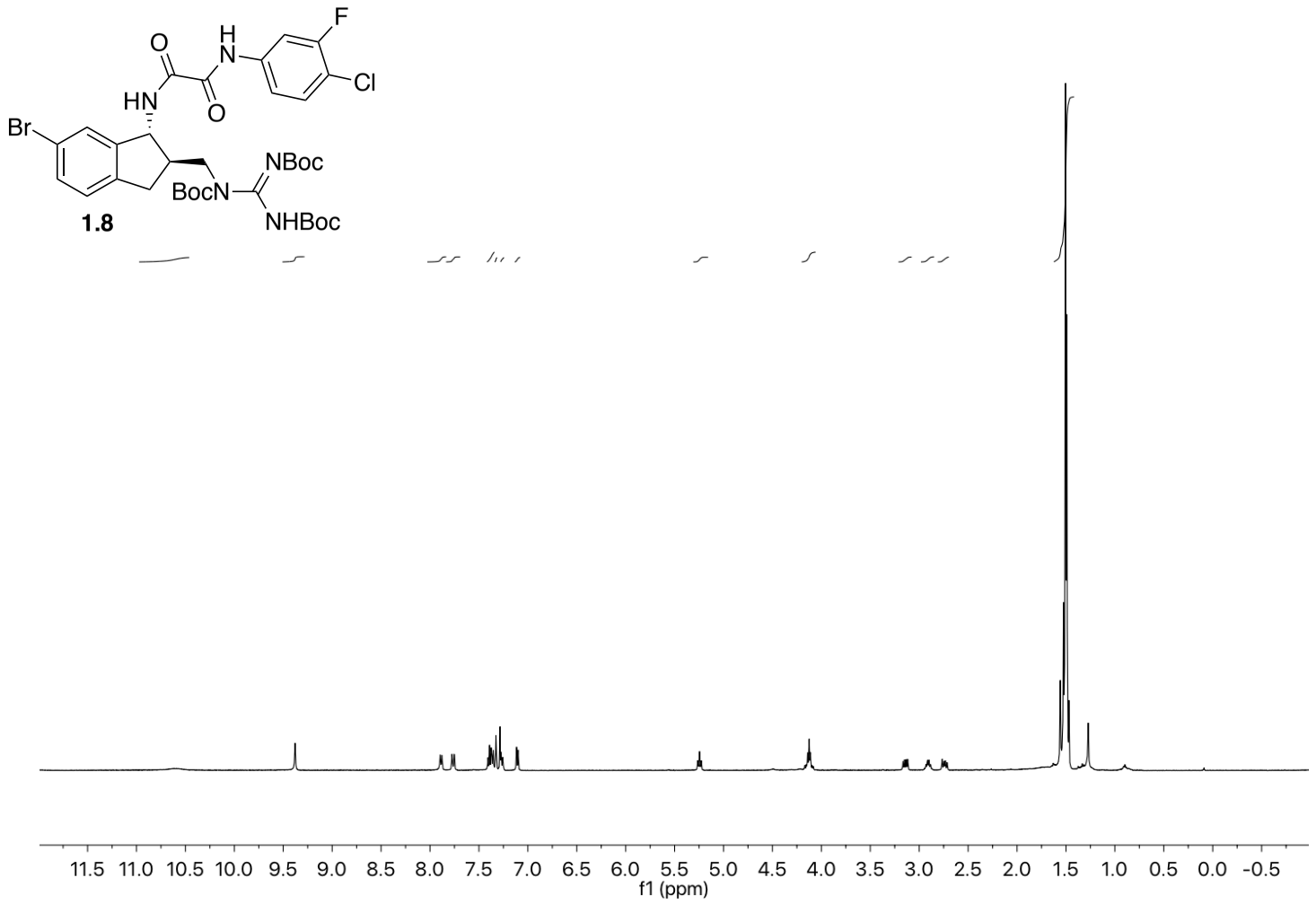

Figure A.1.8.1. The 500 MHz ^{1}H NMR Spectrum of Compound **1.8** in $CDCl_3$.

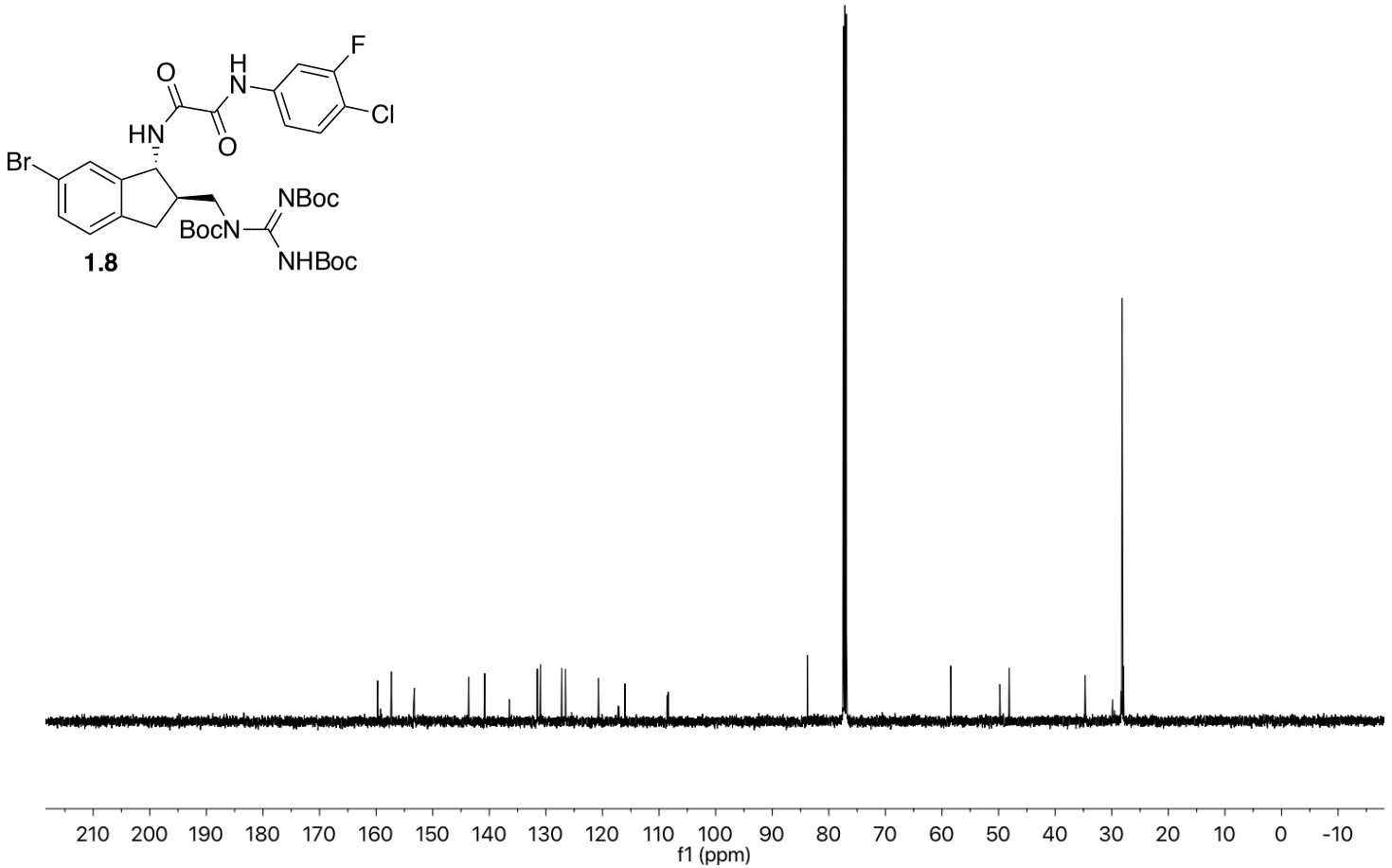

Figure A.1.8.2. The 500 MHz ^{13}C NMR Spectrum of Compound **1.8** in $CDCl_3$.

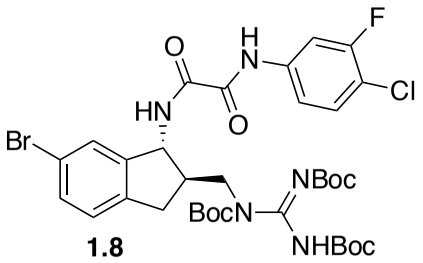

1.8

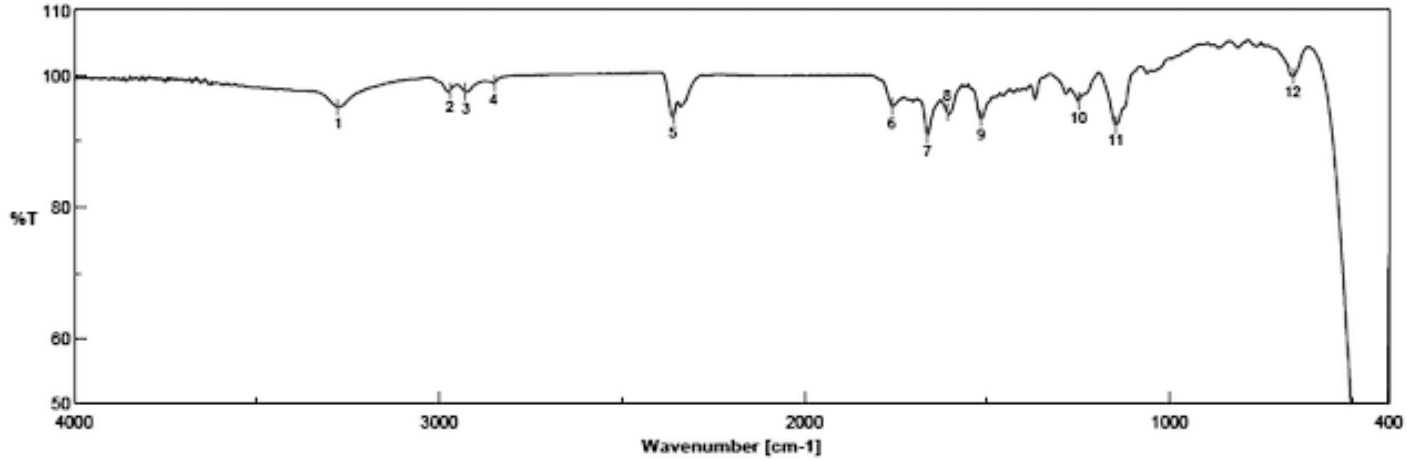

Figure A.1.8.3. The Infrared Spectrum of Compound **1.8**.

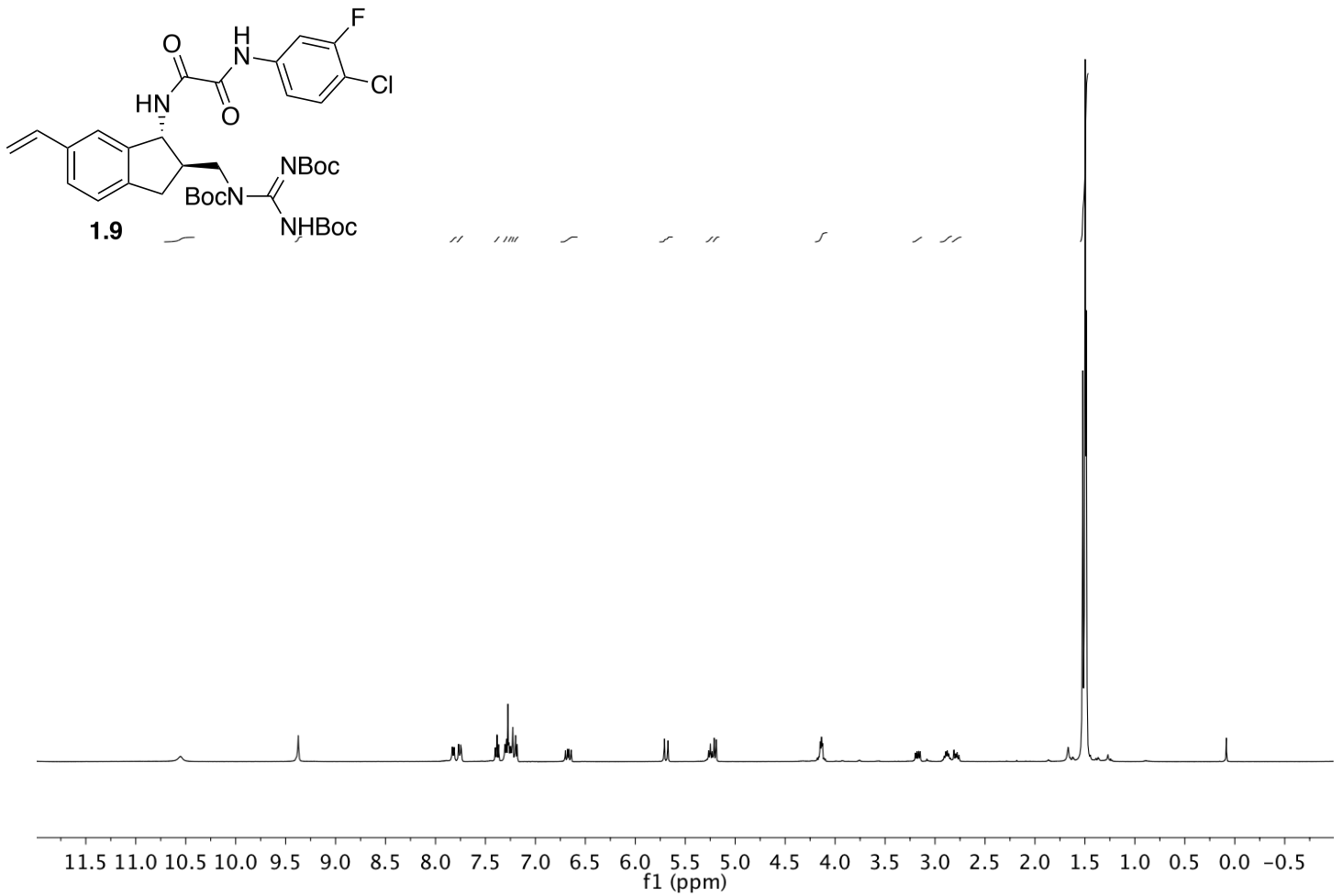

Figure A.1.9.1. The 500 MHz ^{1}H NMR Spectrum of Compound **1.9** in $CDCl_3$.

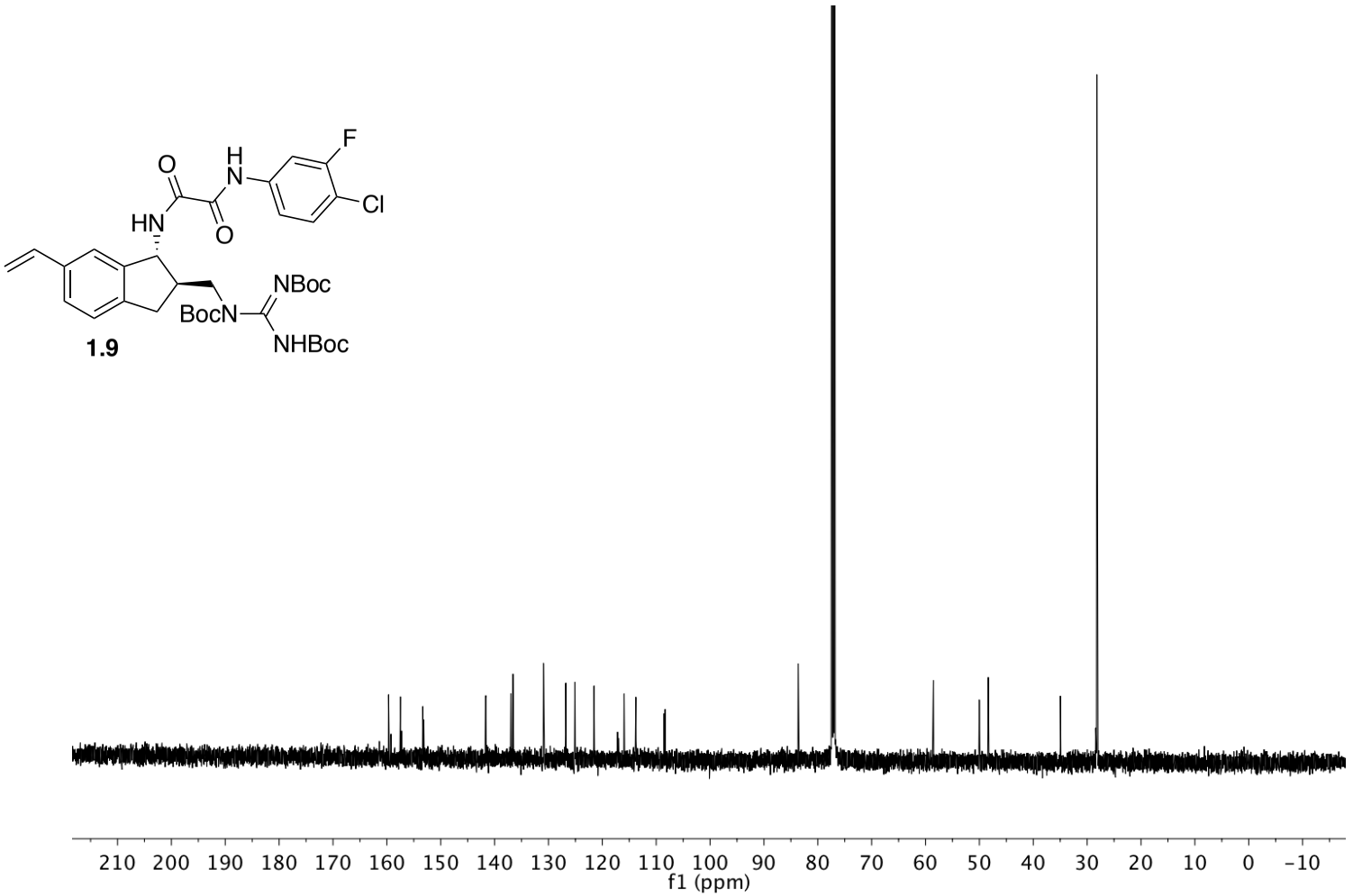

Figure A.1.9.2. The 500 MHz ^{13}C NMR Spectrum of Compound **1.9** in $CDCl_3$.

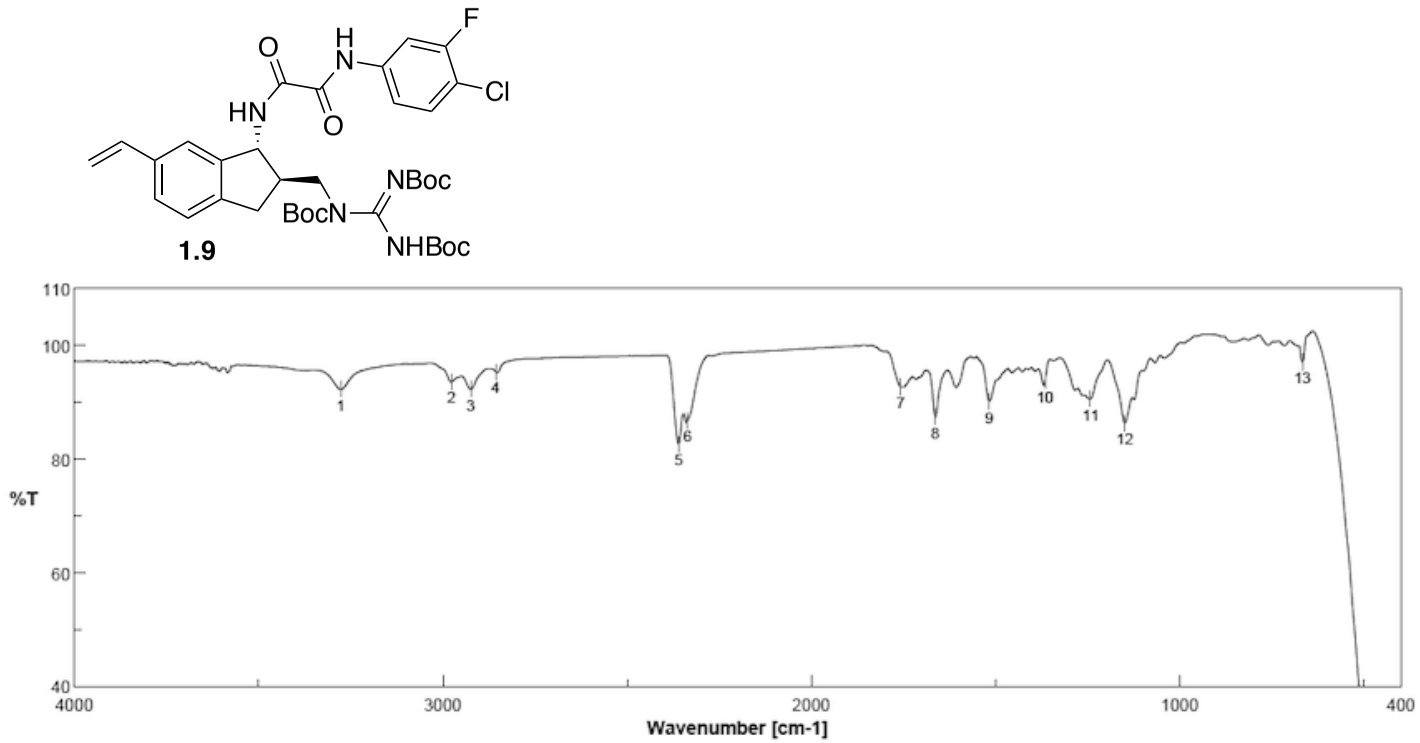

Figure A.1.9.3. The Infrared Spectrum of Compound **1.9**.

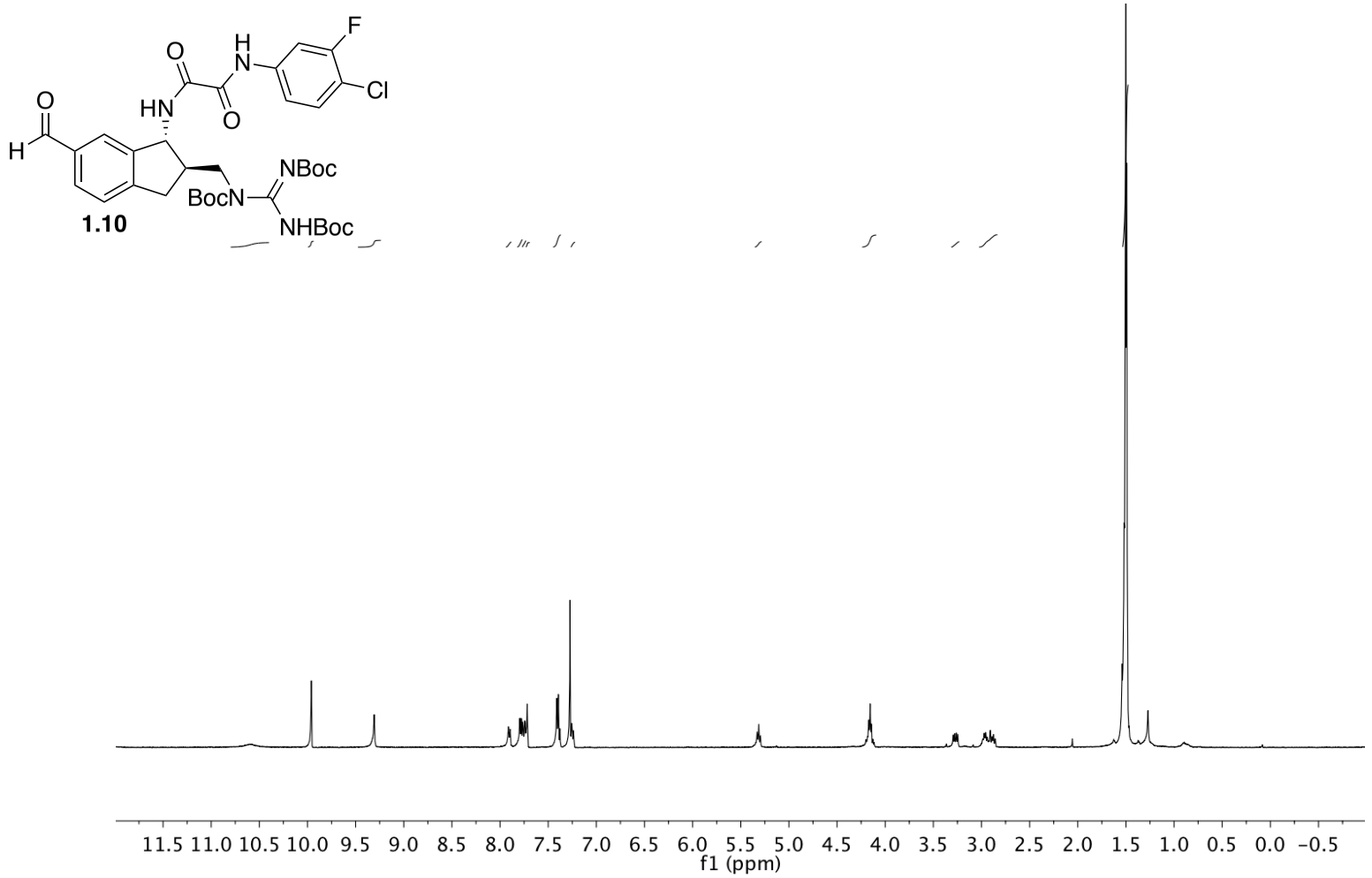

Figure A.1.10.1. The 500 MHz ^{1}H NMR Spectrum of Compound **1.10** in $CDCl_3$.

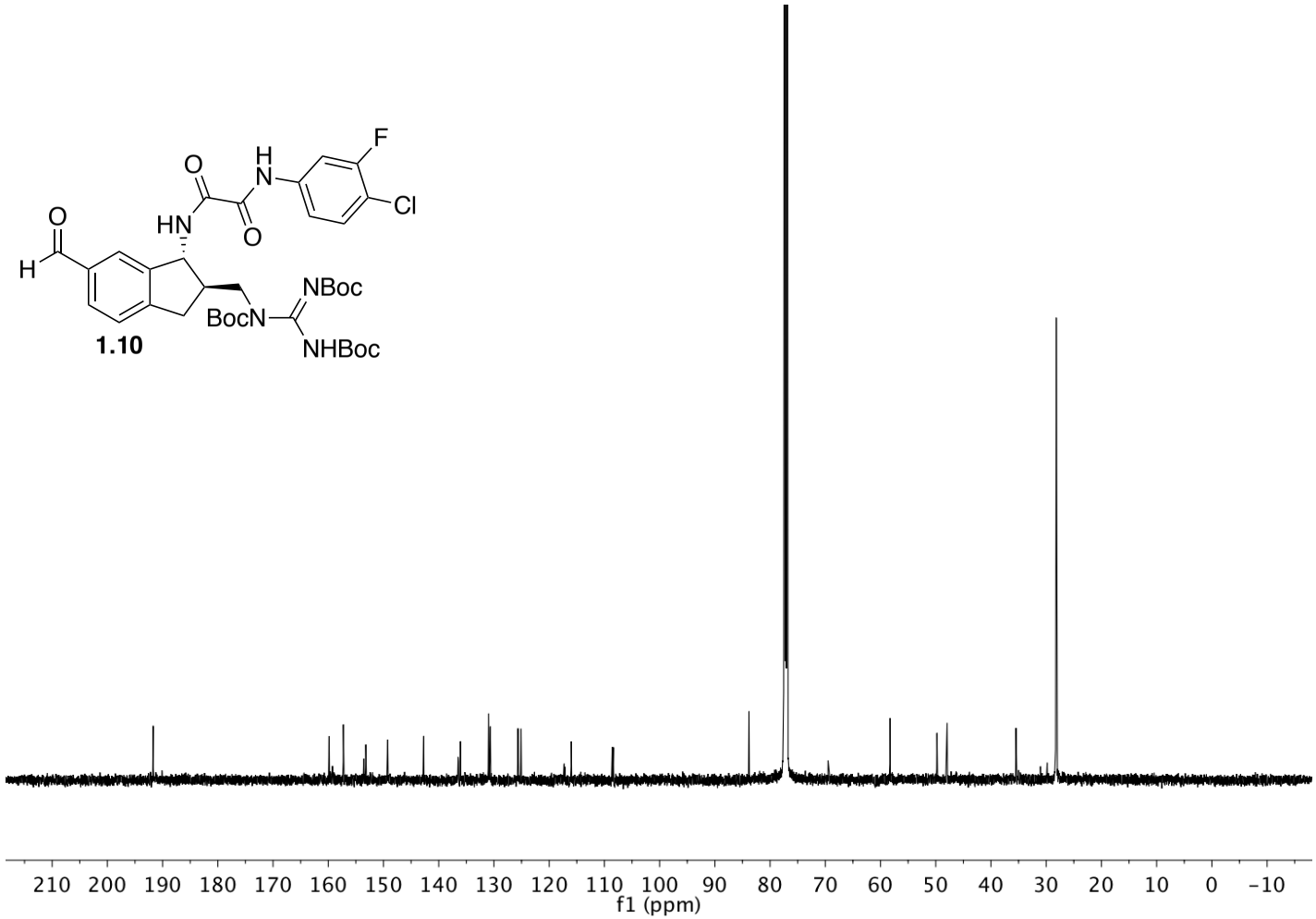

Figure A.1.10.2. The 500 MHz ^{13}C NMR Spectrum of Compound **1.10** in $CDCl_3$.

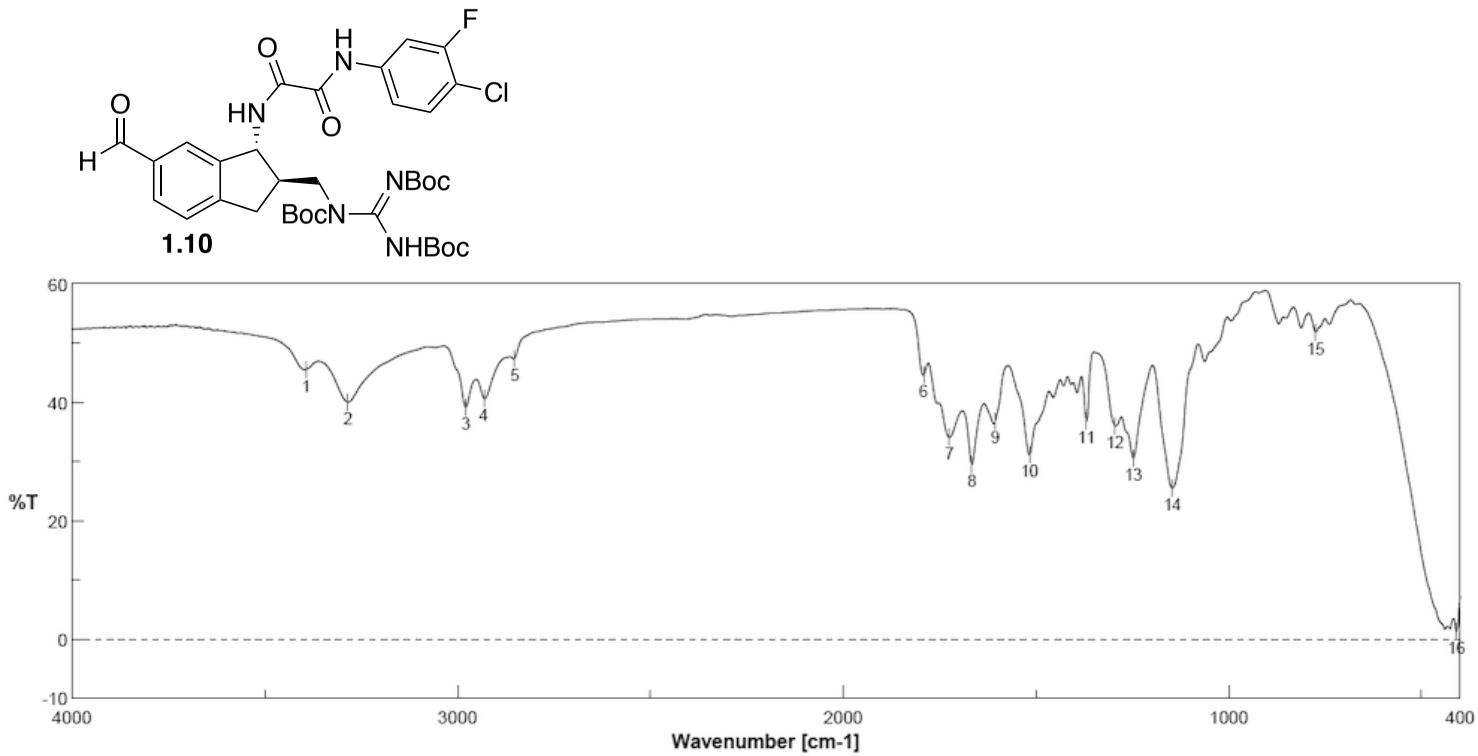

Figure A.1.10.3. The Infrared Spectrum of Compound **1.10**.

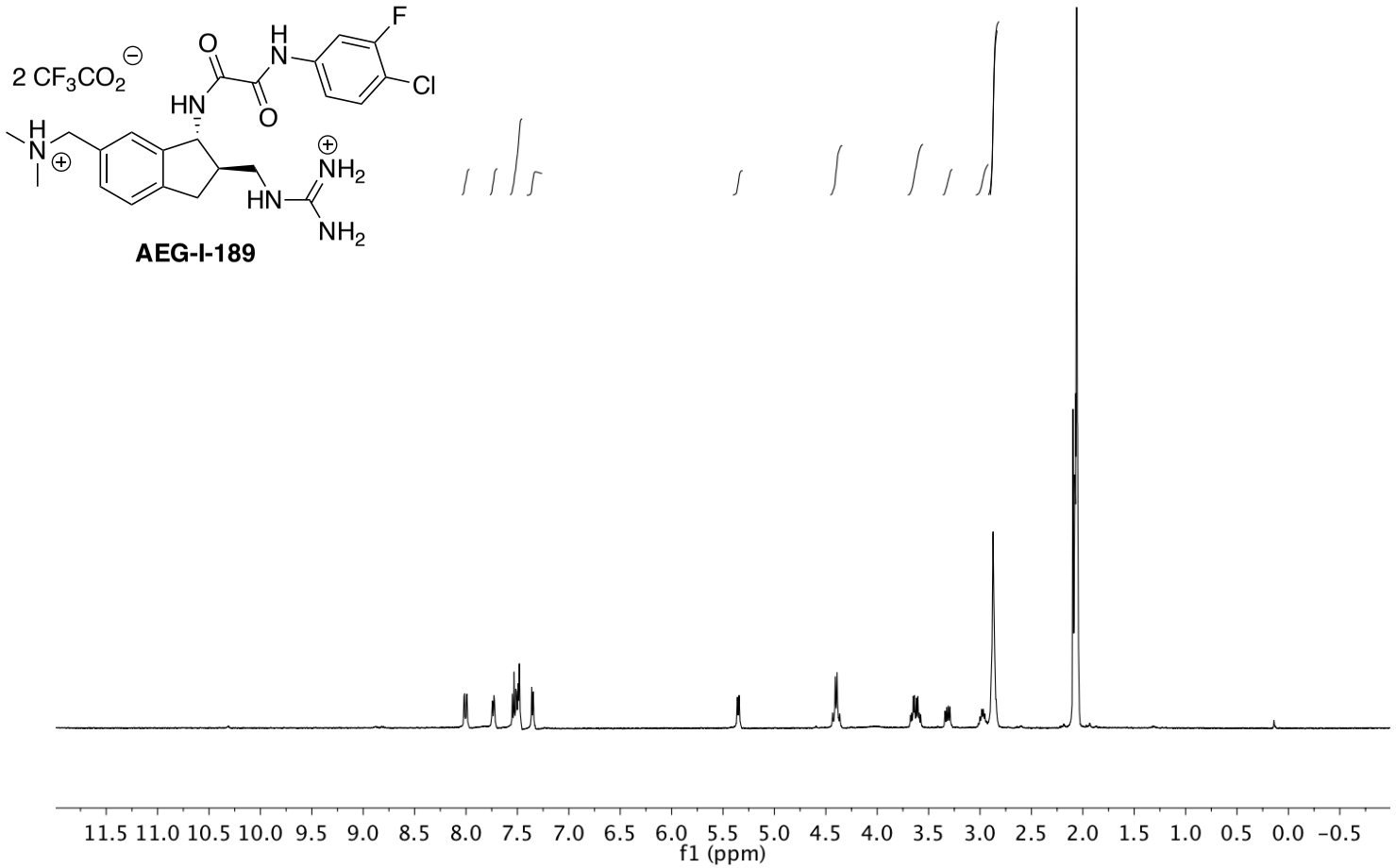

Figure A.1.11.1. The 500 MHz ^{1}H NMR Spectrum of Compound **AEG-I-189** in acetone-d6.

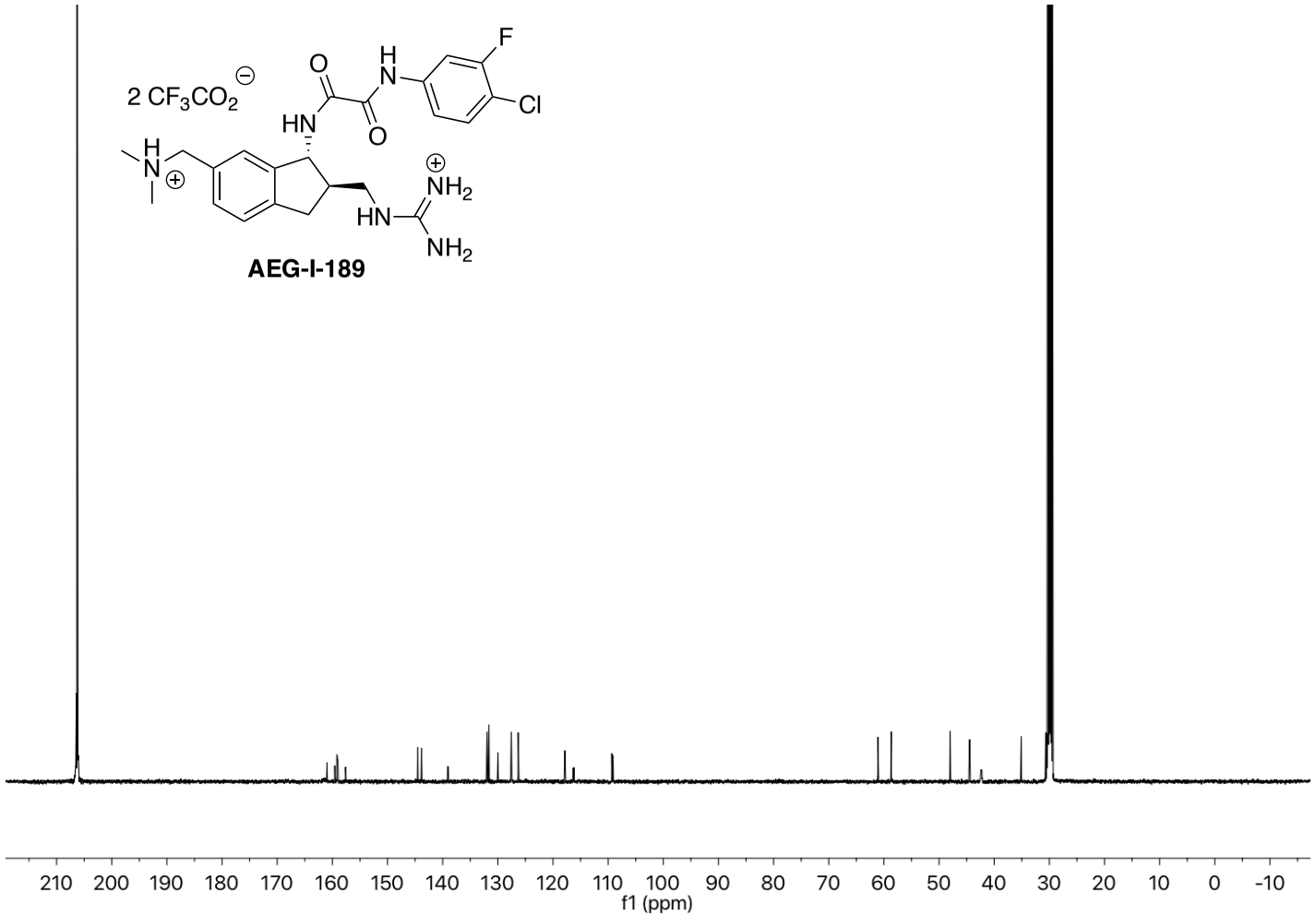

Figure A.1.11.2. The 500 MHz ^{13}C NMR Spectrum of Compound **AEG-I-189** in acetone-d6.

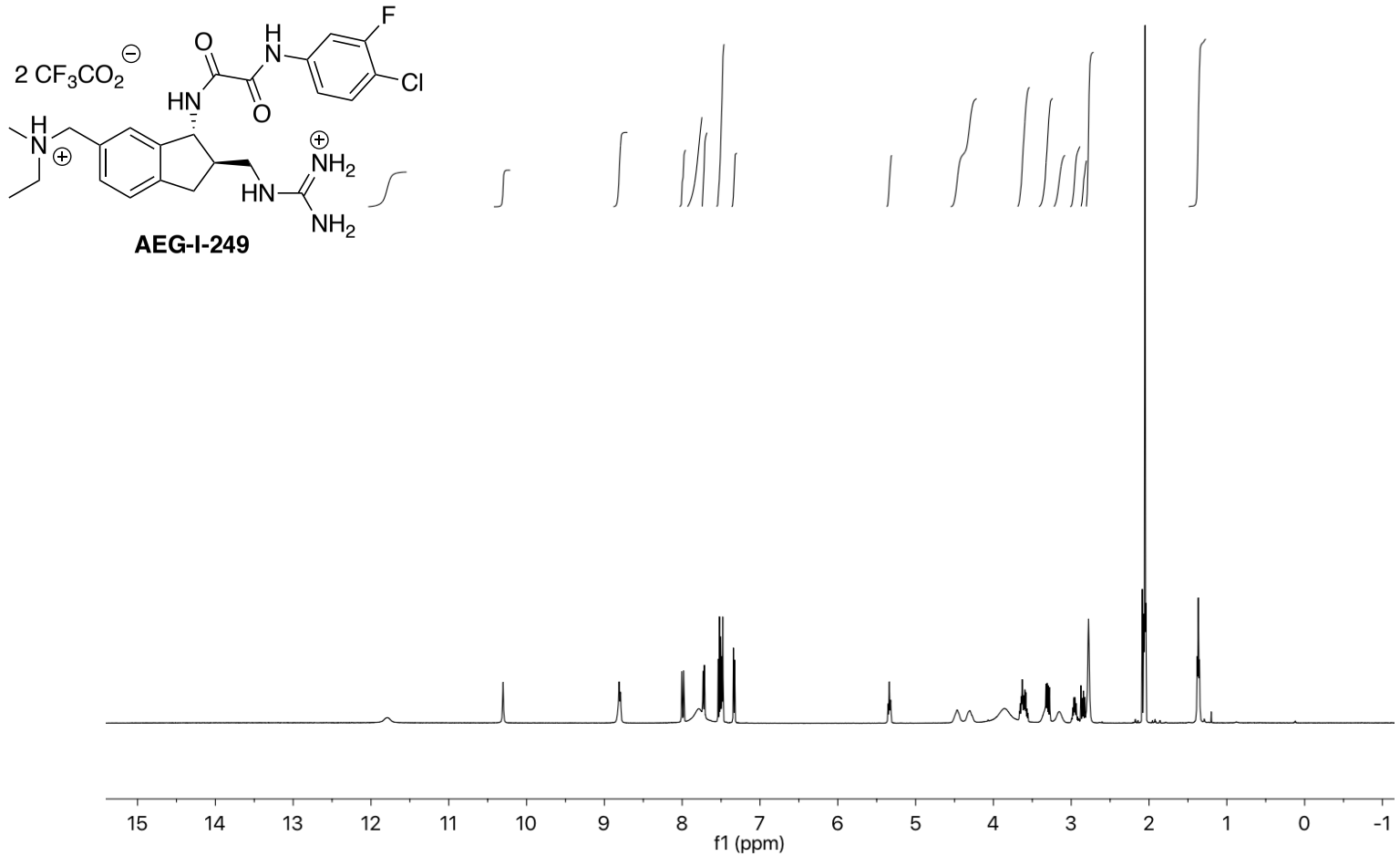

Figure A.1.12.1. The 500 MHz ^{1}H NMR Spectrum of Compound **AEG-I-249** in acetone-d6.

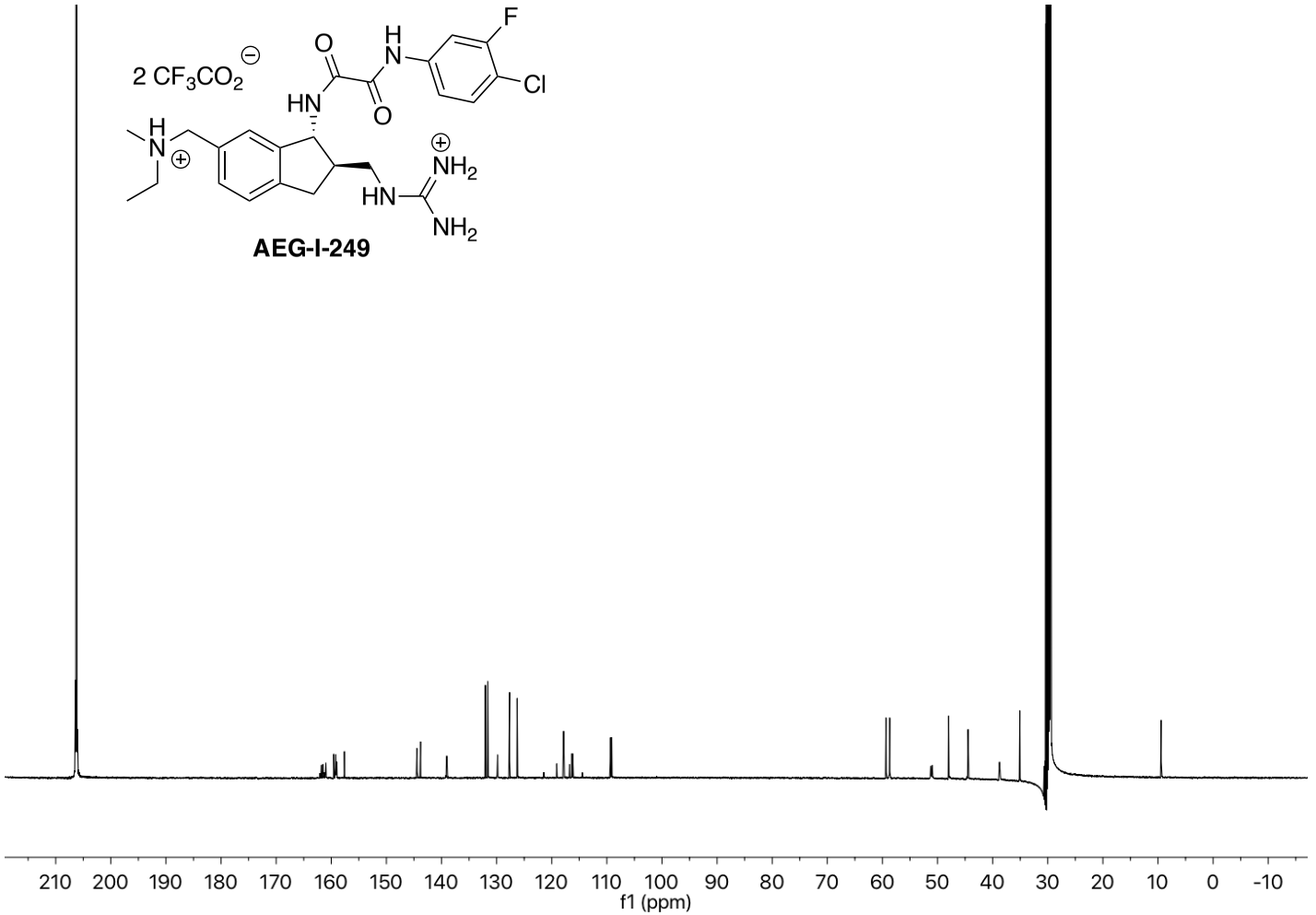

Figure A.1.12.2. The 500 MHz ^{13}C NMR Spectrum of Compound **AEG-I-249** in acetone-d6.

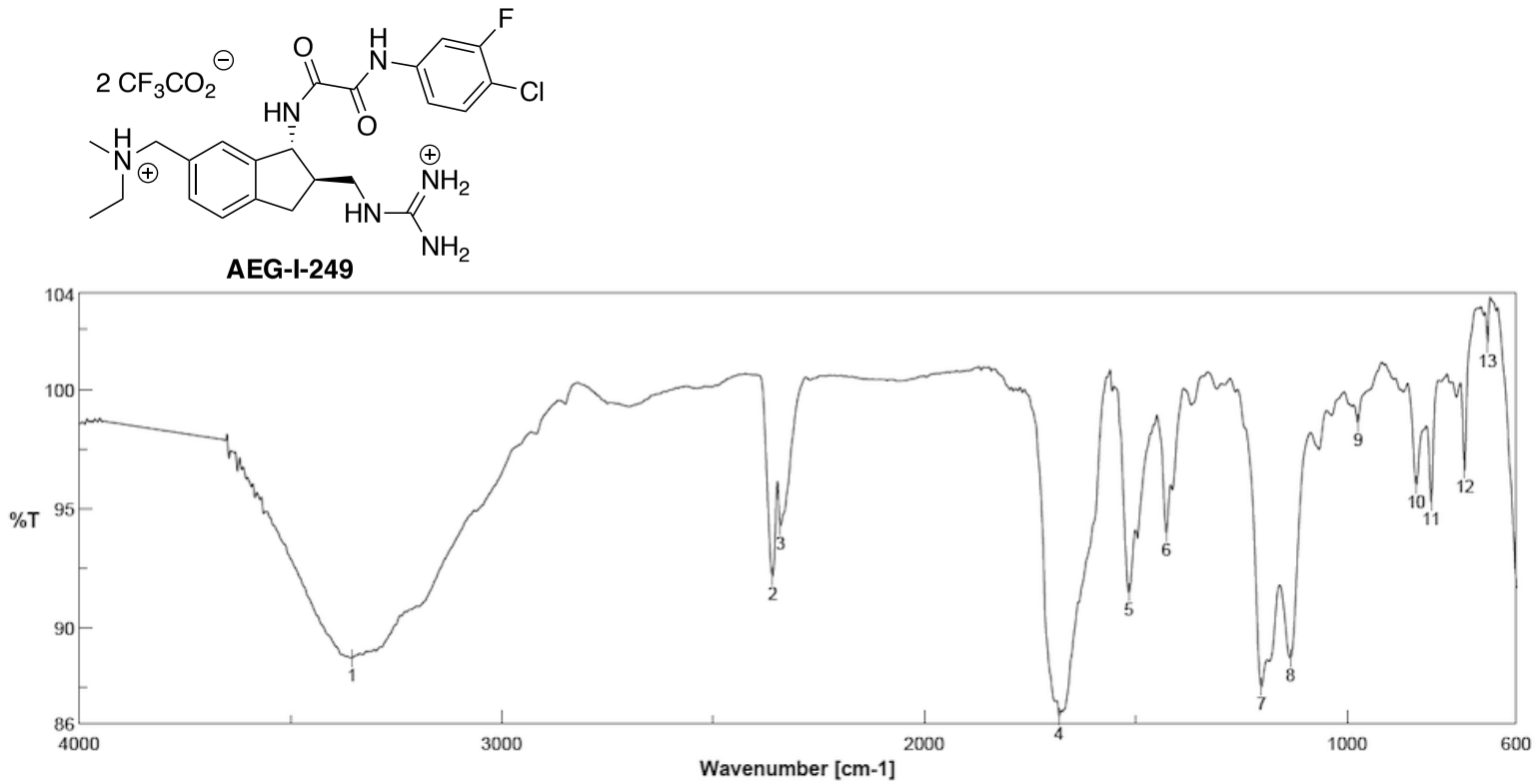

Figure A.1.13.3. The Infrared Spectrum of Compound **AEG-I-249.**

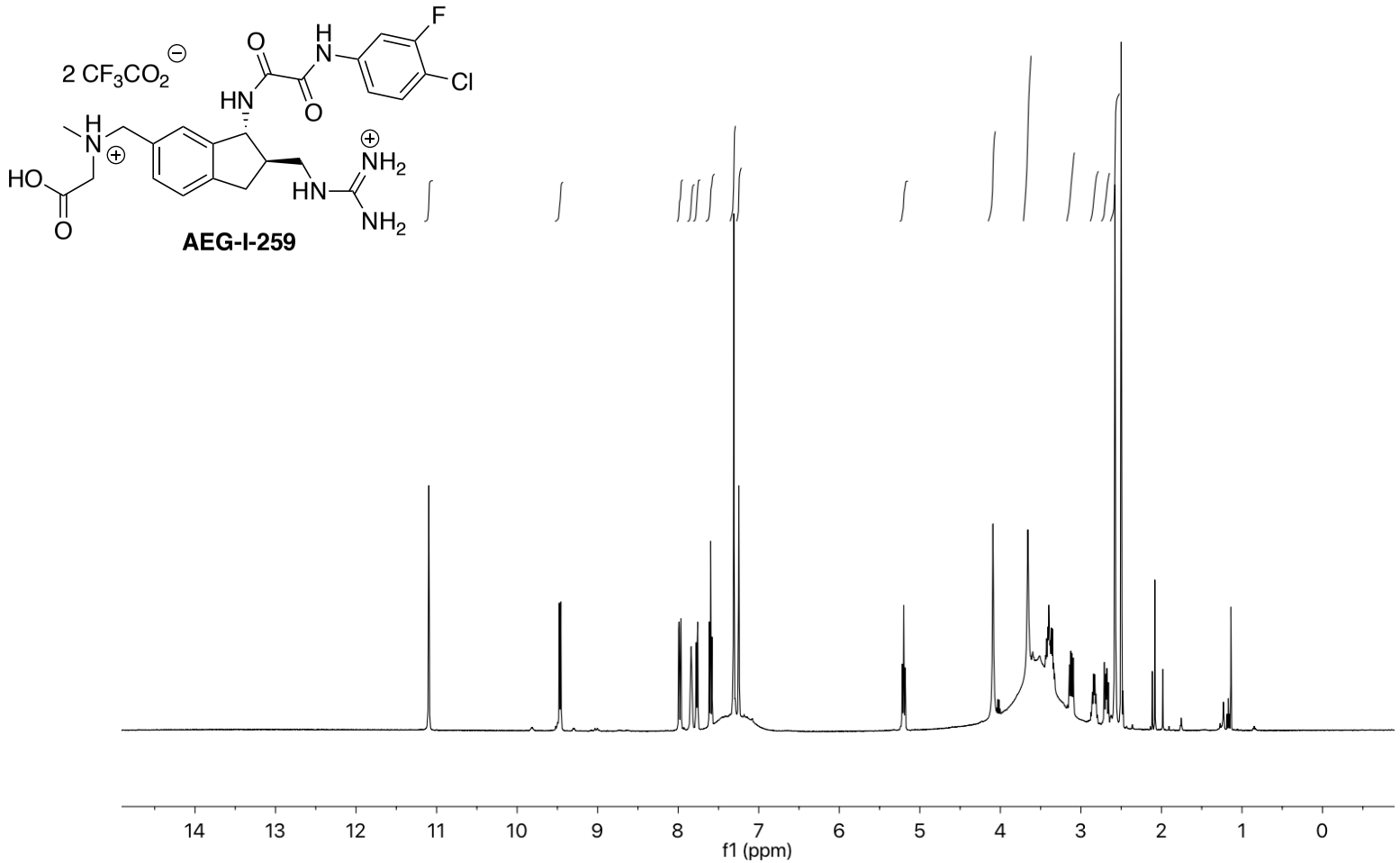

Figure A.1.13.1. The 500 MHz ^{1}H NMR Spectrum of Compound **AEG-I-259** in acetone-d6.

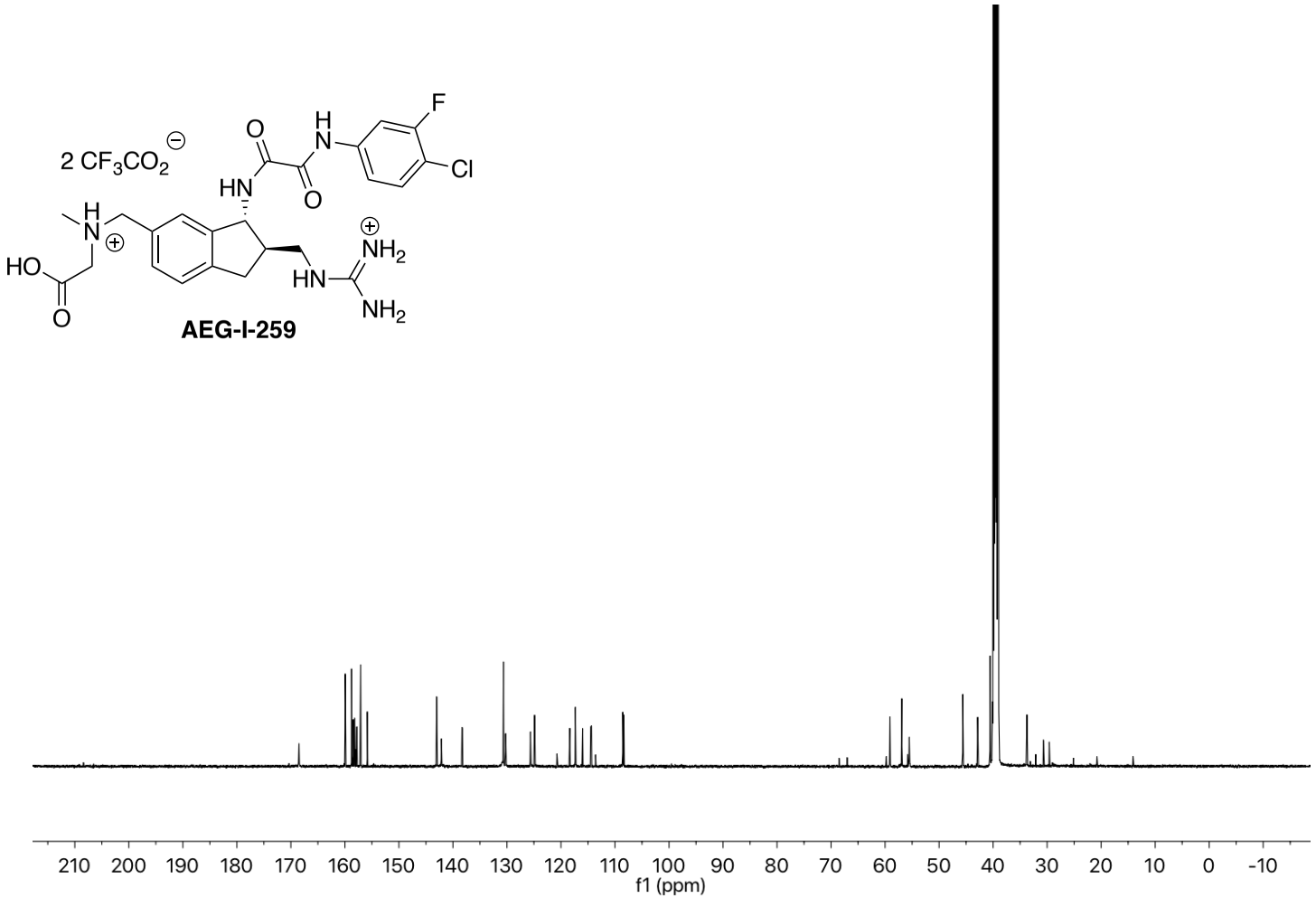

Figure A.1.13.2. The 500 MHz ^{13}C NMR Spectrum of Compound **AEG-I-259** in acetone-d6.

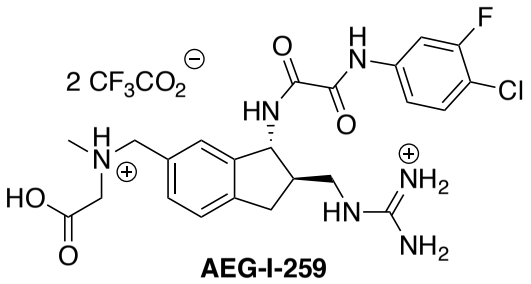

AEG-I-259

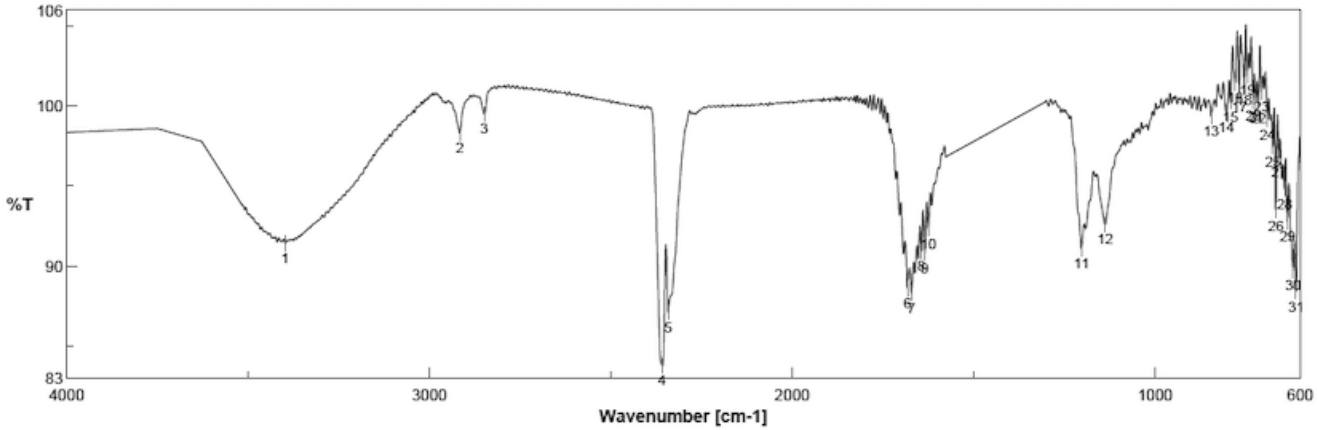

Figure A.1.14.3. The Infrared Spectrum of Compound **AEG-I-259**.

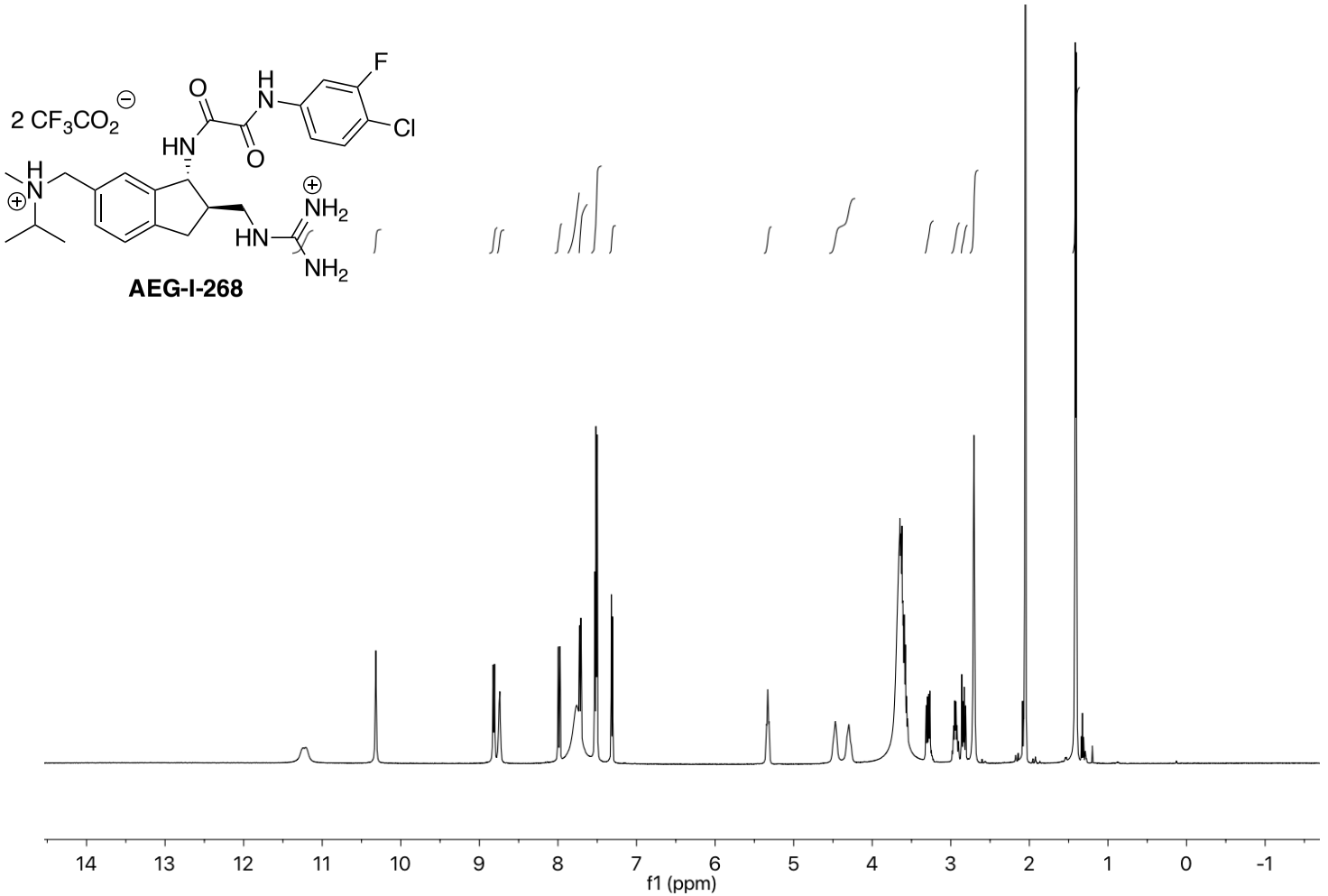

Figure A.1.14.1. The 500 MHz ^{1}H NMR Spectrum of Compound **AEG-I-268** in acetone-d6.

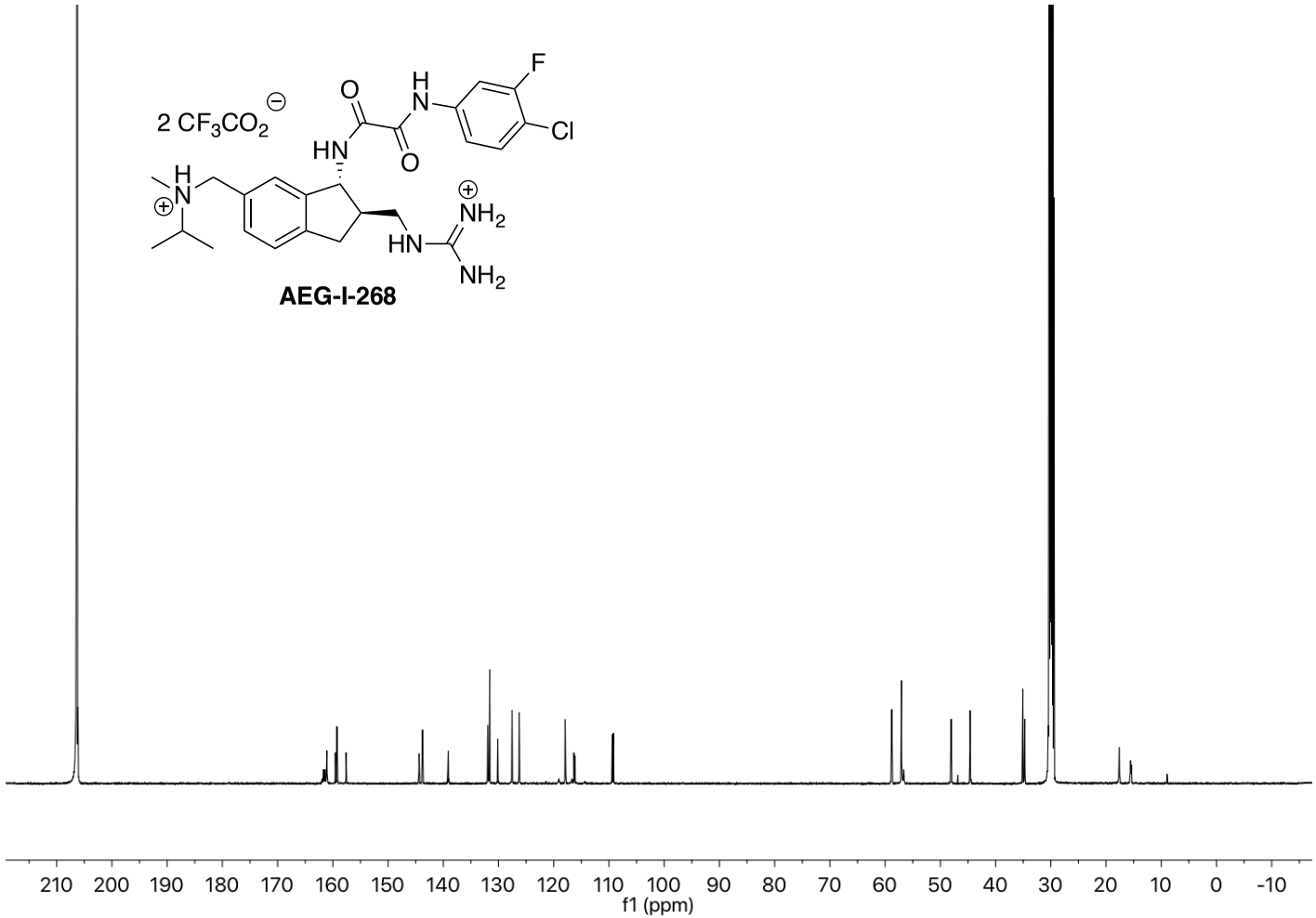

Figure A.1.14.2. The 500 MHz ^{13}C NMR Spectrum of Compound **AEG-I-268** in acetone-d6.

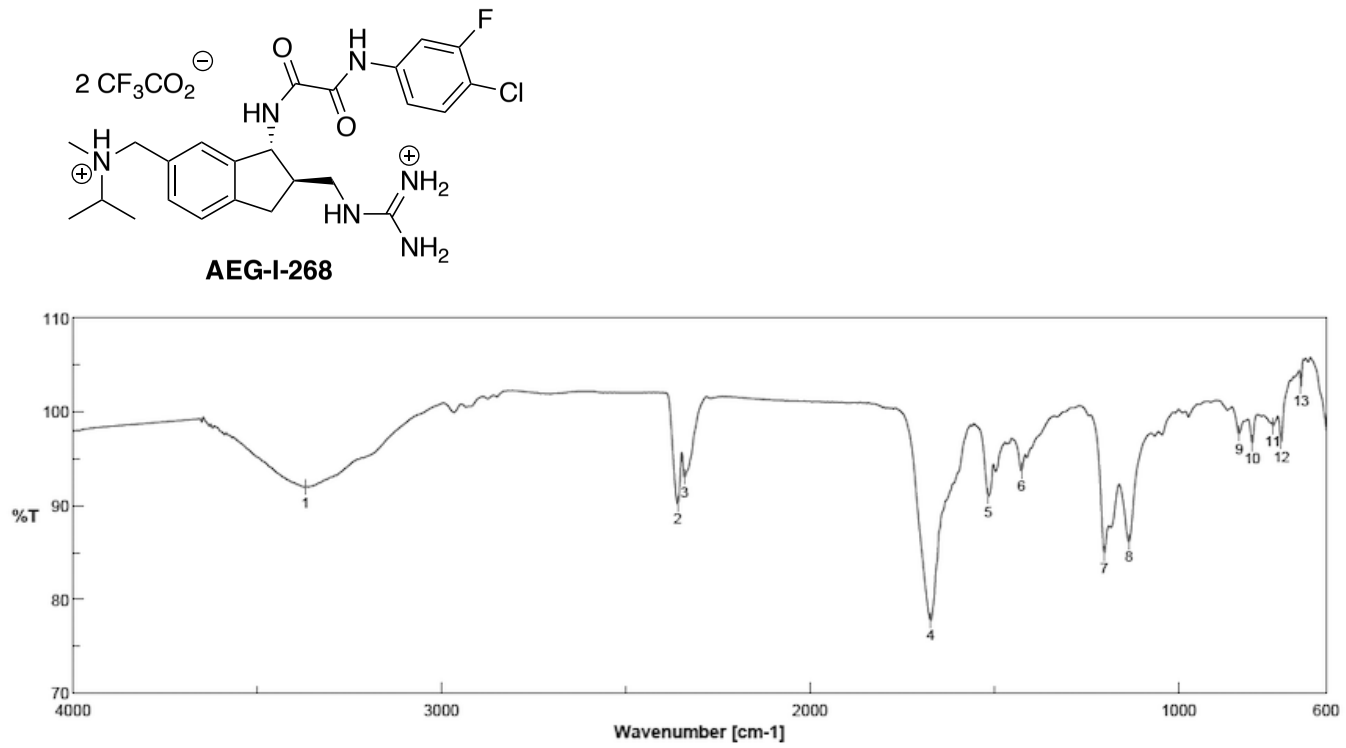

Figure A.1.14.3. The Infrared Spectrum of Compound **AEG-I-268**.

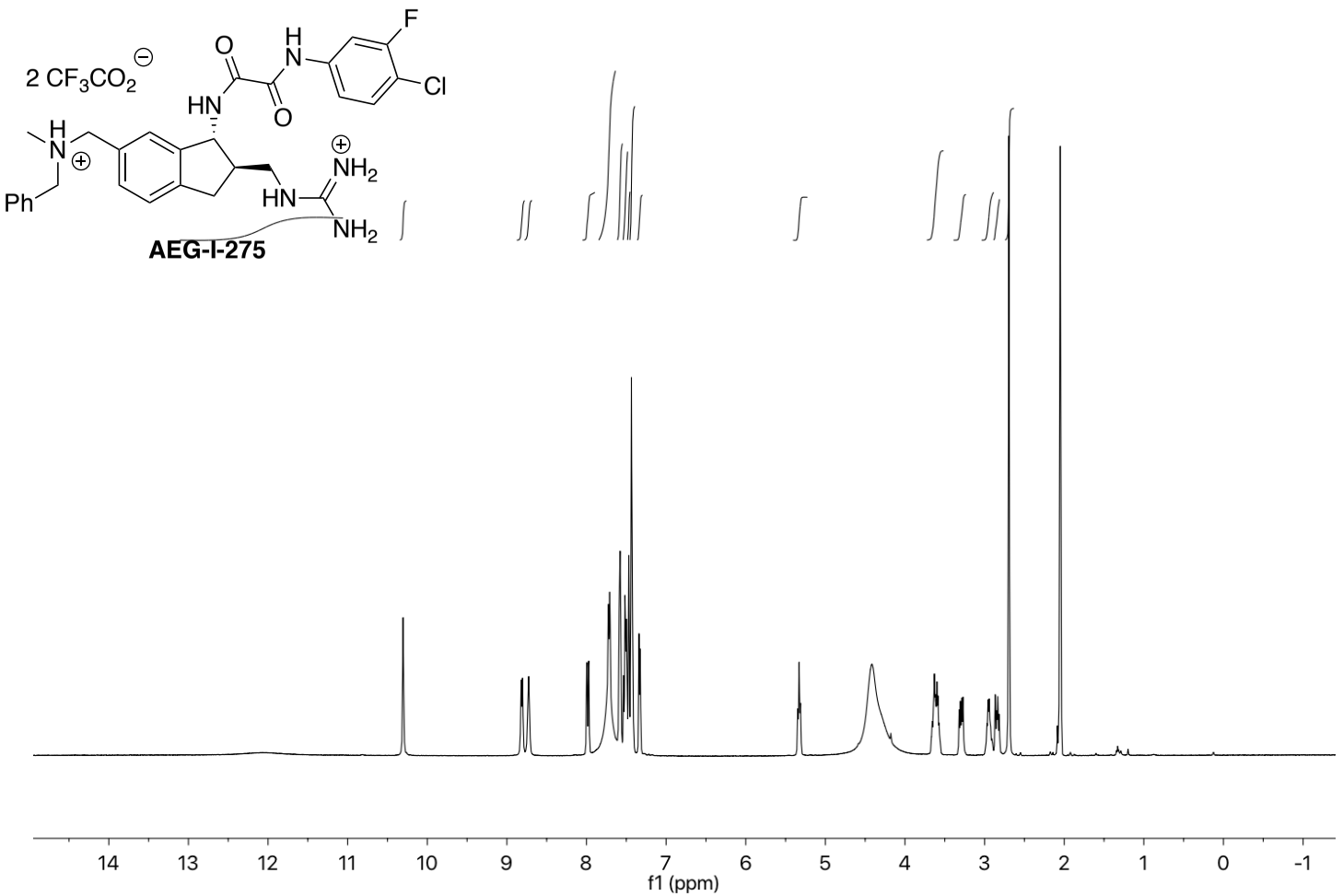

Figure A.1.15.1. The 500 MHz ^{1}H NMR Spectrum of Compound **AEG-I-275** in acetone-d6.

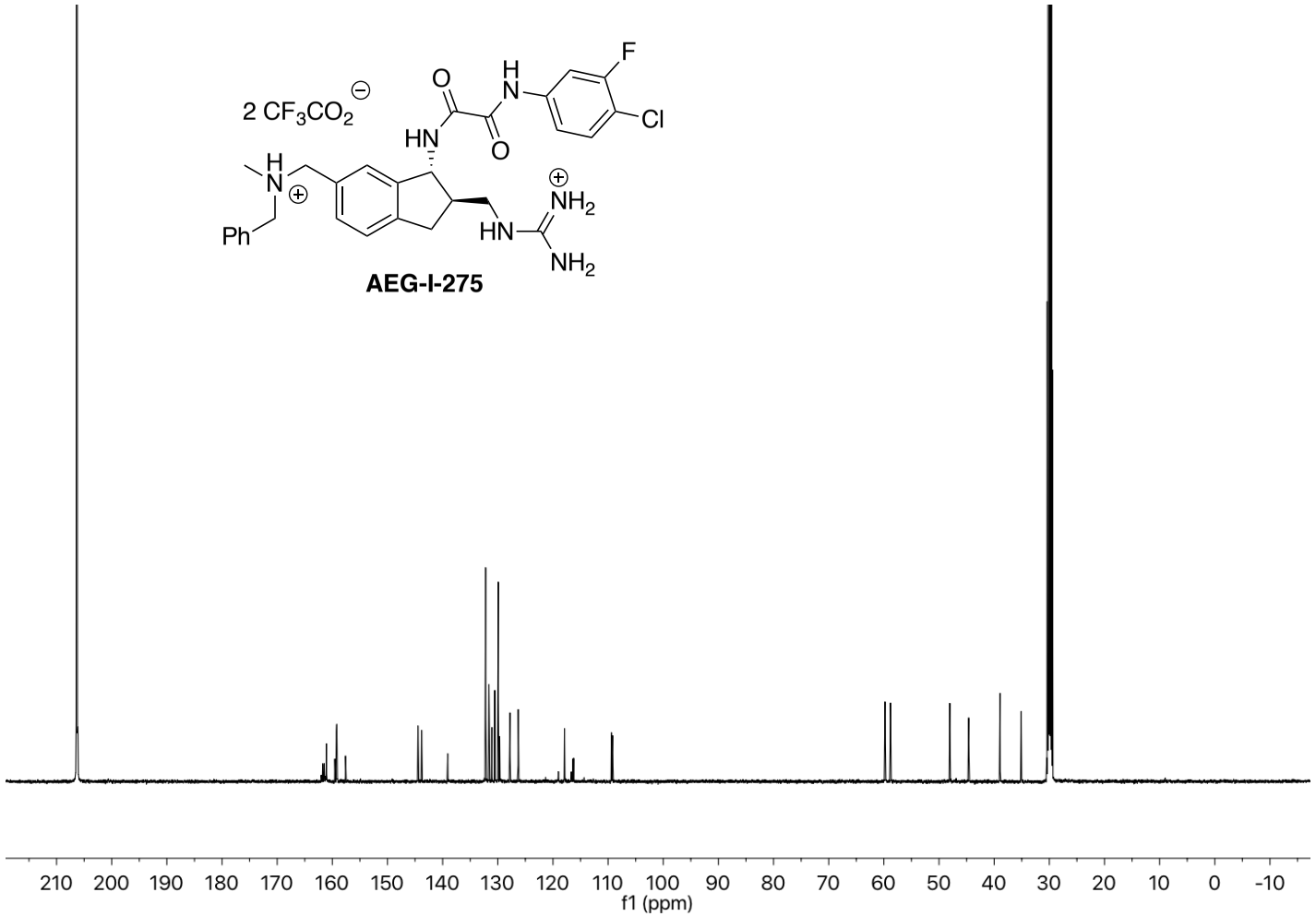

Figure A.1.15.2. The 500 MHz ^{13}C NMR Spectrum of Compound **AEG-I-275** in acetone-d6.

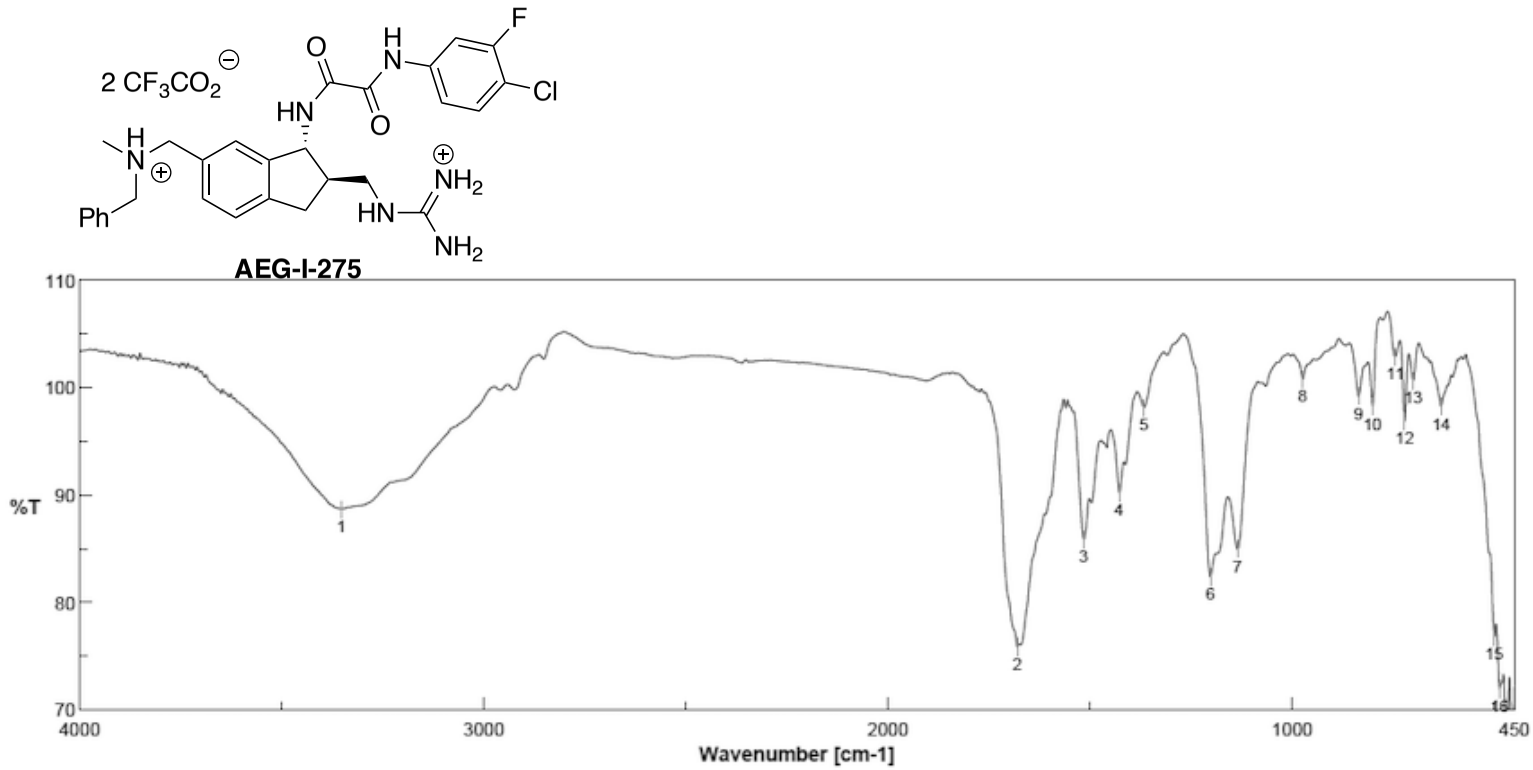

Figure A.1.15.3. The Infrared Spectrum of Compound **AEG-I-275**.

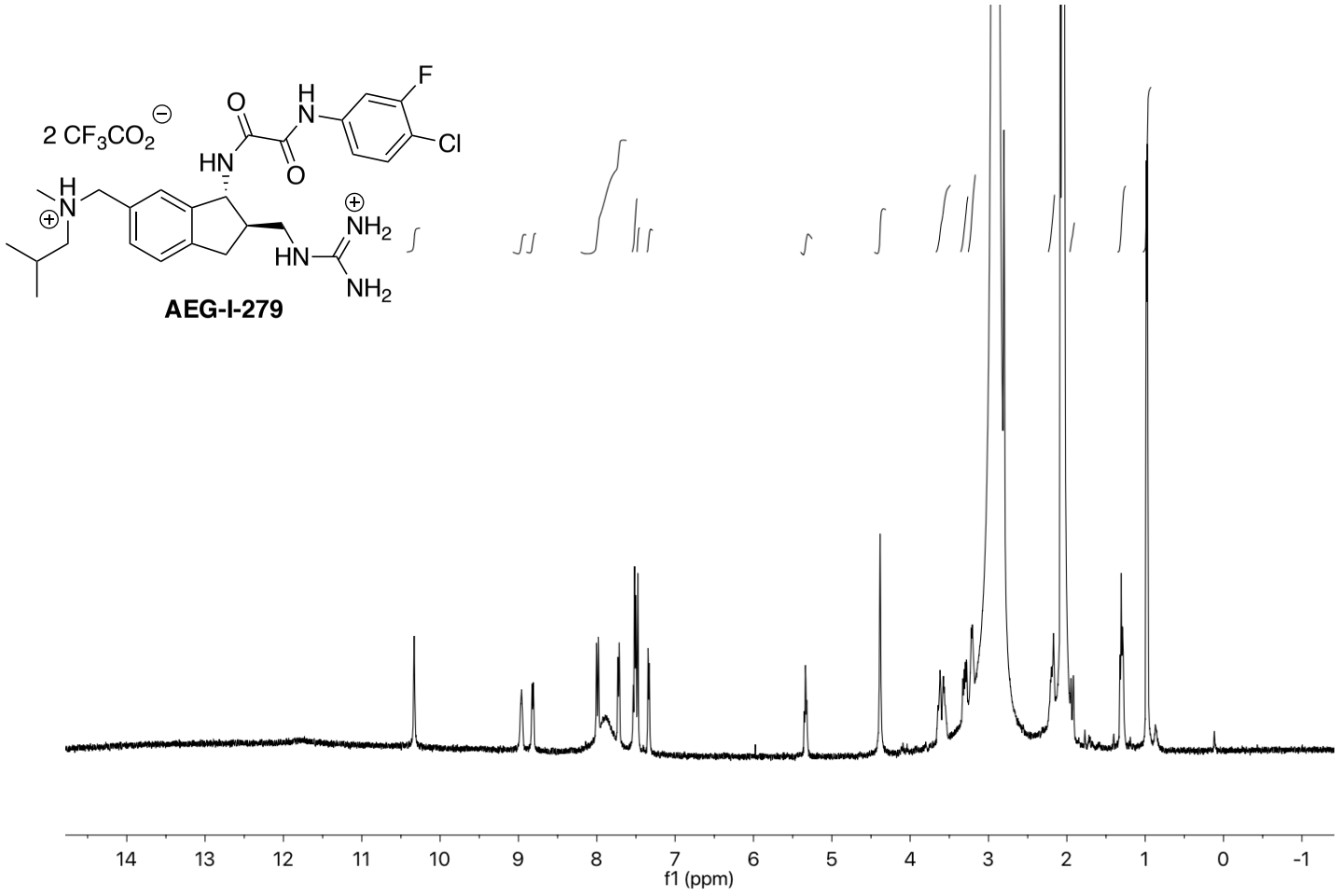

Figure A.1.16.1. The 500 MHz ^{1}H NMR Spectrum of Compound **AEG-I-279** in acetone-d6.

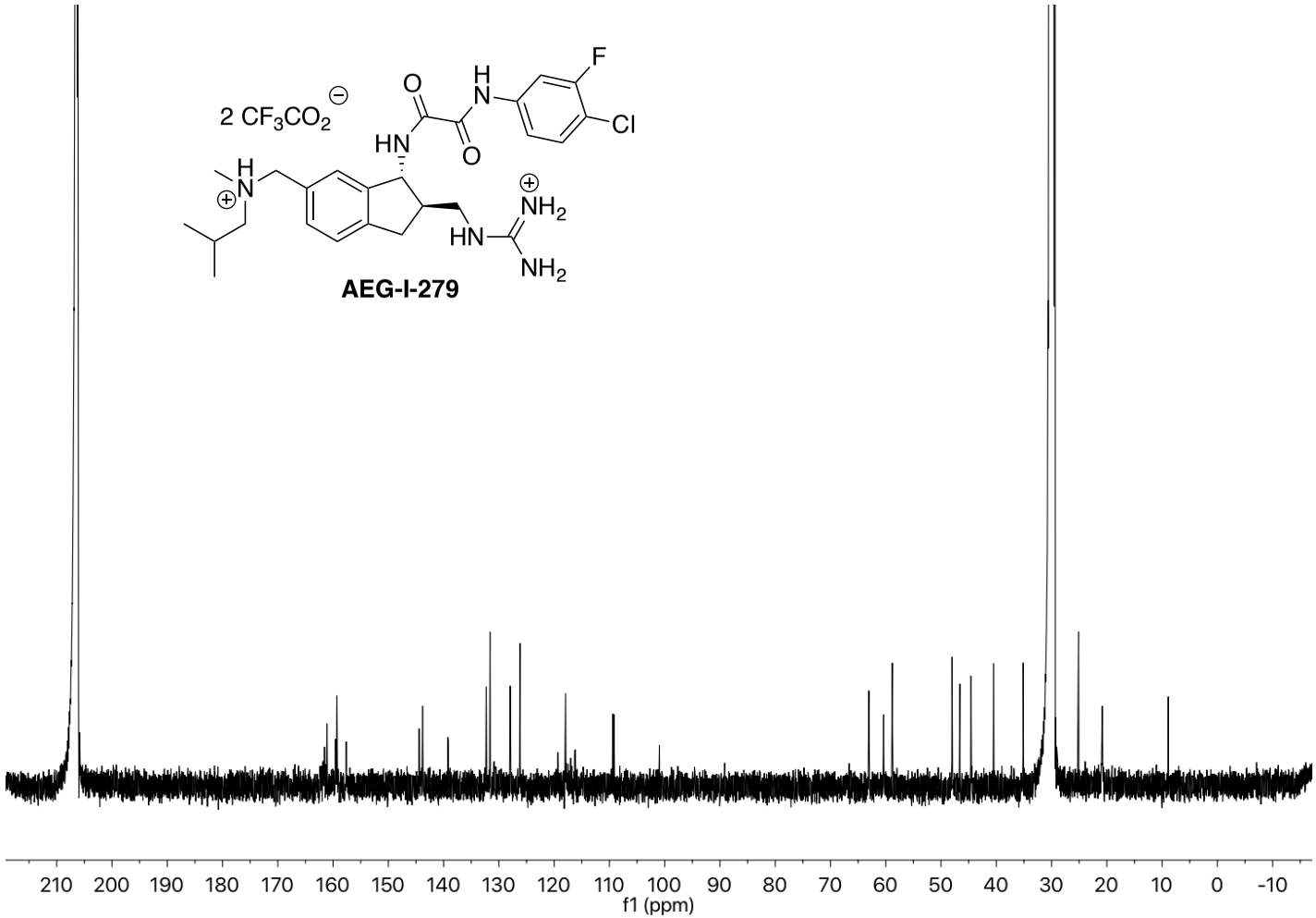

Figure A.1.16.2. The 500 MHz ^{13}C NMR Spectrum of Compound **AEG-I-279** in acetone-d6.

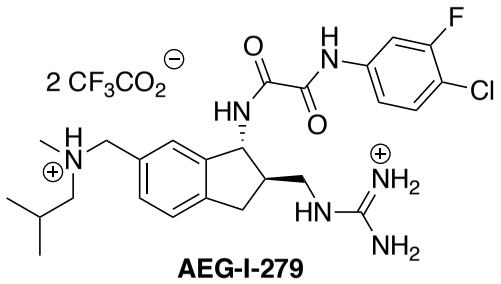

AEG-I-279

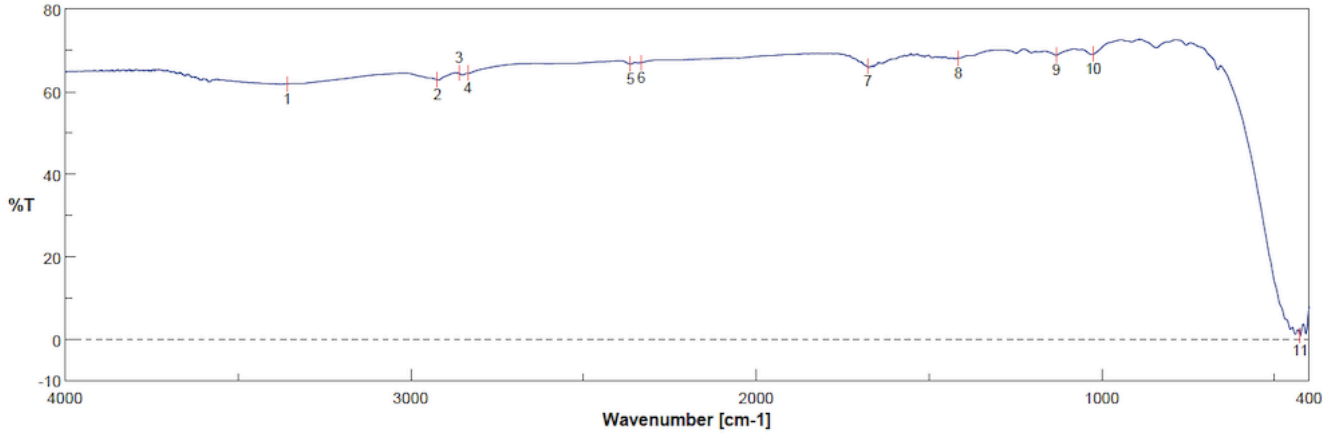

Figure A.1.16.3. The Infrared Spectrum of Compound **AEG-I-279**.

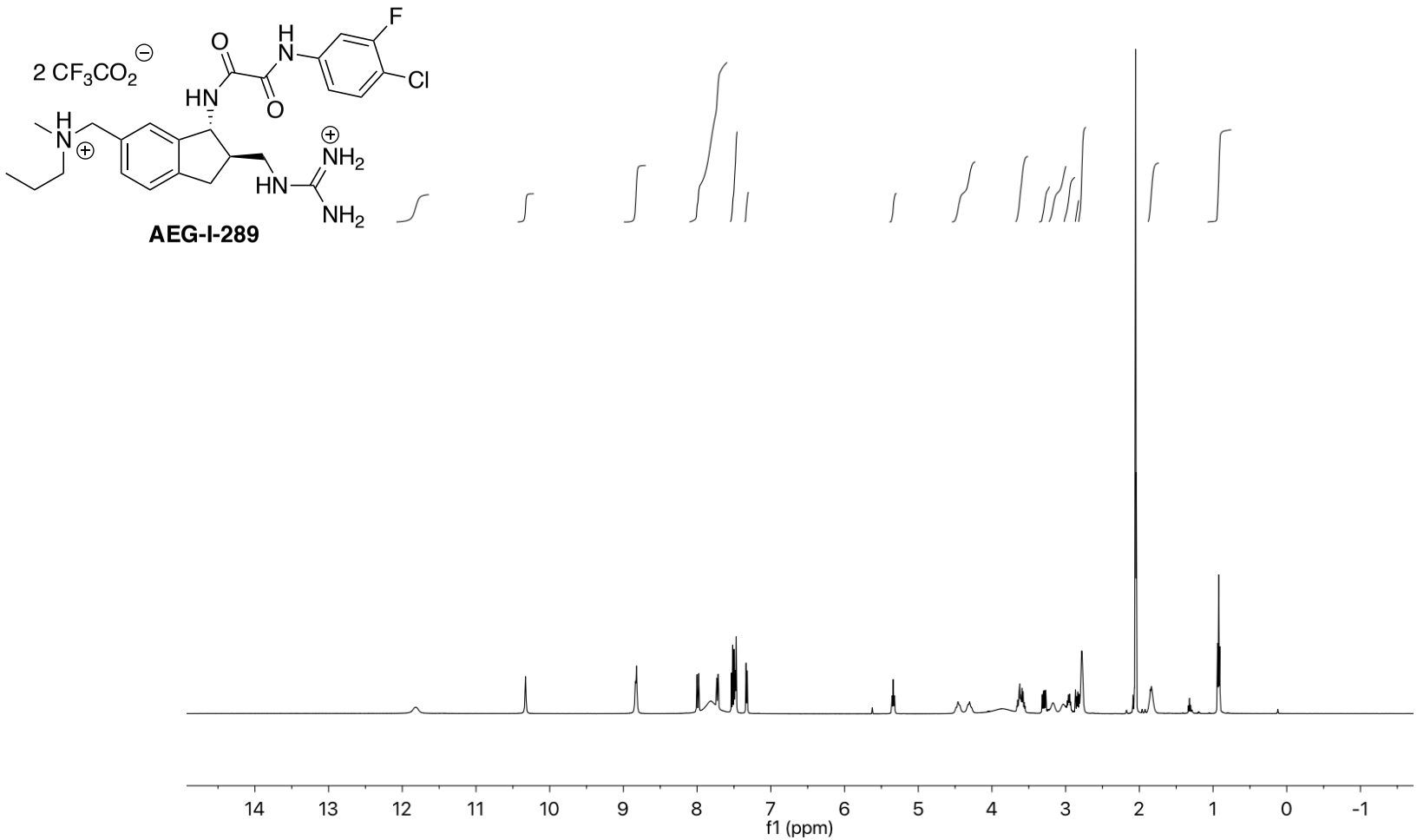

Figure A.1.17.1. The 500 MHz ^{1}H NMR Spectrum of Compound **AEG-I-289** in acetone-d6.

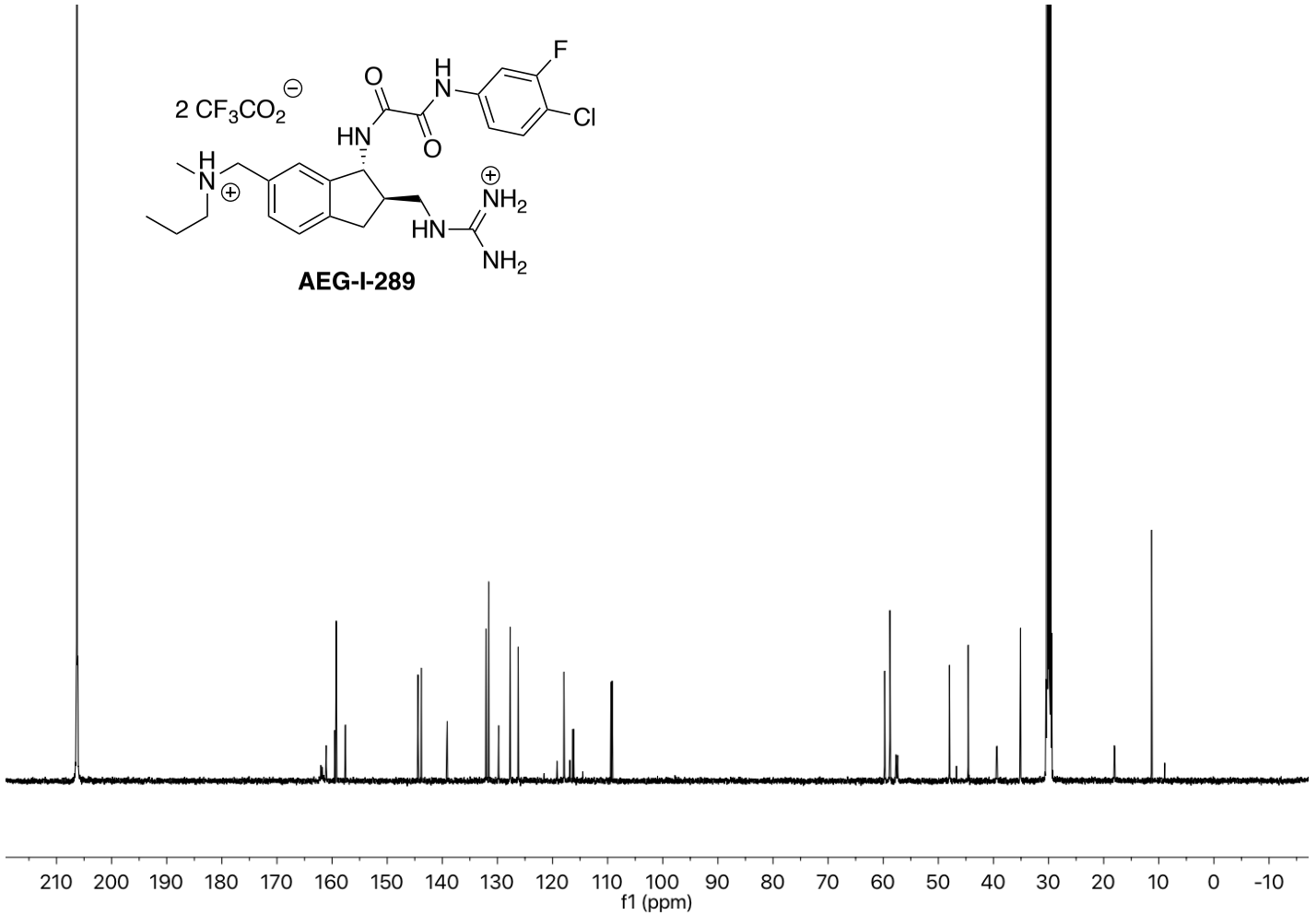

Figure A.1.17.2. The 500 MHz ^{13}C NMR Spectrum of Compound **AEG-I-289** in acetone-d6.

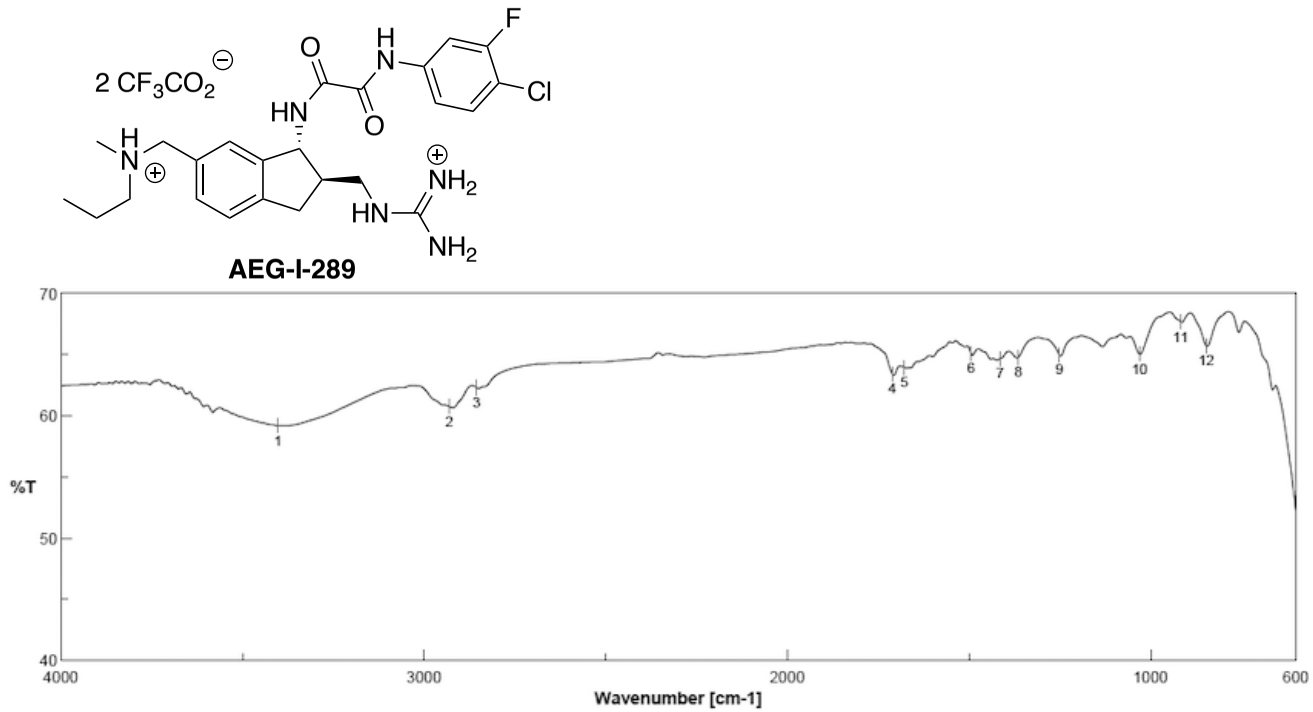

Figure A.1.17.3. The Infrared Spectrum of Compound **AEG-I-289**.

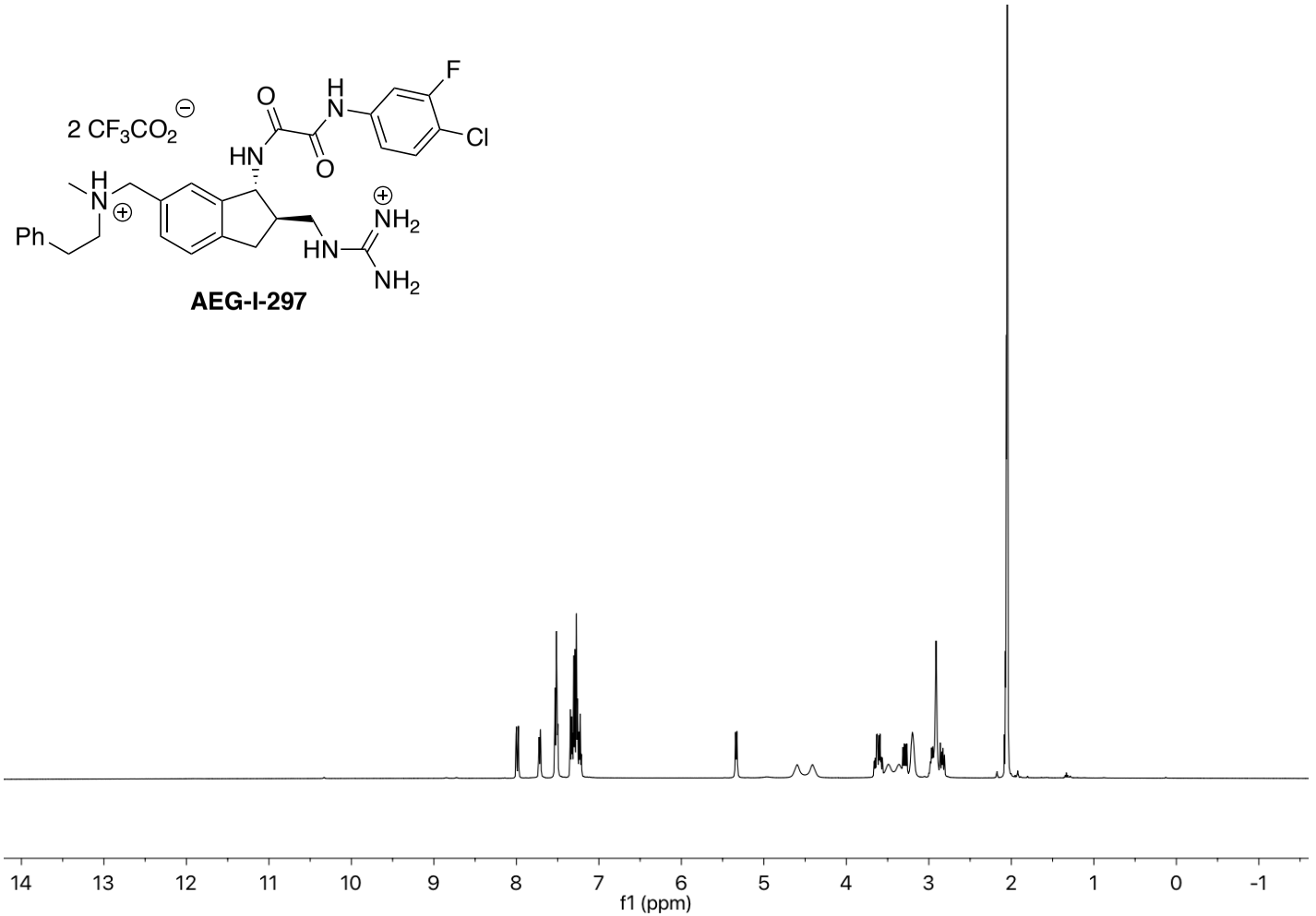

Figure A.1.18.1. The 500 MHz ^{1}H NMR Spectrum of Compound **AEG-I-297** in acetone-d6.

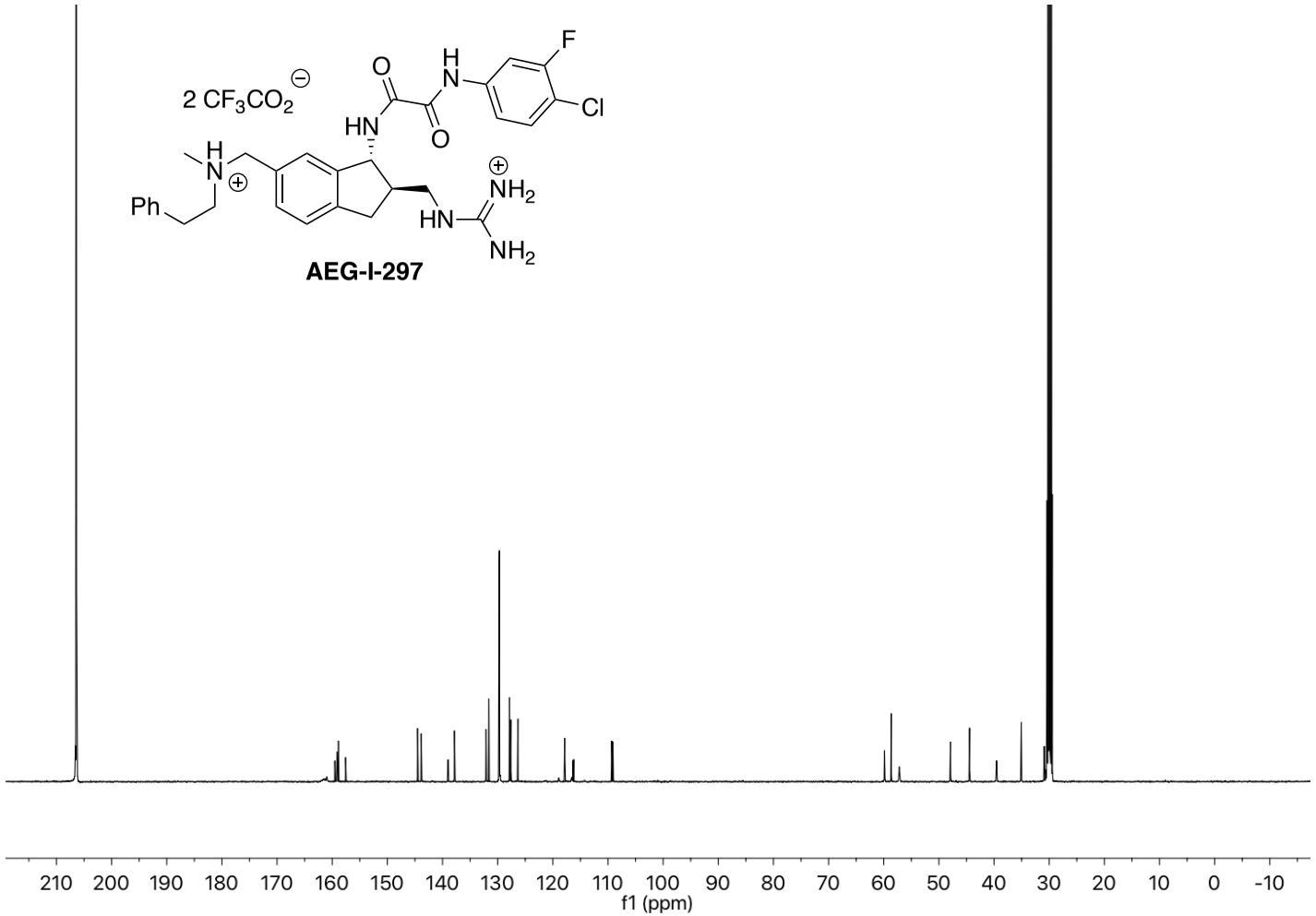

Figure A.1.18.2. The 500 MHz ^{13}C NMR Spectrum of Compound **AEG-I-297** in acetone-d6.

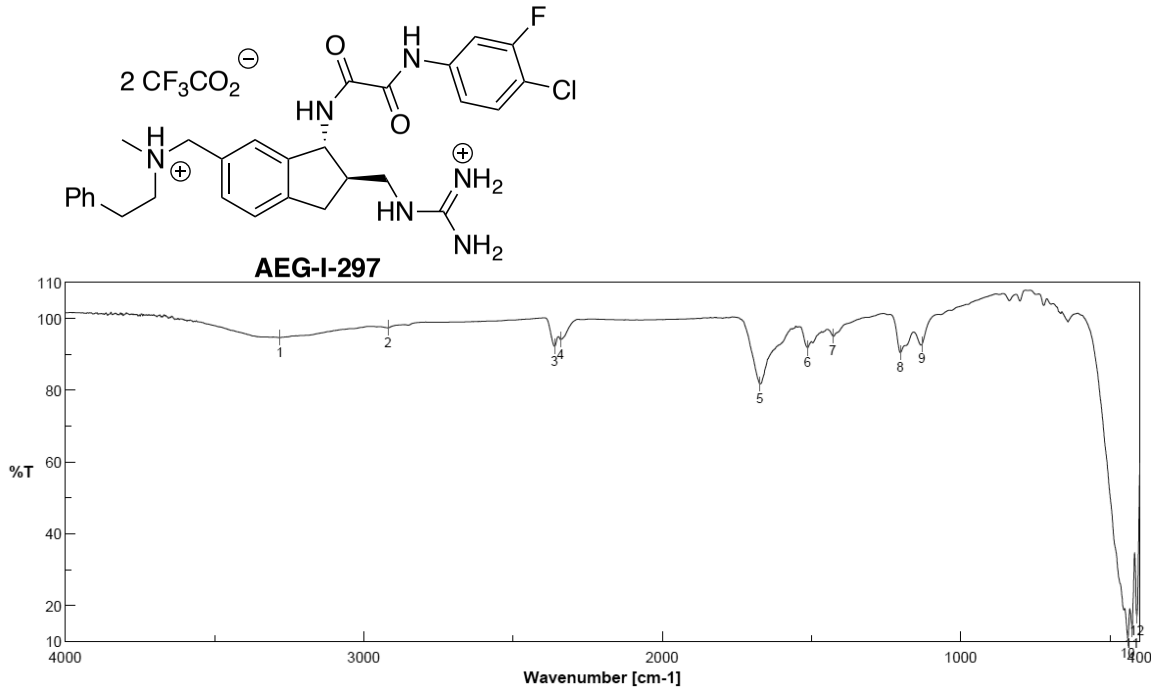

Figure A.1.18.3. The Infrared Spectrum of Compound **AEG-I-297**.

Spectroscopic Data Relevant to Chapter Two

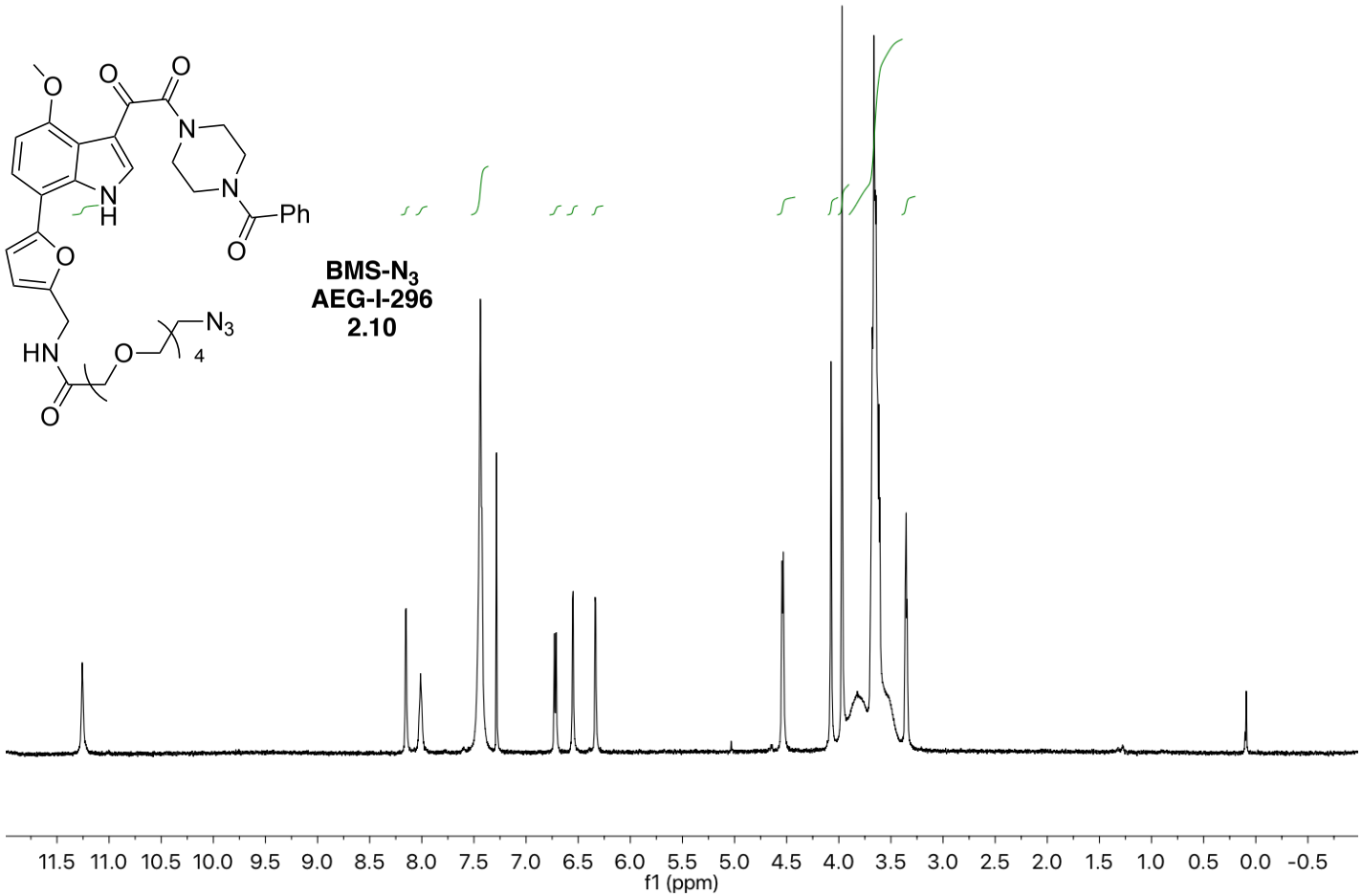

Figure A.2.1.1. The 500 MHz ^{1}H NMR Spectrum of BNM-N_3 **AEG-I-296** in $CDCl_3$.

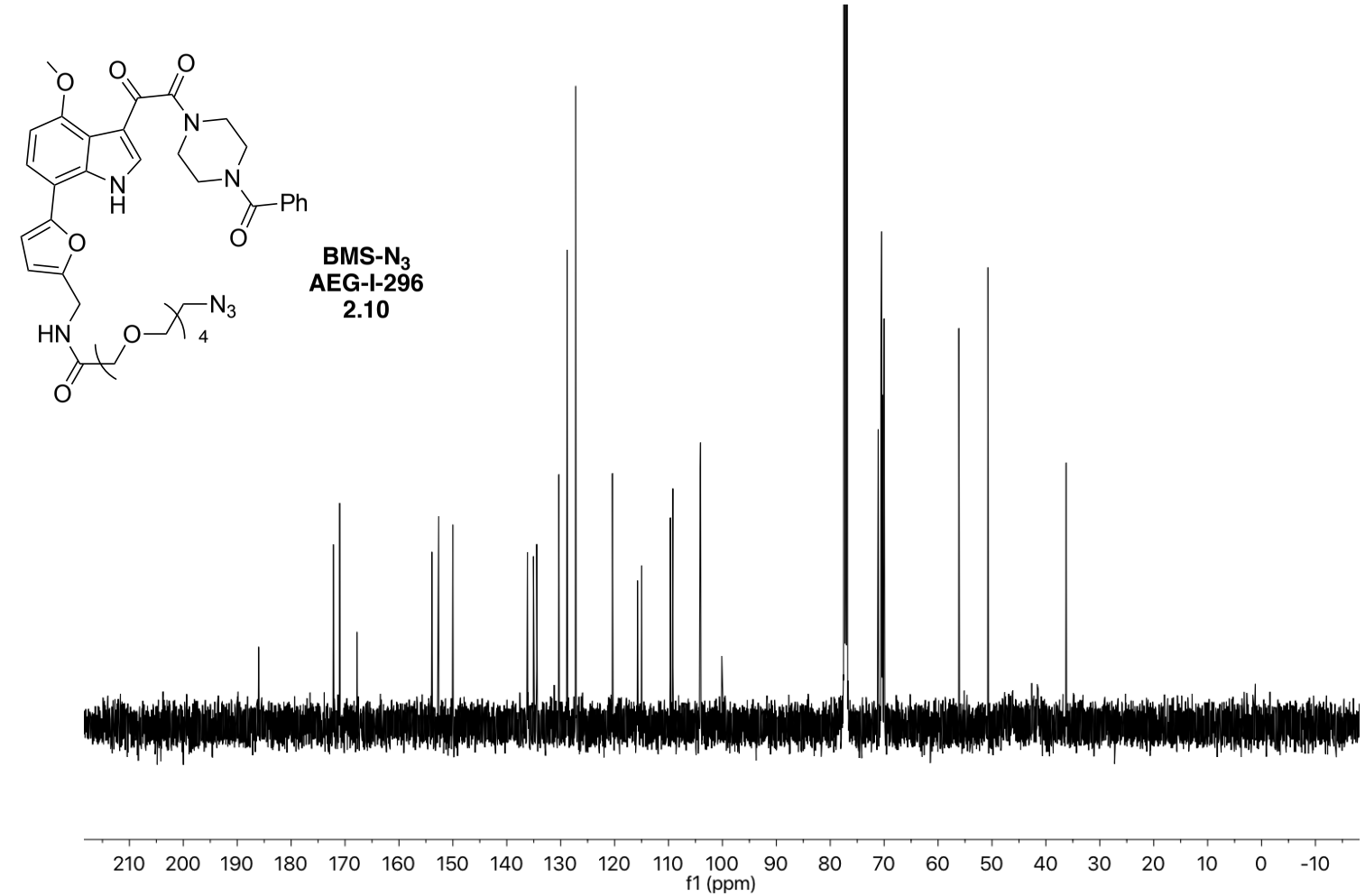

Figure A.2.1.2. The 500 MHz ^{13}C NMR Spectrum of BNM-N_3 **AEG-I-296** in $CDCl_3$.

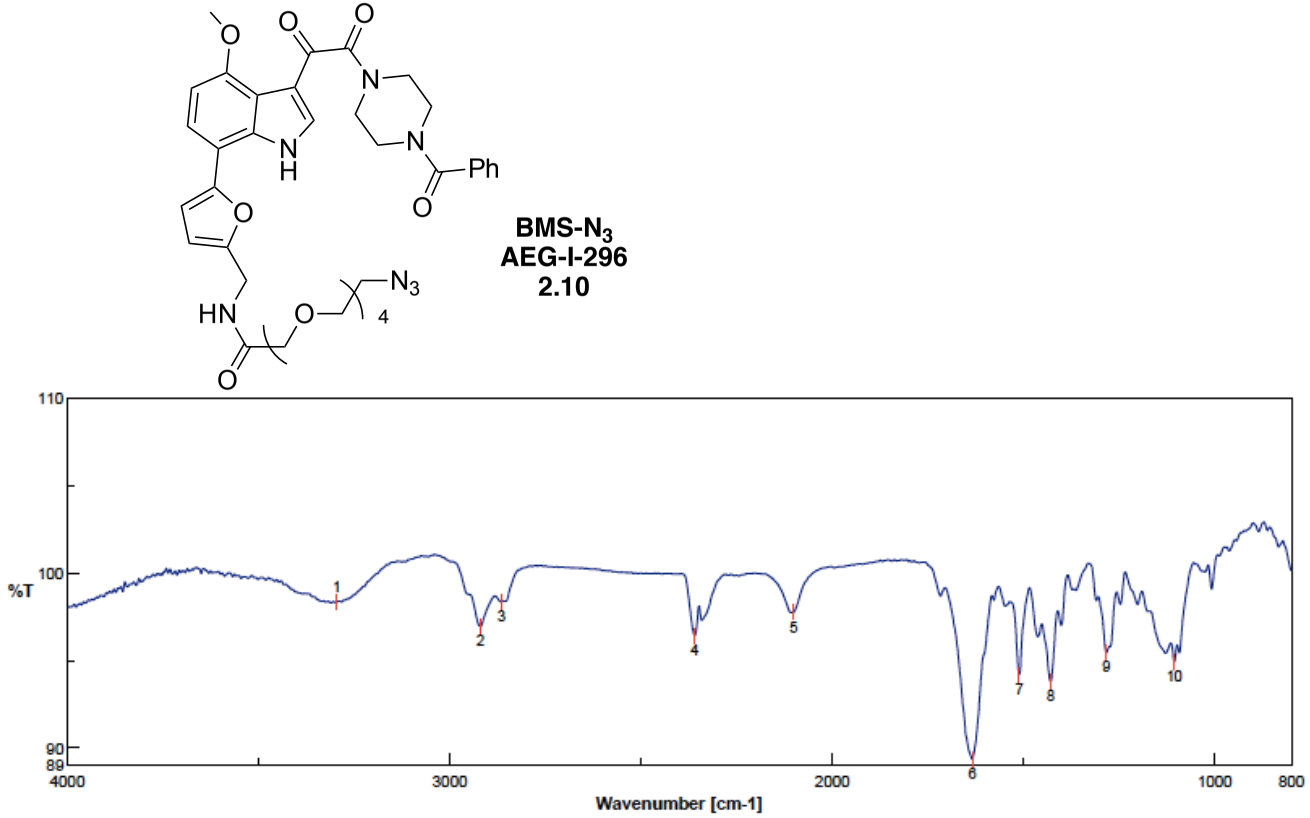

Figure A.2.1.3. The Infrared Spectrum of **AEG-I-296**.

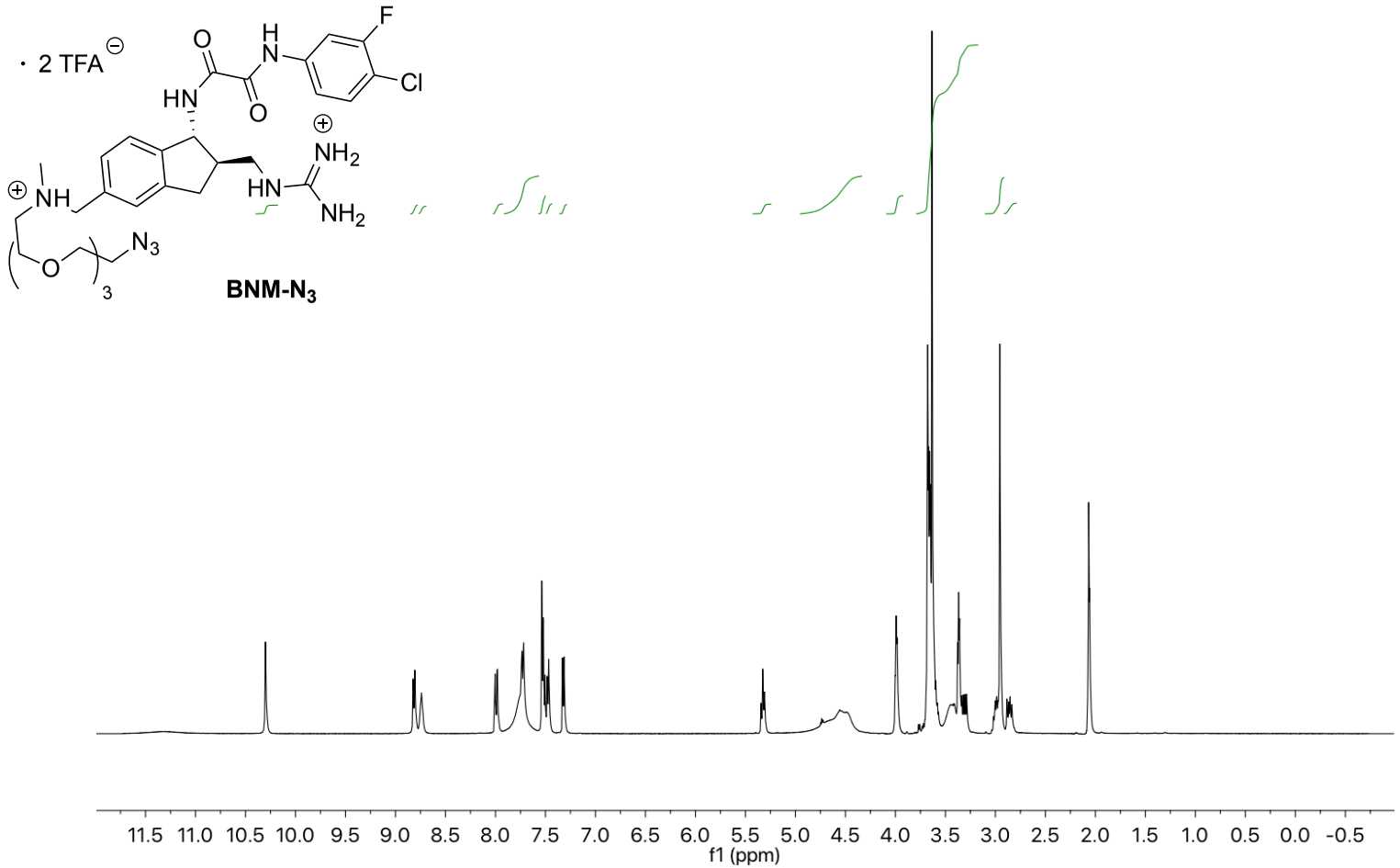

Figure A.2.2.1. The 500 MHz ^{1}H NMR Spectrum of **BMS-N_3** in $CDCl_3$.

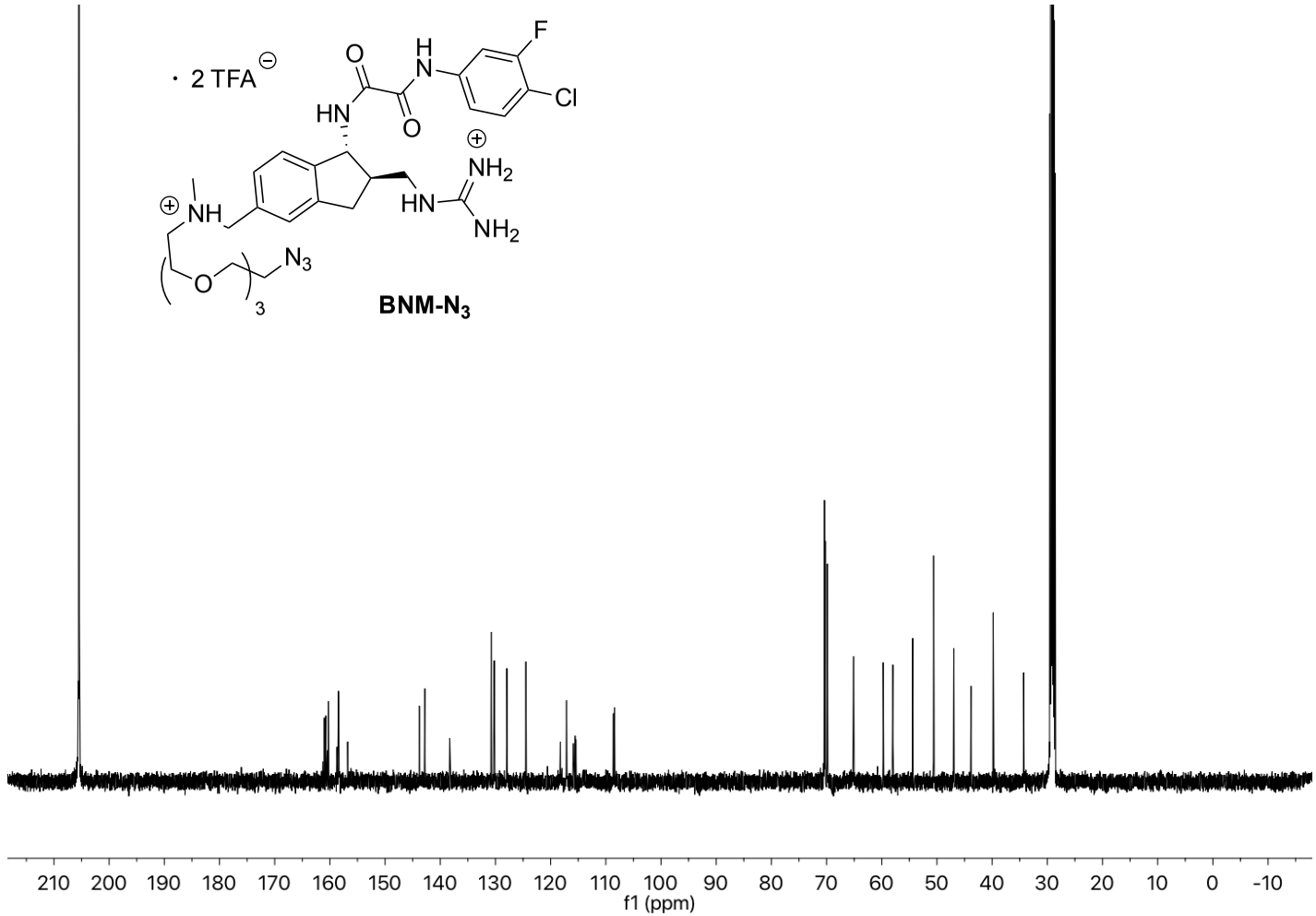

Figure A.2.2.2. The 500 MHz ^{13}C NMR Spectrum of **BMS-N_3** in $CDCl_3$.

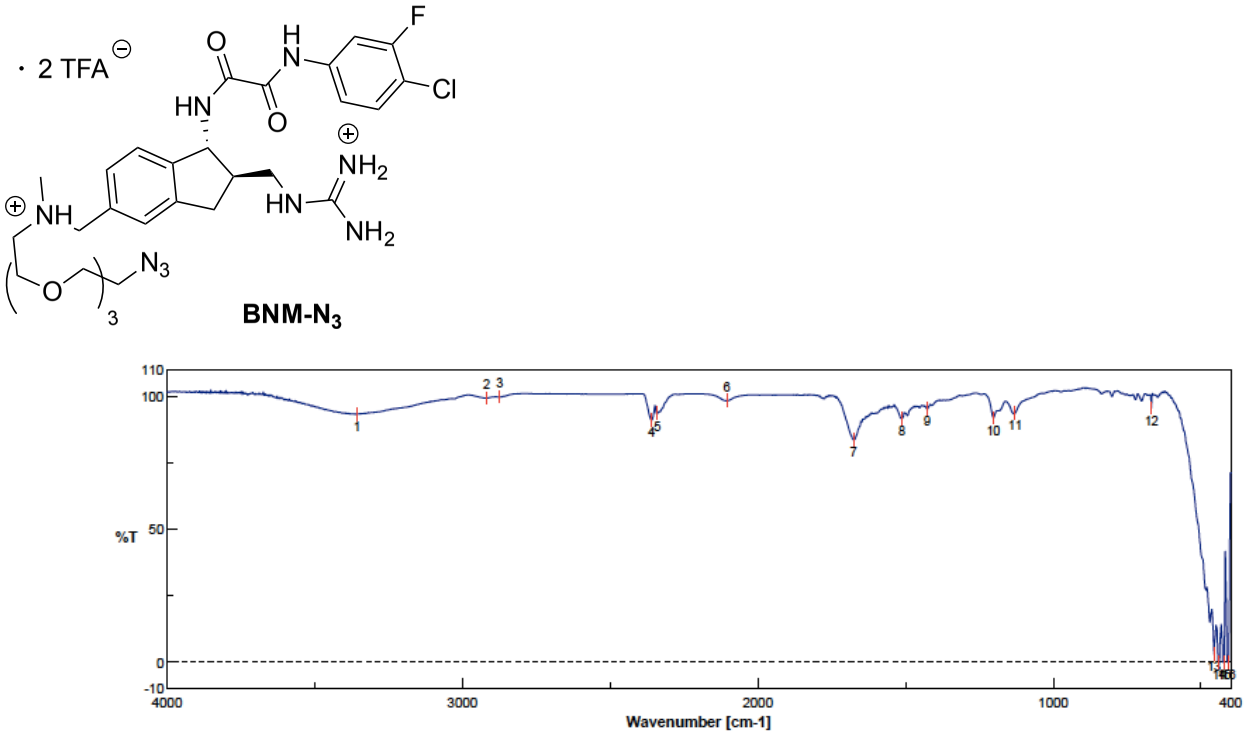

BNM-N_3

Figure A.2.2.1. The Infrared Spectrum of **BMS-N_3**.

Spectroscopic Data Relevant to Chapter Three

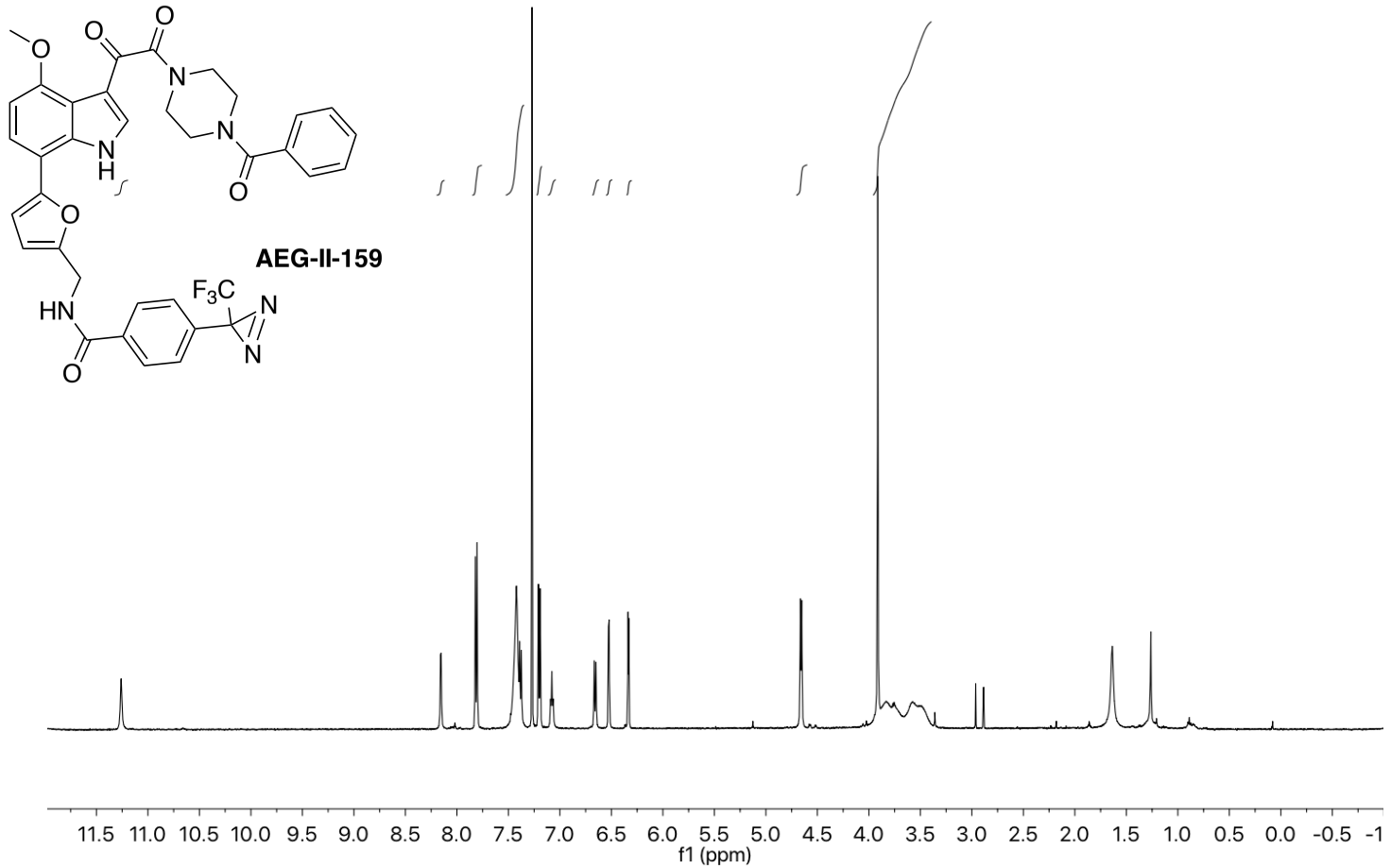

Figure A.3.1.1. The 500 MHz ^{1}H NMR Spectrum of **AEG-II-159** in $CDCl_3$.

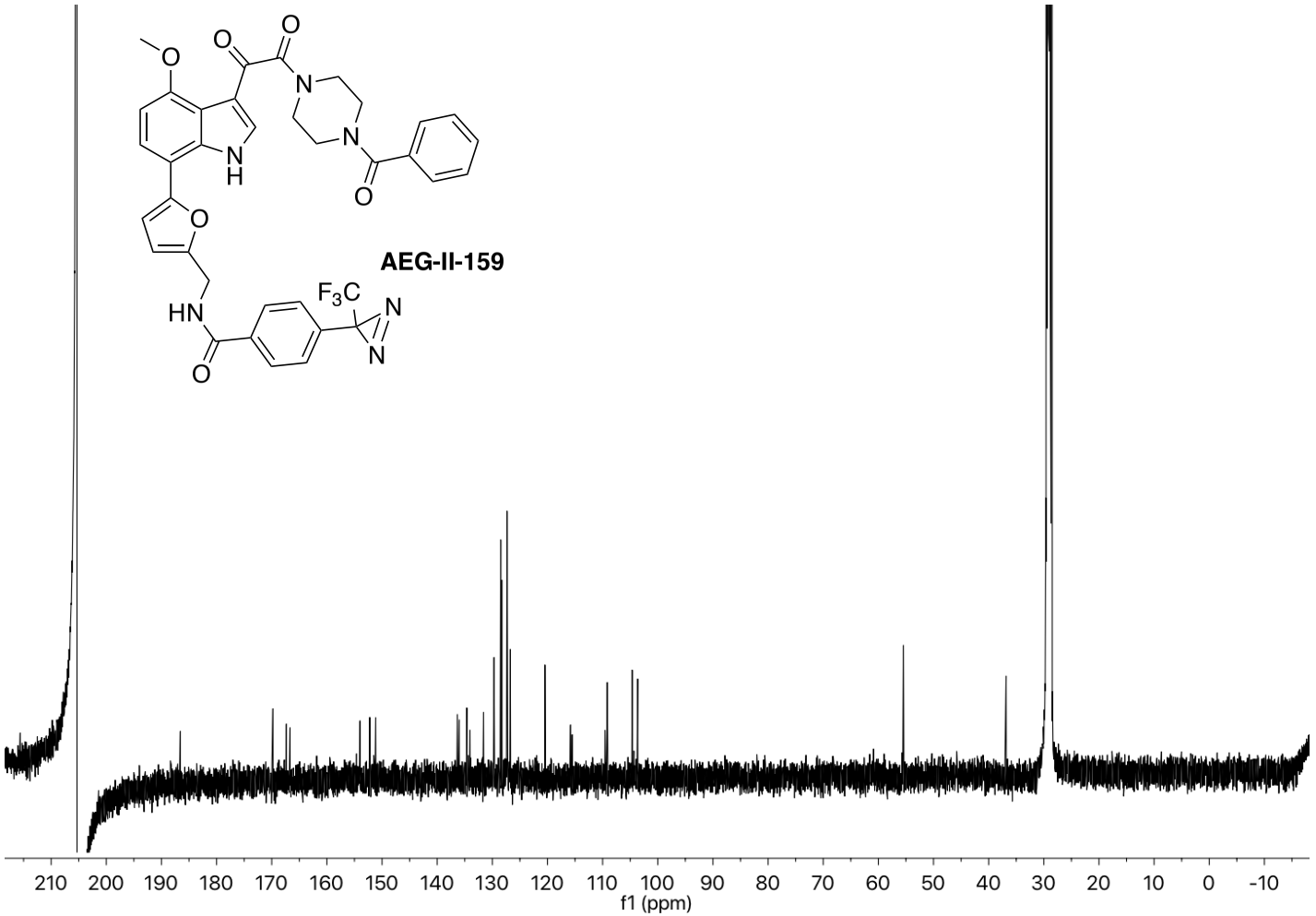

Figure A.3.1.2. The 500 MHz ^{13}C NMR Spectrum of **AEG-II-159** in $CDCl_3$.

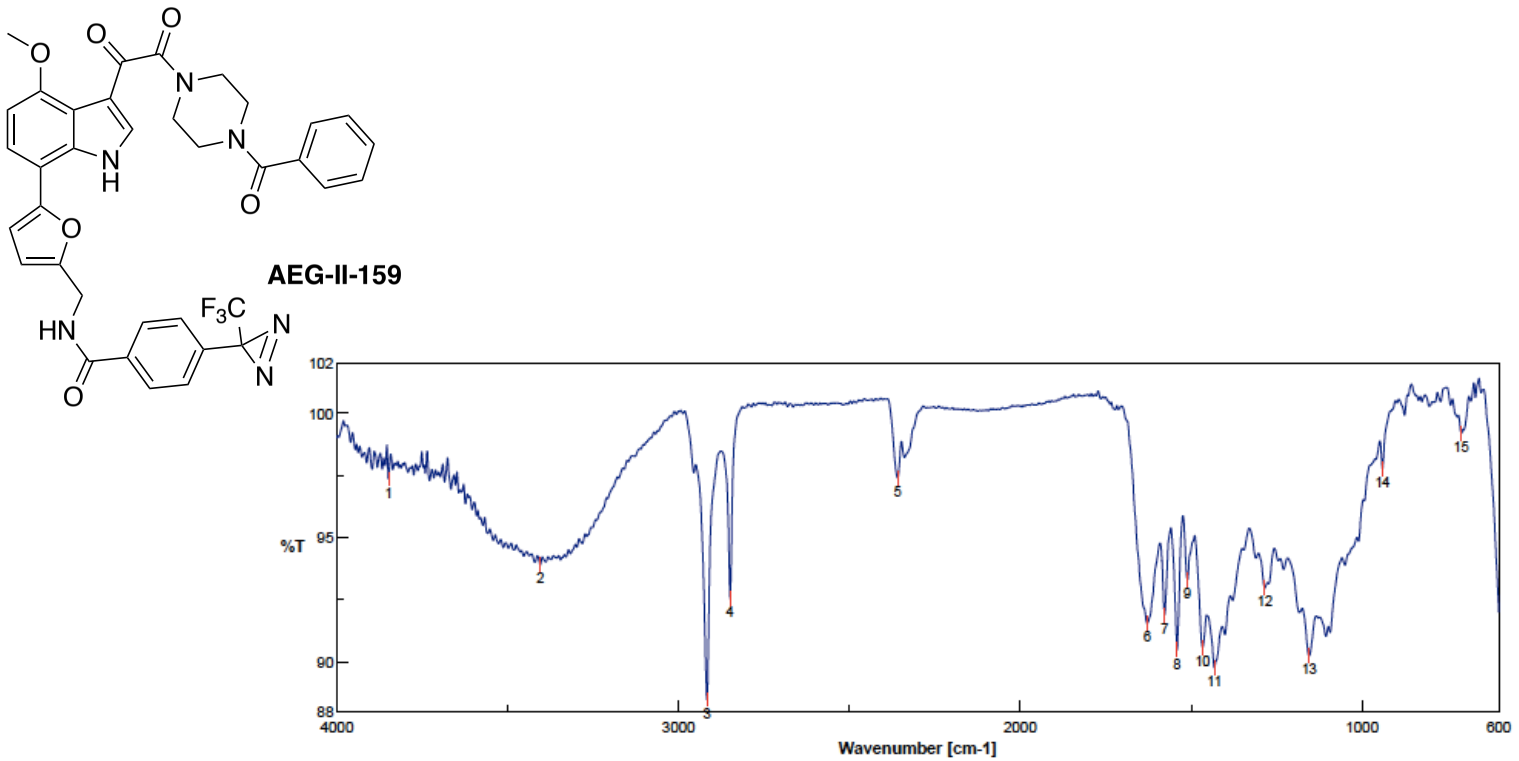

Figure A.3.1.3. The Infrared Spectrum of **AEG-II-159**.

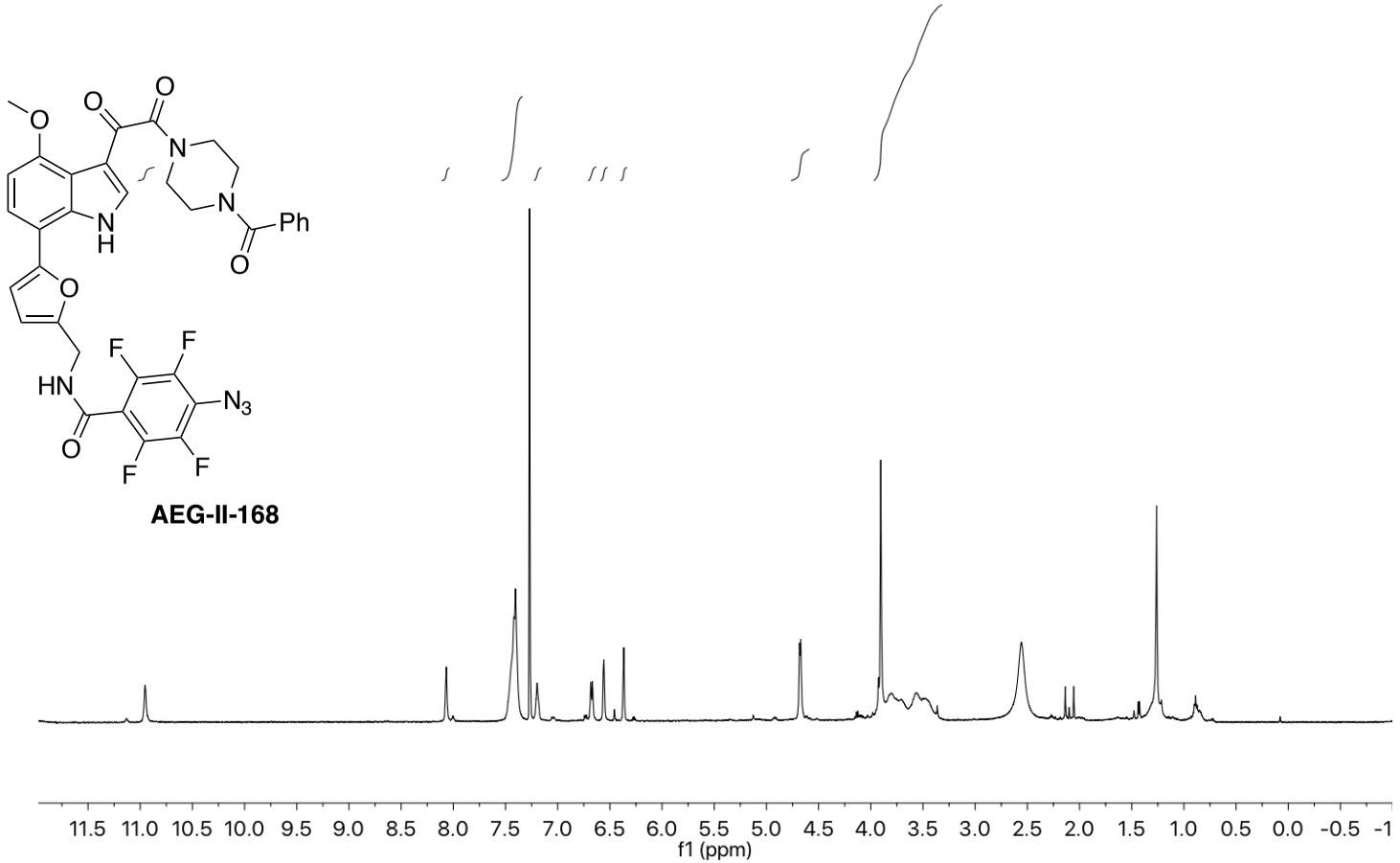

Figure A.3.2.1. The 500 MHz ^{1}H NMR Spectrum of **AEG-II-168** in $CDCl_3$.

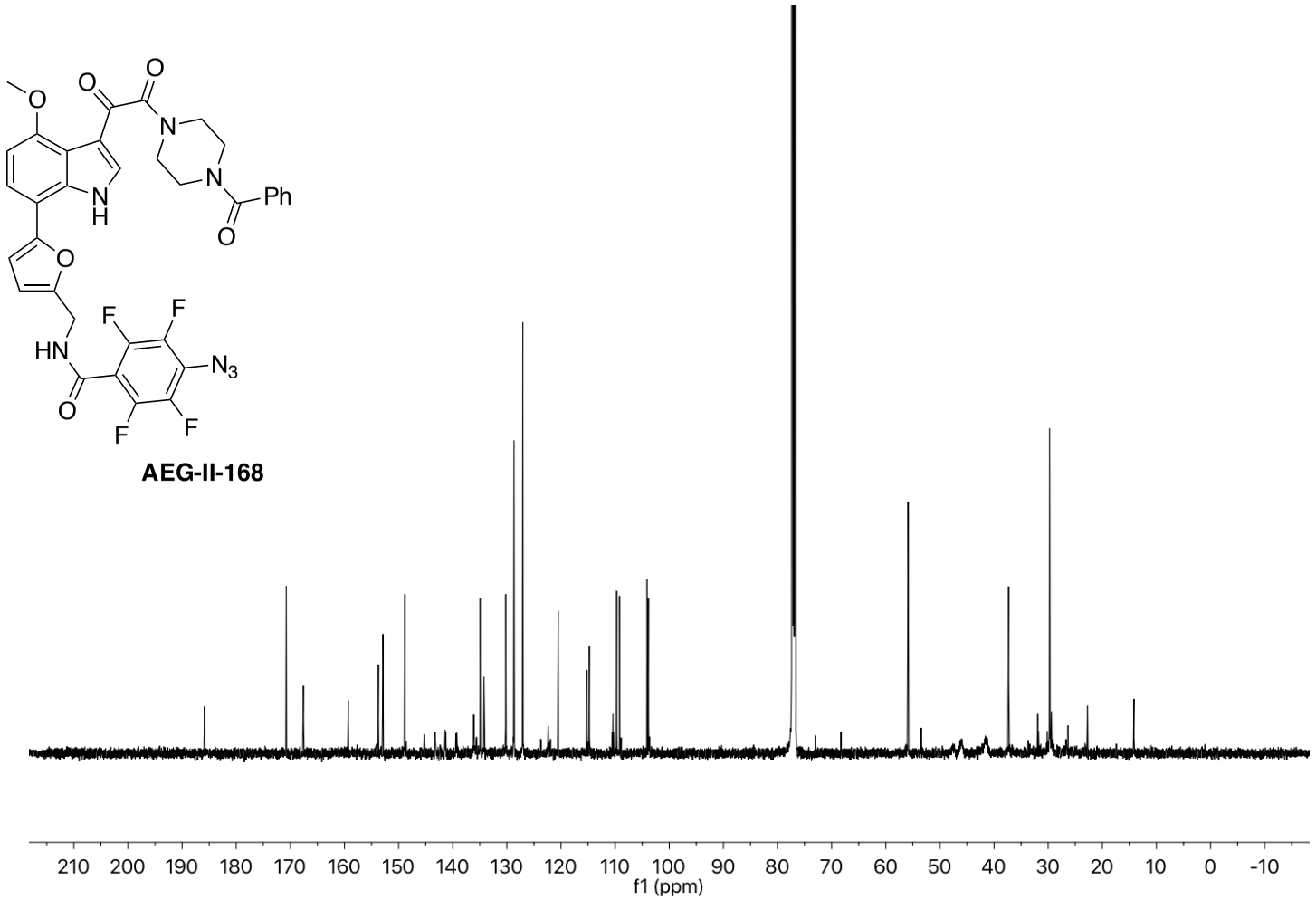

Figure A.3.2.2. The 500 MHz ^{13}C NMR Spectrum of **AEG-II-168** in $CDCl_3$.

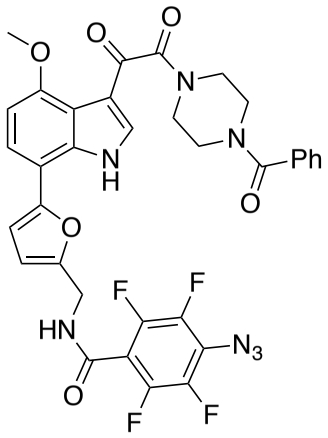

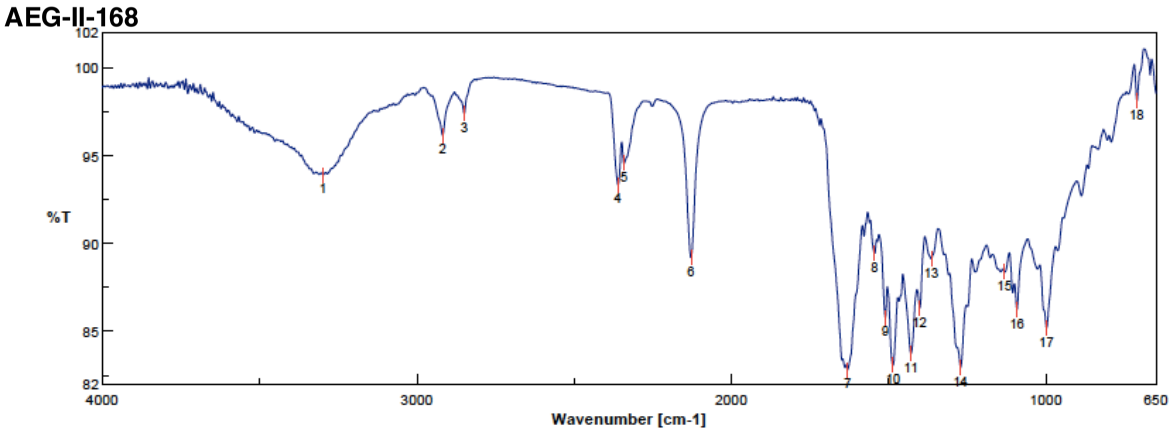

Figure A.3.2.3. The Infrared Spectrum of **AEG-II-168**.

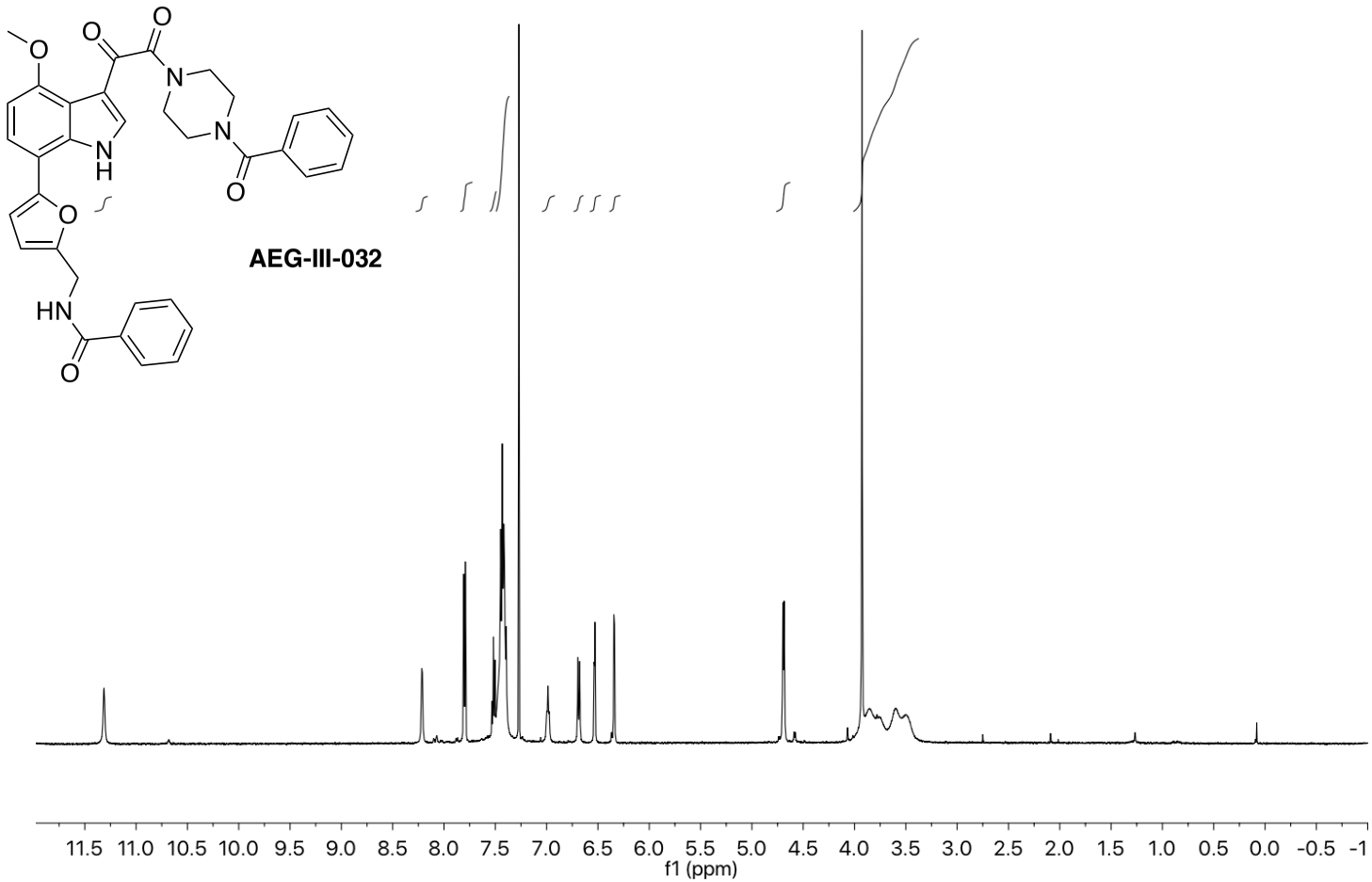

Figure A.3.3.1. The 500 MHz ^{1}H NMR Spectrum of **AEG-III-032** in $CDCl_3$.

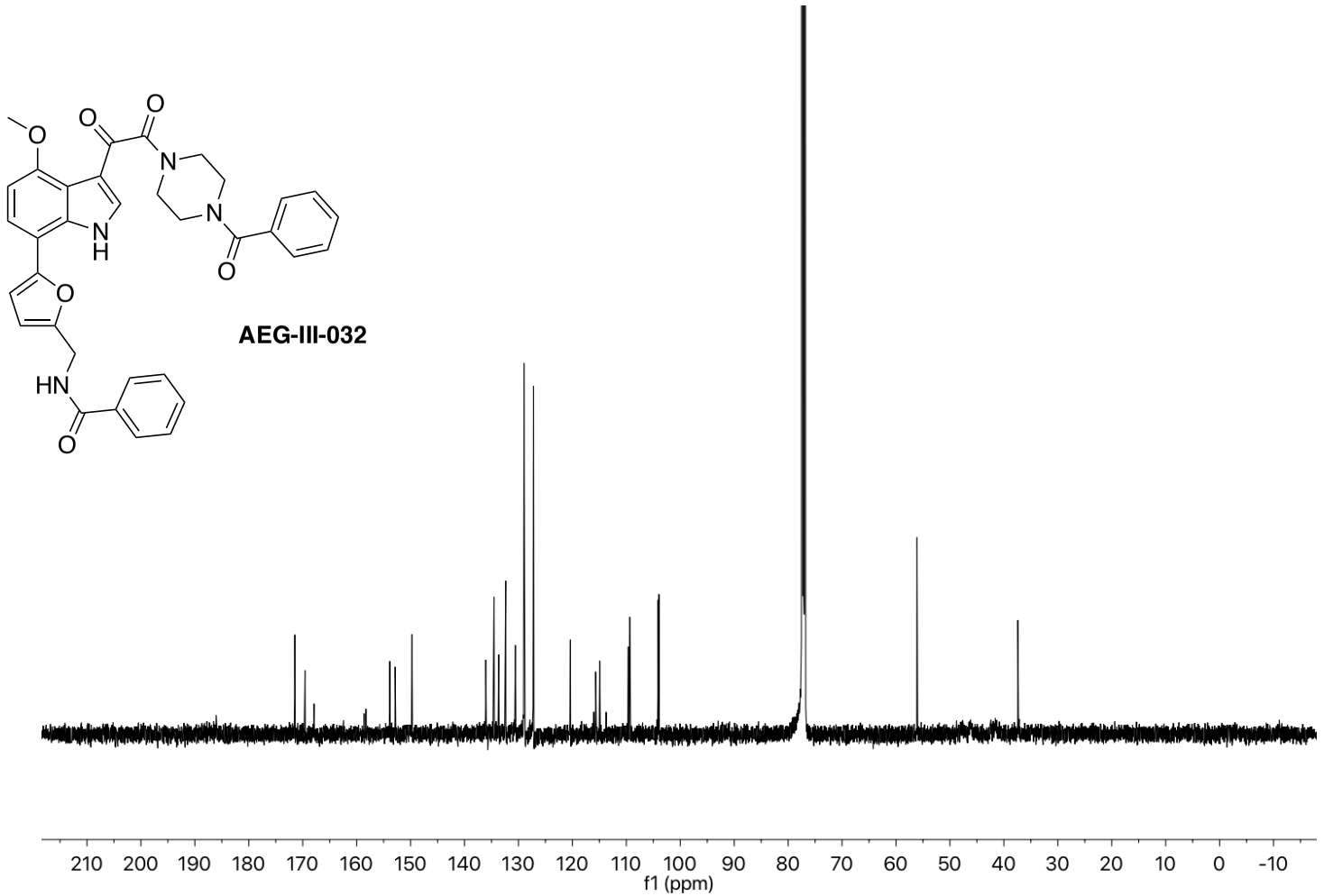

Figure A.3.3.2. The 500 MHz ^{13}C NMR Spectrum of **AEG-III-032** in $CDCl_3$.

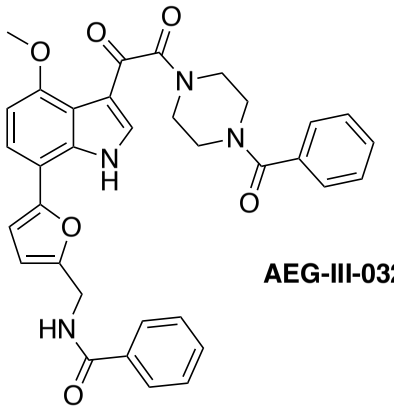

AEG-III-032

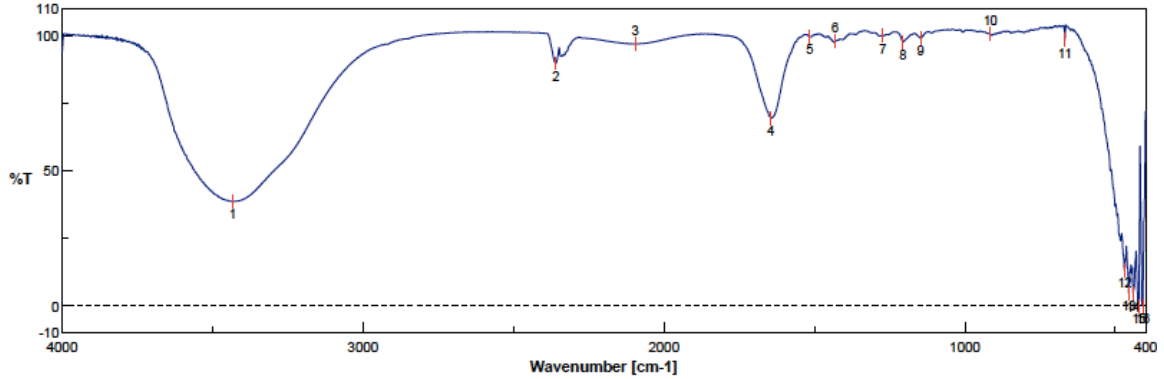

Figure A.3.3.2. Infrared Spectrum of **AEG-III-032**.

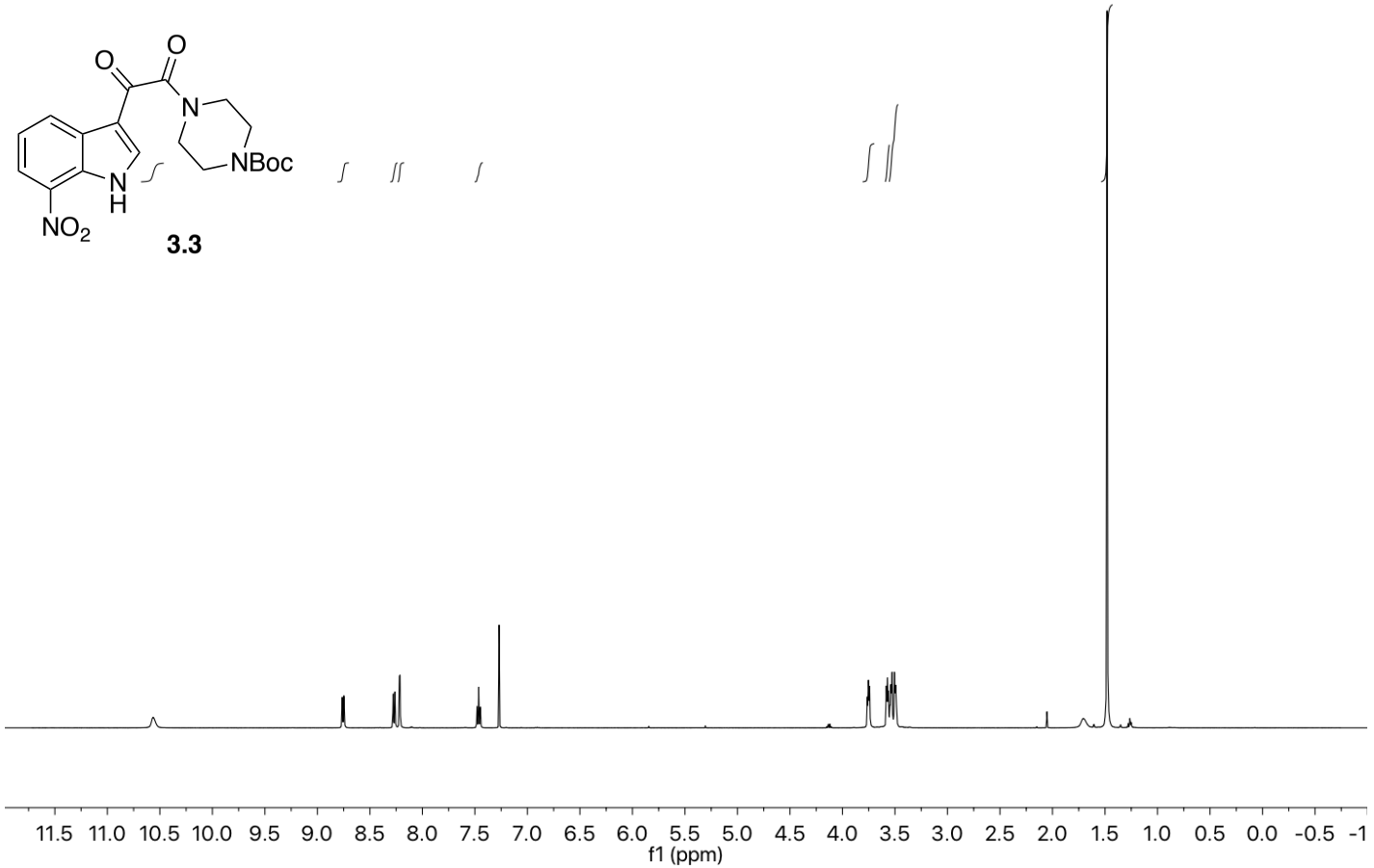

Figure A.3.4.1. The 500 MHz ^{1}H NMR Spectrum of **3.3** in $CDCl_3$.

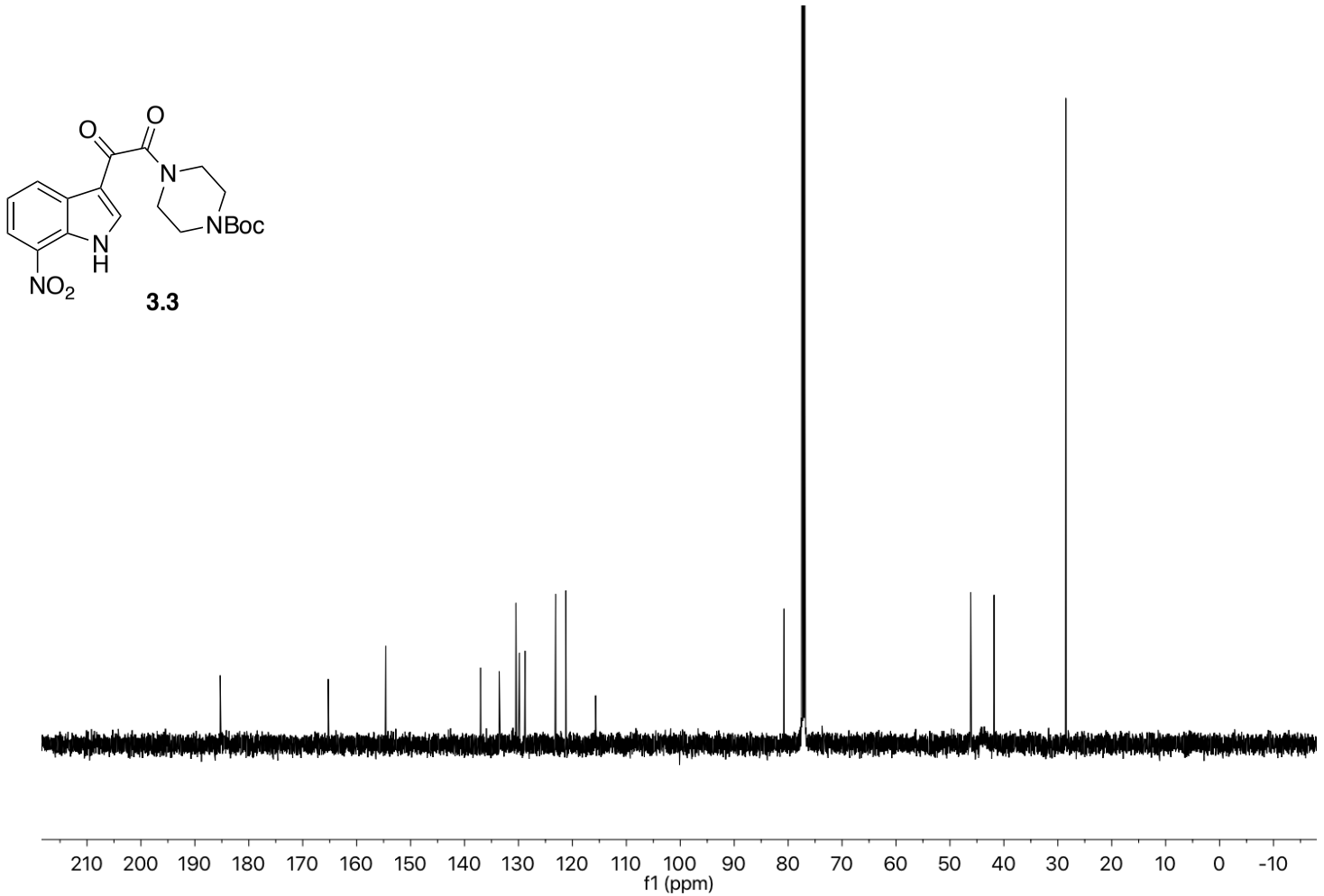

Figure A.3.4.2. The 500 MHz ^{13}C NMR Spectrum of **3.3** in $CDCl_3$.

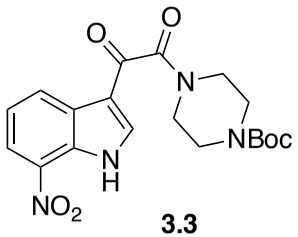

3.3

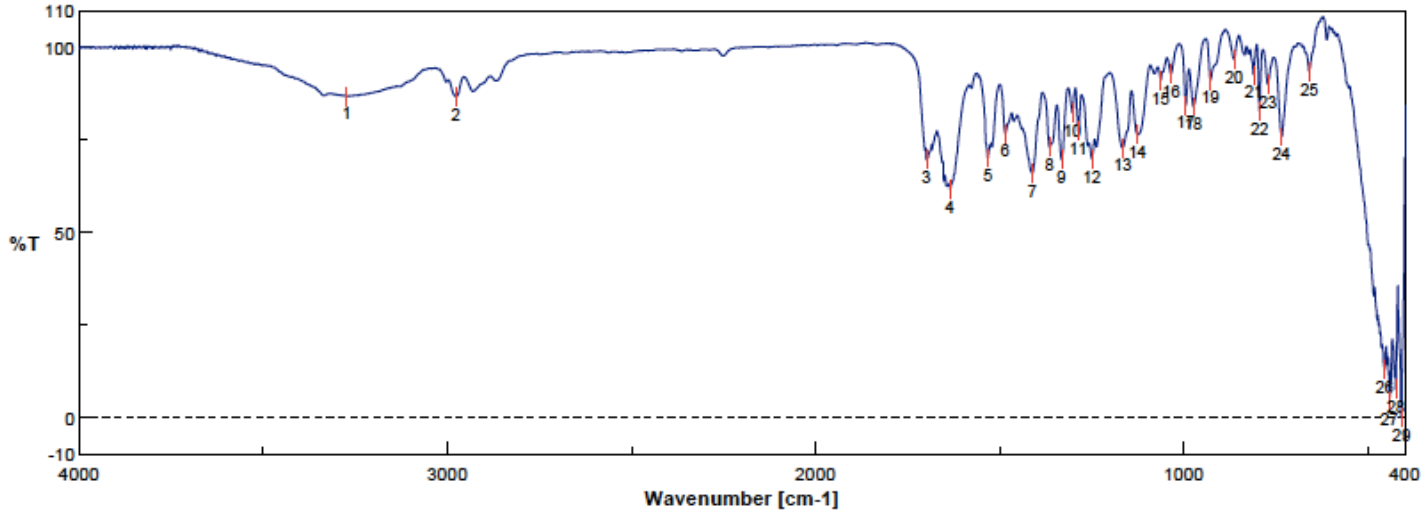

Figure A.3.4.3. The Infrared Spectrum of **3.3**.

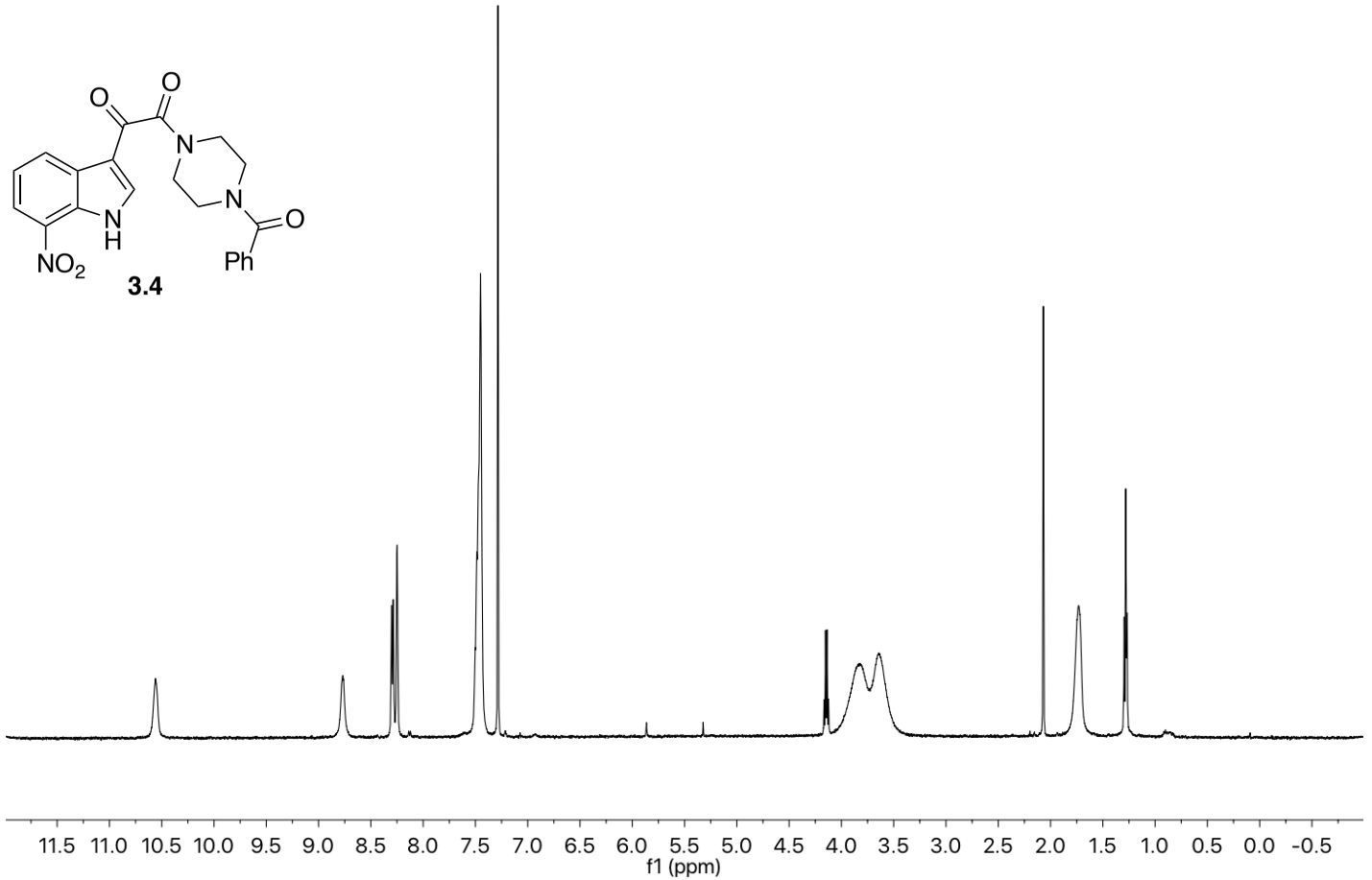

Figure A.3.5.1. The 500 MHz ^{1}H NMR Spectrum of **3.4** in $CDCl_3$.

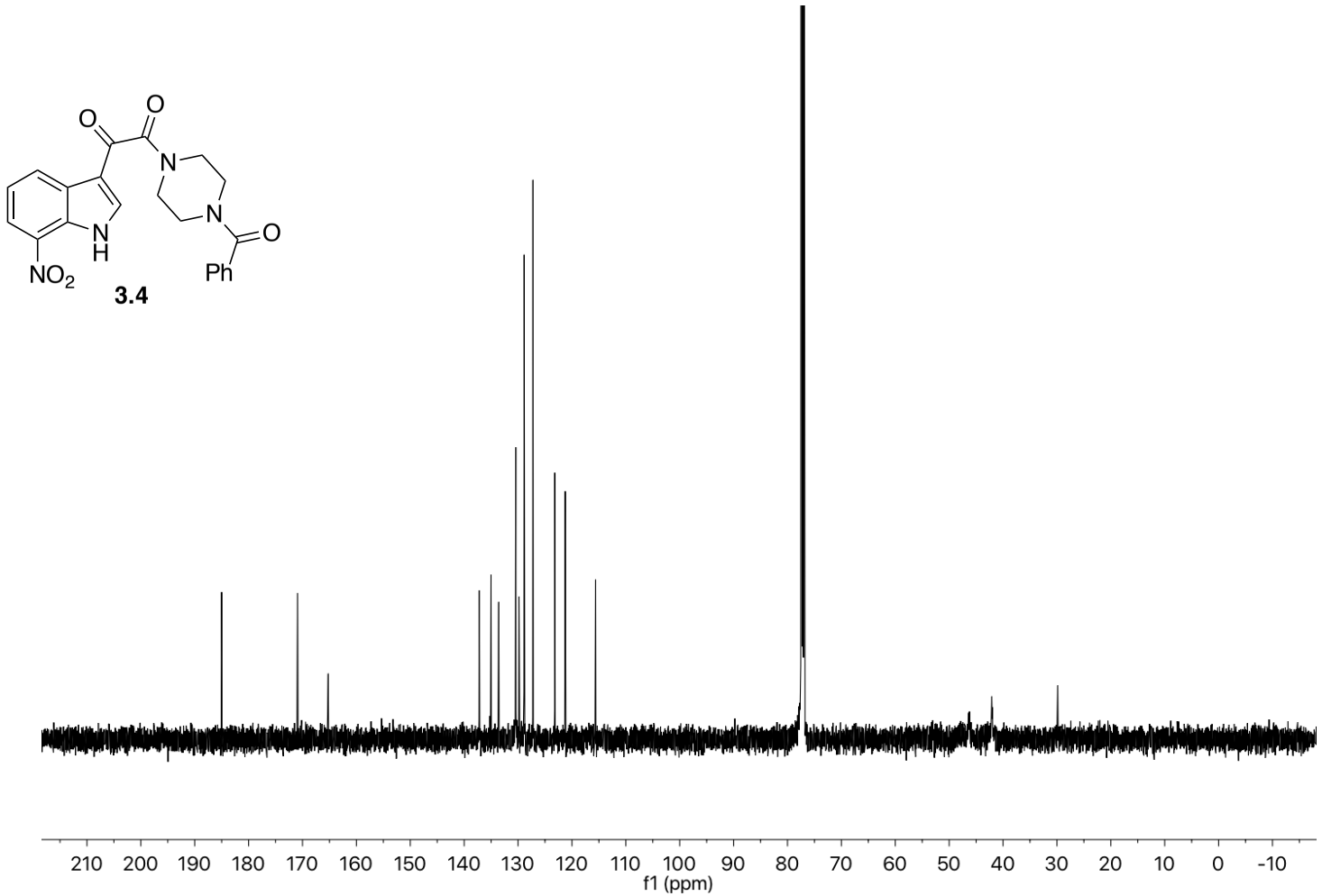

Figure A.3.5.2. The 500 MHz ^{13}C NMR Spectrum of **3.4** in $CDCl_3$.

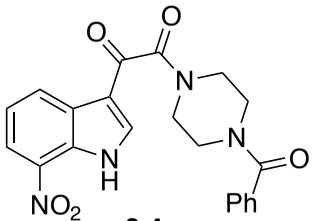

3.4

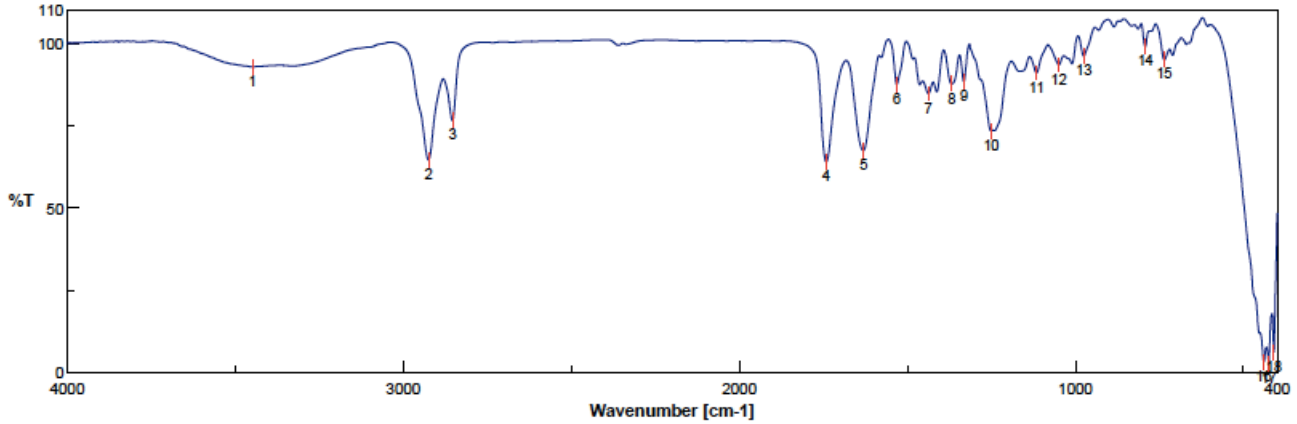

Figure A.3.5.3. The Infrared Spectrum of **3.4**.

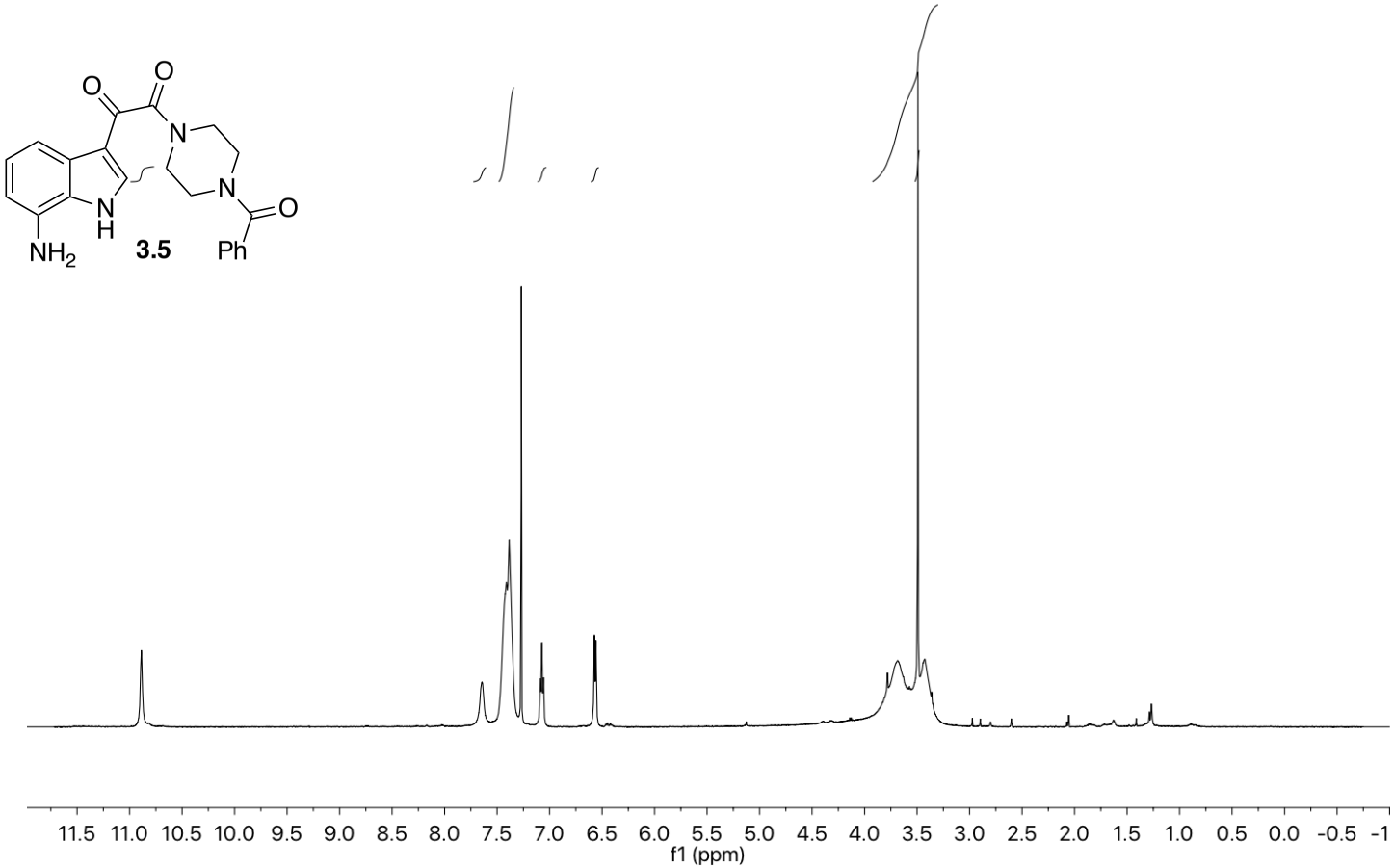

Figure A.3.6.1. The 500 MHz ^{1}H NMR Spectrum of **3.5** in $CDCl_3$.

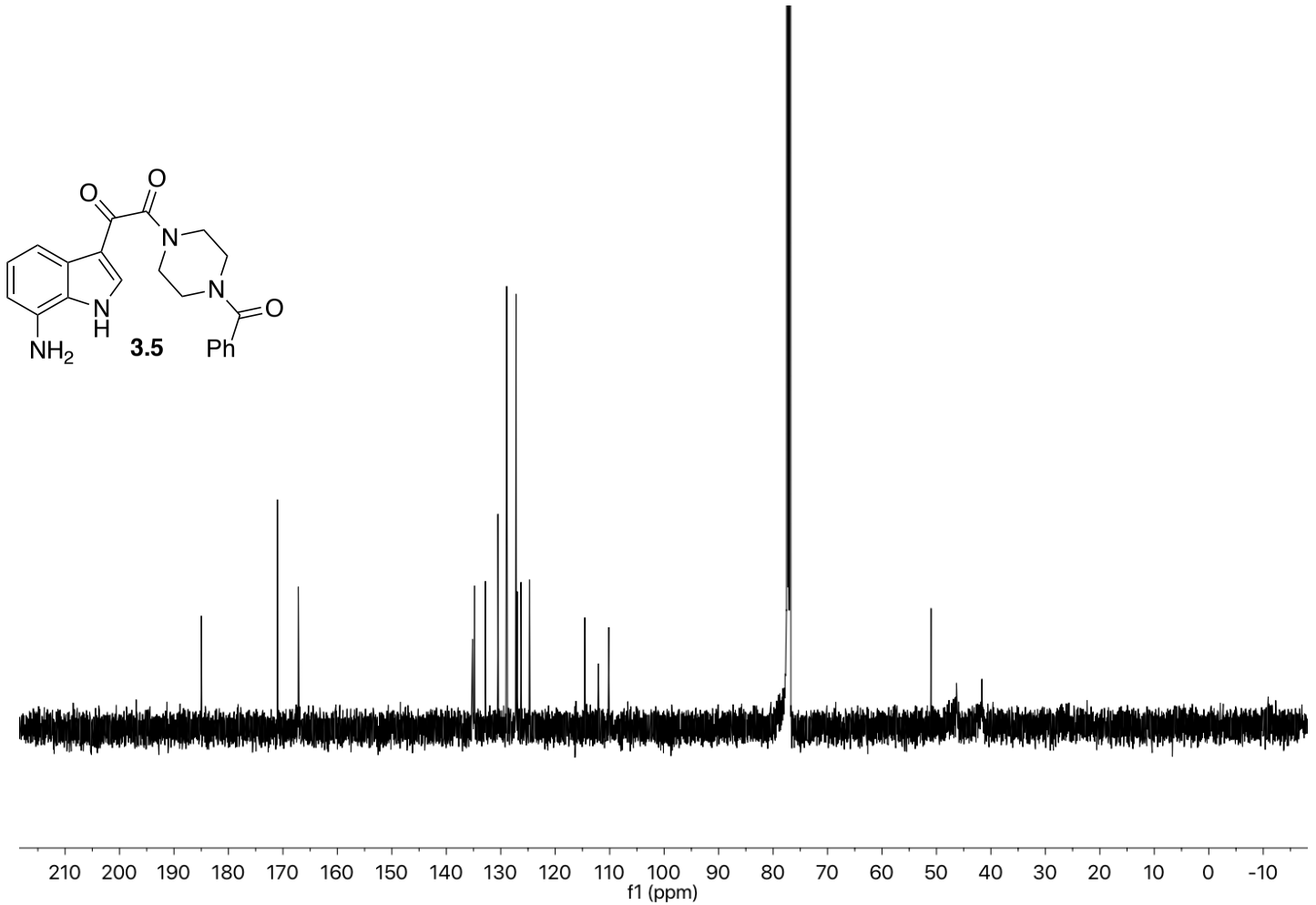

Figure A.3.6.2. The 500 MHz ^{13}C NMR Spectrum of **3.6** in $CDCl_3$.

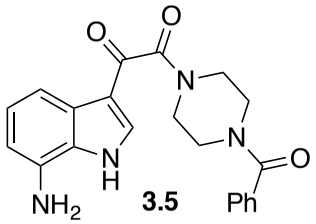

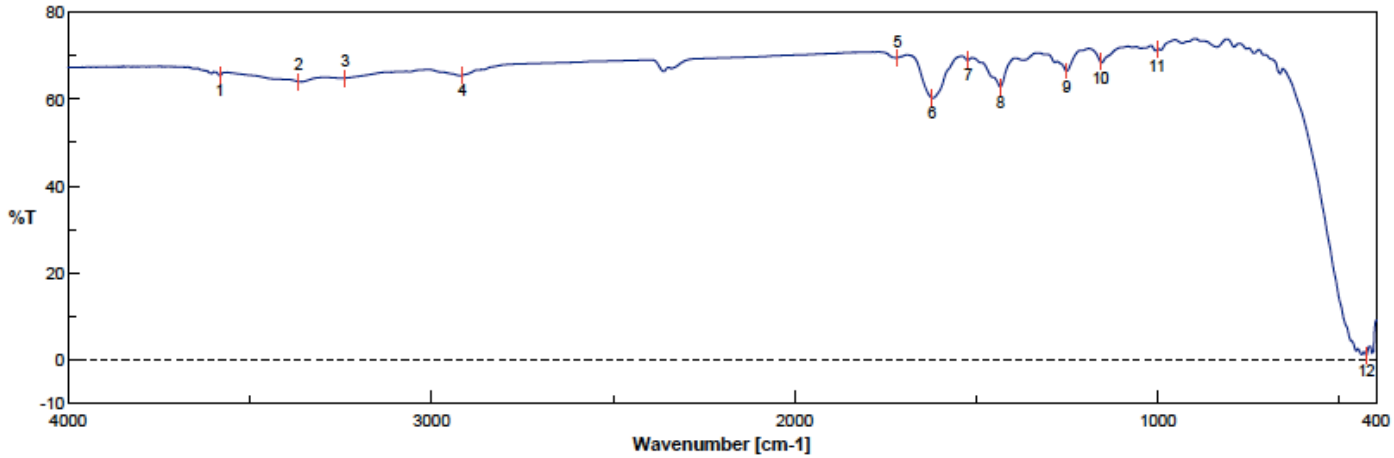

Figure A.3.6.3. The Infrared Spectrum of **3.5**.

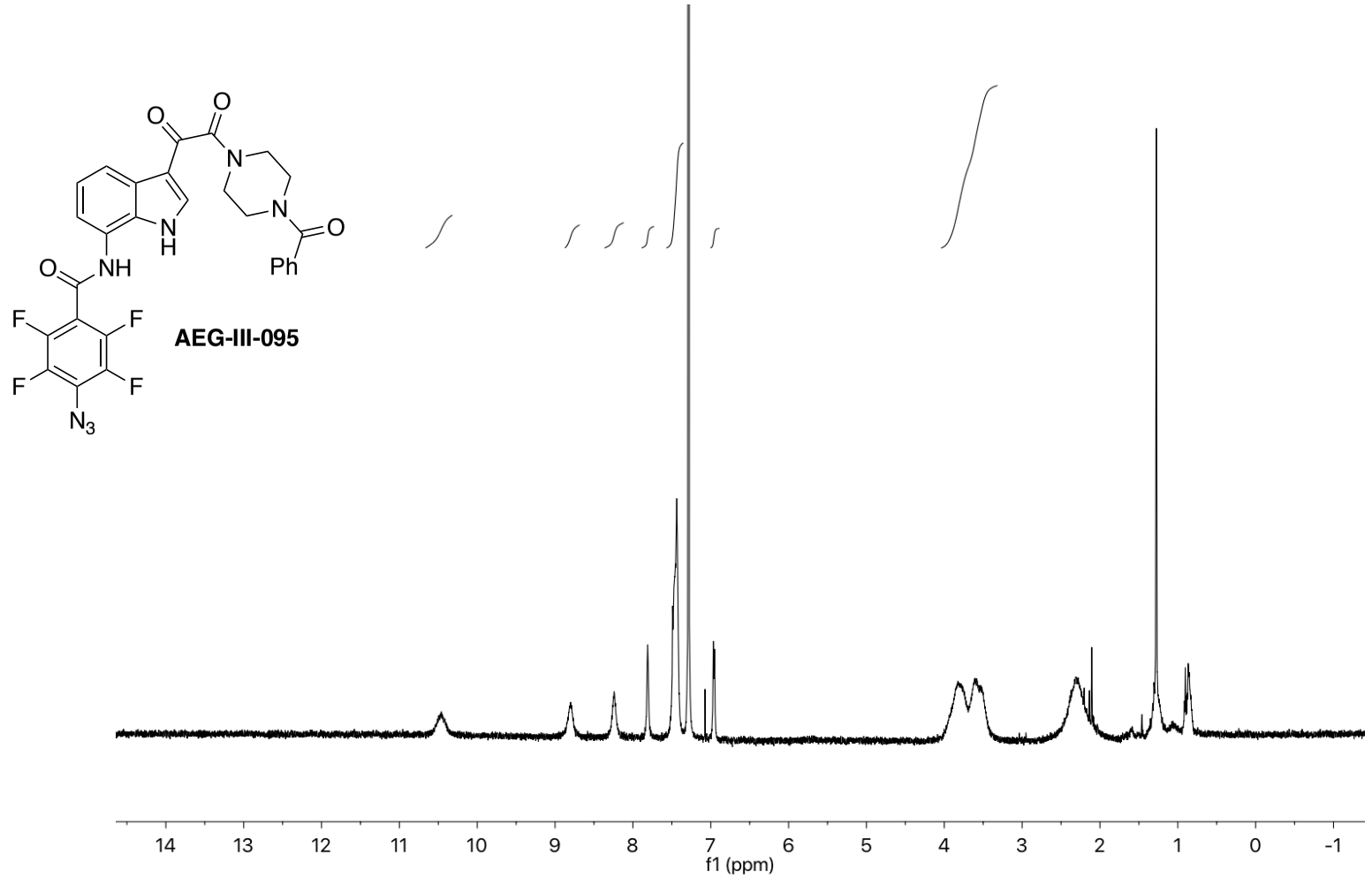

Figure A.3.7.1. The 500 MHz ^{1}H NMR Spectrum of **AEG-III-095** in $CDCl_3$.

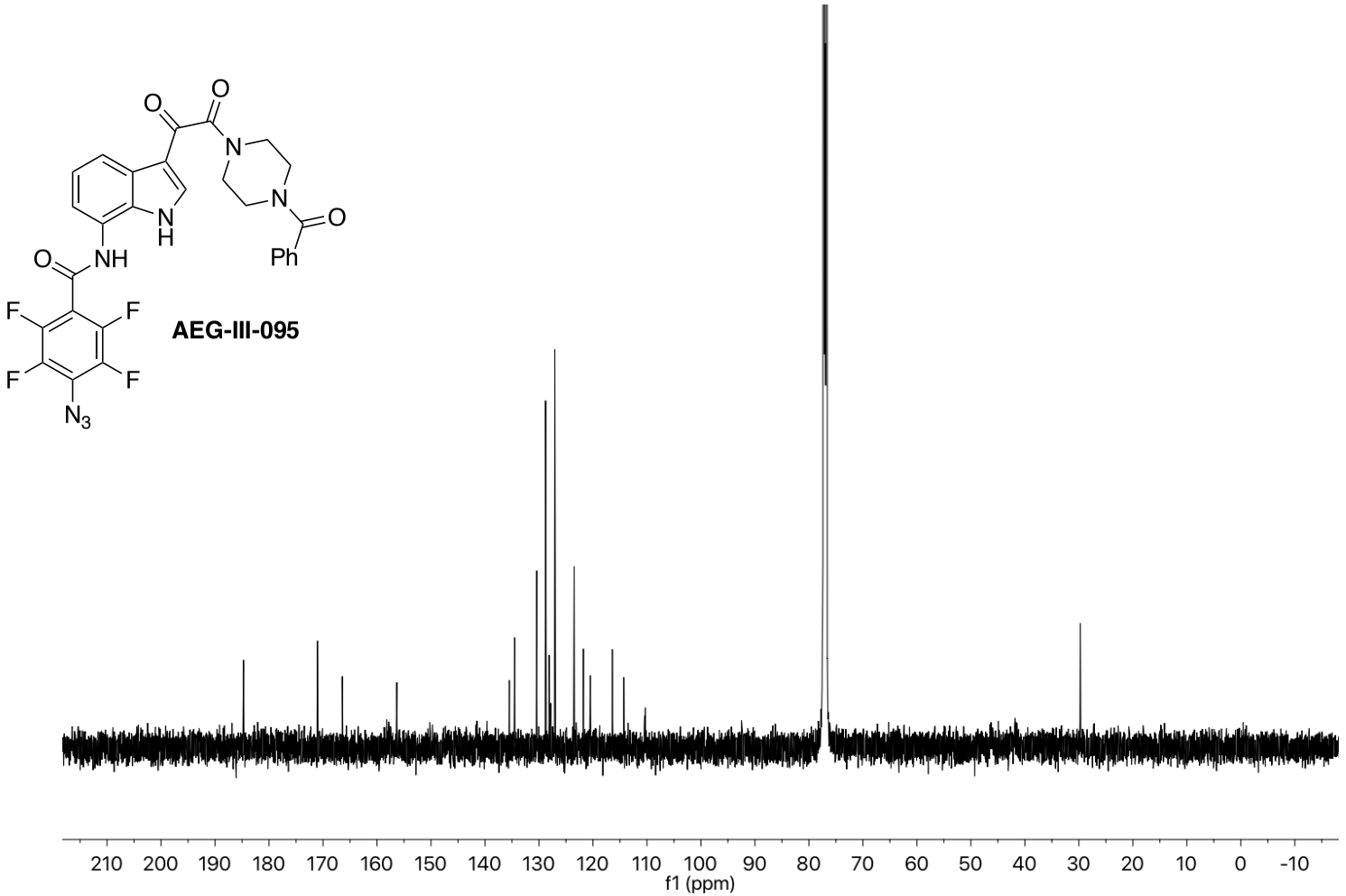

Figure A.3.7.2. The 500 MHz ^{13}C NMR Spectrum of **AEG-III-095** in $CDCl_3$.

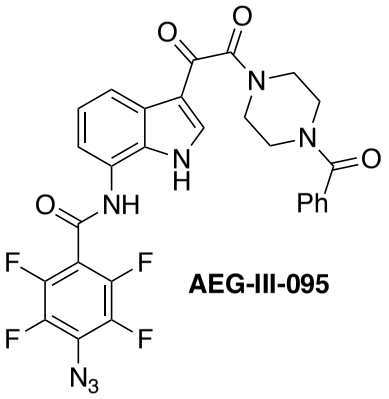

AEG-III-095

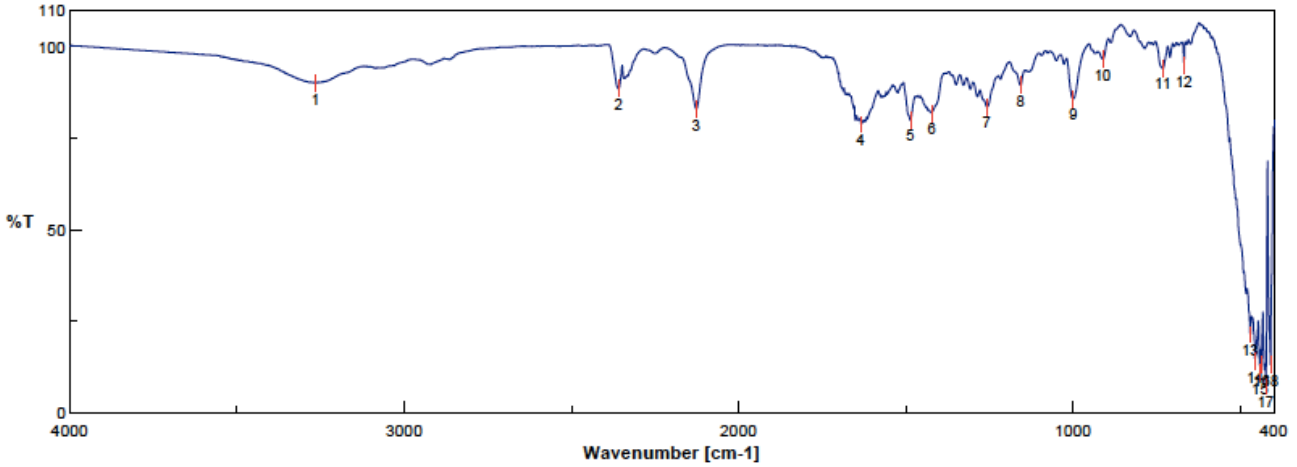

Figure A.3.7.3. The Infrared Spectrum of **AEG-III-095**.

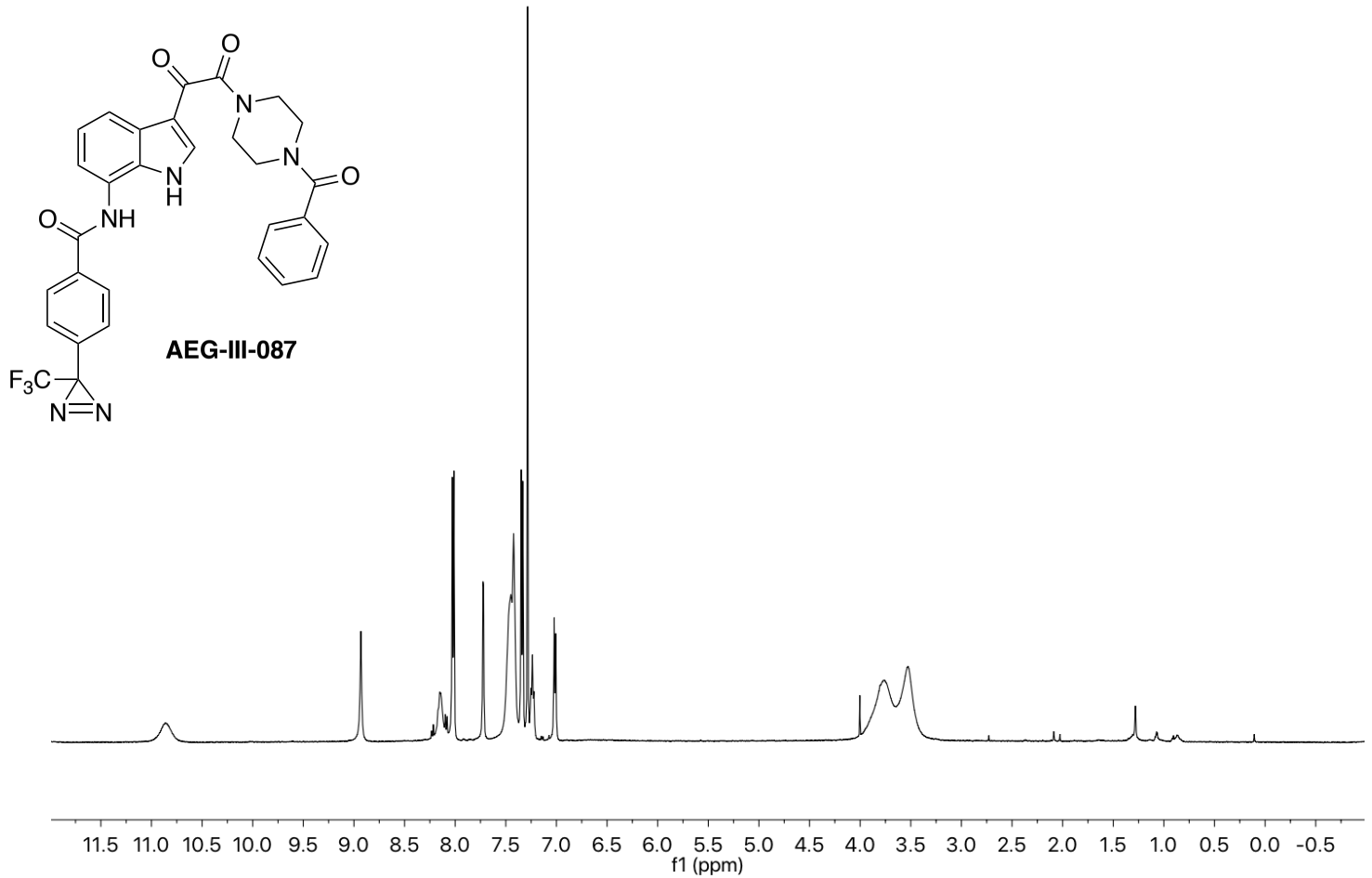

Figure A.3.8.1. The 500 MHz ^{1}H NMR Spectrum of **AEG-III-087** in $CDCl_3$.

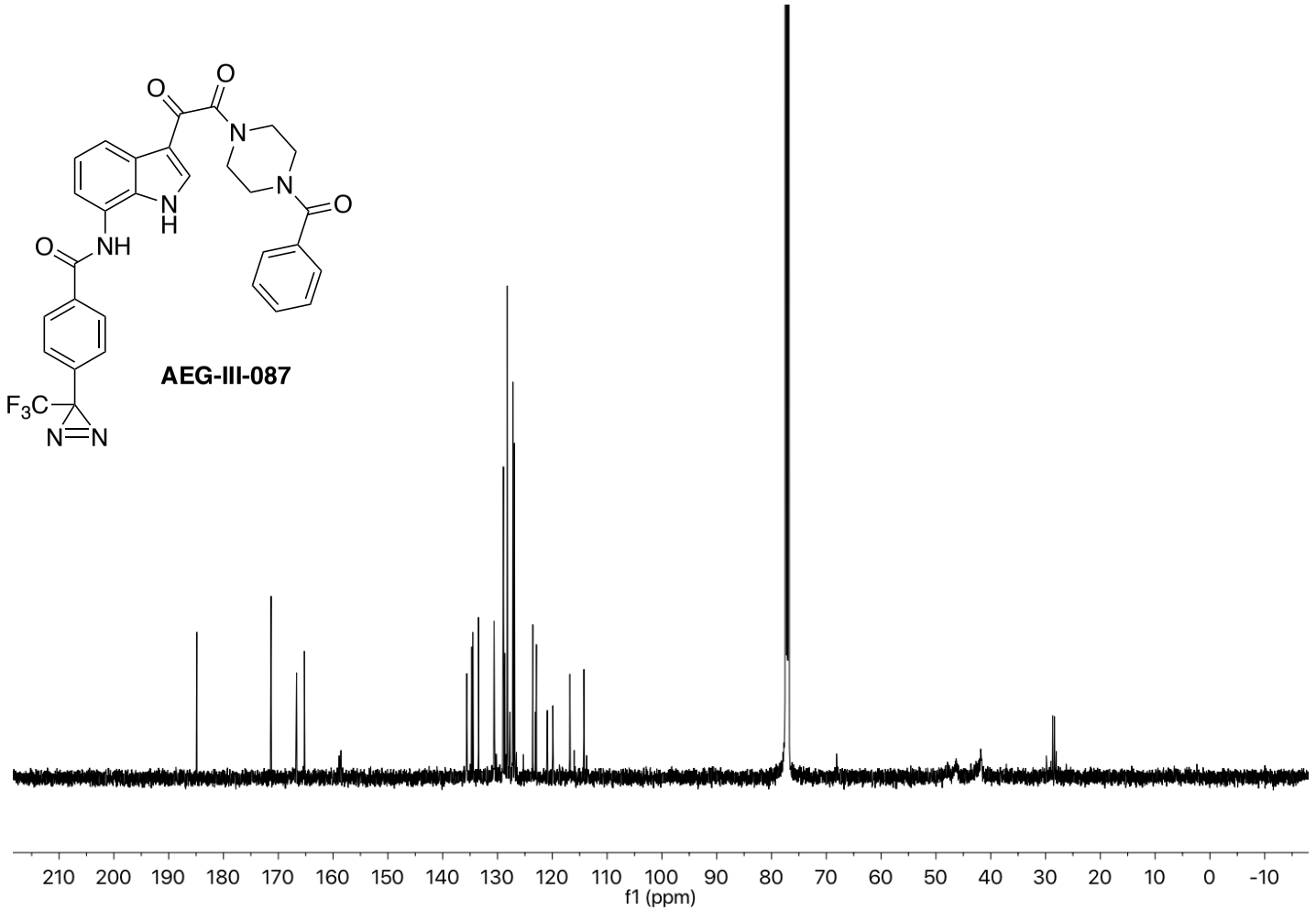

Figure A.3.8.2. The 500 MHz ^{13}C NMR Spectrum of **AEG-III-087** in $CDCl_3$.

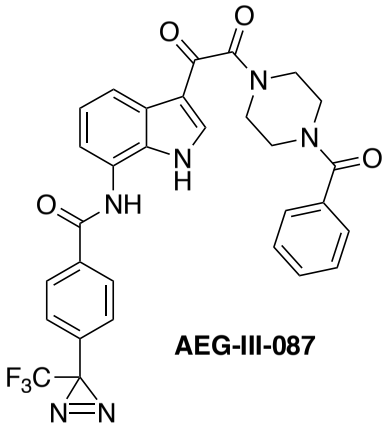

AEG-III-087

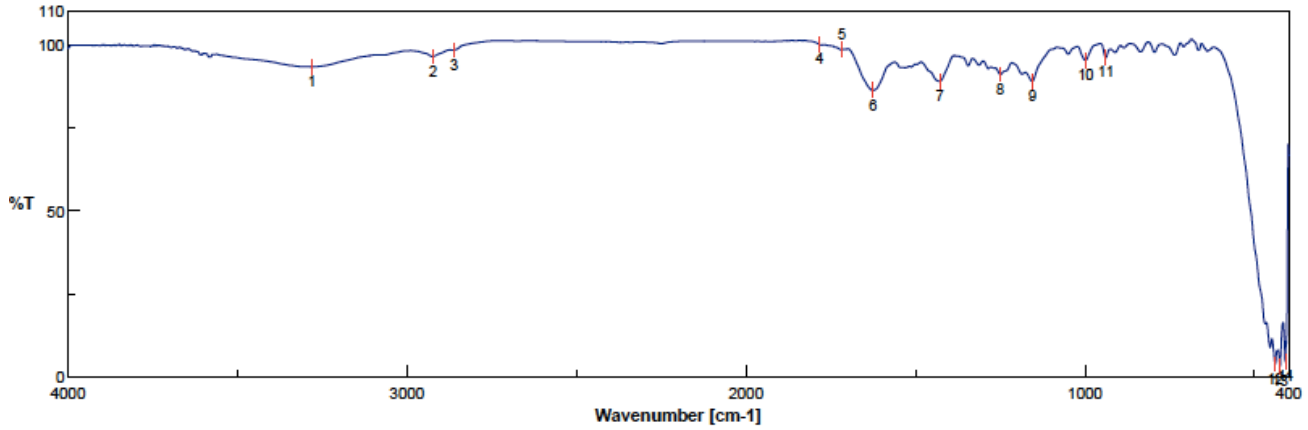

Figure A.3.8.3. The Infrared Spectrum of **AEG-III-087**.

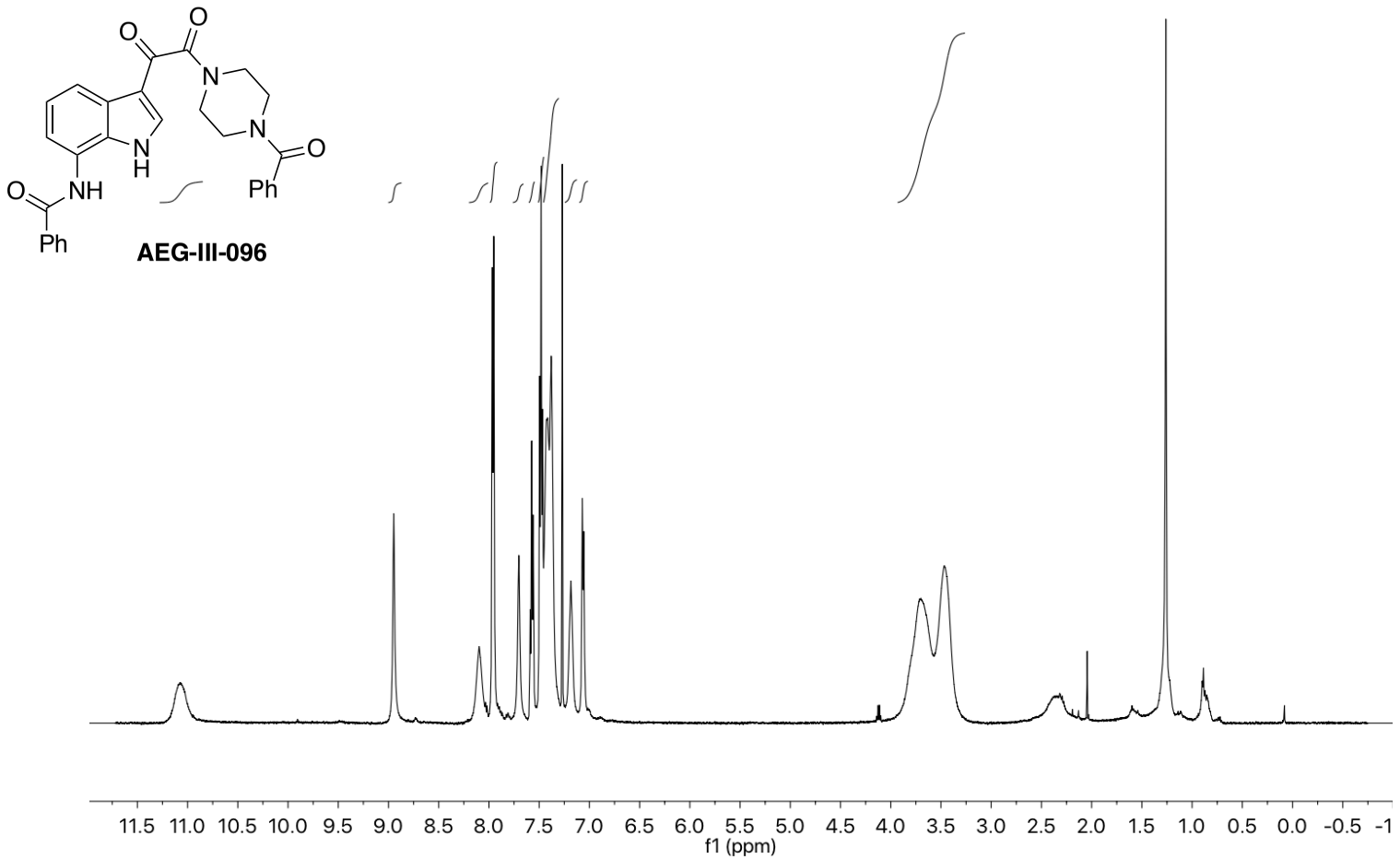

Figure A.3.9.1. The 500 MHz ^{1}H NMR Spectrum of **AEG-III-096** in $CDCl_3$.

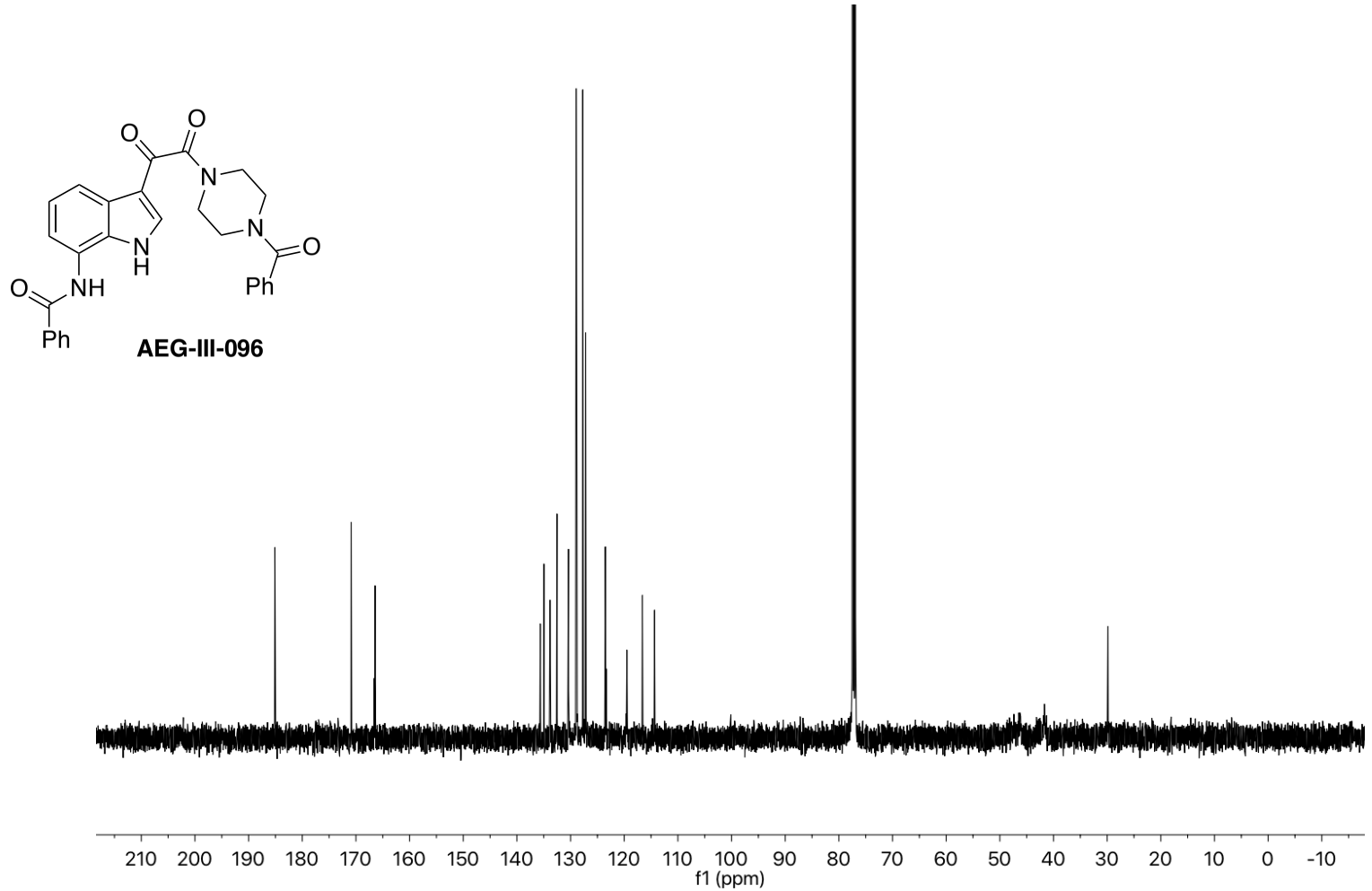

Figure A.3.9.2. The 500 MHz ^{13}C NMR Spectrum of **AEG-III-096** in $CDCl_3$.

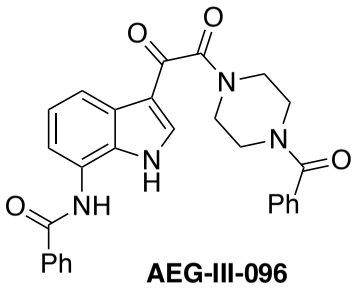

AEG-III-096

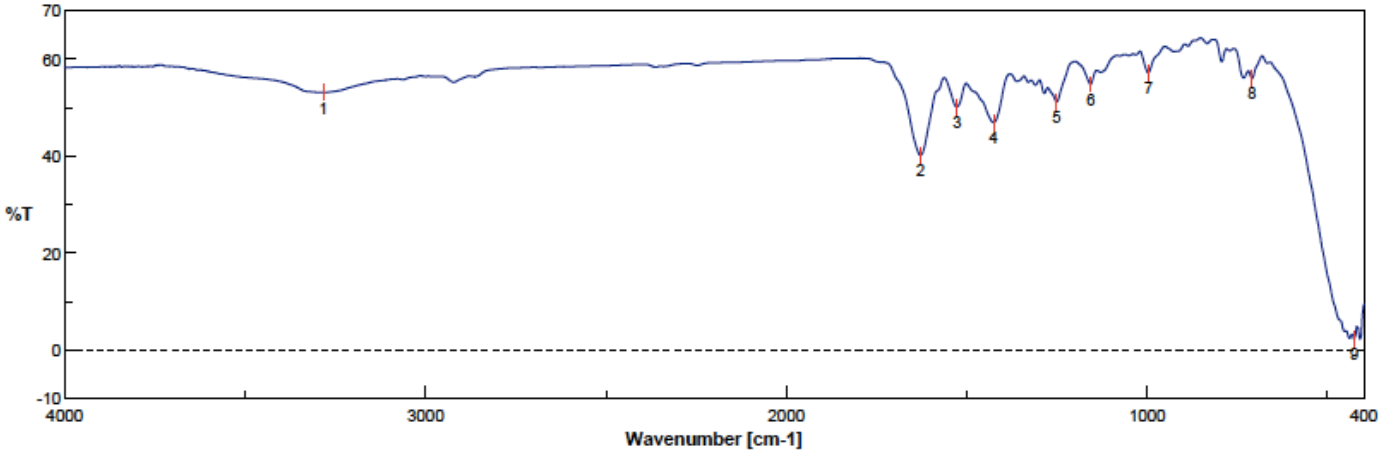

Figure A.3.9.3. The Infrared Spectrum of **AEG-III-096**.

ABOUT THE AUTHOR

Althea Gaffney was born and raised in Los Angeles, California. Althea attended Swarthmore College, where she studied chemistry and was trained in organic synthesis by Professor Robert Paley. She graduated with High Honors with a major in chemistry and a minor in psychology. Althea then went on to work at DuPont Central Research & Development in the Materials Science division. Althea began her career at DuPont researching lithium-ion batteries with the mentorship of Dr. Mark Roelofs before being promoted to Chief of Staff for the Senior Director of the Materials Science long term research division, Dr. Steven Freilich. Althea then decided to pursue graduate study at the University of Pennsylvania in the research group of Prof. Amos B. Smith, III. Upon completion of her PhD, Althea will join the American Institute of Physics as the Assistant Director of Student Programs.